Vibration serviceability of floors subjected to footfall loading of single and multiple occupants

Submitted by Ahmed Salim Mohammed to the University of Exeter as a thesis for the degree of Doctor of Philosophy in Engineering in September 2019

I certify that all material in this thesis which is not my own work has been identified and that no material has previously been submitted and approved for the award of a degree by this or any other University.

Signature: ..... .

Abstract

There is an increasing number of modern floors designed according to current vibration serviceability design guidelines failing to provide satisfactory vibration serviceability performance. This is because the design guidelines are based on assumptions and knowledge that were available in the late 1990s and at the beginning of the 21st century. Since then, there has been developments in the construction trends towards lightweight and modular structures. Numerous number of studies were conducted in the last few years to improve design tools related to vibration serviceability of floors. However, there are still gaps where the realism of these models and design tools can be improved.

This thesis aims to improve the realism of design tools related to footfall-induced vibration of floors based on the usage of floors. An improved method to take into account the influence of dynamic interaction between walking individuals and lightweight floors on the vibration response calculations is proposed. For floors in sensitive facilities, an improved model to predict vibration levels for any probability of exceedance is derived. This model is suitable for single person walking scenario which is relevant for such floors. A model for multiple pedestrian walking scenario is also developed to be utilised for other types of floors where this walking scenario is more likely to occur. To derive such a model, an advanced Ultra-WideBand location tracking system was utilised to collect data regarding people's occupancy and movements on floors. This model was utilised to develop two approaches to predict vibration levels using a simplified method and a more comprehensive framework which includes full simulation of people's movements and their corresponding vibration responses.

Acknowledgements

I would like to thank my supervisor, Professor Aleksandar Pavic for his continuous guidance and support throughout my PhD. The discussions we had in the past four years have inspired me to get the most out of my work. I am also grateful for him and my co-supervisor Professor Paul Reynolds for giving me the opportunity to gain practical experience from other projects related to my PhD topic.

I also would like to thank Mrs Katy Manning for her valuable administrative assistance. The technical support provided by Mr James Bassitt is also gratefully acknowledged. I also would like to thank Atheer, Zandy, Emma, Donald and all my other colleagues in the Vibration Engineering Section for being very kind and supportive.

The financial assistance provided by the College of Engineering, Mathematics, and Physical Sciences at the University of Exeter is also gratefully acknowledged.

My special thanks goes to my parents, my wife and our little son for their limitless love and inspiration. I am also grateful to my brothers and sisters for their incredible support and encouragement. I would like to dedicate this work to all of you.

Contents

List of Figures

List of Tables

List of Abbreviations

BBN	Bolt Beranek and Newman
BIC	Bayesian Information Criterion
C7	7th Cervical Vertebrae
CDF	Cumulative Distribution Function
CFS	Steel Floor System
CLT	Cross Laminated Timber
DAQ	Data Acquisition
DLF	Dynamic Load Factor
GEV	Generalised Extreme Value
GRF	Ground Reaction Force
FE	Finite Element
FRF	Frequency Response Function
HIVOSS	Human induced Vibration of Steel Structures
H2S	Human-to-Structure
HSI	Human-structure interaction
IMU	Inertial Measurement Unit
IP	Inverted Pendulum
L4	4th Lumbar Vertebrae
L5	5th Lumbar Vertebrae
MDOF	Multi-degree-of-freedom
MIMO	Multi-Input Multi-Output
MSD	Mass-Spring-Damper
MTVV	Maximum Transient Vibration Value

R factor	Respone Factor
RMS	Root-Mean-Square
RTLS	Real-Time Location System
S2H	Structure-to-Human
SCI	Steel Construction Institute
SDOF	Single Degree of Freedom
SLS	Serviceability Limit State
SPS	Sandwich Plate System
TP	Test Point
TS	Test Subject
ULS	Ultimate Limit State
UWB	Ultra-WideBand
VC	Vibration Criterion
VDV	Vibration Dose Value
VES	Vibration Engineering Section
WP	Walking Path

Chapter 1

Introduction

The advancements of construction materials and design tools have made it possible to achieve more ambitious architectural concepts of building floors than ever before. The design of such structures is increasingly governed by vibration serviceability criterion related to human occupation of the floor, including their walking and perception of vibration levels. With improved design for vibration serviceability, not only excessive vertical vibration levels can be avoided, but significant reduction in overall cost and carbon emissions related to construction could be achieved. Such reduction has important economic and environmental aspects considering the current size of construction industry. For instance, there were more than 1,000,000 m^2 of office floors under construction in London only during the period between April and September 2018 (Deloitte, 2018). Proper vibration serviceability design of such floors requires availability of reliable design tools and comprehensive understanding regarding their usage.

1.1 Research problem

Current vibration serviceability design guidelines for floors (Pavic and Willford, 2005; Smith et al., 2009; Willford and Young, 2006; Murray et al., 2016; Fanella and Mota) are based on assumptions and knowledge that were available in the late 1990s and at the beginning of the 21st century. Since then, there has been developments in the construction trends towards lightweight and modular structures, as well as advancements in the measurement and testing equipment related to vibration measurements and human activities. Numerous number of studies were conducted in the last few years to address these trends in construction and utilise state-of-the-art equipment to improve design tools related to vibration serviceability of floors. However, there are still gaps where the realism of the models and design tools can be improved based on the usage of buildings, and they are mainly:

- For floors in sensitive facilities, where their fundamental frequency is relatively high, the corresponding footfall loading models in the design guidelines are deterministic or 'partially deterministic'. This contradicts the stochastic nature of footfall loading as proven in the literature (Brownjohn et al., 2004; Racic and Brownjohn, 2011). While probabilistic footfall loading models where proposed in the literature (Živanović and Pavic, 2009; Racic and Brownjohn, 2011; Muhammad and Reynolds, 2020), it appears that none of them was designed for floors in sensitive facilities, proven to be fully probabilistic and can be practically utilised in the design. Extensive database of footfall loading measured using an instrumented treadmill can be utilised to propose a fully-probabilistic model for such floors.

Furthermore, there are discrepancy in the literature regarding the 'cut-off' frequency defining the type of the floor, i.e. floors with a fundamental frequency lower or higher than that are known as 'low-frequency' or 'high-frequency' floors, respectively. This cut-off frequency was proposed in the past when there were limited capabilities of measuring continuous footfall loading, such as those based on a single force plate, which could affect the cut-off frequency reported in the literature. Furthermore, there are reports that build-up resonant response, related to low-frequency floors, can still occurs in floors with fundamental frequency higher than those reported in the literature (Brownjohn and Middleton, 2008). Hence, it appears that the cut-off frequency needs to be updated based on analysis of extensive data of continuous footfall loading, measured using state-of-the-art equipment, to propose a frequency threshold where floors with fundamental frequency higher than that does not experience high build-up resonant responses.

- As the current construction trend is to build lighter and more flexible structures than before, the human-to-mass ratio for these buildings are relatively high. Recent studies showed that for such structures, human-structure interaction (HSI) between walking individuals and supporting floors can have a significant influence on the dynamic properties of the structures (Zhang, 2017; Ahmadi et al., 2018), the gait of the walking individual (Ohlsson, 1982; Dang and Živanović, 2016; Ahmadi et al., 2018; Pimentel, 1997) and, subsequently, the footfall-induced vibrations (Živanović, 2012). Numerous studies were conducted in recent years to take this phenomenon into account for footbridges, but there are limited amount of research conducted for floor structures. As the fundamental frequency of

floor structures are typically higher than those for footbridges, it is not clear how HSI can influence vibration levels of floors in actual buildings and which models can be utilised to take that into account in the vibration response calculation.

- The design guidelines adopt the scenario of a single person walking on the most responsive walking path and a pacing frequency related to the highest vibration level, as a worst-case scenario for the design (Pavic and Willford, 2005; Smith et al., 2009; Willford and Young, 2006; Murray et al., 2016; Fanella and Mota). There are two aspects regarding this walking scenario. Firstly, there are reports that single person walking scenario may not necessarily produce the highest vibration levels (Chen et al., 2015), and in reality, multiple pedestrian walking scenarios are likely to occur frequently (Muhammad et al., 2018). Secondly, depending on the floor layout, it could be unlikely that floor occupants walk on the most responsive walking path, let alone walking there at a pacing frequency related to the highest vibration level. Hence, while this walking scenario could be useful in the design in the absence of information about floor layout, more realistic walking scenarios can be predicted and utilised in the design if floor layout is available. With the recent advancements in indoor location tracking systems and computing capabilities to deal with 'big data' related to people movements and simulations, it appears that measurement and modelling of people occupancy and movements on floors can be utilised to improve the realism of walking scenarios pertinent to vibration serviceability analysis. This could be particularly useful to predict vibration levels of existing floors, before conducting refurbishment works and changing their

floor layout. Interestingly, this aspect is rarely studied in the context of vibration serviceability of floors.

- Vibration serviceability assessment of floors is traditionally assessed using a single number, i.e. the response (R) factor. The R factor typically corresponds to an absolute maximum vibration level which could occur in locations and durations when no floor occupants are exposed to it. Previous studies reported that vibration levels related to R factor, i.e. maximum vibration level, could occur for only a very short duration of time during the day (Reynolds and Pavic, 2015). The vibration dose value (VDV) is an another vibration descriptor that can be utilised to take into account the duration of exposure to vibration throughout the day. However, it is practically difficult to estimate VDV in the absence information regarding the number of floor occupants' walking events and their walking paths. Hence, it is apparent that in the case that floor layout is available, modelling of people occupancy and movements can be utilised to estimate vibration levels likely to be experienced by the occupants which can be used for vibration serviceability checks. Unfortunately, the influence of utilising such models on vibration serviceability assessment of floors is missing in the literature.

It is apparent that the above mentioned gaps in knowledge regarding vibration serviceability of floors are mainly related to lack of understanding of people's occupancy and movements and their influence on the supporting floors. While some of the above mentioned shortcomings can result in an underestimation and others result in overestimation of floors vibration levels, their aggregate outcome is clearly not a reliable vibration serviceability assessment which should not be

based on one error cancelling the other in the modelling process. State -of-the-art measurement and tracking equipment can be utilised to improve the realism of vibration serviceability design tools, related to floors, based on their realistic usage.

1.2 Scope and proposed solution

There are three key elements that characterise vibration serviceability of floor structures related to human footfall dynamic excitation (ISO 10137:2007, 2007):

- Vibration source i.e. human footfall loads applied on the floor,
- Transmission path, which can be categorised by the mass, stiffness, damping and vibration mode shapes of the structure, and
- Vibration receiver i.e. perception of vibration by floor occupants and/or sensitive equipment

This research aims to improve the realism of vibration serviceability design methods related to single and multiple floor occupants' footfall excitation of floors. It focuses on improving the realism of walking scenarios of the occupants, i.e. vibration source, and the their dynamic interaction with the supporting floors, i.e. transmission path. To achieve this, different approaches were followed for each aspect as explained below.

- For floors in sensitive facilities, propose a fully-probabilistic footfall force models, pertinent to floors in sensitive facilities, that takes into account both of inter- and intra-subject variations of the footfall loading. Utilising statistically large amount of measured footfall forces can be utilised to

derive such a model. Hence, database of more than 800 continuously measured ground reaction force time histories for individual people walking on an instrumented treadmill were utilised in this study to propose a fully probabilistic model for such floors. These data were also utilised to perform simulations aimed to update the cut-off frequency of floors and avoid high resonant responses in floors housing sensitive equipment. This cut-off frequency was updated due to lack of practical and universal fully-probabilistic models that can be utilised for both low- and high-frequency floors and considers inter- and intra-subject variabilities.

- For lightweight floors, propose a model that considers HSI in the response calculations of footfall-induced vibration. Different inverted pendulum (IP) and mass-spring-damper (MSD) models are widely utilised to simulate HSI between walking individuals and supporting floors. However, IP models are relatively complex to use in practice. MSD dampers are used more commonly for this aim and they are easier to use, but they are generally utilised to model only the dominant whole-body mode of vibration of the walking individual which has a frequency between 2-4 Hz. Bearing in mind that there are indications of multiple whole-body modes of vibration for walking individuals, and that the fundamental frequency of most floors are above 4-5 Hz, utilising multi-degree-of-freedom (MDOF) or multiple single-degree-of-freedom (SDOF) models can be used to model human dynamics related to multiple modes. However, an alternative method is to utilise transfer functions over a *range of frequencies* which does not require fitting an approximate SDOF or MDOF models. Hence, the model proposed in this study was derived utilising previously conducted tests, from

the literature, involving state-of-the-art wearable sensors attached to test subjects walking on an instrumented treadmill or standing on a platform. The measurements utilised in this part of the study can be, ideally, related to individuals walking on a vibrating platform at various frequencies. However, the focus of this study is on the principle utilised to model HSI, and the model can be updated in the future by utilising data related to individuals walking on such facilities when they become available for such measurements.

- To consider realistic walking scenarios in the design of floors for footfall-induced vibration, data on people's occupancy and movements over an office floor can be collected and analysed. The choice of the location tracking system can influence the errors in the measurements and the derived occupancy model. Such errors can subsequently affect walking paths, simulated using the derived occupancy model, on other floors where the layout is different from that where the measurements were conducted. To minimise such error, an advanced Ultra-WideBand (UWB) location tracking system was utilised in this study. This tracking system produces less errors in the measurements than other practical solutions, such as those based on cameras or sensing devices. The data collected in this experiment were utilised to study the correlation between walking scenarios and their corresponding vibration levels and model realistic walking scenarios on such floors. This is followed by proposing a novel and fully probabilistic framework for vibration serviceability assessment of floors. It utilises the derived people's occupancy and movements model to predict realistic walking scenarios to be used in the design. This will allow for reliable predictions of vibration levels based on the predicted walking

scenarios of single or multiple floor occupants. Although the proposed model can be utilised only when a floor layout is available, it has several applications. For example, it can be utilised to design floors for vibration serviceability before conducting commissioning, or refurbishment, works in a building, or as a vibration remedy by optimising floor layout to minimise vibration levels.

It is worth mentioning that this thesis concentrates only on the main gaps related to improving the realism of design tools pertinent to footfall-induced vibration serviceability of floors. Hence, it has no ambition to resolve all issues related to vibration serviceability of floors.

1.3 Thesis outline

The work presented in this thesis is organised in the form of three scientific journal papers besides five other related conference papers prepared while conducting this research. One journal paper and the conference papers were published while the other two journal papers were submitted for publication. Each chapter-paper was written to stand alone and briefly introduced in a preface to describe its importance and how it is related to the rest of the thesis. Hence, some of the contents of the thesis are repeated in more than one chapter.

This thesis consists of six chapters. Chapter 1 provides an introduction to the research problem followed by the scope and objectives of the proposed solution. A literature review regarding relevant past research is presented in Chapters 2 with focus on the main shortcomings of current design guidelines which represent the research problem of this thesis. Chapter 3 presents an improved version of a design method for floors supporting sensitive equipment with a capability to

estimate vibration levels to any probability of non-exceedance. This is followed by an analytical work to update the so-called 'cut-off frequency' where floors with a natural frequency above which can be designed to support sensitive equipment. Chapter 4 quantifies the influence of HSI on the frequency response function magnitude of floors and proposes a new model that can be used to consider HSI in the prediction of footfall-induced vibration of lightweight floors. A description about utilising an advanced people location tracking system to collect data regarding their movements and the correlation between these movements and the corresponding vibration levels are presented in Chapter 5 which also proposes an occupancy and movement model and a fully probabilistic framework to predict footfall induced vibration of floors, related to multiple occupants, and assess the corresponding vibration levels based on people's experience. Finally, Chapter 6 provides conclusions from this thesis and recommendations for future work.

Chapter 2

Literature Review

2.1 Introduction

The latest version of most of the current guidelines related to the design of floors for vibration serviceability were published more than 10 years ago (Pavic and Willford, 2005; Willford and Young, 2006; Smith et al., 2009). Therefore, they are based on knowledge, regarding vibration serviceability, available at that time. In the mean time, there has been trend in construction towards lightweight and modular structures in recent years. However, there are an increasing number of reported problems related to unsatisfactory vibration serviceability performance of floors (Ebrahimpour and Sack, 2005; Brownjohn et al., 2015; Muhammad and Reynolds, 2019). This indicates that improvements are needed for such design tools. Numerous studies were conducted recently in the literature to improve different aspects of vibration serviceability of floors. Hence, this review aims to address the main drawbacks of these guidelines as well as the recent developments in the literature regarding these drawbacks.

There are three key parameters related to vibration serviceability assessment of

any structure, according to ISO 10137:2007 (2007). They are:

- Vibration source,
- Transmission path, and
- Vibration receiver.

This chapter addresses these parameters, separately, before reviewing modelling strategies of people's occupancy and movements on floors and state-of-the-art people tracking systems which are relevant to this review, as explained below.

2.2 Vibration source

Human walking is the most common activity that causes vibration of building floors, such as offices, hospitals and laboratories. During walking, pedestrians produce a time-varying ground-reaction-force (GRF) at the time-varying location of the pedestrian. GRF related to walking pedestrians is a narrow-band random force where different people produce different GRFs (Brownjohn et al., 2004; Racic et al., 2009; Racic and Brownjohn, 2011). In particular, the vertical component of the GRF is relevant for vibration serviceability of floors, and therefore, the term GRF refers to this component thorough this thesis.

2.2.1 Walking scenarios on floors

Floors are normally used by multiple occupants and their walking patterns are complex and differ for different types of floors, such as offices, hospitals and educational buildings. Current guidelines utilise the scenario of a single person walking in the design (Pavic and Willford, 2005; Willford and Young, 2006; Feldmann and Heinemeyer, 2007; Smith et al., 2009; Fanella and Mota; Murray

et al., 2016). This is adopted on the basis that multiple pedestrians cannot synchronise their footfalls while walking (Racic et al., 2009), and therefore, it is argued that the case of single person walking correspond to the worst-case scenario. However, there are reports indicating that vibration levels related to multiple pedestrians can be higher than those for a single person walking (Chen et al., 2015). Furthermore, the scenario of single pedestrian does not reflect the true nature of walking scenarios on several types of floors, such as offices and retails, where floor occupants are likely to walk individually or simultaneously throughout the day (Muhammad et al., 2018). For other types of floors, such as those in ultra-sensitive facilities, the scenario of single person walking is more likely to occur than that for multiple pedestrians.

Walking paths utilised in the design of floors for vibration serviceability can significantly affect footfall-induced vibration responses (Smith et al., 2009; Hicks and Smith, 2011; Zhang, 2017). Due to the complexity of modelling the movements of floors' occupants', design guidelines adopt a single walking path related to the worst-case scenario (Smith et al., 2009). Such walking path may be unlikely to be used by floor occupants.

Few attempts were made in the literature to utilise pre-defined walking paths to calculate the predicted vibration response of floors (Nguyen, 2013; Zhang, 2017). Most of them utilised walking paths related to maximum vibration levels. Hudson and Reynolds (2013) utilised start and end points for walking paths, shown in Figure 2.1, based on an existing floor layout, to estimate vibration levels of an office floor. The resulting vibration responses were then used statistically for vibration serviceability assessment. While their work represents an improvement towards utilising more realistic walking scenarios in the design, it lacks crucial

parameters regarding the timing of walking events, number of pedestrians walking simultaneously and arrival and departure rates. Therefore, an improved vibration serviceability design tool can be derived by simulating realistic walking scenarios on floors. Section 2.5 describes a potential modelling strategy that can be used for this purpose.

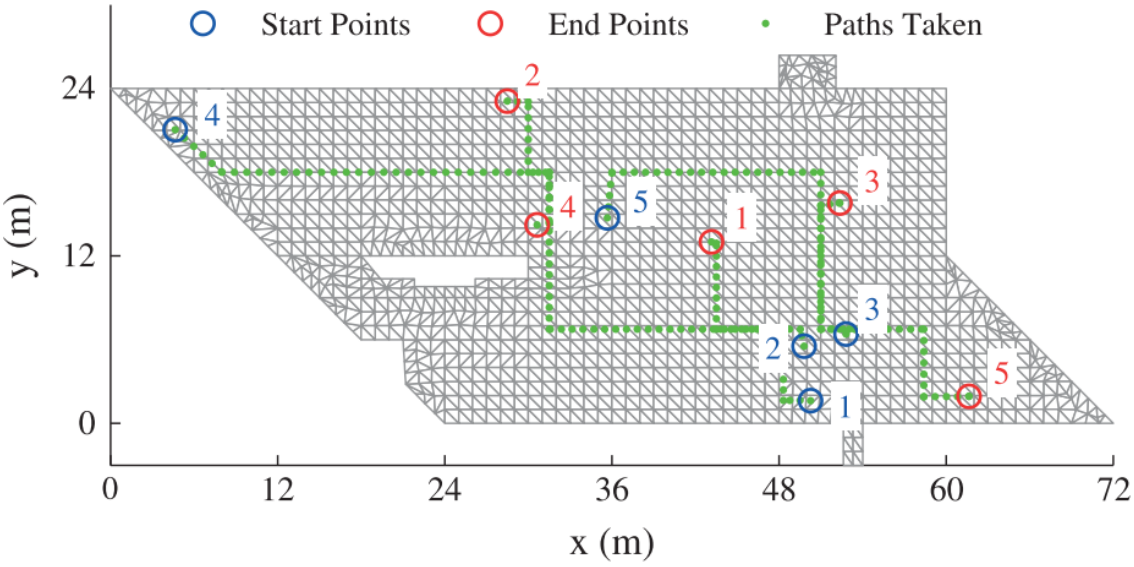

Figure 2.1: Example of routes taken by five individuals based on existing layout of the floor (Hudson and Reynolds, 2013).

2.3 Transmission path

Footfall excitation transfers through the building, i.e. transmission path, to the receivers of vibration. In the context of vibration serviceability of floors, the transmission path includes structural and non-structural, e.g non-structural partitions, elements of the building (Pavic and Reynolds, 2002). Transmission path can be categorised by the modal properties of the floor, which are natural frequencies, modal damping ratios, modal masses and mode shapes (Inman, 2007). The modal properties are utilised by various design methods to calculate the vibration responses. The following two subsections focus on two common types of construction where vibration serviceability related to footfall excitation is

crucial in the design.

2.3.1 Floors housing vibration sensitive equipment

Wyatt (1989) proposed that the design of floors for footfall-induced vibration should be performed depending on the nature of the response. He suggested that floors with fundamental frequency lower than a specific frequency threshold, known as the *cut-off frequency*, are dominated by a build-up resonant response. On the other hand, floors with fundamental frequency higher than the cut-off frequency are dominated by sequence of transient responses, corresponding to the footfalls. Therefore, the former type of floors is known as *low-frequency floors* and the later is known as *high-frequency floors*. Current design guidelines adopt this classification of floors in the design and recommend designing floors carrying sensitive equipment as high-frequency floors (Pavic and Willford, 2005; Willford and Young, 2006; Smith et al., 2009; Murray et al., 2016).

The cut-off frequency between low- and high-frequency floors varies significantly for different authors and design guidelines, as shown in Table 2.1.

Floors supporting sensitive equipment are required to have low-level transient vibration responses due to human footfall excitation (Hanagan and Murray, 1997; Liu and Davis, 2014), thus they are traditionally designed as high-frequency floors. A number of studies (Ellis et al., 2000; Brownjohn and Middleton, 2008) reported that the cut-off frequencies given in Table 2.1 are too conservative, which has a major effect on the design and cost of ultra-sensitive facilities. They showed that the resonant build-up response can occur even for floors with a fundamental frequency of above 15 Hz (Brownjohn and Middleton, 2008). This is because there are higher dominant harmonics of footfall loading at frequencies above

Table 2.1: Cut-off frequency between low- and high-frequency floors adopted by different authors and design guidelines.

Author	Cut-off frequency
Ohlsson (1988)	8 Hz
Wyatt (1989)	7 Hz
Allen and Murray (1993)	9 Hz
The Concrete Society (Pavic and Willford, 2005)	10 Hz
The Concrete Centre (Willford and Young, 2006)	10 Hz
The Steel Construction Institute P354 (Smith et al., 2009)	8-10 Hz
American Institute of Steel Construction (Murray et al., 2016)	9 Hz
Human induced vibration of steel (HIVOSS) (Feldmann and Heinemeyer, 2007; Feldmann et al., 2009)	10 Hz
ISO 10137:2007 (2007)	8-10 Hz
BS 6472-1:2008 (2008)	7-10 Hz
AS 3623—1993 (1993)	8 Hz

10 Hz, which contain a significant amount of energy. For example, according to the design guidelines, a floor with a fundamental frequency of 11.5 Hz is a high-frequency floor. However, a person walking at a pacing rate 2.3 Hz, still can induce the resonant vibrations by the harmonic corresponding to the fifth integer multiple of pacing frequency. This error in the floor type yields an underestimated vibration response, hence a floor may not be fit for purpose. The uncertainty linked to the cut-off frequency could be explained by the lack of knowledge and/or reliable experimental data pertinent to human footfall excitation when these cut-off frequency values were suggested. Large database of footfall forces measured using state-of-the-art equipment could be analysed to update the cut-off in a way that avoids resonant vibration of floors in sensitive facilities.

Another major drawback of the available guidelines related to high-frequency floors is their adoption of deterministic mathematical description of human-induced loading (Middleton and Brownjohn, 2010; Liu and Davis,

2014). The model presented by Arup (Willford et al., 2005) allows for 75% of non-exceedance in vibration response predictions, while a probabilistic approach is arguably more suitable due to the inherent stochastic nature of human footfall forces (Racic and Brownjohn, 2011; Brownjohn et al., 2004; Živanović and Pavic, 2009; Brownjohn et al., 2015).

Živanović and Pavic (2009) merged together the design methods related to low- and high-frequency floors in a probabilistic model that takes into account the inter-subject variability, which refers to the variability of the footfall loading induced by different people. The model can be used to estimate the probability distribution of vibration responses generated by different people. However, Middleton (2009) showed that the variations between successive steps, i.e. intra-subject variations, during walking have more influence on the vibration responses than the inter-subject variations. Neglecting intra-subject variations can also result in an overestimated vibration response of high-frequency floors (Middleton, 2009).

Other studies attempted to produce probabilistic and universal footfall loading models to be used for both low- and high-frequency floors. Racic and Brownjohn (2011) proposed a stochastic footfall loading model using Gaussian functions. The model utilises random parameters derived from experimentally measured footfall loading to generate synthetic footfall loading. As access to such experimental database may not be available to public access, the usage of this model is limited. Muhammad and Reynolds (2020) proposed a probabilistic model for footfall loading related to both left and right legs and their combined loading. The model appears to produce comparable synthetic footfall loading to those obtained from the measurements. The study shows that the energy at the first four dominant harmonics for the synthetic footfall loading is comparable to that

obtained from the measurements. However, it is not obvious how the energy at higher frequencies, i.e. higher than 10 Hz, are compared between the synthetic and the measured footfall loading. Hence, it is apparent that there is a lack of probabilistic and practical footfall force models, pertinent to floors in sensitive facilities, that takes into account both of inter- and intra-subject variations.

2.3.2 Lightweight floors

Lightweight floors are increasingly becoming popular in the construction industry due to recent advancements in construction materials and design tools. Petrovic-Kotur (2016) suggests that floors can be classified as lightweight if they weigh less than 250 kg/m^2, heavy floors if they weigh more than 500 kg/m^2 or normal weight if they weigh between 250 kg/m^2 and 500 kg/m^2. This is similar, but slightly different, to the classification suggested by the National Building Code of Canada (2005) which implies that lightweight floors have less than 100 kg/m^2, heavy floors weigh more than 500 kg/m^2 and medium weight floors weigh between 250 kg/m^2 and 500 kg/m^2. On the other hand, Ohlsson (1982) suggests that heavy floors have modal masses of at least 1000 kg for each mode of vibration of interest.

Due to the comparable masses between floor occupants and lightweight floors, dynamic interaction between walking individuals and these floors could significantly affect the corresponding footfall-induced vibration (Zhang, 2017). Zhang (2017) argued that this can occur for steel floor systems (CFS) if the mass ratio between the floor's occupants and the supporting floor is equal or higher than 0.1. This is in-line with previous studies, related to footbridges, which reported that such interaction is dependant on the pedestrians-to-structure mass ratio

(Shahabpoor, 2014; Ahmadi et al., 2018). Therefore, there are indications that the phenomenon of HSI between walking pedestrians and floors in real buildings can significantly affect the predicted vibration levels, but there is only limited amount of research conducted to quantify it for floor structures.

Numerous studies were conducted previously to understand this phenomenon. For example, Ohlsson (1982) found that the spectrum of the footfall force measured on a rigid surface was different from that measured on a floor, especially for frequencies close to the frequency of the floor, i.e. resonance. He also reported that a walking pedestrian can alter the damping and mass of the supporting floor. Pimentel (1997) reported that dynamic load factors (DLFs) related to a walking pedestrian on a footbridge are lower than that those for a pedestrian walking on a rigid surface. Similarly, Baumann and Bachmann (1988) reported up to 10% lower DLFs for pedestrians walking on a flexible prestressed beam. More recently, Dang and Živanović (2016) and Ahmadi et al. (2018) have directly measured the footfall loading of a individual walkers on flexible footbridges. They reported a drop in the DLFs around the frequency of the bridge and the drop was more prominent in the case of resonance. Other studies reported that pedestrians walking on structures can alter their natural frequency or modal damping. Ebrahimpour et al. (1989) showed that walking occupants increased the damping of their supporting platform. Similar conclusions were made later by Shahabpoor et al. (2017b), Živanović (2012) and Van Nimmen et al. (2015) who reported that pedestrians walking on footbridges can alter the structural modal damping and natural frequency.

Hence, it can be concluded from the literature that HSI has two components: the influence of the walking on the modal properties of the supporting structure

(H2S) and the influence of the structure on the footfall loading of the walker (S2H). These two components were described by a recent study conducted by Ahmadi et al. (2019) who quantified these two components on two footbridges.

Regarding the modelling aspect of HSI, currently available models are related to pedestrians walking on footbridges. The majority of them are based on modelling the walking individual as either an inverted pendulum (IP) (Bocian et al., 2013; Qin et al., 2013; Dang, 2014) or a mass-spring-damper (MSD) (Caprani et al., 2011; da Silva and Pimentel, 2011; Van Nimmen et al., 2015; Zhang et al., 2015; Shahabpoor et al., 2016a). IP models are generally complex to implement in the design and have limited robustness (Shahabpoor et al., 2016b). MSD models are more common and easier to use. Current MSD models for walking individuals take into account human dynamics related to only the dominant whole-body mode of vibration. Their corresponding single-degree-of-freedom (SDOF) natural frequency, 2-4 Hz, is close to the fundamental frequency of a typical footbridge, and therefore, they are proven to be useful and reliable in the design of such structures for vibration serviceability. Despite that MSD models were suggested for simulating HSI between walking individuals and floors (Zhang, 2017), their frequency is considerably lower than the fundamental frequency of building floors, typically higher than 4-5 Hz. While multiple modes of of vibration are reported in the literature for standing people, there are indications that higher order human whole-body mode of vibration exists for walking individuals (Shahabpoor, 2014), but quantification of its parameters is generally missing. Hence, design methods related to footfall-induced vibration of floors can be improved by taking into account whole-body dynamics of walking individuals in frequency ranges relevant to dominant modes of vibration for building floors, i.e. higher than 4-5 Hz. This can

be achieved by incorporating multiple SDOF or multi-degree-of-freedom (MDOF) models calibrated for this purpose. Another way to achieve this is by utilising experimentally-based transfer functions, to describe the dynamics of walking individuals *over a range of frequencies*, which eliminates the need to derive approximate SDOF or MDOF models.

2.4 Vibration receiver

Receivers of floors' vibration could be the occupants or vibration sensitive equipment, such as those in hospitals and laboratories. Vibration is considered unacceptable if it causes adverse reaction from the occupants or impaired performance for sensitive equipment (ISO 10137:2007, 2007).

2.4.1 Floor occupants

Griffin (1990) stated that the root-mean-square (RMS) acceleration related to human perception to continuous vibration can be arranged as frequency-dependant curves, known as the base curves. These curves are different between z-axis, as shown in Figure 2.2, and the two other perpendicular axes (BS6472:1992).

To take into account the dependency of human comfort on the frequency of vibration, different weighting curves were introduced based on the human activity and direction of vibration (BS6472:1992). Figure 2.3 shows the W_b weighting curve, which is the most commonly used weighting curve (BS6472:1992).

Wyatt and Dier (1989) utilised the concept of RMS acceleration to propose the response (R) factor for vibration serviceability checks. The R factor is a multiplication of the base curve, i.e. multiplication of the RMS acceleration related

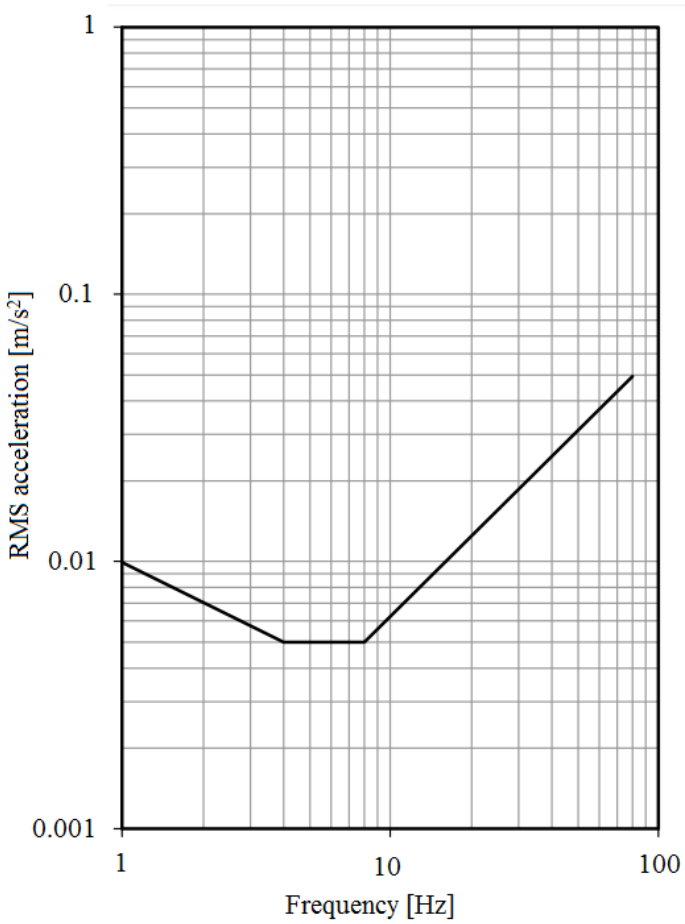

Figure 2.2: Base curve related to perception to vertical vibration (BS6472:1992).

to human perception to vibration. This concept of R factor was adopted by the Steel Construction Institute's design guideline SCI076 (Wyatt, 1989) and ISO (1989), and is currently widely used by the current design guidelines for vibration serviceability assessment related to footfall-induced excitation of floors (Pavic and Willford, 2005; Willford and Young, 2006; Smith et al., 2009). The most widely used RMS averaging for R factor is 1 s, which is equivalent to the maximum transient vibration value (MTVV). Table 2.2 shows the multiplication factor adopted by BS6472:1992 corresponding to different types of floors.

The main advantage of utilising R factor in vibration serviceability assessment is its simplicity . However, it is argued that it is too sensitive to, and depends on, very short duration peaks. i.e. 1 s, in the response and may not describe vibration

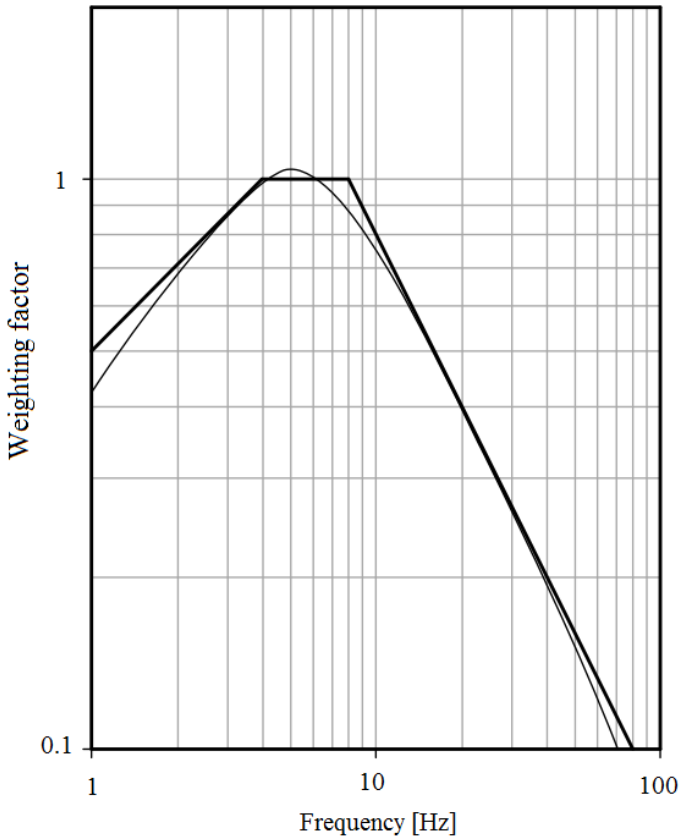

Figure 2.3: W_b frequency weighting curve for z-axis (light curve) and its approximation (thick curve) (BS6472:1992).

levels for the vast majority of the time (Reynolds and Pavic, 2015; Muhammad et al., 2018). Reynolds and Pavic (2015) carried out vibration monitoring of an in-service office floor for 10 days. They found that the peak R factor was reached for a very short duration and the R factor related to 90% probability of non-exceedance was significantly lower than the peak R factor. Interestingly, ISO 2631-2-2003 (2003), and its following versions, no longer provide guidance values, for such metric, above which adverse comments due to building vibration could occur since "their possible range is too widespread to be reproduced in an International Standard" (ISO, 1989). However, the concept of RMS acceleration and response factor are still utilised in practice.

The vibration dose value (VDV) of the acceleration is an another metric for vibration serviceability assessment. It is the fourth root of the time integral of

Table 2.2: Multiplication factor for human perception to vertical vibration (BS6472:1992).

Place	Time	Multiplication factor
Critical working areas	Day	1
	Night	1
Residential	Day	2-4
	Night	1.4
Office	Day	2
	Night	2
Workshops	Day	8
	Night	8

the fourth power of the acceleration (BS6472:1992). Its tolerance limits, adopted BS 6472-1:2008 (2008), are shown in Table 2.3. A multiplication factor of 2 and 4 should be applied to the limits related to the 16-hour VDV, shown in Table 2.3, for offices and workshops, respectively.

Table 2.3: Vibration dose value tolerance ranges within residential buildings (BS 6472-1:2008, 2008).

Place and time	Low probability of adverse comment m/s$^{1.75}$	Adverse comment possible m/s$^{1.75}$	Adverse comment probable m/s$^{1.75}$
Residential buildings 16-hour day	0.2-0.4	0.4-0.8	0.8-1.6
Residential buildings 8-hour day	0.1-0.2	0.2-0.4	0.4-0.8

The VDV approach incorporates the duration of exposure to vibration as well as the magnitude of vibration. However, it has been reported that VDV limit for low probability of adverse comment for office floors, 0.4-0.8 m/s$^{1.75}$ as provided by BS 6472-1:2008 (2008), is too high and need to be calibrated (Reynolds and Pavic, 2015; Muhammad et al., 2018). Furthermore, a potential challenge with utilising the VDV in the design is the prediction of the number of floor occupants' walking events and their walking paths (Pavic and Willford, 2005; Smith et al., 2009).

2.4.2 Sensitive machinery

For vibration sensitive equipment, such as those in hospitals and laboratories, the permissible vibration limits are below those related to human perception. The vibration criterion (VC) curves are widely used in the design of such floors for vibration serviceability. BBN VC (Gorodon, 1988) is the most widely used VC for sensitive facilities. Table 2.4 shows its corresponding limits given in terms of the RMS (one-third octave frequency) velocity response, and the corresponding multiplication factor.

Table 2.4: BBN VC limits and the corresponding multiplication factor for sensitive facilities (Gorodon, 1988).

Place/criterion curve	RMS velocity [μm/s]	Multiplication factor
Workshop	800	8
Office	400	4
Residential day	200	2
Operating theatres	100	1
VC-A	50	0.5
VC-B	25	0.25
VC-C	12.5	0.125
VC-D	6.25	0.0625
VC-E	3.13	0.03125

2.5 People occupancy and movements on floors

Vibration levels related to normal occupancy could be significantly different from those related to walking scenarios recommended by the current design guidelines. Živanović et al. (2012) monitored vibration levels of an in-service office floor and showed that the occupants were exposed to lower vibration levels during normal occupancy than in single pedestrian walking tests along the most responsive walking paths, which is the recommended walking scenario by design guidelines. They suggested that models with capability to produce

various probability of exceedance related to walking paths and events can be used to improve the predictability of vibration levels. To achieve this, they suggested that experimental data regarding actual walking paths and movements on in-service floors are needed (Živanović et al., 2012). In general, measurement and modelling of people occupancy and movements on floors can be potentially utilised to improve design tools for vibration serviceability of floors by:

- Deriving occupancy and movement models on floors from experimental data. Such models can be used to model realistic walking scenarios and their corresponding vibration levels.
- Utilising vibration levels exposed by floors' occupants in the design instead of relying on vibration levels occurring at positions that may not be occupied by the occupants during most of the day.
- Studying the subjective rating of vibration levels by floors' occupants, experimentally, by comparing the actual vibration levels they perceived, based on their positions, and their assessment to these vibration levels.

Tracking and modelling of indoor people occupancy and movements have wide range of applications including improving energy performance of buildings, architectural design and emergency evacuation planning (Dong et al., 2018; Balvedi et al., 2018). Therefore, there are different models available in the literature, with various complexity, that serve different applications and there is no universal model that serves all building occupancy applications. It is argued that fit-for-purpose modelling strategy should be utilised, and the objective of the application should lead the modelling approach (Gaetani et al., 2016; Balvedi et al., 2018). For vibration serviceability applications, such models can be

categorised into two groups: occupancy and movements models. Occupancy models are related to the spatial and temporal occupancy patterns of floor occupants within specific areas and they are useful to quantify the vibration levels experienced by floor occupants based on their locations. Movement models refer to the movements of floor occupants and their interaction with each other and the surrounding objects and they can be utilised to predict walking paths and their timings when used with occupancy models.

There are different models related to people movements and their interaction with each other and the surrounding environment (walls, tables, etc). It has been reported that the most widely used model, the social force model (Helbing et al., 2000; Helbing and Farkas, 2002), can produce a balanced performance between computational cost and accuracy in simulating pedestrians' movements (Duives et al., 2013). The model was originally derived to model evacuation scenarios, but it was proven to be relevant for modelling people movements in normal situations (Helbing and Farkas, 2002) where the occupants are not crowded. While the model is sensitive to the parameters related to physical contact between the occupants and the surroundings (Helbing and Farkas, 2002), this is not expected to be an issue when the model is used to simulate movements in normal conditions, i.e. not evacuation scenarios as pedestrians are less likely to physically touch the walls and other boundaries during walking.

Occupancy models can be grouped into three categories (Balvedi et al., 2018): static schedules, rule-based models and stochastic models. Rule-based models depends heavily on measurements, rather than its statistical features, which may differ from one measurement to another. Static schedules models assume a deterministic characteristics for occupant behaviour. Stochastic models, which

focus on the statistical features of the occupants, have shown a strong potential for modelling realistic behaviour of building occupancy (Page et al., 2008). Previous studies suggest that this type of models reflect the nature of patterns of presence on floors, such as the timings of first arrival, final departure and intermediate transitions (Page et al., 2008). Page et al. (2008) reported that the Markov chain works well at reproducing short presence and absence durations, and hence, it has the potential to be used for modelling realistic behaviour of occupancy on office floors. To utilise the Markov chain in such analysis, experimental data related to people occupancy should be utilised to make future predictions of occupants' activities.

2.5.1 Indoor people location tracking systems

There are various devices and techniques related to indoor people location tracking, such as cameras, motion sensors, ranging devices and inertial sensors. The nature of the collected data depends on the system utilised. Figure 2.4 shows various levels of data that can be collected.

The terms of the occupancy resolution, in figure 2.4, are (Teixeira et al., 2010):

- *Presence* corresponds to binary information regarding the presence or absence of single or multiple persons is a specific area.
- *Count* refers to the number of recorded occupants.
- *Location* refers to the ability to locate a stationary or moving occupant.
- *Track* corresponds to tracking floor occupants during specific occasions. For example, a camera can be used to track an occupant and assign a corresponding temporary identification to him/her. However, once the

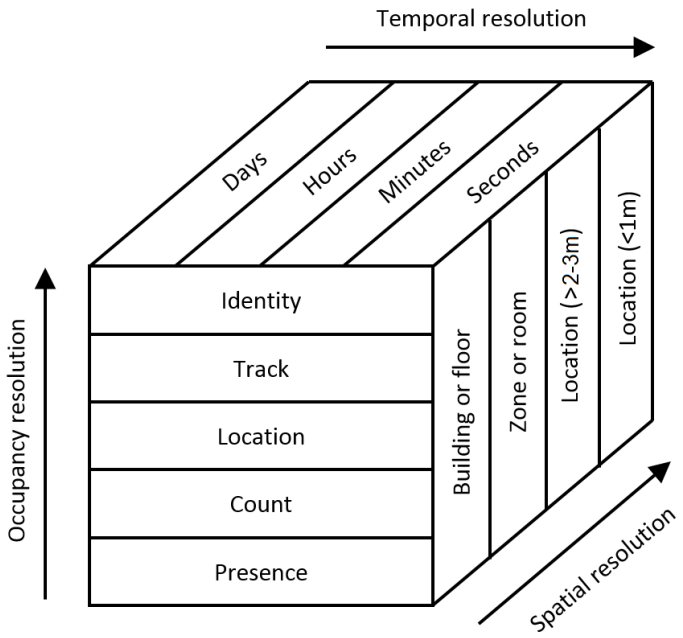

Figure 2.4: Temporal, spatial and occupancy resolution related to the data that can be collected using currently available people tracking systems (after Azizi et al. (2019)).

occupant leaves the field of view related to the camera and comes back again, a new identification will be assigned to him/her.

- *Identity* refers to the case when the same identifications can be assigned to the same individuals no matter how often they become undetectable during the day.

For vibration serviceability applications, data related to different levels of resolution can be used differently . Data with *temporal* resolution of lower than a minute, i.e. one recording per one or few minutes, may not include information about short walking events. This means if the data was recorded with a low temporal resolution, a person can make few walking events while being recorded as stationary. A sensible *spatial* resolution can be used to reduce errors related to the derived models. While the exact locations of floor occupants might not be needed, if a tracking system is not precise enough, it might report an occupant

as he/she is sitting in, say, a meeting room while he/she is, in reality, sitting in an adjacent office or kitchen. This may affect the derived occupancy models and the corresponding walking paths and vibration levels of other floors with different layout where the meeting room, as for the example above, is located away from the office or the kitchen. The *occupancy* resolution of the data may limit the type of the derived occupancy and movements model, but the *identity* level of occupancy resolution can provide the most comprehensive understanding of people occupancy and movements.

Teixeira et al. (2010) conducted a comprehensive study regarding the reliability of people's occupancy and location tracking systems and concluded that the highest occupancy, spatial and temporal resolutions for floor occupants can be collected using wearable ranging devices. The most commonly-used device from this family of systems is the system based on the UWB signals. This system has the ability to track the location with a spatial resolution of less than a meter and *identity* of floor occupants with high temporal resolution of less than 1 s (Dardari et al., 2015). However, it requires installation of anchors (signal receivers) at various locations on the floor and the floor occupants need to wear tags (signal emitters).

Other techniques, such as those based on Bluetooth signals can be easily used to track the location of mobile phones of the occupants without the need to use wearable devices but their accuracy is considerably low, i.e. higher than 2-3m, (Teixeira et al., 2010). Vision-based tracking techniques, based on cameras, are gaining a growing interest in the past few years. Existing security cameras inside buildings can be utilised for tracking without the need to set-up extra devices. While the data collected using such systems are useful to trace the movements on floors, it is difficult to use them for modelling the occupancy and movements of

individual occupants, especially where multiple cameras are needed to monitor the movements (Teixeira et al., 2010).

2.6 Final remarks

This chapter reviews key past research relevant to vibration serviceability of floors subjected to footfall excitation. It also highlights key issues related to different types of floors where the rest of this thesis is directed.

It is shown that, for floors housing sensitive facilities, a probabilistic, rather than deterministic, model can be used for an improved design tool for vibration serviceability. For such floors, the single person walking scenario is relevant for the design for vibration serviceability. Furthermore, the cut-off frequency between low- and high-frequency floors varies significantly between different authors and its value may can be updated to avoid high-level build-up resonant response in such floors.

For other types of floors, such as office floors, it is shown that utilising reliable people's occupancy and movements models in the design can improve vibration level predictions. Such occupancy and movements models can provide realistic walking scenarios related to single and multiple floor occupants in the design for vibration serviceability. Furthermore, these models can be also utilised for conducting vibration serviceability assessment based on the exposure of the occupants to vibration levels rather than the maximum vibration level occurring at a single point on the floor which may not be occupied by occupants. To derive such models, experimental data regarding people locations on floors can be utilised in the model development. Although the usage of such models can be limited to floors with known layouts, they have several applications. For

example, they can be utilised to design floors for vibration serviceability before conducting commissioning, or refurbishment, works in a building, or as a vibration remedy by optimising floor layout to minimise vibration levels. It is apparent that the UWB tracking system has the capability to provide comprehensive data regarding people occupancy and movements and can be utilised to provide these measurements.

There are limited number of studies regarding the influence of walking occupants on the dynamic properties of floors. Lightweight floors, with comparable masses to those for the occupants, are prone to be influenced by dynamic interaction between walking occupants and the supporting floors. As the fundamental frequency of such floors are typically above 4-5 Hz, improved HSI models can be developed to take into account whole-body dynamics of walking individuals in frequency ranges relevant to dominant modes of vibration of floors.

Preface to Chapter 3

Chapter 3 presents an improved version of the model proposed by Arup related to the design of floors housing sensitive equipment. The improved model has a capability to estimate vibration levels related to any probability of non-exceedance. The model presented in this chapter is based on a single person walking scenario as it is the relevant design scenario for such floors.

To reduce the influence of resonance on the response of such floors, a comprehensive analysis was conducted to update the so-called 'cut-off frequency' where floors with a natural frequency above which can be designed to support sensitive equipment.

The ground reaction force data utilised in this chapter was provided by Vitomir Racic, but all of the analysis was performed by the author of this thesis. The materials presented in this chapter has been published under the following reference, but slight amendments were made to make the style of the chapter compatible with the rest of the thesis.

Mohammed, A. and Pavic, A. and Racic, V. (2018). Improved model for human induced vibrations of high-frequency floors. *Engineering Structures*, 168:950–966. ISSN 01410296. doi: $10.1016/j.engstruct.2018.04.093$.

Chapter 3

Improved model for human induced vibrations of floors housing sensitive equipment

Abstract

The key UK design guidelines published by the Concrete Society and Concrete Centre for single human footfall excitation of high-frequency floors were introduced more than 10 years ago. The corresponding footfall force model is derived using a set of single footfalls recorded on a force plate and it features a deterministic approach which contradicts the stochastic nature of human-induced loading, including intra- and inter- subject variability. More recent studies were also developed based on deterministic approaches. This chapter presents an improved version of this force model for high-frequency floors with statistically defined parameters derived using a comprehensive database of footfall force time histories, comprising multiple successive footfalls that are continuously measured

on an instrumented treadmill. The improved model enables probability-based prediction of vibration levels for any probability of non-exceedance, while the existing model allows for vibration prediction related to 75% probability of non-exceedance for design purposes. Moreover, the improved model shifts the suggested cut-off frequency between low- and high-frequency floors from 10 Hz to 14 Hz. This is to account for higher force harmonics that can still induce the resonant vibration response and to avoid possible significant amplification of the vibration response due to the near-resonance effect. Minor effects of near-resonance are taken into account by a damping factor. The performance of the existing and the improved models is compared against numerical simulations carried out using a finite element model of a structure and the treadmill forces. The results show that while the existing model tends to overestimate or underestimate the vibration levels depending on the pacing rate, the new model provides statistically reliable estimations of the vibration responses. Hence, it can be adopted in a new generation of the design guidelines featuring a probabilistic approach to vibration serviceability assessment of high-frequency floors.

3.1 Introduction

The advancements in construction materials and design software have boosted the current architectural trend of building lighter structures than ever with increasingly longer spans and reduced carbon footprint. While the Ultimate Limit State (ULS) requirements are related to the strength of the building and the safety of its occupants, Serviceability Limit State (SLS) criteria increasingly govern design. This is particularly the case with vibration serviceability of structures due to human activities, such as walking, running and jumping (Racic and Pavic,

2009; Middleton and Brownjohn, 2010).

Building floors have traditionally been designed mainly to accommodate people, who are by their nature very sensitive vibration receivers (BS 6472-1:2008, 2008). Nowadays there is a growing need for floors accommodating vibration sensitive equipment, such as microscopes and lasers in hospitals and hi-tech laboratories. Their optimal functioning commonly permits extremely low vibration levels (often micro-levels) of the supporting structure which are far below human perception. Vibration criteria (VC) for sensitive equipment is normally provided by the manufacturer, leaving the provision of the adequate floor to clients and structural designers (Middleton and Brownjohn, 2010).

Early studies made vibration assessment based on static deflection of a floor and suggested increasing the stiffness and therefore the fundamental frequency to reduce the vibration response. The same concept features the work by Ungar and White (1979) who were the first to use an "idealised footfall force" (Galbraith, 1970) in a design method to calculate the maximum velocity response. This method has been further developed by Amick et al. (1991) and adopted in a number of design guidelines (Murray et al., 1997; Fanella and Mota).

A more sophisticated approach was based on the nature of the vibration response (Wyatt, 1989; Wyatt and Dier, 1989). If the response is dominated by a resonant build-up they are known as *low-frequency floors*, while those that show a sequence of transient responses due to each successive footfall are called *high-frequency floors*. The division between low- and high-frequency floors depends on whether the fundamental frequency of the floor is relatively low or high, respectively. The threshold frequency, known as *cut-off frequency*, varies significantly for different authors and design guidelines, as shown in Table 3.1.

Table 3.1: Cut-off frequency between low- and high-frequency floors adopted by different authors and design guidelines.

Author	Cut-off frequency
Ohlsson (1988)	8 Hz
Wyatt (1989)	7 Hz
Allen and Murray (1993)	9 Hz
The Concrete Society (Pavic and Willford, 2005)	10 Hz
The Concrete Centre (Willford and Young, 2006)	10 Hz
The Steel Construction Institute P354 (Smith et al., 2009)	8-10 Hz
American Institute of Steel Construction (Murray et al., 2016)	9 Hz
Human induced vibration of steel (HIVOSS) (Feldmann and Heinemeyer, 2007; Feldmann et al., 2009)	10 Hz
ISO 10137:2007 (2007)	8-10 Hz
BS 6472-1:2008 (2008)	7-10 Hz
AS 3623—1993 (1993)	8 Hz

Floors supporting sensitive equipment are required to have low-level transient vibration responses due to human footfall excitation (Hanagan and Murray, 1997; Liu and Davis, 2014), thus they are traditionally designed as high-frequency floors. A number of studies (Ellis et al., 2000; Brownjohn and Middleton, 2008) reported that the cut-off frequencies given in Table 3.1 are too conservative, which has a major effect on the design and cost of ultra-sensitive facilities. They showed that the resonant build-up response can occur even for floors with a fundamental frequency of above 15 Hz (Brownjohn and Middleton, 2008). This is because there are higher dominant harmonics of footfall loading at frequencies above 10 Hz, which contain a significant amount of energy. For example, according to the design guidelines, a floor with a fundamental frequency of 11.5 Hz is a high-frequency floor. However, a person walking at a pacing rate 2.3 Hz, whose corresponding footfall force has Fourier amplitudes shown in Figure 3.1, still can induce the resonant vibrations by the harmonic corresponding to the fifth integer

multiple of pacing frequency. This error in the floor type yields an underestimated vibration response, hence a floor may not be fit for purpose. The uncertainty linked to the cut-off frequency could be explained by the lack of knowledge and/or reliable experimental data pertinent to human footfall excitation when these cut-off frequency values were suggested. Large database of footfall forces measured using state-of-the-art equipment could be analysed to update the cut-off in a way that avoids resonant vibration of floors in sensitive facilities.

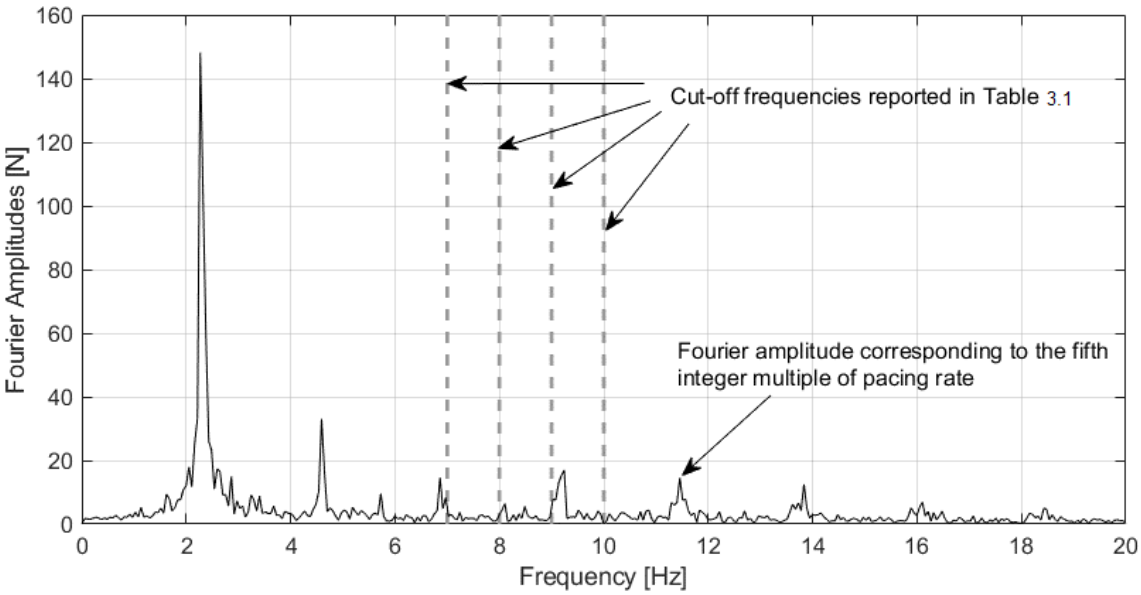

Figure 3.1: Fourier amplitudes of a footfall force signal measured using an instrumented treadmill corresponding to a pacing rate of 2.3 Hz.

Another major drawback of the available guidelines related to high-frequency floors is their adoption of deterministic mathematical description of human-induced loading (Middleton and Brownjohn, 2010; Liu and Davis, 2014). The model presented by Arup (Willford et al., 2005) allows for 75% of non-exceedance in vibration response predictions, while a probabilistic approach is arguably more suitable due to the inherent stochastic nature of human footfall forces (Racic and Brownjohn, 2011; Brownjohn et al., 2004; Živanović and Pavic, 2009; Brownjohn et al., 2015).

Živanović and Pavic (2009) merged together the design methods related to low- and high-frequency floors in a probabilistic model that takes into account the inter-subject variability, which refers to the variability of the footfall loading induced by different people. The model can be used to estimate the probability distribution of vibration responses generated by different people. However, Middleton (2009) showed that the variations between successive steps, i.e. intra-subject variations, during walking have more influence on the vibration responses than the inter-subject variations. Neglecting intra-subject variations can also result in an overestimated vibration response of high-frequency floors (Middleton, 2009).

Other studies attempted to produce probabilistic and universal footfall loading models to be used for both low- and high-frequency floors. Racic and Brownjohn (2011) proposed a stochastic footfall loading model using Gaussian functions. The model utilises random parameters derived from experimentally measured footfall loading to generate synthetic footfall loading. As access to such experimental database may might not be available to public access, the usage of this model is limited. Muhammad and Reynolds (2020) proposed a probabilistic model for footfall loading related to both left and right legs and their combined loading. The model appears to produce comparable synthetic footfall loading to those obtained from the measurements. The study shows that the energy at the first four dominant harmonics for the synthetic footfall loading is comparable to that obtained from the measurements. However, it is not obvious how the energy at higher frequencies, i.e. higher than 10 Hz, are compared between the synthetic and the measured footfall loading. Hence, it is apparent that there is a lack of probabilistic and practical footfall force models, pertinent to floors in sensitive facilities, that takes into account both of inter- and intra-subject variations.

While frequency domain approaches (Brownjohn et al., 2004; Ohlsson, 1982; Eriksson, 1994) are widely used in the literature, time domain models can describe the peak responses corresponding to footfall strikes. Hence, this study proposes an improved and probability-based version of the widely used Arup's force model for high-frequency floors (Willford et al., 2005). This model was chosen as it provides closest and least conservative predictions of floor vibrations compared with experimental results (Liu and Davis, 2014; Brownjohn and Middleton, 2008; Willford et al., 2007; Pavic et al., 2003). The improved model was derived using a large number of continuously measured footfall forces generated by many people walking on an instrumented treadmill (Racic and Brownjohn, 2012, 2011). The parameter estimation of the proposed model and the model implementation take statistical approaches. To reduce high-amplitude resonant responses in such floors, a cut-off frequency was determined after conducting extensive numerical analysis based on the above mentioned experimental data. Moreover, the effect of structural damping is introduced in this model to take into account any "near-resonance" effects. The performance of the new model has been verified via numerical simulations utilising the treadmill forces and a finite element model of a high-frequency floor.

Section 3.2 of this chapter describes the nature of the human-induced vibration responses and the procedure followed to derive a more reliable cut-off frequency between low- and high-frequency floors. The new model and its implementation procedure are elaborated in Section 3.3, while its verification is demonstrated in Section 3.4. Finally, a discussion of the results and the main conclusions are presented in Section 3.5.

3.2 Resonant and transient vibration responses due to human footfall excitation

This section demonstrates the nature of the resonant and transient vibration responses due to human footfall excitation based on numerical simulations using measured footfall forces (Section 3.2.1) applied to different Single Degree of Freedom (SDOF) oscillators (Section 3.2.2). Moreover, it aims to derive a reliable value of the cut-off frequency (Section 3.2.3) relevant to the model development presented in Section 3.3.

3.2.1 Footfall forces

The authors have at their disposal a comprehensive database of 715 continuously measured vertical force time histories, generated by more than 70 test subjects walking individually on an instrumented treadmill using their own shoes (Racic and Brownjohn, 2011, 2012). Although the type of the shoes can have an influence on the measured footfall forces (Yi, 2011), this was not the choice of the author as the measurements were performed previously. Each test subject followed the same test protocol designed to record a force signal at a constant speed of rotation of the treadmill belts per each test. The speed was varied randomly from slow to fast across successive tests, so the database comprises forces for a wide range of pacing rates. Each force time history contains at least 60 successive footfalls, rather than a single footfall only used in development of Arup's model. This makes it possible to study the intra-subject variability of the footfall loads, i.e. the inability of a person to generate two identical footfalls during a walking test. The large number of test subjects processed in the

experiment enables studies of inter-subject variability, i.e. differences between force records generated by different people under nominally identical conditions. These forces can be considered statistically more reliable data than that used in the development of the original Arup model (Kerr, 1998).

The range of pacing rates corresponding to these footfall forces is between 1.4-2.5 Hz. The force signals were cropped for the time duration of 50 footfalls from the middle of the force signal. Several first and last footfalls were discarded to eliminate potential negative effects related to the start and the end of the walking test, yielding footfalls that might not reliably represent the real walking of a person. This length of the force signal was used everywhere else in this chapter unless otherwise stated. Moreover, the effect of body weight was excluded by normalising the forces (Racic and Brownjohn, 2011, 2012) to 750 N before they were used in the analysis. This is because the weight of the limited number of test subject participated in the measurements may not represent the weight of the general population. Hence, this study assumes no correlation between human body mass and the normalised walking force.

3.2.2 Resonant and transient vibration responses

Depending on the natural frequency (f_n) of the first vibration mode, the vibration response due to human footfall excitation can take three distinct shapes, as shown in Figure 3.2:

- When the fundamental frequency is relatively small, i.e. $f_n <$ 8-10 Hz, and close to one of the integer multiples of the pacing rate (f_p), a resonant build-up response occurs (Figure 3.2a).

- If the fundamental frequency is much higher than the pacing rate, i.e. $f_n >>$

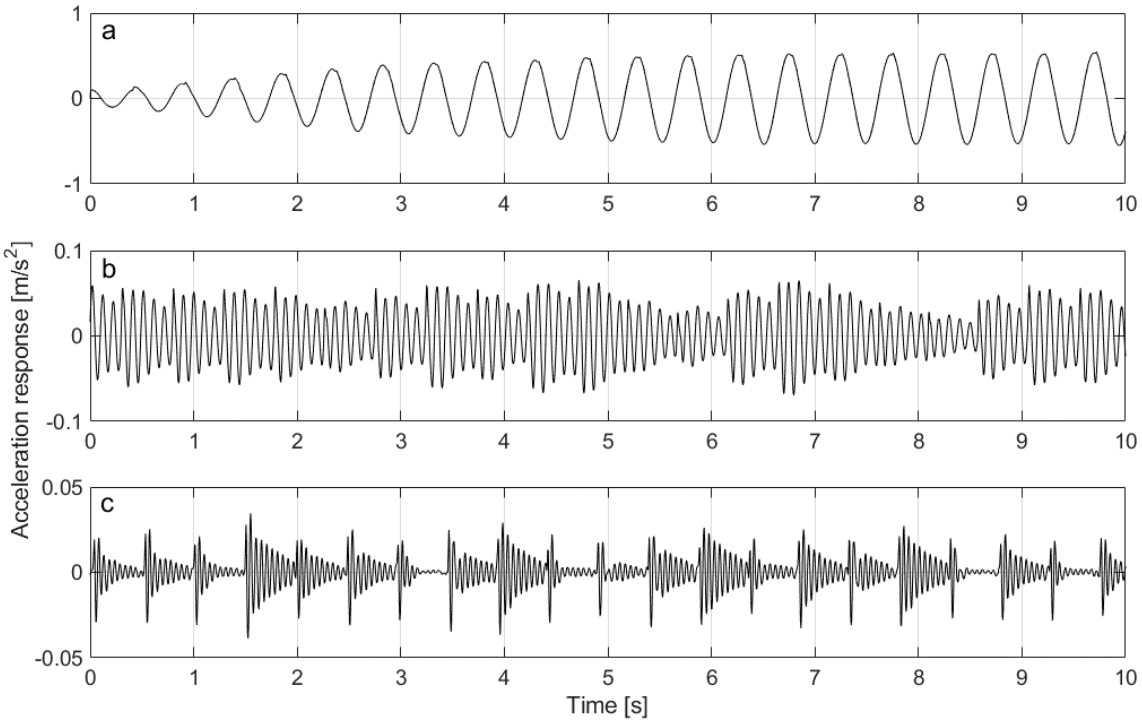

Figure 3.2: Simulated vibration responses due to a recorded footfall force with f_p=2.0 Hz and natural frequency of the oscillator (a) f_n=2.0 Hz, (b) f_n=10 Hz and (c) f_n=20 Hz.

f_p, a transient response will dominate the vibration response (Figure 3.2c).

- When the fundamental frequency lies between the two above mentioned ranges, the sharp transient decays are reduced considerably, and the overall vibration levels are increased (Figure 3.2b).

This chapter focuses on modelling the transient vibration response (Figure 3.2c), which is the typical case for high-frequency floors.

Besides the natural frequency, the shape of the vibration response, as described above, is affected by the harmonics of the footfall force that excite the dominant vibration modes of the structure (Murray et al., 2016; Pavic and Willford, 2005). The common knowledge is that a build-up of the resonant response is unlikely to occur if the fundamental frequency is higher than three or four integer multiples of the pacing rate as the harmonics at this range of frequencies are relatively small (Murray et al., 2016; Pavic and Willford, 2005). The normalised Fourier

amplitudes of all the forces in the database (Racic and Brownjohn, 2011, 2012) are overlapped in Figure 3.3 with a logarithmic scale in its vertical axis. To reduce signal leakage while performing the Fast Fourier Transformation, the length of the force time history was reduced to slightly less than 20.48 s, i.e. for a duration equal to an integer multiple of T, where $T = 1/f_p$. There is no apparent sign that beyond, say, 10 Hz (see Table 3.1) the Fourier amplitudes of the harmonics do not exist and cannot produce a resonant build-up response. They are smaller in amplitude, but they definitely exist at integer multiples of the pacing rate. The relatively high amplitudes of the harmonics at frequencies higher than 10 Hz are also obvious for the footfall forces presented by other studies in the literature (Brownjohn et al., 2004; Živanović and Pavic, 2009; Caprani, 2014).

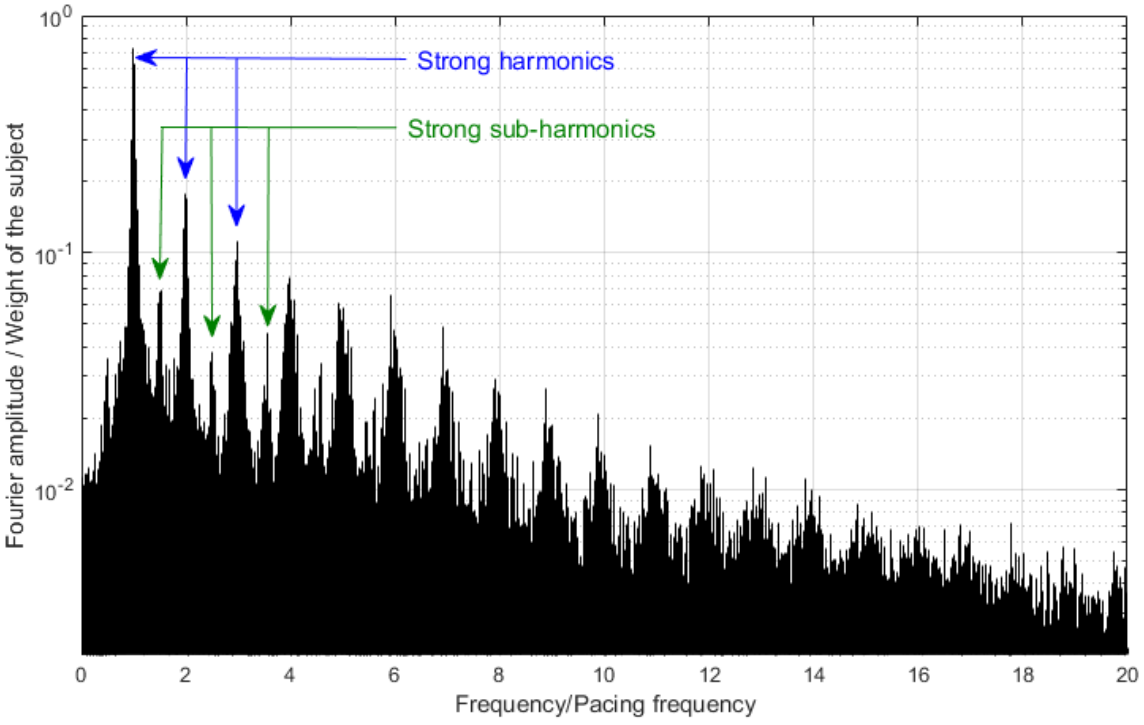

Figure 3.3: Normalised Discrete Fourier amplitudes for all available footfall forces (Racic and Brownjohn, 2011, 2012) with pacing rates between 1.4-2.5 Hz (Brownjohn et al., 2004).

To assess the effect of the harmonics of the footfall excitation on the vibration response, each footfall force from the database was applied to a series of SDOF

oscillators, which had natural frequencies between 1-40 Hz with an increment of 0.1 Hz. Therefore, the total number of the oscillators is 391 and the total number of simulated vibration responses is 279,565. The modal mass was assumed 1 kg and the damping ratio was assumed 3% in all simulations. The duration of each simulation is equal to the length of the corresponding footfall force time history, while the integration time step is 0.005 s. For the response of each simulation, the running 1-second root mean square (1-s RMS) was calculated as described in Equation 3.1.

$$v_{rms} = \sqrt{\frac{1}{T}\int_0^T v^2(t)dt} \quad , \tag{3.1}$$

where v_{rms} is the velocity 1-s RMS [m/s] and T is the duration of the averaging [1 s]. The reason behind utilising velocity here, rather than acceleration response, is that many of the process in sensitive facilities are photographic in nature where there are limits on blurring which can be defined as the distance travelled during the exposure, i.e. velocity (Middleton, 2009).

The maximum transient vibration value (MTVV), which is equal to the maximum 1-s RMS, corresponding to each simulation was used for comparison, as shown in Figure 3.4. The grey colour represents the MTVV velocity corresponding to each footfall force and varying SDOF natural frequencies, while the black colour represents the average MTVV velocity at each SDOF natural frequency. The vibration descriptor MTVV is utilised in this study to describe the maximum velocity response related to *multiple footfalls*, i.e. one force time history, while peak velocities refer to maximum velocity response related to *one footfall*.

The MTVV velocity is relatively high at integer multiples of pacing rates (Figure

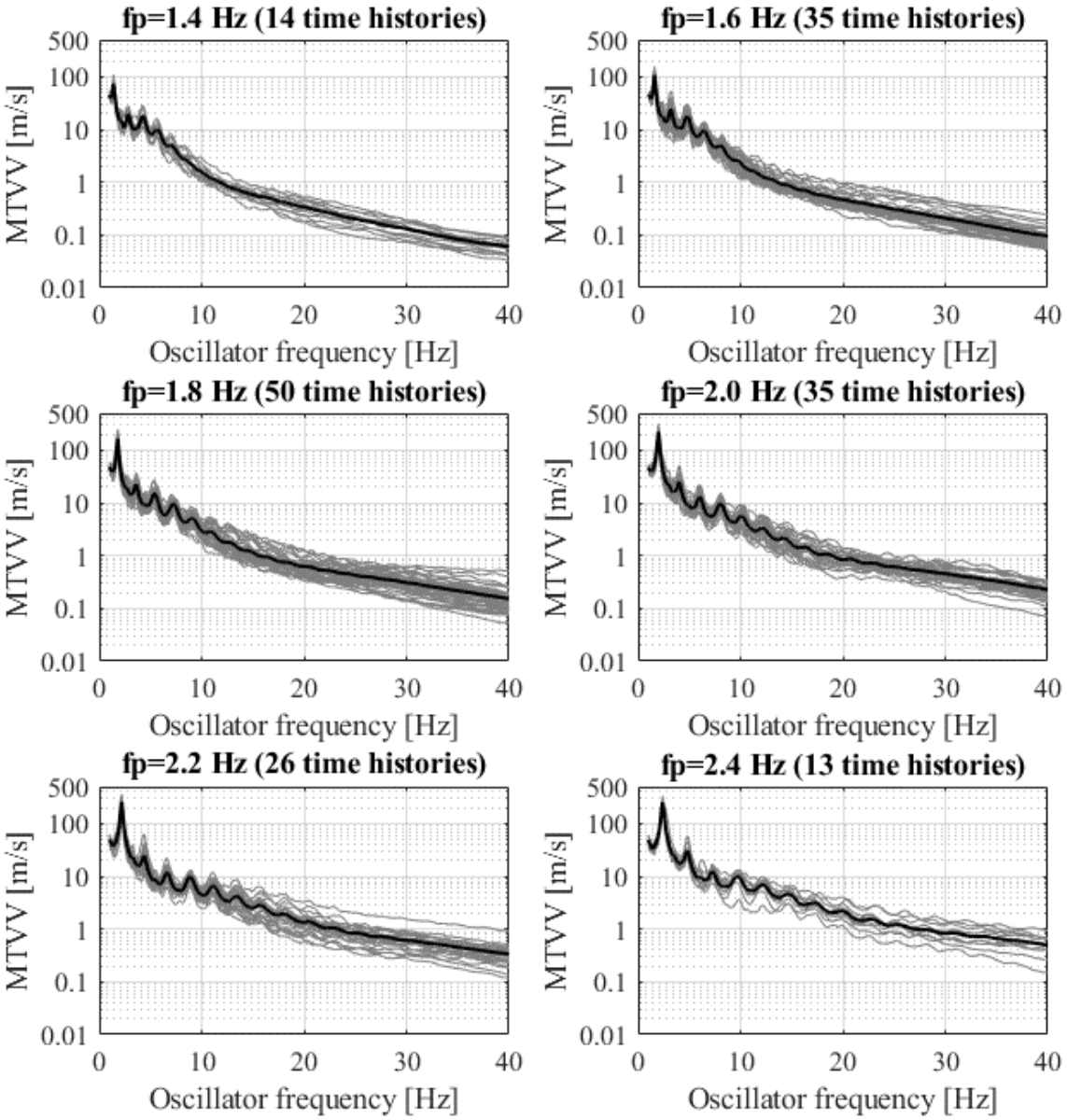

Figure 3.4: MTVV velocity (grey) for pacing rates (f_p) from 1.4 Hz (up left) to 2.4 Hz (bottom right). Black represents the average MTVV velocity at each natural frequency.

3.4). This is the case even for the oscillators, with a natural frequency of up to 30 Hz. Therefore, there is no evidence that the harmonics of footfall forces, which correspond to frequencies above the reported cut-off frequency in the literature (Table 3.1), cannot induce a resonant build-up response. This implies that a more detailed study should be carried out to derive the cut-off frequency, as elaborated in the next section.

3.2.3 Determining cut-off frequency between low- and high-frequency floors

As already observed above, a typical transient response due to walking comprises a series of velocity peaks corresponding to heel strikes, followed by a decaying vibration response to around zero before the beginning of the next footfall, as shown in Figure 3.2c (Brownjohn and Middleton, 2008). This means that the response due to previous footfalls has a negligible contribution to the response due to the present footfall. On the other hand, for non-transient vibration responses, such as those shown in Figure 3.2a and Figure 3.2b, the response is affected by a number of previous footfalls depending on the structural damping.

Theoretically speaking, a transient response time history, related to one mode of vibration, can be reconstructed from the peak responses, corresponding to successive footfalls, followed by an exponentially decaying response in between them. In this case, the reconstructed vibration response level is similar to that of the original time history response (Figure 3.5). Therefore, the proposed methodology to identify the cut-off frequency is as follows:

- Simulate vibration responses by applying measured footfall forces (Racic and Brownjohn, 2011, 2012) on SDOF oscillators with different natural frequencies.
- For each response time history, extract the peak velocity responses corresponding to each footfall strike with their exact times.
- Use the peak velocities to reconstruct the time history response which comprises only a decaying response after each peak velocity, as shown

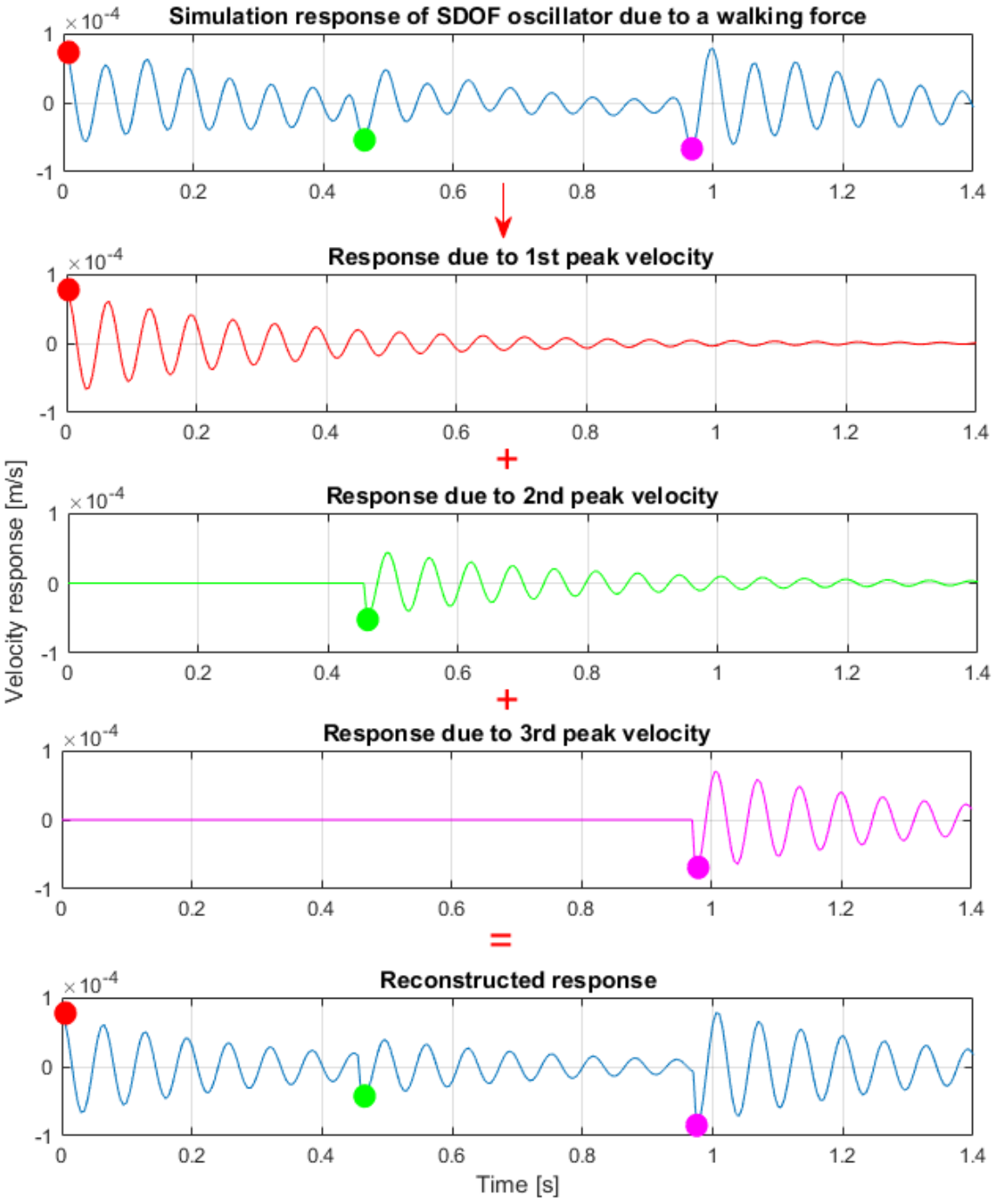

Figure 3.5: Typical reconstructed vibration response from simulation of a footfall force with pacing rate (f_p) of 2.0 Hz applied on SDOF oscillator with a natural frequency (f_n) of 16 Hz. Red, green and pink dots refer to the 1st, 2nd and 3rd peak velocities, respectively.

in Figure 3.5.

- Establish the difference between the original and the reconstructed responses by calculating the ratio of their MTVVs (, i.e. MTVV velocity of the reconstructed response over that for the original response.

- Repeat this process for the different natural frequencies of the SDOF oscillator and the measured footfall forces (Racic and Brownjohn, 2011, 2012).
- Identify the frequency corresponding to a value of the MTVV ratio which is reasonably close to 1.0, as explained below.

The closer the MTVV ratio to 1.0, the more similar are the reconstructed response and its corresponding simulated transient response. Figure 3.6 compares two cases when the MTVV ratio is close or far from 1.0. The process of generating reconstructed vibration responses was repeated for all available footfall forces (Racic and Brownjohn, 2011, 2012) when the natural frequency of the SDOF oscillator is an integer multiple of the pacing rate, up to 20 Hz. This is to consider the effect of the harmonics at these frequencies. The damping ratio used in the simulations was 3% while the modal mass was assumed 1 kg. The MTVV ratios corresponding to this analysis are presented as box plots in Figure 3.7. The upper and lower ends of the rectangles represent the values corresponding to a 75% and 25% chance of non-exceedance, respectively. The whiskers, i.e. ends of the extended lines from the boxes, represent the maximum and minimum values.

At relatively low pacing rates, the MTVV ratio approaches 1.0 at a lower SDOF natural frequency than that for higher pacing rates (Figure 3.7). This indicates the dependency of the cut-off frequency on the pacing rates. One way to specify a cut-off frequency is to suggest a frequency above which footfall induced vibration of floors is dominated by transient response. For natural frequencies at or above 14 Hz, the median of the MTVV ratios for all pacing rates (horizontal lines in the middle of the rectangles in Figure 3.7) were within 10% of 1.0, i.e. 0.90-1.10,

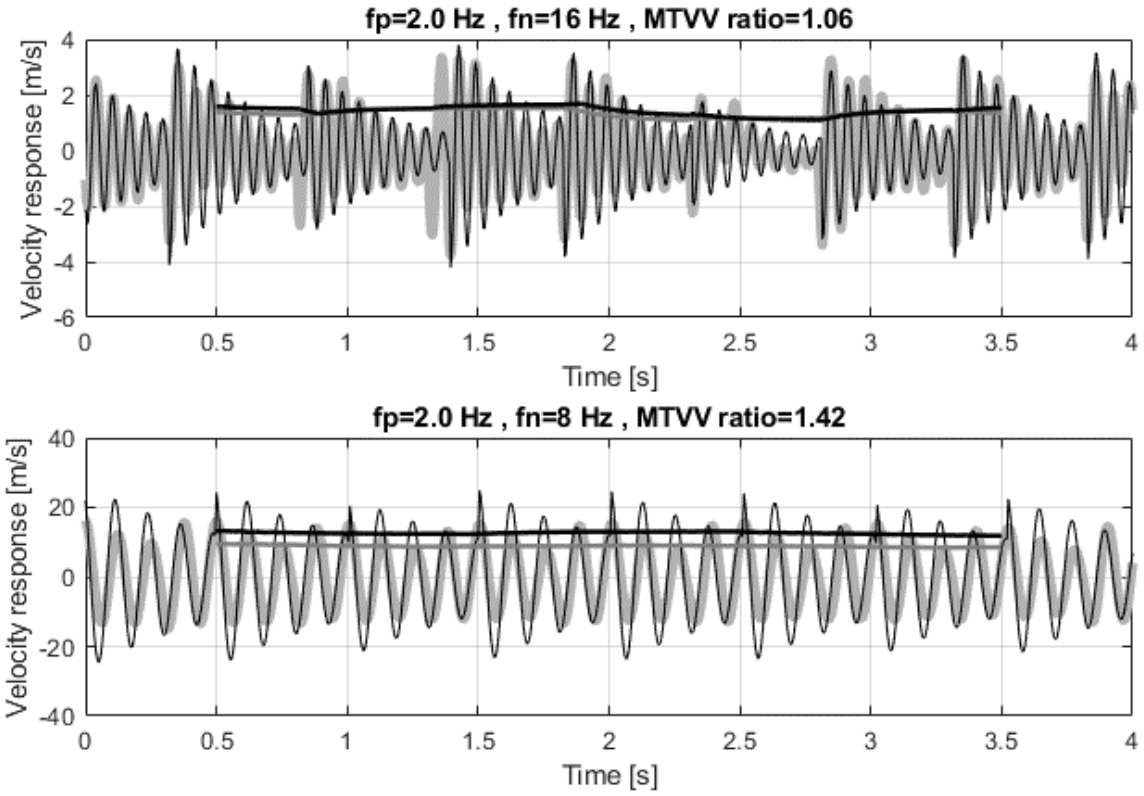

Figure 3.6: Comparison between simulated (grey) and reconstructed (black) vibration responses with their corresponding 1-s running RMS for natural frequency (f_n) of 16 Hz (top) and 8 Hz (bottom).

which is reasonably close to 1.0. This implies that the shape of vibration responses corresponding to SDOF oscillators with natural frequencies above 14 Hz resemble typical transient responses regardless of the pacing rate. The harmonics of footfall forces (Racic and Brownjohn, 2011, 2012) corresponding to frequencies above 14 Hz are more likely to increase the amplitude of the vibration responses rather than to induce a clear resonant build-up response. Therefore, this study suggests using this frequency as the cut-off frequency above which the footfall induced vibration of floors is dominated by transient response.

While this may not be the only way to determine the cut-off frequency, this study suggests using 14 Hz as the cut-off frequency as it is shown that footfall induced vibration of floors which have fundamental frequency above 14 Hz is dominated by transient responses.

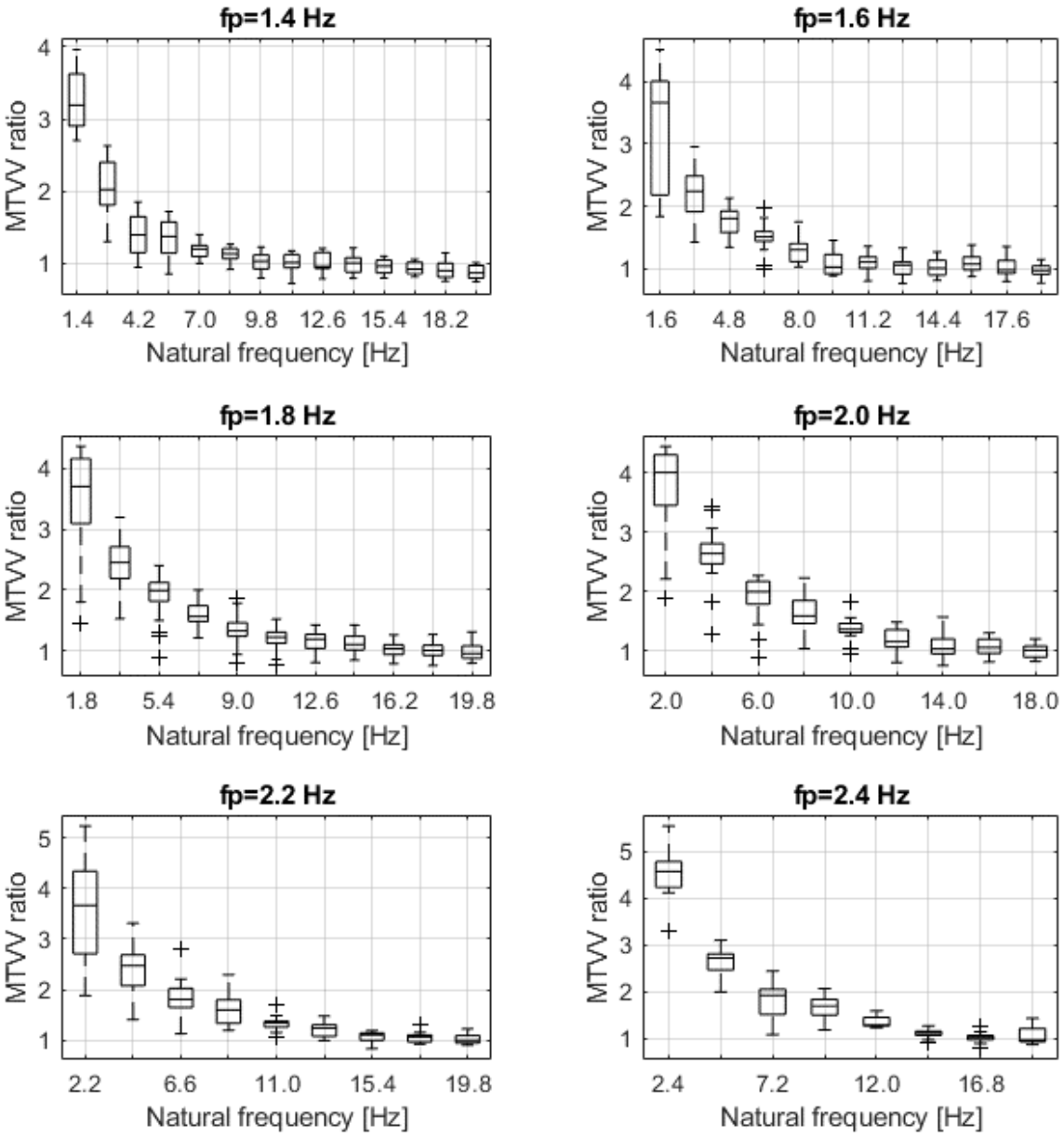

Figure 3.7: MTVV ratio between simulated and reconstructed vibration responses at different pacing rates (f_p).

3.3 Modelling human-induced vibrations of high-frequency structures

This section starts with necessary details of Arup's force model (Section 3.3.1), followed by its expansion into a more sophisticated probability-based successor proposed in this study (Section 3.3.2 and Section 3.3.3) and its implementation in vibration serviceability assessment of high-frequency floors (Section 3.3.4).

3.3.1 Arup's model

The model was derived using a database of over 800 single footfalls recorded for 40 individuals stepping on a force plate while walking at a range of pacing rates controlled by a metronome (Kerr, 1998). The measured footfalls were shifted repeatedly along the time axes to synthesise the corresponding artificial and perfectly periodic force time history (Figure 3.8). Each such force was applied to a series of SDOF oscillators with natural frequencies of 10-40 Hz and only the peak velocity for each simulation was extracted. The modal mass was assumed 1 kg for all simulations, so that the peak velocity response was numerically equivalent to the impulse represented by the shaded area in Figure 3.8 and expressed in [N s]. Such an impulse is termed *effective impulse*.

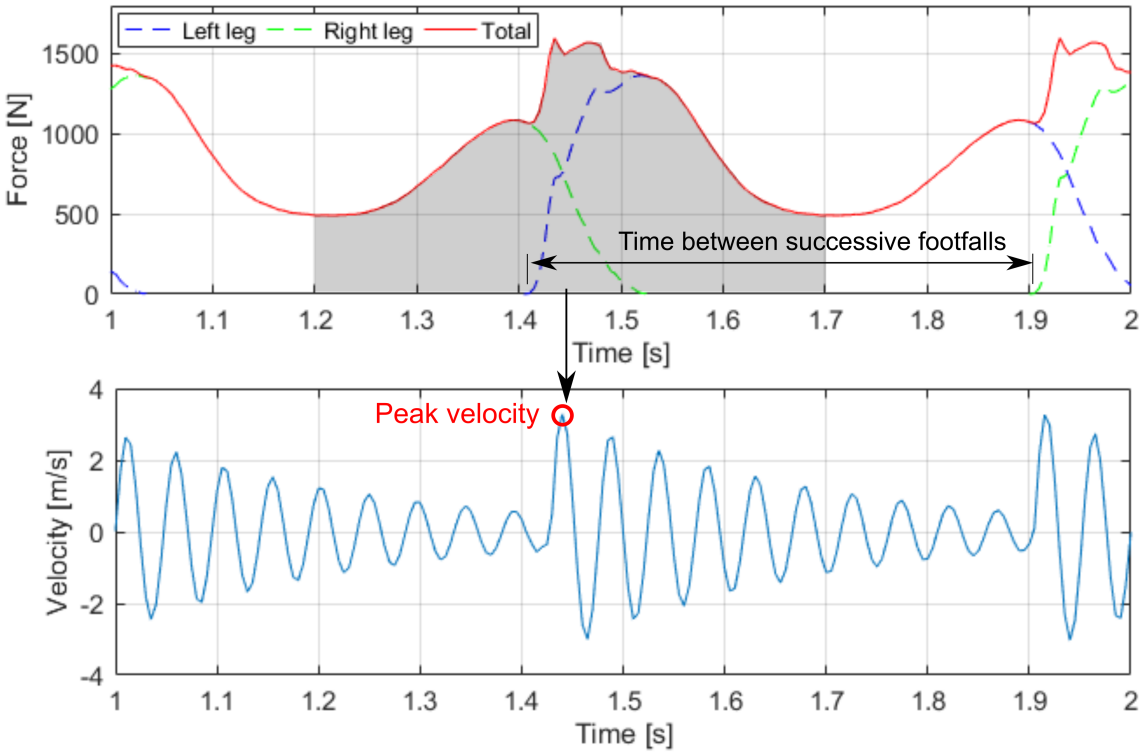

Figure 3.8: Arup's approximation of the typical footfall force (top) and its corresponding velocity vibration response (bottom).

For varying pacing rates, the mean of the extracted effective impulses are shown in Figure 3.9 as a function of the 'floor frequency (Hz)', which is the natural

frequency of the 1 kg SDOF system. The corresponding curve fit is:

$$I_{eff} = A\frac{f_p^{1.43}}{f_n^{1.3}} \quad , \tag{3.2}$$

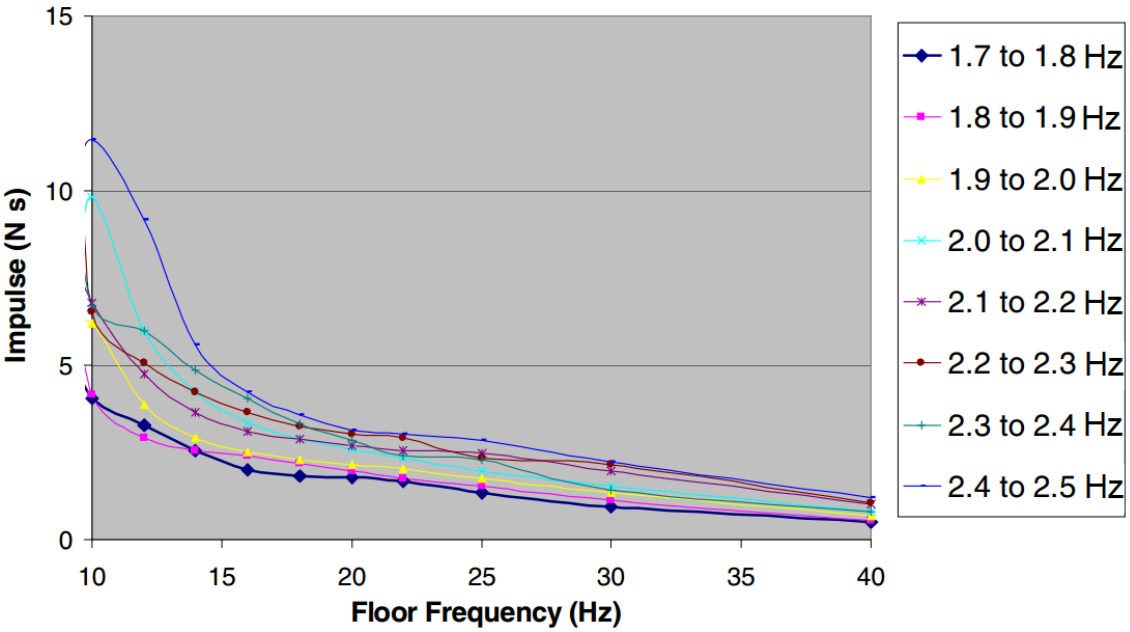

Figure 3.9: Effective impulse derived from Kerr (1998) footfall traces (after Willford et al. (2005))

where, I_{eff} is the effective impulse [N s], f_p is the pacing rate [Hz], f_n is the SDOF natural frequency [Hz] and A is a coefficient which has a mean value of 42 and a standard deviation of 0.4 while its corresponding design value for 75% chance of non-exceedance is 54.

This effective impulse is used in Equation 3.3 to calculate the contribution of the time history response of each vibration mode in the total response. This response corresponds to one footfall strike.

$$v_n(t) = u_i u_j \frac{I_{eff}}{M_n} e^{-\zeta_n \omega_n t} \sin\left(\omega_{nd} t\right) \quad , \tag{3.3}$$

Here, $v_n(t)$ [m/s] is the contribution to the velocity response from mode n at each time step t, u_i and u_j are the mode shape amplitude at the node of application

of the force and the node of interest, respectively, M_n [kg] is the modal mass of the mode n, ζ_n is the modal damping ratio, ω_n and ω_{nd} [rad/s] are the angular frequency and damped angular frequency of mode n, respectively.

The contribution of each mode in the total response, calculated using Equation 3.3, should be determined individually for N vibration modes with a natural frequency up to twice the fundamental frequency. The total velocity response $v_t(t)$ is calculated using Equation 3.4 based on the assumption that the structure remains linear during vibration, and therefore, the principle of superposition applies.

$$v_t(t) = \sum_{n=1}^{N} v_n(t) \quad , \tag{3.4}$$

The criterion of the vibration serviceability assessment for high-frequency floors is based on the maximum 1-s RMS of the total response calculated using Equation 3.1.

3.3.2 Improved modelling procedure

Based on the analysis presented in Section 3.2, the key differences between the steps followed to derive Arup's model and its advanced version explained in the following sections are:

- The range of natural frequencies of the SDOF oscillators used to derive the present model is 14-40 Hz with an increment of 0.1 Hz, compared with 10-40 Hz used to derive Arup's model. This is to account for the proposed cut-off frequency of 14 Hz, as described in Section 3.2.3.

- In the new model, SDOF simulations, which utilised continuously measured

treadmill forces (Racic and Brownjohn, 2011, 2012), were carried out to extract the peak velocities corresponding to 50 successive footfalls. These peak velocities are treated as the effective impulse (I_{eff}) explained in Equation 3.3 but they belong to the improved model presented in this chapter.

- Contrary to Arup's model, the damping effect is considered in the new model. This is to take into account the slight amplification of the vibration response of high-frequency floors induced by the near-resonance effects corresponding to the higher harmonics of footfall loading, as explained in Section 3.2.

Apart from the above mentioned differences, the new model was derived using the same procedure as that used for Arup's model. The damping ratio was assumed 3% in the SDOF simulations, while the effect of other damping ratios is elaborated in Section 3.3.3.3. The Newmark integration method (Paz and Leigh, 2004), with a step time of 0.005 s, was used to calculate vibration responses where no algorithmic damping was introduced. The peak velocities, i.e. the effective impulses, were calculated from SDOF oscillators with natural frequencies in the range 14-40 Hz and 0.1 Hz increments.

3.3.3 Formulation of the effective impulse

The peak velocities corresponding to a single footfall and multiple SDOF oscillators can be presented as shown in Figure 3.10, which corresponds to a pacing rate of 2.25 Hz. For example, for this pacing rate there are 28 continuously measured footfall force time histories in the database (Racic and Brownjohn, 2011, 2012), each having 50 footfalls. This means there are 1,400 set of data,

similar to that shown in Figure 3.10, created and analysed for this pacing rate. The differences between them can be explained by the inter- and intra-subject variabilities of human footfall forces (Section 3.2.1). Previous studies in the literature have focused on modelling the dynamic load factor of footfall force for the first few harmonics (Brownjohn et al., 2004; Živanović and Pavic, 2009; Caprani, 2014). This section describes how to statistically model the peak velocities shown in Figure 3.10 as a function of SDOF natural frequency, pacing rate and damping ratio. This is similar to the work presented by previous studies which aimed to derive spectral models of footfall loading (Brownjohn et al., 2004; Živanović and Pavic, 2009; Caprani, 2014).

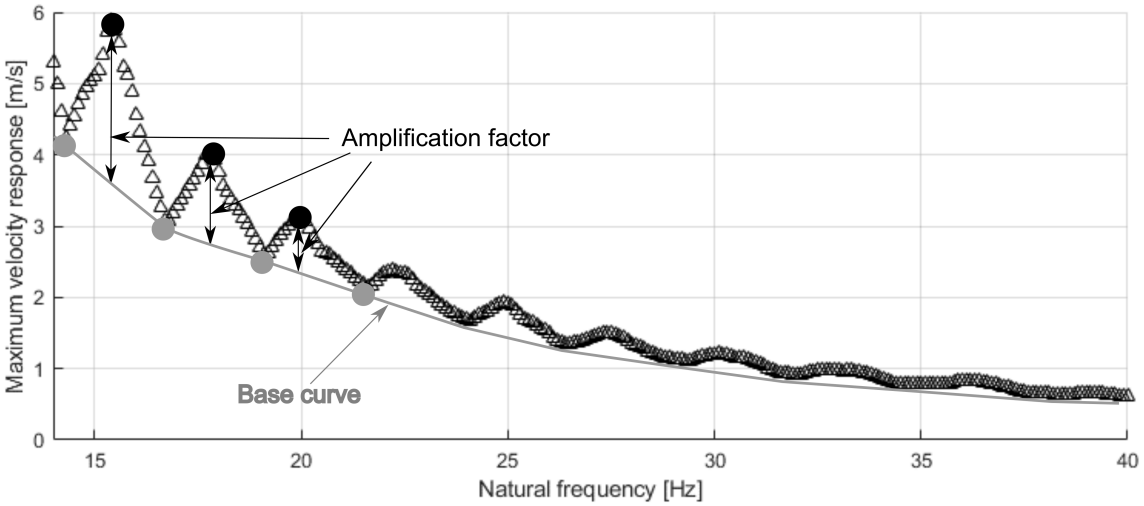

Figure 3.10: Peak velocities (black triangles) corresponding to one footfall, within a continuous footfall force, with a pacing rate of 2.25 Hz and multiple natural frequencies.

In Figure 3.10 peaks can be noticed around integer multiples of the pacing rate due to resonance or near-resonance effects. This can be explained by the effect of harmonics of the footfall excitation at integer multiples of pacing rates as explained in Section 3.2.2.

To simplify the modelling of the peak velocities shown in Figure 3.10, they were split into two components: a 'base curve' and an 'amplification factor', i.e.

grey curve and black dots, respectively, in Figure 3.10. The base curve was assumed continuous across all SDOF frequencies, while the amplification factor was assumed to be present at locations of each integer multiple of the pacing rate (black dots in Figure 3.10). The grey dots represent the locations where the amplification factor has no effect and its location is assumed to be in the middle of each two successive integer multiples of pacing rate, i.e. subsequent pairs of the black dots. Between black and grey dots, the amplification factor can be assumed to change linearly and its value can be interpolated between them.

Hence, the peak velocity at each integer multiple of the footfall frequency is theoretically equal to the base curve value at that natural frequency, $B\left(f_n, f_p\right)$, in m/s, multiplied by the corresponding contribution of the amplification factor at the same natural frequency, $A_f\left(f_n, f_p\right)$, a dimensionless parameter, as shown in Figure 3.10 and mathematically described in Equation 3.5.

$$I_{eff} = B\left(f_n, f_p\right) A_f\left(f_n, f_p\right) P_\zeta\left(f_n, f_p, \zeta\right) \quad , \tag{3.5}$$

where, P_ζ (f_n,f_p, P_ζ) is the damping factor (dimensionless parameter), which is described in Section 3.3.3.3.

The remaining part of this section describes the fitting process of $B(f_n,f_p)$, A_f (f_n,f_p) and P_ζ (f_n,f_p, P_ζ).

3.3.3.1 Base curve

$B\left(f_n, f_p\right)$ has different sets of values for different combinations of f_p and f_n. However, they can be reasonably fitted by gamma distribution for the data in most f_p and f_n combinations. Figure 3.11 shows an example of $B\left(f_n, f_p\right)$ values and the corresponding theoretical gamma distribution.

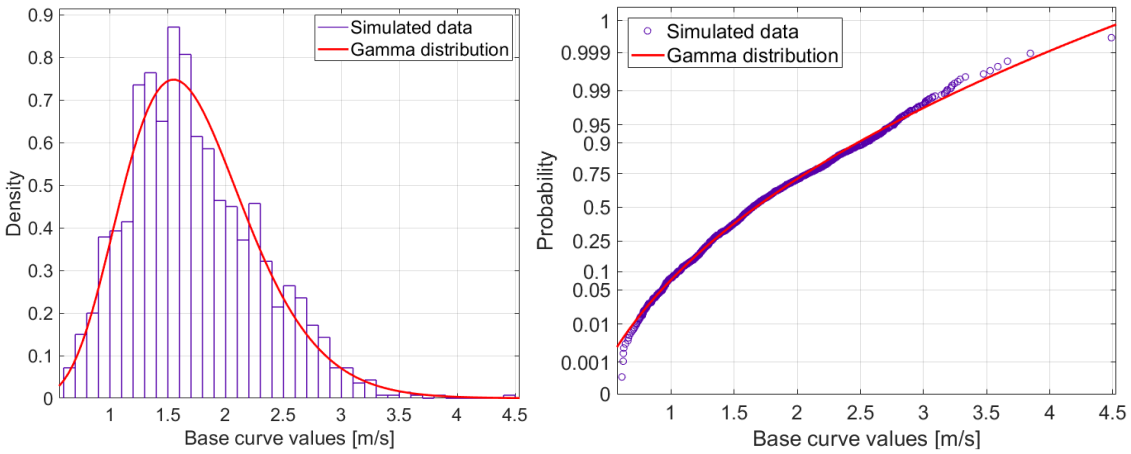

(a) (b)

Figure 3.11: Probability density function (left) and cumulative probability density function (right) derived using best fit of gamma distribution for a sample of base curve values corresponding to a pacing rate 2.25 Hz and SDOF natural frequency 24.8 Hz.

Gamma distribution can be defined as (Scheaffer et al., 2010):

$$f\left(B\left(f_n, f_p\right)\right) = \frac{B\left(f_n, f_p\right)^{k-1} e^{-\frac{B\left(f_n f_p\right)}{\theta}}}{\theta^k r(k)} \quad , \tag{3.6}$$

where $f\left(B\left(f_n, f_p\right)\right)$ is the probability density function, k and θ, dimensionless parameters, are the shape and scale parameters and $\mathrm{r}(k)$ is the gamma function evaluated at k.

The fitting process is repeated for each pair of f_p and f_n. Hence, there are different values for k and θ, for each pair of f_p and f_n. A surface fitting was used to fit k and θ. The form of the equation related to the surface fitting was chosen based on the Bayesian Information Criterion (BIC) (Schwarz, 1978), a useful method for model selection among a finite number of models. The values of the parameters were calculated using the Nonlinear Least Squares method (Teunissen, 1990). The fitting is shown in Figure 3.12 and described by Equations 3.7 and 3.8.

$$k = 4.5 - 0.12 f_n + 3 f_p \quad , \tag{3.7}$$

$$\theta = 0.08 + 2 \frac{f_p^{3.3}}{f_n^{1.58}} \quad , \tag{3.8}$$

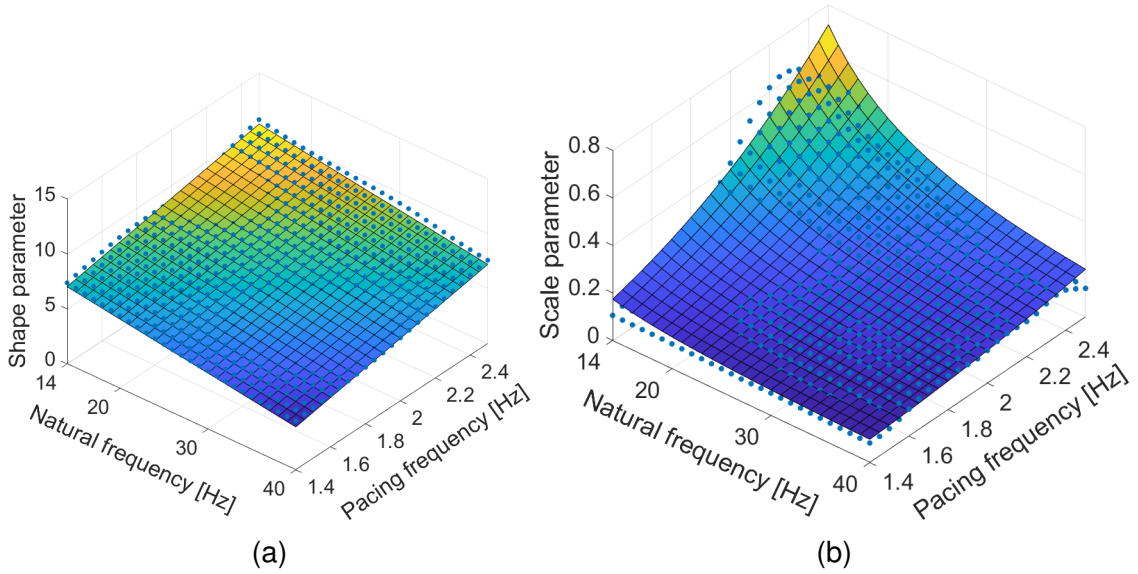

(a) (b)

Figure 3.12: Best fits of the shape (left) and scale (right) parameters for the gamma distribution.

3.3.3.2 Amplification factor

For $A_f(f_n, f_p)$, the generalised extreme value (GEV) distribution (Kotz and Nadarajah, 2000) can be reasonably used to fit its fluctuations, especially around integer multiples of f_p. GEV distribution is useful to fit data with relatively extreme values (Beirlant et al., 2005) which are needed in this case to simulate high peak vibration responses. Figure 3.13 shows an example of $A_f(f_n, f_p)$ values and the corresponding theoretical GEV distribution.

The probability density function $f(A_f(f_n, f_p))$ is characterised by location μ, scale σ and shape τ parameters, dimensionless parameters, as described in Equation 3.9 (Kotz and Nadarajah, 2000).

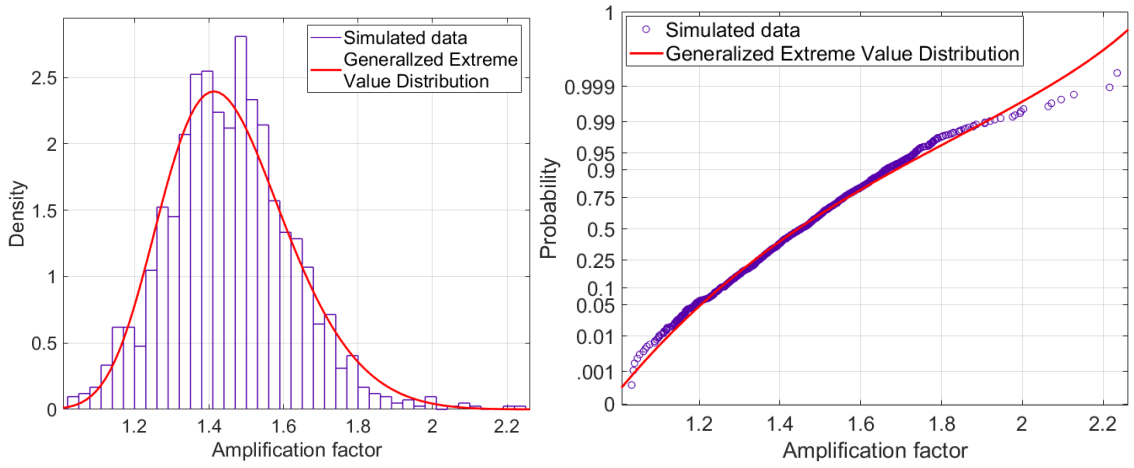

(a) (b)

Figure 3.13: Probability density (left) and cumulative probability density (right) functions using best fit of GEV distribution for a sample of amplification factor values corresponding to a pacing rate of 2.25 Hz and natural frequency of 24.8 Hz.

$$f\left(A_f\left(f_n, f_p\right)\right) = \frac{1}{\sigma}\tau\left[1+\tau\left(\frac{A_f\left(f_n, f_p\right)-\mu}{\sigma}\right)\right]^{-1-1/\tau} e^{\left\{-\left[1+\tau\left(\frac{A_f(q_n, f_p)-\mu}{\sigma}\right)\right]^{-1/\tau}\right]} \quad , \tag{3.9}$$

The GEV distribution is fitted to peak velocities, and the extracted values of μ, σ and τ are further fitted to surfaces as functions of f_n and f_p, measured in Hz, in a similar way to that used for $B\left(f_n, f_p\right)$. The results are illustrated in Figure 3.14 and the mathematical formulation is described by Equations 3.10-3.12.

$$\mu = 0.98 + 7.6\frac{f_p^{2.5}}{f_n^{1.82}} \quad , \tag{3.10}$$

$$\sigma = -0.03 + 0.85\frac{f_p^{1.3}}{f_n} \quad , \tag{3.11}$$

$$\tau = 0.18 - 0.00013f_n^2 - 0.015f_nf_p + 0.0004f_pf_n^2 \quad , \tag{3.12}$$

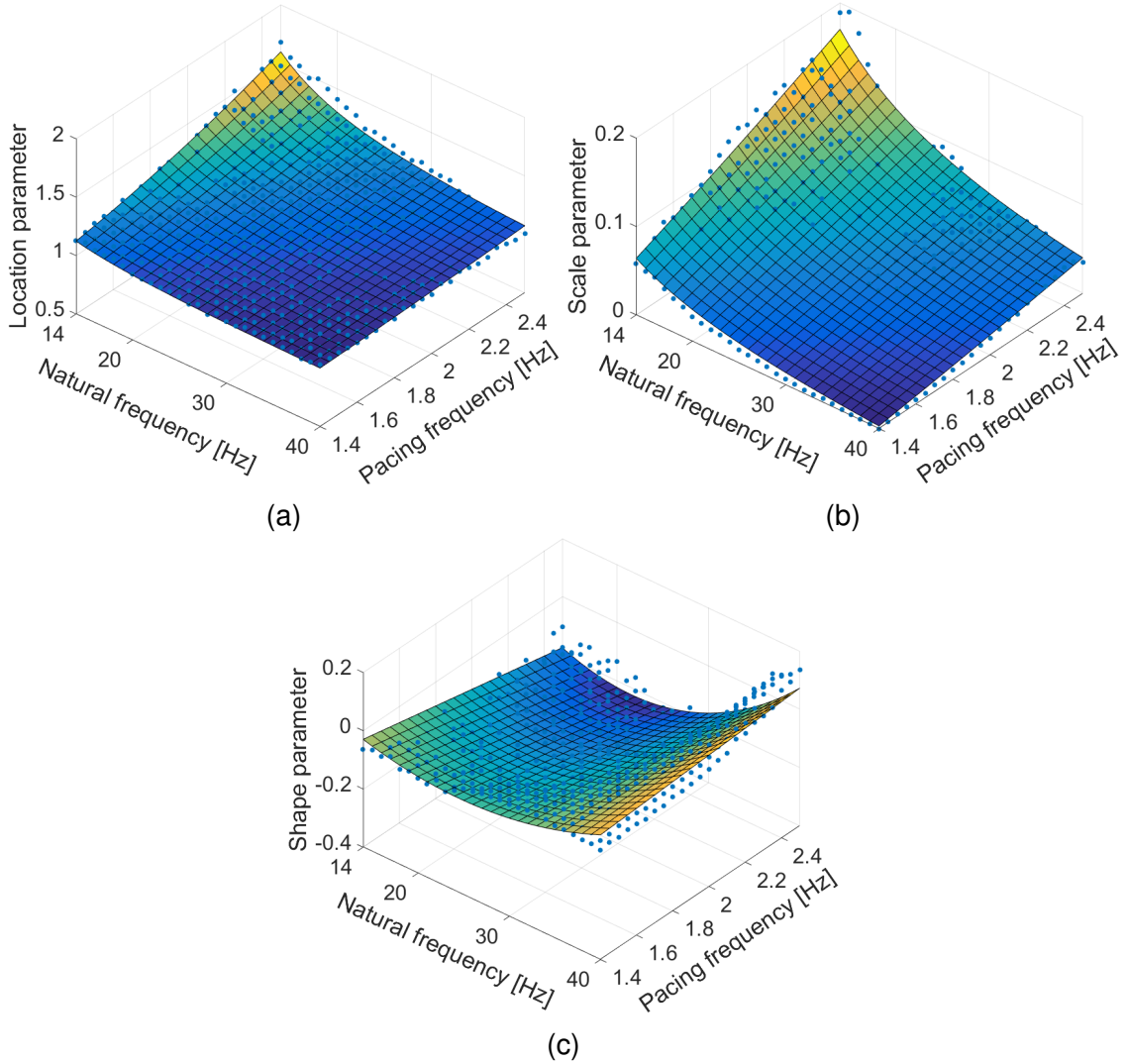

Figure 3.14: Best fits of the location (top left), scale (top right) and shape (bottom) parameters for the GEV distribution.

Interpolation of $A_f\left(f_n, f_p\right)$ should be considered if the natural frequency is not an integer multiple of the pacing rate (Figure 3.10). For instance, if the natural frequency lies exactly in the middle of two successive integer multiples of the pacing rate, the amplification factor will have no effect on the response, i.e. $A_f\left(f_n, f_p\right) = 1.0$. This takes into account that the amplification factor has a reduced effect between the integer multiples of the pacing rate, as shown in Figure 3.10.

3.3.3.3 Damping effect

A damping factor is developed in this section to scale amplification factor $A_f\left(f_n, f_p\right)$ to account for the effect of a floor near-resonance with the harmonics of footfall excitation above 14 Hz and to account for damping ratios ζ of the SDOFs different from 3%. Hence, the numerical simulations presented in the previous section are repeated here to derive amplification factors $A'_f\left(f_n, f_p, \zeta\right)$ for damping ratios in the range 0.5%-6%, with an increment of 0.1%. The damping factor $P_\zeta\left(f_n, f_p, \zeta\right)$ can be expressed as:

$$P_\zeta\left(f_n, f_p, \zeta\right) = \frac{A_f\left(f_n, f_p\right)}{A'_f\left(f_n, f_p, \zeta\right)} \quad , \tag{3.13}$$

The plane defined by Equation 3.14 is fitted to $P_\zeta\left(f_n, f_p, \zeta\right)$ for different damping ratios:

$$P_\zeta\left(f_n, f_p, \zeta\right) = a + bf_p + cf_n \quad , \tag{3.14}$$

where, a, b and c are the parameters of the equation, dimensionless parameters. Figure 3.15 shows the fitted plane corresponding to a damping ratio of 5%, where the maximum error, i.e. the difference between a single damping factor value and the corresponding value on the fitted plane, is around 10%.

Finally, values of the parameters a, b and c are curve fitted as functions of the damping ratio. The resulting curve fits are illustrated in Figure 3.16 and described by Equations 3.15, 3.16 and 3.17. The shapes of these equations are decided based on the trends observed in the data (Figure 3.16).

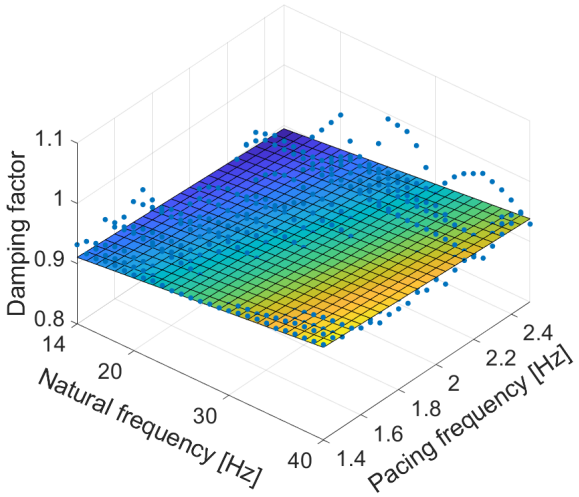

Figure 3.15: Best fit of the damping factors corresponding to a damping ratio of 5%.

$$a = 2.82 - 2.58\zeta^{0.1} \quad , \tag{3.15}$$

$$b = -0.0174 + \frac{0.38}{e^{100\zeta}} \quad , \tag{3.16}$$

$$c = 0.0028 - \frac{0.0138}{e^{50\,\zeta}} \quad , \tag{3.17}$$

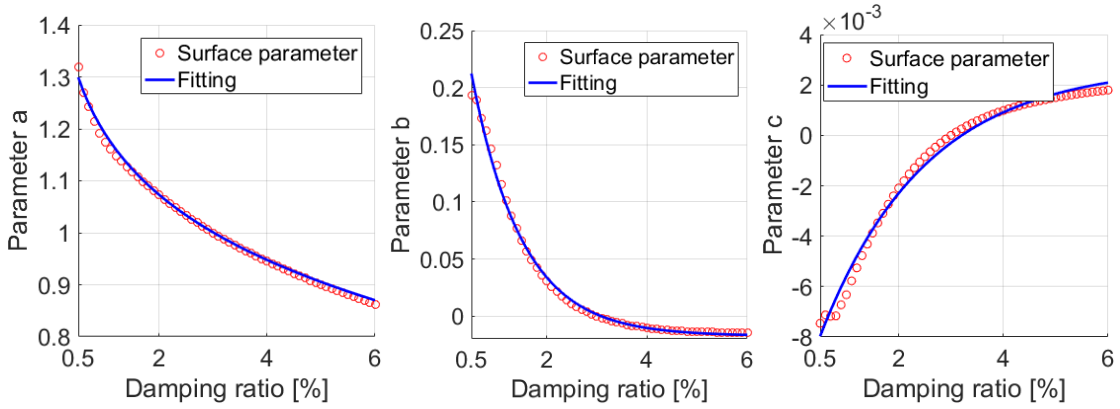

(a) (b) (c)

Figure 3.16: Fitting parameters a (left), b (middle) and c (right).

According to Equation 3.14, the range of $P_\zeta\,(f_n, f_p, \zeta)$ is 0.86-1.72. The lower and upper limits correspond to f_p=2.5 Hz, f_n=14 Hz and ζ=6% and ζ=0.5%,

respectively. It is assumed that the damping factor $P_\zeta(f_n, f_p, \zeta)$ has the highest effect when f_n is an integer multiple of f_p due to the near-resonant effect with the higher harmonics of footfall loading, as was the case with $A_f(f_n, f_p)$ in the previous section. Hence, if the natural frequency is not an integer multiple of the pacing rate, $P_\zeta(f_n, f_p, \zeta)$ need to be interpolated in the same way as $A_f(f_n, f_p)$.

3.3.4 Implementation of the new model

Vibration serviceability assessment of a high-frequency floor using the new model takes the following steps:

- The modal properties are derived from either modal testing or a finite element (FE) model of the floor.
- The walking path, pacing rate and its corresponding walking speed or step length can be utilised to calculate the time that a walking person spends while walking on the floor. This is necessary to determine the number of footfalls and the duration of the vibration response. Further discussion about deciding an appropriate pacing rate and walking path is beyond the scope of this study. However, a reader is advised to generate value of the pacing rate based on probability density functions available in the literature (Racic et al., 2009).
- For each vibration mode, Equations 3.7, 3.8, 3.10-3.12 are used to calculate the distribution parameters related to the gamma and the GEV distributions. Random values of these distributions are generated based on Equations 3.6 and 3.9 corresponding to $A_f(f_n, f_p)$ and $B(f_n, f_p)$, respectively. The number of the generated values is the same as the number of footfalls

calculated above. The effect of damping is considered by calculating $P_\zeta(f_n, f_p, \zeta)$ using Equation 3.14, which parameters can be calculated using Equations 3.15, 3.16 and 3.17. The generated values of $A_f(f_n, f_p)$ and $P_\zeta(f_n, f_p, \zeta)$ need to be scaled depending on the natural frequency of the considered vibration mode and the pacing rate, as explained in Section 3.3.3.2 and Figure 3.10.

- The effective impulse I_{eff} corresponding to each footfall can be determined using Equation 3.5. The time history of decaying vibration response due to each effective impulse is calculated utilising Equation 3.3 and the modal properties of each mode under consideration. The total time history response due to each mode can be obtained when the decaying responses are sequenced one after another to form a continuous response time history for the duration of walking. The time between each two successive footfalls needs to be consistent with the pacing rate. The residual of each decaying response at the beginning of the next footfall is assumed to be zero.

- The total response corresponding to the contribution from all vibration modes having frequencies up to twice the fundamental frequency is calculated using Equation 3.4. This number of vibration modes is adopted from the Arup's model.

By following the above mentioned procedure, a single response time history can be obtained. To consider the statistical nature of $A_f(f_n, f_p)$ and $B(f_n, f_p)$, a sufficient number of responses needs to be generated as explained below. This number of samples n is defined by Equation 3.18 (Rubinstein and Kroese, 2017).

$$n = (\frac{s}{SE_{\overline{x}}})^2 \quad , \tag{3.18}$$

where, s is the standard deviation of the population and $SE_{\overline{x}}$ is the standard error of their mean.

In this study, the samples are a set of MTVV velocity calculated following the above mentioned procedure, while the population refers to all possible MTVV velocities. As the standard deviation of the population s is unknown, it is estimated to be the standard deviation of the samples. Assuming the samples are independent and identically distributed, there is a 95% chance that their mean is within the population mean $\mp$ a tolerance of 1.96 $SE_{\overline{x}}$ (Rubinstein and Kroese, 2017). This tolerance should be specified based on the required accuracy (Rubinstein and Kroese, 2017). This study suggests using a tolerance value of 1% of the mean of the samples.

Hence, the sufficient number of responses can be found in an iterative approach. After generating each sample, i.e. MTVV velocity, the sufficient number of samples n can be calculated using Equation 3.18 and compared with the actual number of generated samples. When Equation 3.18 is fulfilled, i.e. the number of generated samples is equal or higher than the sufficient number of samples n, the simulations can be stopped.

Finally, the cumulative distribution function (CDF) of the MTVV velocity, corresponding to the generated responses, can be obtained and the vibration serviceability assessment can be carried out based on the desired probability. The whole process explained in this section is summarised in Figure 3.17.

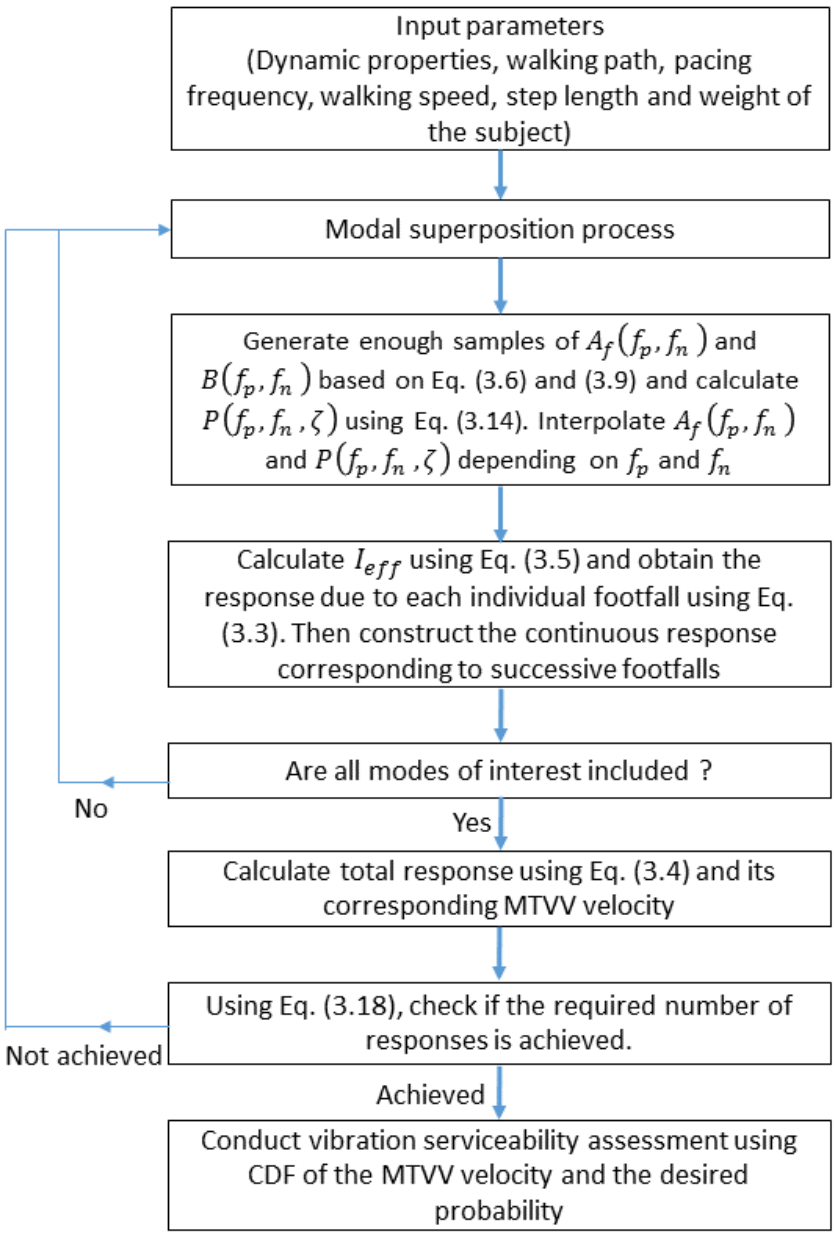

Figure 3.17: Implementation procedure of the new model.

3.4 Verification

The performance of the model elaborated in the previous section is verified here against numerical simulations (Section 3.4.3) of the vibration response calculated using the measured treadmill forces (Section 3.2.1) and a FE model of a high-frequency floor (Section 3.4.1). Simulations are also carried out using the original Arup model (Section 3.4.3) for comparison (Section 3.4.4).

3.4.1 Finite element model

The FE model utilised in this section is developed using ANSYS FE software (ANSYS Inc., 2016) and is updated to match the experimentally measured modal properties of the corresponding real floor but with increased stiffness (Figure 3.18). The floor is a 58m $\times$ 14m composite slab supported by steel beams and columns. The slab has a concrete deck with thickness 130 mm and it was modelled using a shell element, i.e. SHELL181 in ANSYS, assuming isotropic behavior with a mesh size of 0.5m. BEAM188 element was used to model the supporting steel beams and columns. The elastic modulus used to model the concrete and steel materials are 38 GPa and 210 GPa, while their corresponding Poisson's ratios are 0.2 and 0.3, respectively. The elastic modulus of the steel material was increased, to 420 GPa, to raise the fundamental frequency of the FE model to the region of high-frequency floors, i.e. above 14 Hz. The structure has a maximum span of 7.0 $\times$ 6.0 m and similar, but not identical, structural configuration between its two wings (left and right). The columns were fixed at the far ends and the lateral movement of the floor was restrained at the perimeter of the floor.

Figure 3.19 shows the first six vibration modes of the structure. While the first 18 vibration modes have contributions from either the left or the right wing of the structure, the other eight vibration modes have contributions from both wings. The dynamic properties of all vibration modes with a natural frequency up to twice the fundamental frequency, i.e. 26 vibration modes, were extracted from the FE model and used in the analysis presented in the next section.

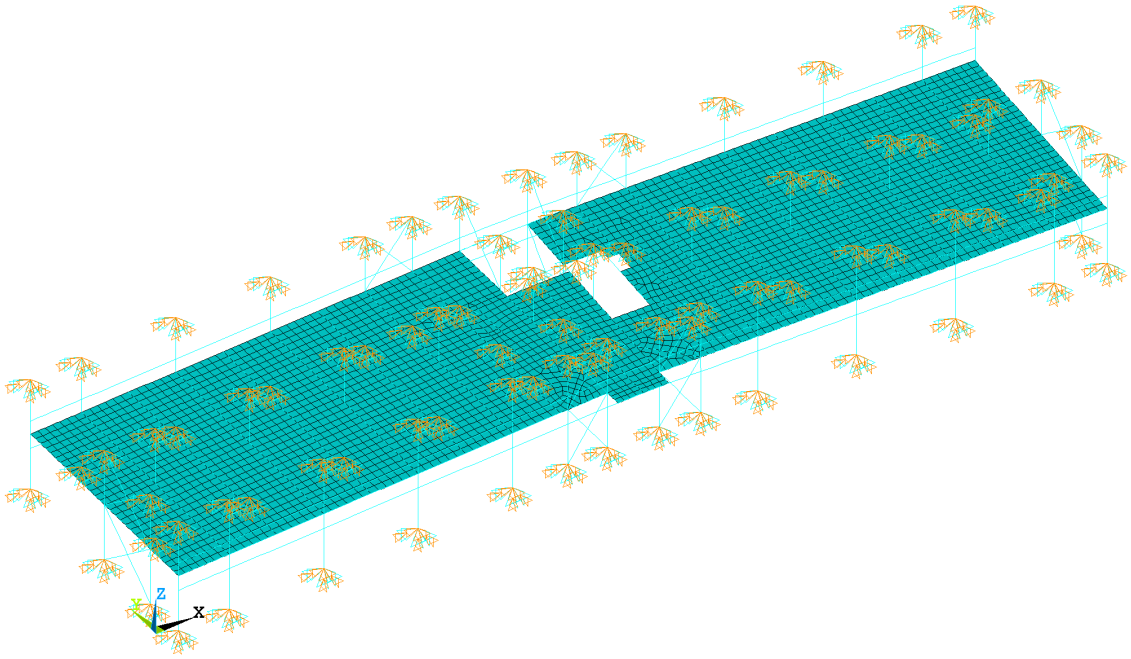

Figure 3.18: FE model of the floor structure.

3.4.2 Simulations based on measured footfall forces and FE model

The simulations are carried out using 60 measured forces (Section 3.2.1) due to people walking at six walking frequencies, i.e. ten footfall forces for each pacing rate 1.4, 1.6, 1.8, 2.0, 2.2 and 2.4 Hz, representing slow to fast walking scenarios.

A walking path expected to produce the maximum response is specified before performing the simulations (Figure 3.19). A constant value of 0.75 m was used for the step length. Unity-scaled, i.e. normalised to a maximum value of 1.0 mode shapes $\{\phi_r\}$ were used to calculate the modal force time histories $P_r(t)$ for each mode r for the footfall force moving along the walking path, as described in Equation 3.19:

$$P_r(t) = f(t)\ \phi_r(v.t) \quad , \tag{3.19}$$

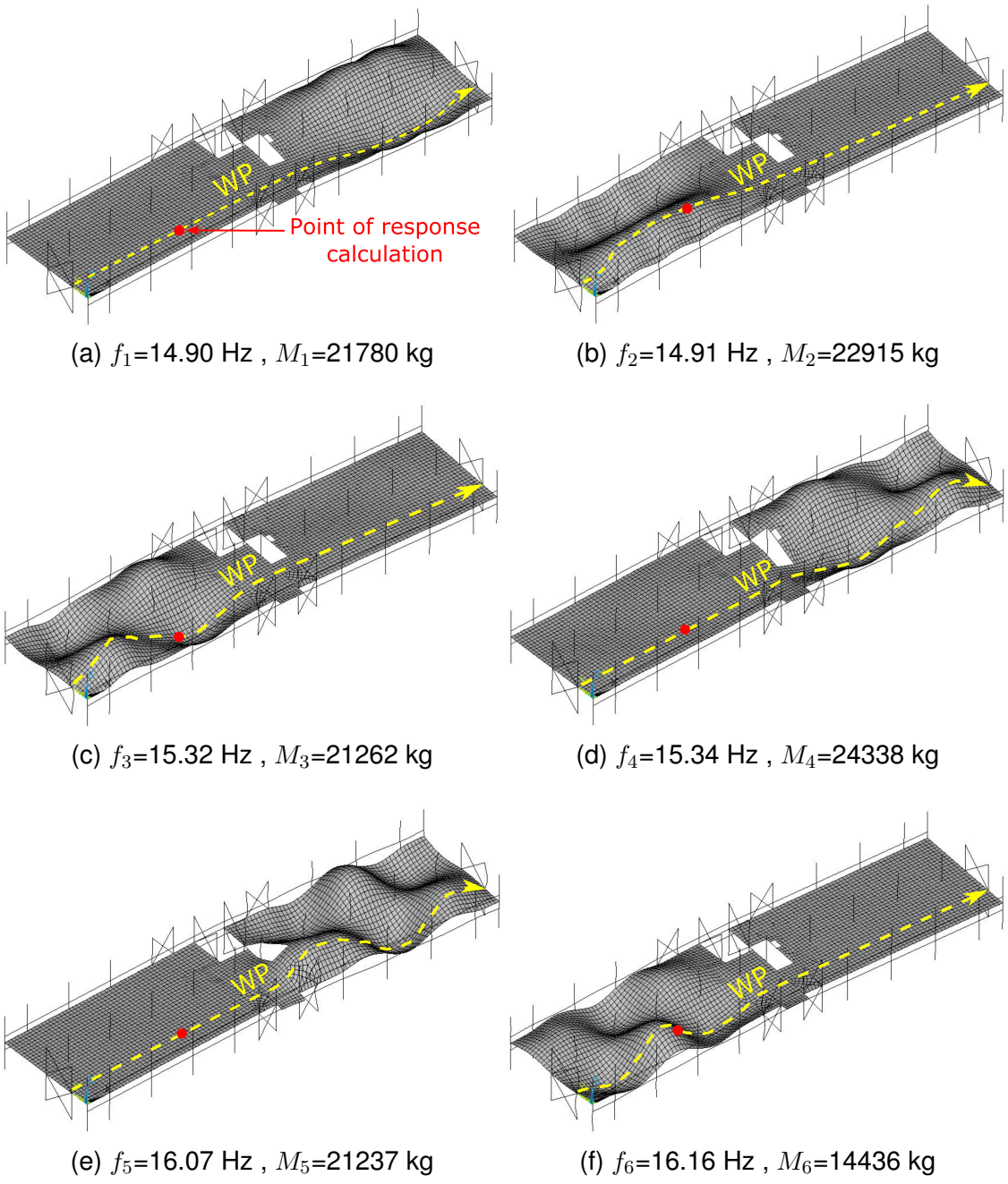

(a) f_1=14.90 Hz , M_1=21780 kg

(b) f_2=14.91 Hz , M_2=22915 kg

(c) f_3=15.32 Hz , M_3=21262 kg

(d) f_4=15.34 Hz , M_4=24338 kg

(e) f_5=16.07 Hz , M_5=21237 kg

(f) f_6=16.16 Hz , M_6=14436 kg

Figure 3.19: Mode shapes, natural frequencies (f_n) and modal masses (M_n) of the first six modes showing the walking path (WP) (dashed yellow line) and the point of the response calculations (red dot).

where, $f(t)$ is the physical footfall force, t is time, v is the constant walking speed, r =1, 2,... refers to different modes of vibration and $\phi_r(v.t)$ is amplitude of the mode shape r at the location of the pedestrian at time t. Essentially Equation 3.19 describes scaling of footfall force $f(t)$ by mode shape amplitudes $\phi_r(v.t)$ along the walking path. Due to the discrete locations of the nodes, the amplitudes of the unity-scaled mode shapes corresponding to the location of the pedestrian at each

time step were obtained by interpolation.

The contribution of each mode in the total response was obtained by applying the modal force time history to a SDOF oscillator having the same modal properties as that extracted from the FE model. The Newmark integration method was used to solve the corresponding equation of motion with a time step of 0.005 s. The modal damping ratio was assumed 3% in all simulations. The vibration responses were calculated at a node which has contributions from as many vibration modes as possible (red dot in Figure 3.19). Hence, the contribution of each mode in the total response was multiplied by its corresponding mode shape value at that node (u_j). The total responses were determined based on the superposition principle, i.e. by adding responses from all vibration modes having a natural frequency up to twice the fundamental frequency.

This procedure was repeated to simulate the vibration response due to each measured footfall force. Therefore, there are 60 vibration response time histories, here called “oscillator based responses”, used in the next section for comparison with the vibration responses calculated using both the new model and Arup’s model.

3.4.3 Calculated responses using the new model and Arup’s model

The same walking path, pacing rates, step length and modal properties from the previous section were used here to calculate the responses, using both the newly proposed model and Arup’s model. For the new model, the procedure described in Section 3.3.4 was followed to estimate the vibration response time histories and their corresponding MTVV velocity. After generating each response, an

estimation of the required number of generated responses, according to Equation 3.18, is obtained and compared with the actual number of generated responses, as shown in Figure 3.20.

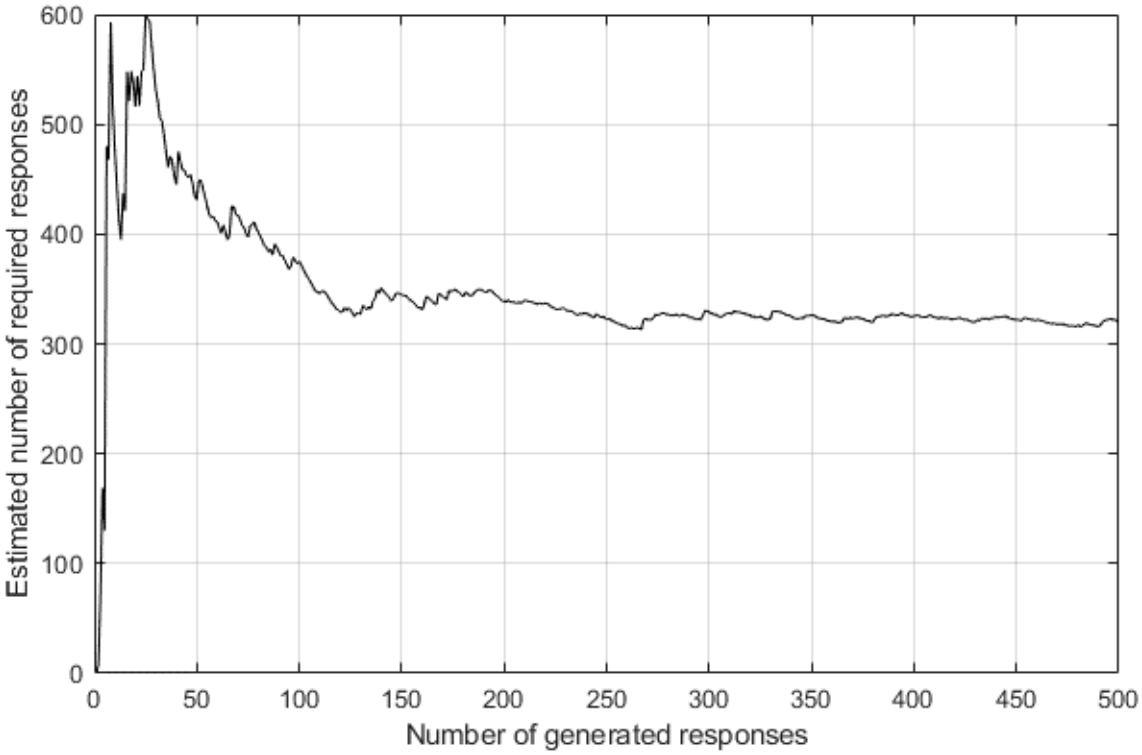

Figure 3.20: Stability of the estimated number of the required simulations related to the response calculation at pacing rate of 1.4 Hz. The required number of generated responses was achieved after 326 iterations.

The vibration response using Arup's model was estimated in a similar procedure. The main difference is that the effective impulse is calculated based on Equation 3.2 instead of Equation 3.5.

3.4.4 Results and comparison

Examples of velocity time history responses calculated using the oscillator based simulations and the new model are presented in Figure 3.21.

A numerical comparison between the vibration responses can be made using their cumulative probability distribution. Figure 3.22 shows the overlaid plot of the cumulative probability distribution corresponding to each vibration response time

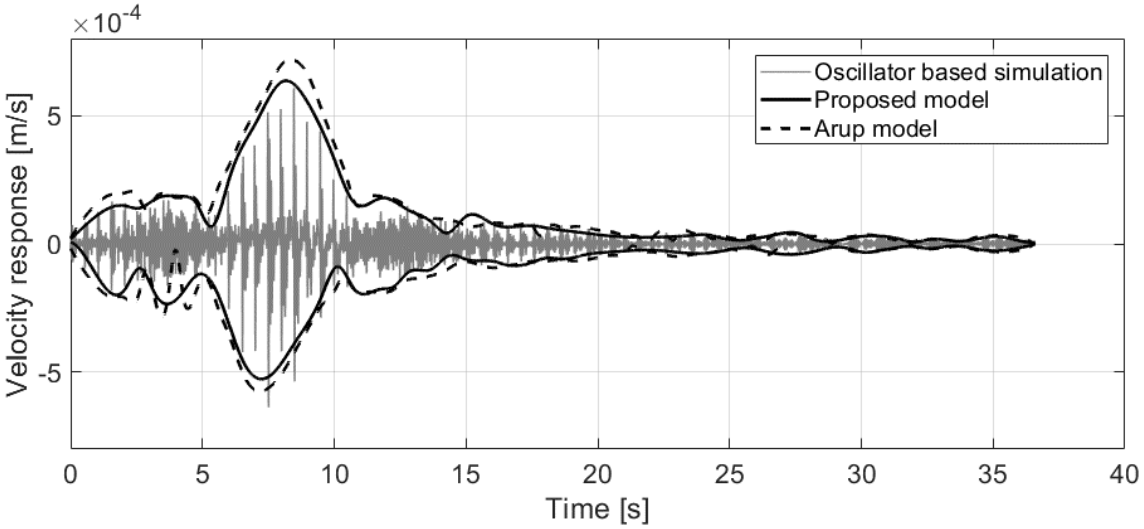

Figure 3.21: Time-history response samples from the oscillator based simulations, the new model and Arup's model corresponding to a pacing rate of 2.0 Hz. For the responses calculated using the new model and Arup's model, only their envelopes are shown in this figure for comparison purposes.

history obtained using the oscillator based simulations, the new model and Arup's model.

This figure shows that the vibration response levels calculated using the new model (light grey curves in Figure 3.22) are relatively close to that obtained from the oscillator based simulations (dark grey curves in Figure 3.22). The vibration responses calculated using Arup's model slightly overestimate the responses corresponding to the pacing rates of 1.4 Hz and 1.6 Hz, while less conservative results were obtained for vibration responses corresponding to other pacing rates (Figure 3.22).

A more obvious and appropriate comparison between the considered vibration responses can be carried out using the MTVV of the velocity responses. Figure 3.23 presents the cumulative probability distribution of the MTVV velocity corresponding to the generated responses using the new model. This represents the MTVV velocity prediction range of the proposed model. For comparison purposes, the projections of the MTVV velocity, corresponding to the responses

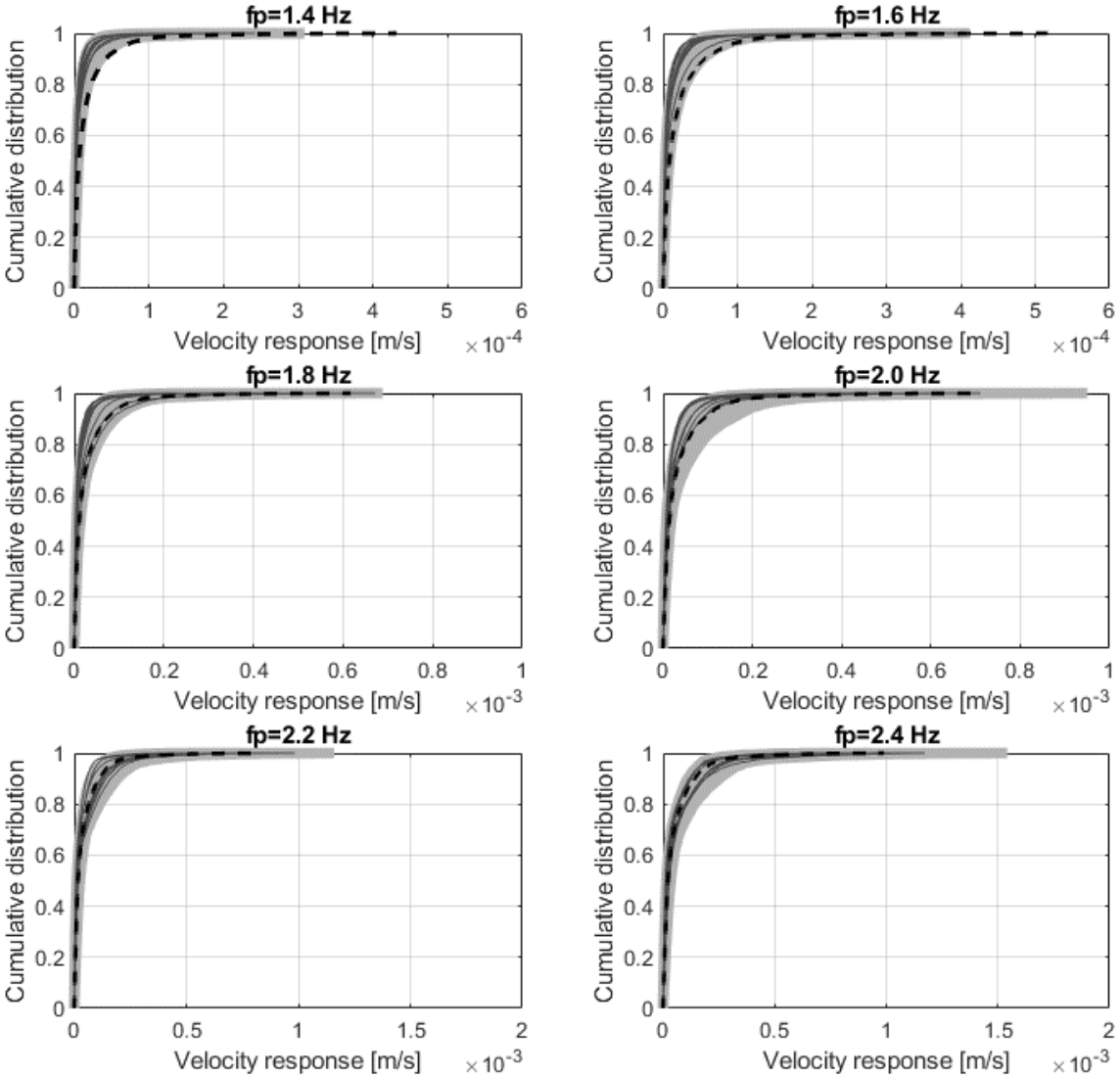

Figure 3.22: Cumulative probability distribution function of the time history responses obtained from the new model (light grey curves), oscillator based simulations (dark grey curves) and Arup's model (dashed black curves).

obtained using the oscillator based simulations and Arup's model, on the cumulative probability distribution in Figure 3.23 were illustrated in the same figure.

Most of the MTVV velocity corresponding to the oscillator based simulations are within the predicted range of the vibration responses obtained using the new model (Figure 3.23). Only four vibration responses, out of 60, obtained from the oscillator based simulations are outside but relatively close to the predicted range of the vibration levels calculated using the new model. Ideally, the MTVV

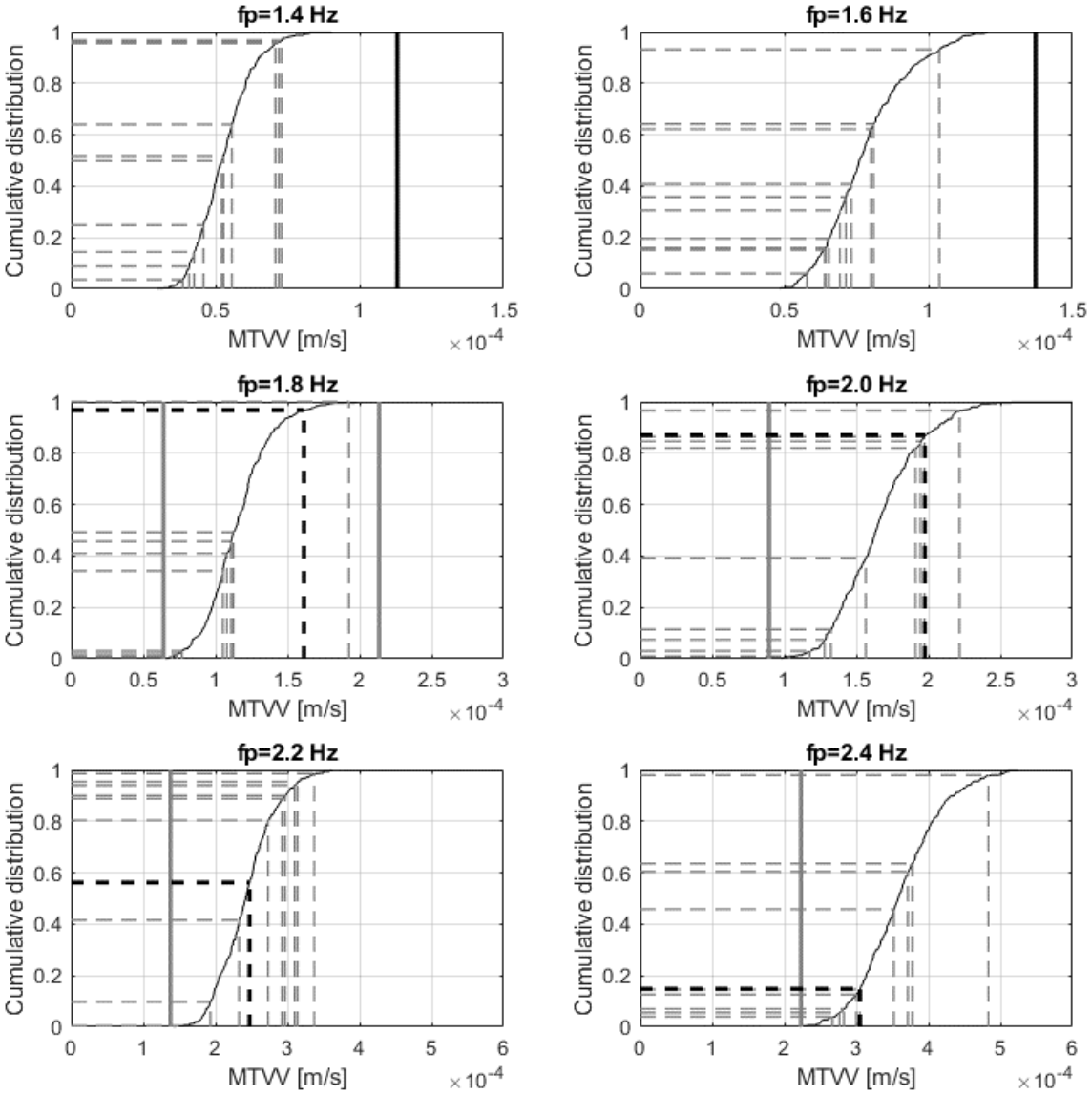

Figure 3.23: MTVV velocity of the time history responses obtained from the new model (black thin curves), Arup's model (black thick lines) and the oscillator based simulations (grey lines). Solid vertical lines represent the values outside the ranges of the new model.

velocity of the oscillator based simulations should be clustered around vibration levels corresponding to a cumulative probability distribution value of 0.5 (Figure 3.23). This is broadly achieved by most of the simulated MTVV velocity values (dashed grey lines in Figure 3.23).

Arup's methodology for vibration prediction has an implicit 75% chance of non-exceedance probability for a certain vibration level as explained in Section 3.3.1. This implies that the MTVV velocity corresponding to the responses

obtained using Arup's model should be higher than that corresponding to seven responses, out of 10 obtained from the oscillator based simulations related to each pacing rate. By comparing these MTVV velocity values, it is obvious that the vibration levels calculated using Arup's model are significantly overestimated for low pacing rates, i.e. 1.4 Hz and 1.6 Hz, and slightly underestimated for a high pacing rate, i.e. 2.4 Hz. Closer vibration levels were obtained for responses corresponding to pacing rates 1.8 Hz and 2.0 Hz (Figure 3.23). The same trend can be observed when they are compared with the MTVV velocity corresponding to the new model (Figure 3.23).

3.5 Discussion and conclusions

This chapter presents an improved version of Arup's approach for the vibration serviceability assessment of high-frequency floors. The main advances are the new cut-off frequency of 14 Hz rather than 10 Hz between low- and high-frequency floors and the probabilistic rather than deterministic approach to modelling individual footfall loading. Note that using cut-off frequency 14 Hz in the existing models for high-frequency floors, including Arup's model, may not be appropriate, as they were developed using simulations of different oscillators than in this study.

Another key advantage of the proposed force model is its capability to provide probability-based vibration serviceability assessment related to any given probability of exceedance of the floor vibration levels. This is far more flexible than Arup's original model providing vibration levels corresponding to 75% probability of non-exceedance. The probabilistic approach of the proposed individual footfall loading and the related criterion for assessing vibration serviceability describes

better the stochastic nature of human-induced vibrations than that of the existing model.

The simulation results showed that the new model can predict the vibration levels for more than 90% of cases. Those outside the range showed vibration levels mostly below, yet close to, their targets (Figure 3.23). Although the verification of the new model was conducted using the data used to derive the model, the fact that the new model is capable of predicting vibration levels simulated by experimental data means that the new model can, in theory, predict actual vibration levels. However, further verification using experimentally measured responses can be conducted in the future.

For Arup's model, the predicated vibration responses appear to be well correlated with that from the simulations. It tends to overestimate the response for low pacing rates, but slightly underestimate vibration levels at high pacing rates. The best performance of Arup's model was observed for pacing rates corresponding to an average walking speed, i.e. 1.8 Hz and 2.0 Hz. This is in line with previous findings that Arup's model can underestimate the response for high-frequency floors with relatively low fundamental frequency and high pacing rate (Brownjohn and Middleton, 2008). The reason for this could be related to using synthetic rather than continuously measured footfall forces (Racic and Brownjohn, 2011, 2012) and the range of the SDOF frequencies used to derive the model. Hence, it is apparent that Arup's model performs well when it is utilised for initial predictions of vibration levels of high frequency floors, but its 'partially-deterministic' nature means that it cannot provide response predictions for any probability of non-exceedance, and this is what the new model appears to be capable of.

As the new model requires repetitive simulations, vibration serviceability assessment in design practice would benefit from a computer software where the results can be obtained within a few seconds on a standard PC configuration. In future this approach could also involve in the calculations statistical treatment of walking paths and other force parameters, such as pacing rate and body weight. Finally, the new model needs to be verified against vibration serviceability surveys of real high-frequency floors when occupied by walking people.

Preface to Chapter 4

Chapter 4 Quantifies the influence of single and multiple pedestrians on the magnitudes of the frequency response functions, which describe the corresponding modal properties, of the supporting floors. This is followed by a description of a proposed model that takes human structure interaction into account in the response calculation of footfall-induced vibration of floors.

The author did not participated in the tests conducted on Floor B discussed in this chapter and the corresponding data, i.e. time-history data of walking tests and all frequency response functions, were provided by the first supervisor. The data related to measurements of individuals walking on an instrumented treadmill were provided by James Brownjohn. All other experimental works and analyses were conducted by the writer. Members in the Vibration Engineering Section at the University of Exeter provided assistance in the experimental tests of Floor C.

The contents of this chapter were adopted from a manuscript of the following journal paper submitted to the Mechanical Systems and Signal Processing. Slight amendments were made to adjust the style of this chapter.

Mohammed, A. and Pavic, A. Human-structure dynamic interaction between building floors and walking occupants in vertical direction. *Mechanical Systems and Signal Processing*.

Chapter 4

Human-structure dynamic interaction between building floors and walking occupants in vertical direction

Abstract

While modern building floors feature lightweight materials and slender structural elements, their dynamic interaction with walking occupants has not been quantified. This is despite the proven and significant influence of this interaction on human-induced vibration levels of other types of lightweight structures, such as footbridges. This work presents an experimental study to quantify the effect of walking pedestrians on the magnitude of frequency response functions (FRFs), which describe the corresponding modal properties, of three floors. It also proposes a methodology to take into account the interaction between walking

pedestrians and supporting floors in the response calculation of human-induced vibration. Instead of the conventional mass-spring-damper or inverted-pendulum models, the proposed model utilises two experimentally-driven transfer functions, related to the dynamics of walking individuals over a range of frequencies between 1 Hz and 10Hz, to mathematically describe the dynamics of this interaction. The results show that walking occupants can cause significant reduction in the amplitudes of the FRFs. This reduction ranges from 44% and 62% for a floor occupied by two or six walking pedestrians, respectively, to 10% for a heavier floor with a higher fundamental frequency occupied by six walking pedestrians. This implies ignoring this phenomenon in the design can result in an overestimation of the predicted vibration levels. This is especially the case for floors with relatively low fundamental frequency and modal mass. Furthermore, the derived transfer functions related to the dynamics of walking individuals indicated the existence of three whole-body modes of vibration with frequency less than 10 Hz. The performance of the proposed human-structure interaction model is verified with experimental measurements of vibration responses related to individual occupants walking on three floors. The simulated vibration levels are consistent with their measured counterparts indicating the applicability of the proposed model.

4.1 Introduction

The new generation of building floors feature more slender structural elements and larger column-free areas than ever before (Nag, 2018; Ferdous et al., 2019). This is due to architectural trends and the recent development of lightweight construction materials and design tools. The design of such floors is increasingly

governed by vibration serviceability criteria related to human activities, such as walking (Nguyen, 2013; Brownjohn et al., 2015).

These trends in building floor design mean that they are livelier and have lower modal mass than typical older floors. Therefore, their dynamic interaction with walking occupants in the vertical direction is more likely to influence their vibration serviceability performance than previously. Such interaction is not taken into account in any of the current vibration serviceability design guidelines used worldwide and pertinent to building floors (Pavic and Willford, 2005; Willford and Young, 2006; Feldmann and Heinemeyer, 2007; Smith et al., 2009; Fanella and Mota; Murray et al., 2016). This is because, when most of these guidelines were published, more than 10 years ago, floors were generally heavier and stiffer than modern floors, and therefore, human-structure interaction (HSI) did not have a significant influence on their dynamic performance. However, neglecting HSI for modern floors could result in a significant overestimation of human-induced vibrations.

Numerous studies were conducted previously to understand this phenomenon. For example, Ohlsson (1982) found that the spectrum of the footfall force measured on a rigid surface was different from that measured on a floor, especially for frequencies close to the frequency of the floor, i.e resonance. He also reported that a walking pedestrian can alter the damping and mass of the supporting floor. Pimentel (1997) reported that dynamic load factors (DLFs) related to a walking pedestrian on a footbridge are lower than that those for a pedestrian walking on a rigid surface. Similarly, Baumann and Bachmann (1988) reported up to 10% lower DLFs for pedestrians walking on a flexible prestressed beam. More recently, Dang and Živanović (2016) and Ahmadi et al. (2018)

have directly measured the footfall loading of a individual walkers on flexible footbridges. They reported a drop in the DLFs around the frequency of the bridge and the drop was more prominent in the case of resonance. Other studies reported that pedestrians walking on structures can alter their natural frequency or modal damping. Ebrahimpour et al. (1989) showed that walking occupants increased the damping of their supporting platform. Similar conclusions were made later by Shahabpoor et al. (2017b), Živanović (2012) and Van Nimmen et al. (2015) who reported that pedestrians walking on footbridges can alter their modal damping and natural frequency.

Hence, it can be concluded from the literature that HSI has two components: the influence of the walking on the modal properties of the supporting structure (H2S) and the influence of the structure on the footfall loading of the walker (S2H). These two components were described by a recent study conducted by Ahmadi et al. (2019) who quantified these two components on two footbridges.

Regarding the modelling aspect of HSI, currently available models are related to pedestrians walking on footbridges. The majority of them are based on modelling the walking individual as either an inverted pendulum (IP) (Bocian et al., 2013; Qin et al., 2013; Dang, 2014) or a mass-spring-damper (MSD) (Caprani et al., 2011; da Silva and Pimentel, 2011; Van Nimmen et al., 2015; Shahabpoor et al., 2016a). IP models are generally complex to implement in the design and have limited robustness (Shahabpoor et al., 2016b). MSD models are more common and easier to use. Current MSD models for walking individuals take into account human dynamics related to only the dominant whole-body mode of vibration. Their corresponding single-degree-of-freedom (SDOF) natural frequency is around 2-4 Hz which correspond to the frequency of

the dominant whole body mode of vibration for individual walkers. Such frequency is close to the fundamental frequency of a typical footbridge, and therefore, these models are proven to be useful and reliable in the design of such structures for vibration serviceability. Despite that such models were suggested in the literature to be utilised to simulate HSI between walking individuals and floors (Zhang, 2017), their frequency is considerably lower than the fundamental frequency of building floors, typically higher than 4-5 Hz. While multiple modes of of vibration are reported in the literature for standing people, there are indications that higher order human whole-body mode of vibration exists for walking individuals (Shahabpoor, 2014), but quantification of its parameters is generally missing. Hence, design methods related to footfall-induced vibration of floors can be improved by taking into account whole-body dynamics of walking individuals in frequency ranges relevant to dominant modes of vibration for building floors, i.e. higher than 4-5 Hz. This can be achieved by incorporating multiple SDOF or multi-degree-of-freedom (MDOF) models calibrated for this purpose. Another way to achieve this is by utilising experimentally-based transfer functions, to describe the dynamics of walking individuals over a range of frequencies, which eliminates the need to derive approximate SDOF or MDOF models. Hence, this study:

- Quantifies the influence of HSI between single or multiple walking pedestrians and supporting floors on the frequency response function (FRF) magnitude, and
- Presents an improved HSI model for individuals walking on floors where the dynamics of walking individuals were simulated using experimentally-based transfer functions which take into account the dynamics of the walker over a range of frequencies, i.e. 1-10 Hz.

The influence of HSI on the DLF was not quantified in this study due to lack of equipment needed to directly measure the GRFs related to pedestrians walking on flexible floors. However, the DLF was not explicitly utilised in the proposed HSI model, as described below.

Three floors were tested when they were empty and occupied by single or multiple walking occupants. The influence of the walking occupants on the FRF magnitude is quantified. The proposed HSI model considers whole-body dynamics of walking individuals for frequency range 1-10 Hz, i.e. close to the fundamental frequency of most floors. It is represented by two transfer functions describing the transmissibility of structural acceleration to the human body and the corresponding interaction force applied on the floor. Their influence on the vibration response is assumed, in this study, to be equivalent to that caused by H2S and S2H components of HSI. The transfer functions were derived from two separate sets of experimental measurements available in the literature (Matsumoto and Griffin, 1998; Bocian et al., 2016). The measurements involve individual test subjects instrumented with sensors and walking on an instrumented treadmill or standing on an instrumented force plate shaking in the vertical direction, to study their whole-body dynamics. The performance of the proposed HSI model is verified by comparing *simulated* human-induced structural vibration using the proposed HSI model with corresponding *measurements* of individuals walking on the three floors considered in this study.

It is worth mentioning that the measurements utilised to derive the proposed model can be, ideally, related to individuals walking on a vibrating platform at various frequencies. However, the focus of this study is on the principle utilised to model HSI, and the model can be updated in the future by utilising data related

to individuals walking on such facilities when they become available for such measurements.

Section 4.2 in this chapter quantifies the effect of HSI on the FRF magnitude of three floors before proposing a methodology to model this phenomenon in Section 4.3. Section 4.4 validates the proposed model, while Section 4.5 presents a parametric study regarding the influence of dynamic properties of the structure on HSI. Finally, Section 4.6 presents the concluding remarks.

4.2 Influence of HSI on FRF magnitude of floors

It has been widely reported that the influence of HSI on human-induced vibration of structures is equivalent to the modification of dynamic properties of the supporting structure, namely, natural frequencies and damping ratios (Živanović, 2012; Shahabpoor et al., 2016b). The modal properties of a structure are closely related to its FRFs. Hence, this section quantifies the influence of HSI on the FRF magnitude of three floors. This was done by conducting a modal testing on the three floors to identify the modal properties of their dominant modes of vibration. This is followed by measuring the magnitude of the FRFs at specific test points (TPs) of the floors when they were empty and occupied by single or multiple walking occupants. The FRFs corresponding to empty and occupied structures were compared, and relevant discussion about the results is provided at the end of this section.

4.2.1 Modal testing

Modal testing was conducted to measure the FRFs which are used to estimate natural frequency, mode shape, damping ratio and modal mass corresponding

to modes of vibration of interest for the three structures explained in this study. Multi-input multi-output (MIMO) modal testing was conducted where multiple APS400 (APS Dynamics Inc., 2013) and APS113 (APS Dynamics Inc., 1996) electrodynamic shakers were used to apply uncorrelated random force on the floor structure. Their input force was calculated by multiplying the acceleration of the moving armature, measured using an Endevco 7754A-1000 piezoelectric accelerometer, by its mass. The corresponding structural response was measured by Honeywell QA750 accelerometers placed on specific TPs in the vertical direction.

The floor input force and output acceleration signals were processed using Data Physics Spectrum Analyser DP730 to calculate the FRFs (Ewins, 2000). A Hanning window with a 75% overlap was used for this purpose. Curve fitting of the calculated FRFs was carried out using ME'scope software (Vibrant Technology Inc., 2018) to estimate the natural frequency, mode shape, damping ratio and modal mass corresponding to modes of vibration of interest. The duration of each test and other test-specific details are explained below.

4.2.2 Floor A

The laboratory full-scale test floor, shown in Figure 4.1, is a reconfigurable structure weighting 15 tonnes and located at the University of Exeter and dedicated for research purposes. It comprises Sandwich Plate System (SPS) plates attached, using steel splices, to steel beams resting on four columns (Figure 4.2). A detailed description of the structure is available elsewhere (Hudson and Reynolds, 2016).

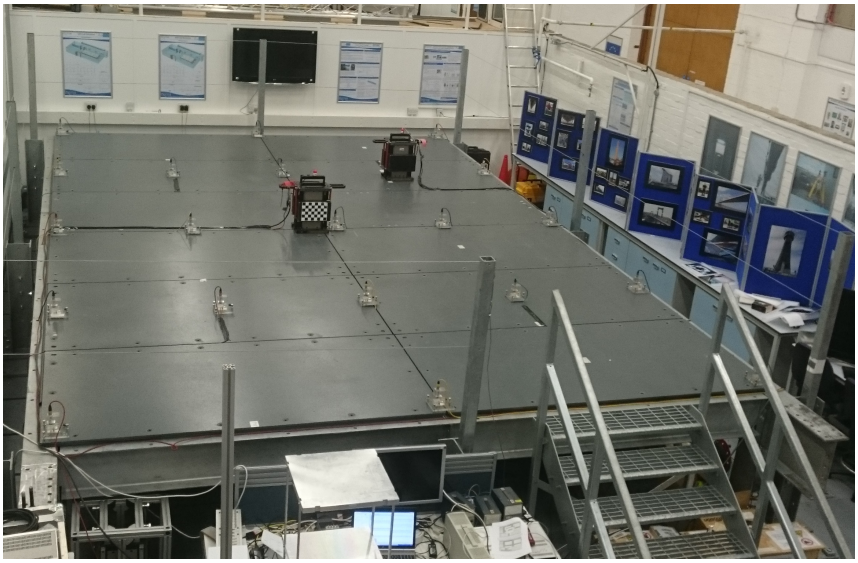

Figure 4.1: Overview of Floor A (Mohammed and Pavic, 2017).

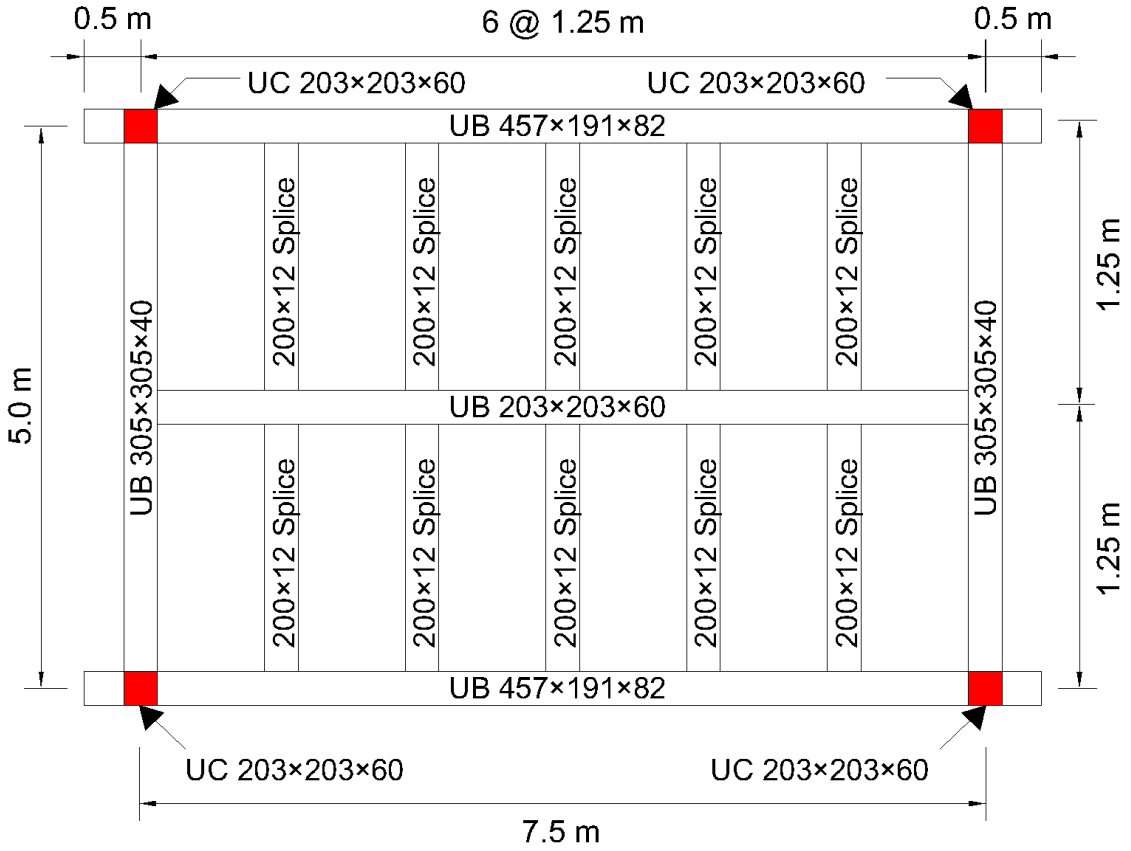

Figure 4.2: Key structural elements of Floor A. Red squares represent columns locations.

4.2.2.1 FRF measurements of the empty and occupied floor

The test grid corresponding to this floor comprises 21 TPs, as shown in Figure 4.4. Two APS400 shakers (APS Dynamics Inc., 2013) were placed at TP11 and

TP17, green dots in Figure 4.4, and 21 Honeywell QA750 accelerometers were placed at the test grid, as shown in Figure 4.4. The FRFs measurements were conducted when the floor was empty of occupants (Mohammed and Pavic, 2017). The test lasted approximately eight minutes, during which six data blocks, each lasting 80 s, were collected with a frequency resolution of 0.0125 Hz. Figure 4.3 shows one block of input force, related to the shaker at the midspan, and the corresponding vibration response measured at the same point.

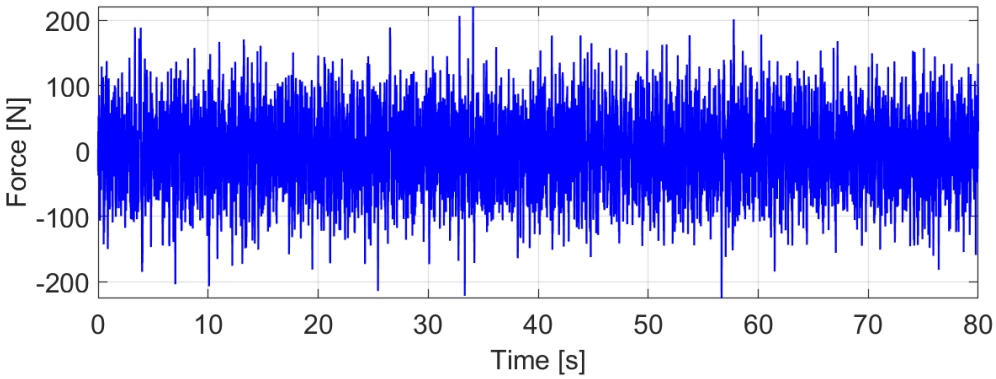

(a) Input force.

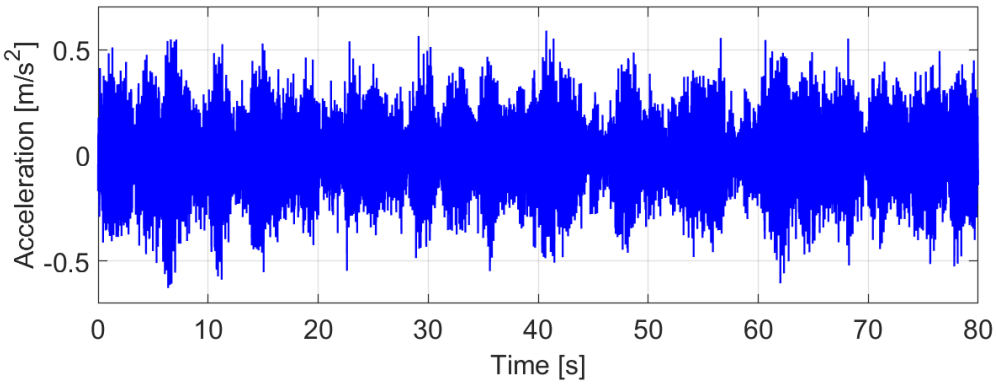

(b) Measured acceleration.

Figure 4.3: (a) Input force, related to the shaker at the midspan, and (b) the corresponding acceleration response measured at the same point.

The corresponding mode shapes of the lowest four vertical modes of vibration corresponding to the empty floor are shown in Figure 4.5.

Nominally identical measurements of the FRFs, as for the empty floor, were conducted when the floor was occupied by two (TSs 1 and 2), four (TSs 1-4) or

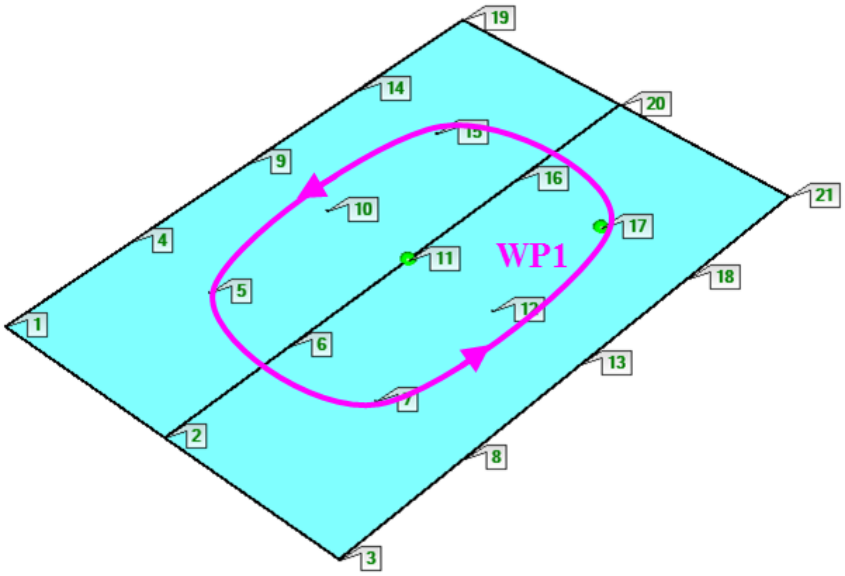

Figure 4.4: Test grid used for the FRF measurements of Floor A. Green dots represent shakers locations (TP11 and TP17).

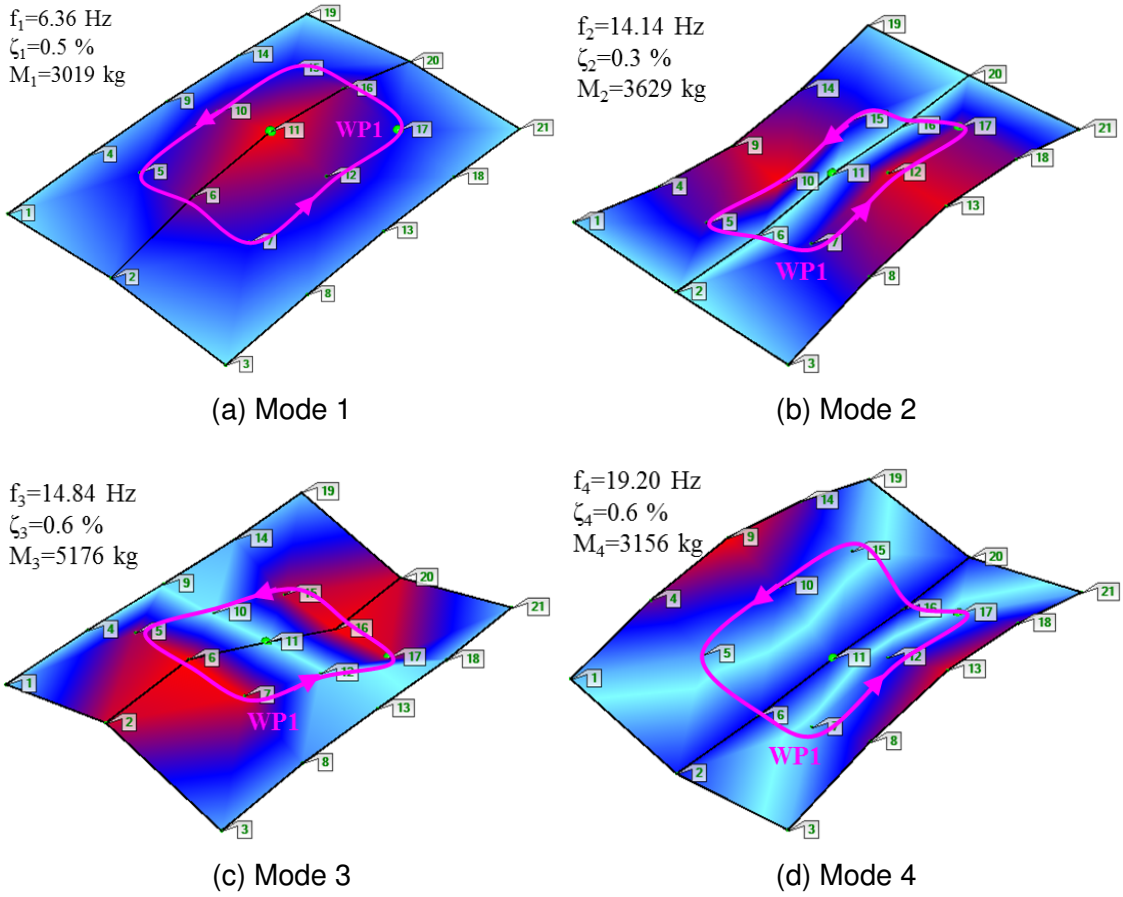

Figure 4.5: Mode shapes of the lowest four modes of vibration for Floor A when it was empty from occupants.

six (TSs 1-6) pedestrians walking on Floor A (Figure 4.6). These measurements were conducted immediately after the FRF measurement of the empty floor, so

the change in temperature is unlikely to influence the measurements. Each test was conducted once for each group size apart from the test which involved six TSs which was repeated twice to test the repeatability of such measurements, as explained below. Before each test, the occupants were asked to walk continuously in random walking paths on Floor A and avoid colliding with each other during. The aim of these tests was to study whether walking occupants have an effect on the FRF magnitude of the floor or not for various walking paths and scenarios, rather than targeting a walking path related to the highest influence of walking occupants on the FRF magnitude.

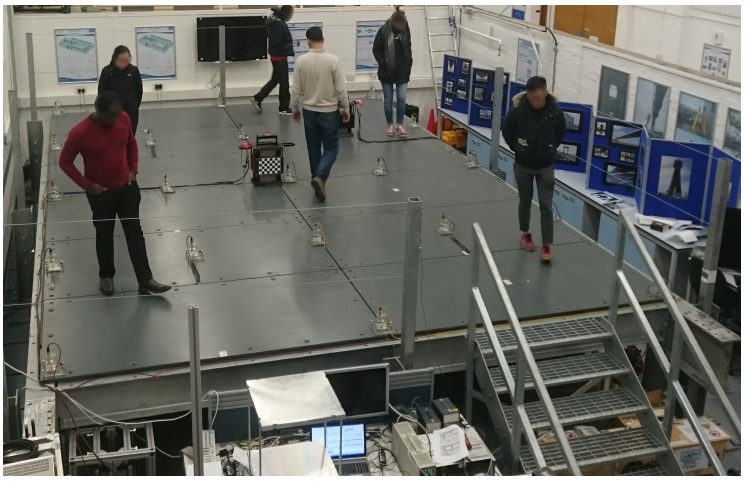

Figure 4.6: FRF measurement of Floor A when occupied by six pedestrians (Mohammed and Pavic, 2017).

It is worth mentioning that the input for the FRF measurements was only the shakers' forces, i.e. the moving masses of the shakers multiplied by their acceleration, while the footfall loading of the walking occupants was assumed to be a background noise that can be averaged out throughout the FRF measurements. This assumption was utilised previously by Živanović and Pavic (2009) while conducting similar measurements on a footbridge. The magnitude of the FRFs measured in this study is shown in Figure 4.7.

Figure 4.7a shows that there was a significant reduction in the FRF magnitude

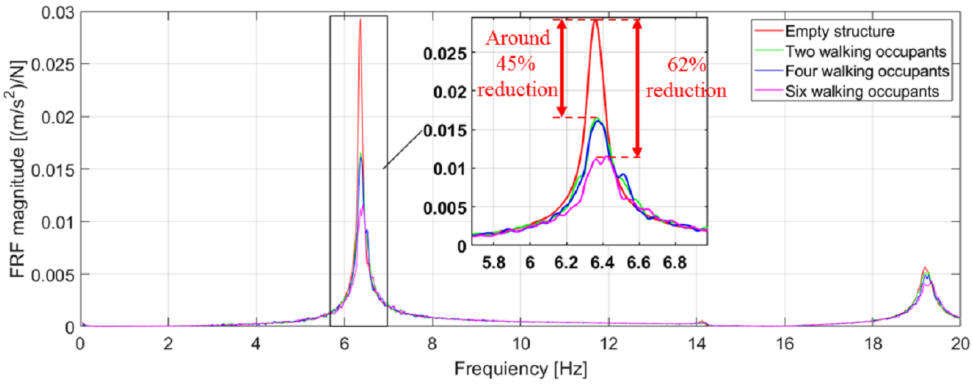

(a) TP11

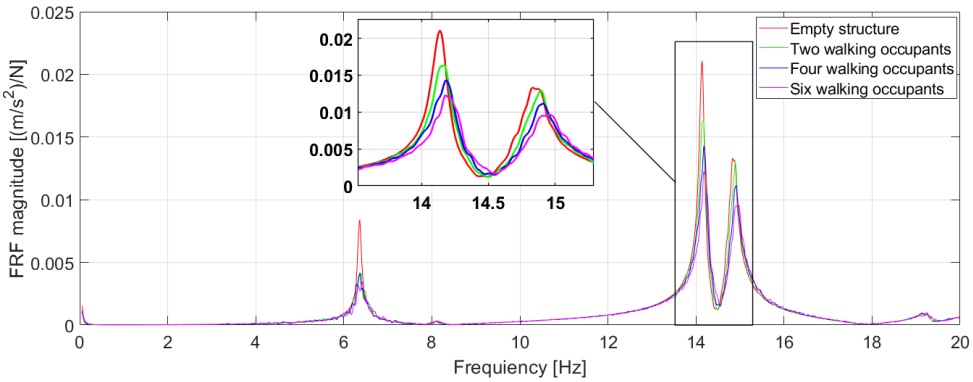

(b) TP17

Figure 4.7: FRF magnitude measured at (a) TP11 and (b) TP17 (Figure 4.4) on Floor A when it was empty and occupied by walking pedestrians.

at the fundamental frequency, i.e. up to around 50% reduction, even when only two pedestrians were walking on the floor. A slight increase of the fundamental frequency could also be noticed as the number of walking occupants increased (Figure 4.7b). Such an increment in fundamental frequency for structures occupied by walking individuals was also reported by Živanović and Pavic (2009), although the reason for such frequency increment is not clear. Interestingly, the reduction in FRF magnitude at the fundamental frequency was apparently similar when two and four pedestrians were walking on the floor. The reason for this could be explained by the random walking path followed by the walking pedestrians during each test and the corresponding mode shape amplitude for the first mode of vibration (Figure 4.5a). In essence, walking close to the edges of the floor could involve less interaction between the walking occupants and the

1st mode of the floor but more interaction between the occupants and the 2nd and 3rd modes (Figure 4.5).

To assess how repeating these tests can affect the measured FRF magnitude, the measurement related to six TSs were repeated twice, and the corresponding results are shown in Figure 4.8. This figure shows that while the FRF magnitude related to the two tests, when six TSs were walking on the floor, are not identical, they are quite similar, especially when they are compared to those related to the empty structure.

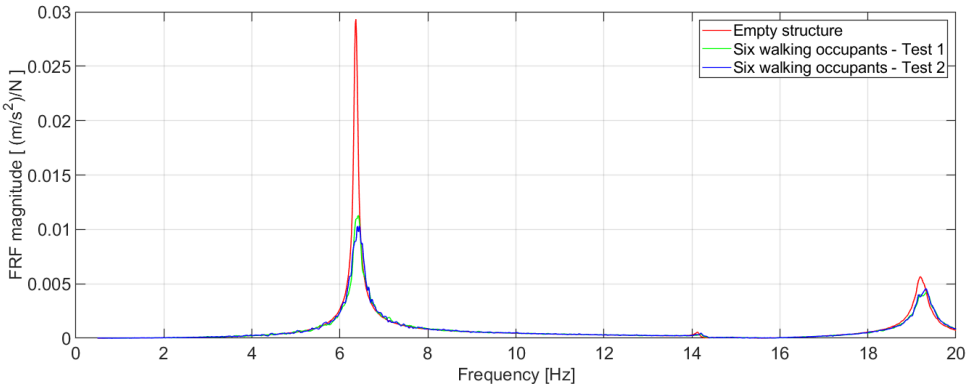

(a) TP11

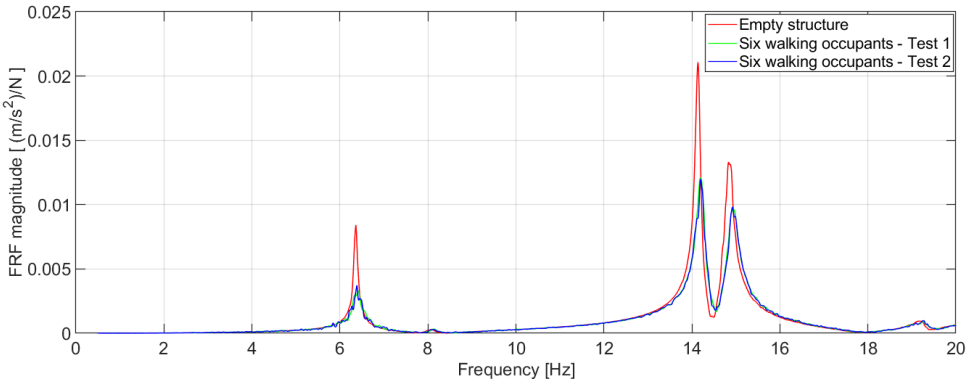

(b) TP17

Figure 4.8: FRF magnitude for two nominally identical tests related to six TSs walking on Floor A at (a) TP11 and (b) TP17 (Figure 4.4).

4.2.3 Floor B

Floor B is a full-scale prototype with a deck made of cross laminated timber (CLT). The floor, shown in Figure 4.9, was constructed for research purposes. The CLT

panels are supported by the lower flanges of two primary (longitudinal) and six secondary (transverse) beams covered by a raised floor (Figure 4.10). All primary and secondary beams, apart from the secondary beams at the two edges, feature web openings, as shown in Figure 4.10. All tests described in this chapter related to this floor were conducted by members of the Vibration Engineering Section (VES) at the University of Exeter for a separate project.

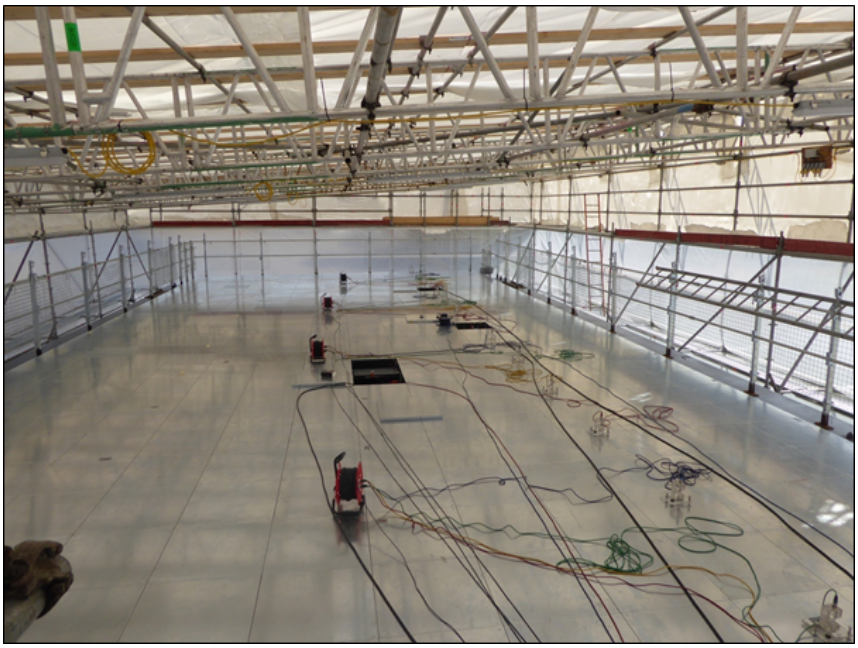

Figure 4.9: Overview of Floor B.

4.2.3.1 FRF measurements of the empty and occupied floor

Figure 4.11 shows the test grid used in the FRF measurements of the floor when it was empty. Four shakers - three APS400 (APS Dynamics Inc., 2013) and one APS113 (APS Dynamics Inc., 1996) shakers, located at TP3, TP33, TP62 and TP42, respectively (Figure 4.11) were used in the modal testing. The corresponding vertical acceleration at the test grid was measured using 16 Honeywell QA750 accelerometers in five 'swipes'. The measurements of the FRFs were conducted when the floor was empty. The test lasted less than seven minutes, during which 15 data blocks, each lasting 32 s, were collected

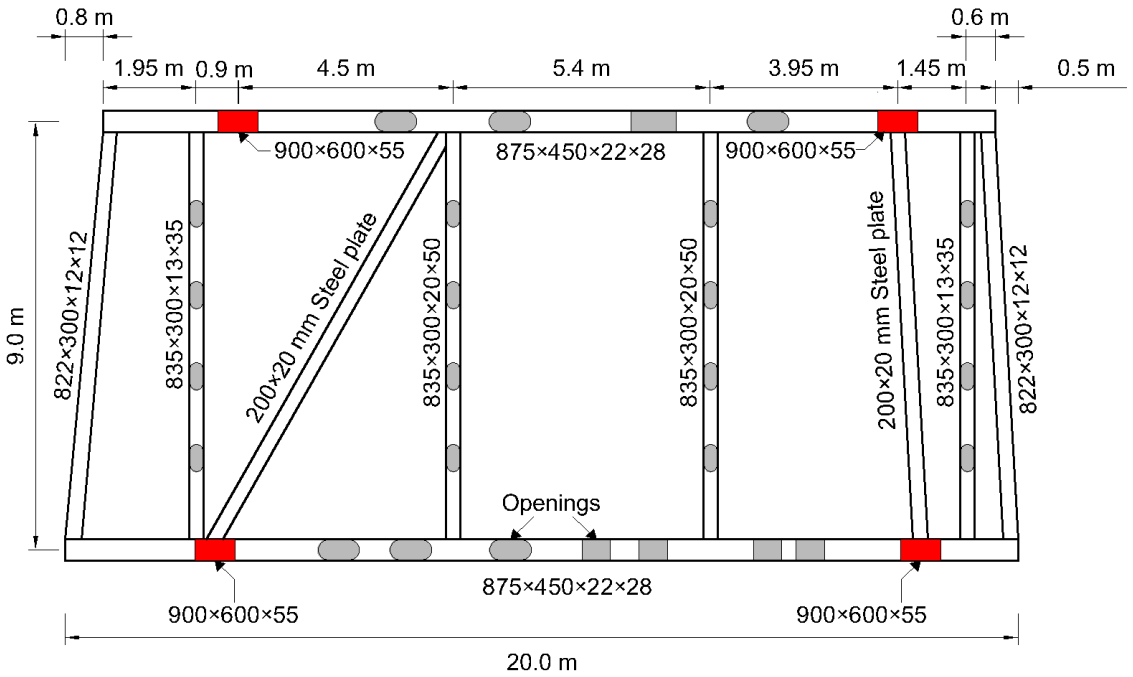

Figure 4.10: Key structural elements of Floor B. Red rectangles represent columns locations. The sections of the steel members are not standard, and their dimensions are shown in the figure.

with a frequency resolution of 0.03125 Hz. As the writer only has the FRFs regarding modal testing, the input force and measured acceleration time histories are not shown here. The mode shapes of the lowest four modes of vibration corresponding to an empty floor are presented in Figure 4.12.

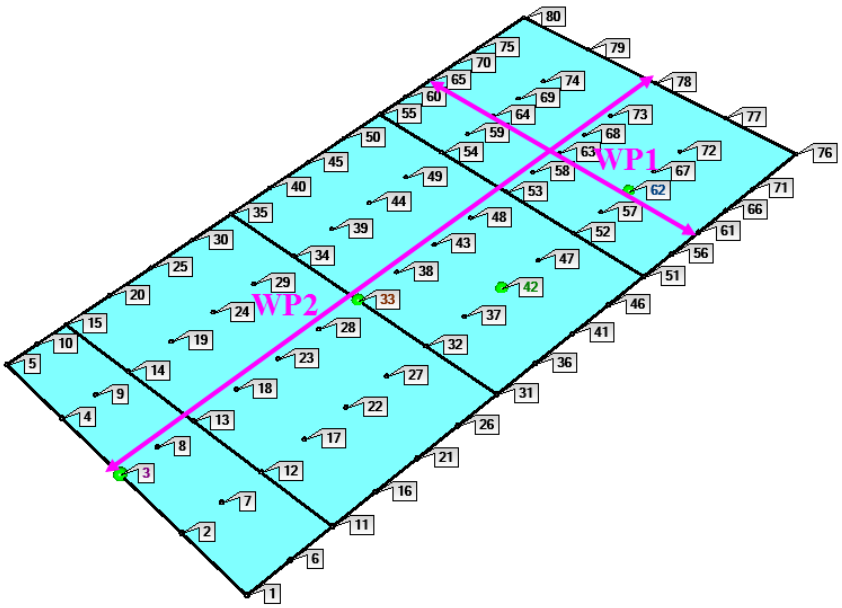

Figure 4.11: Test grid used for the FRF measurements of Floor B.

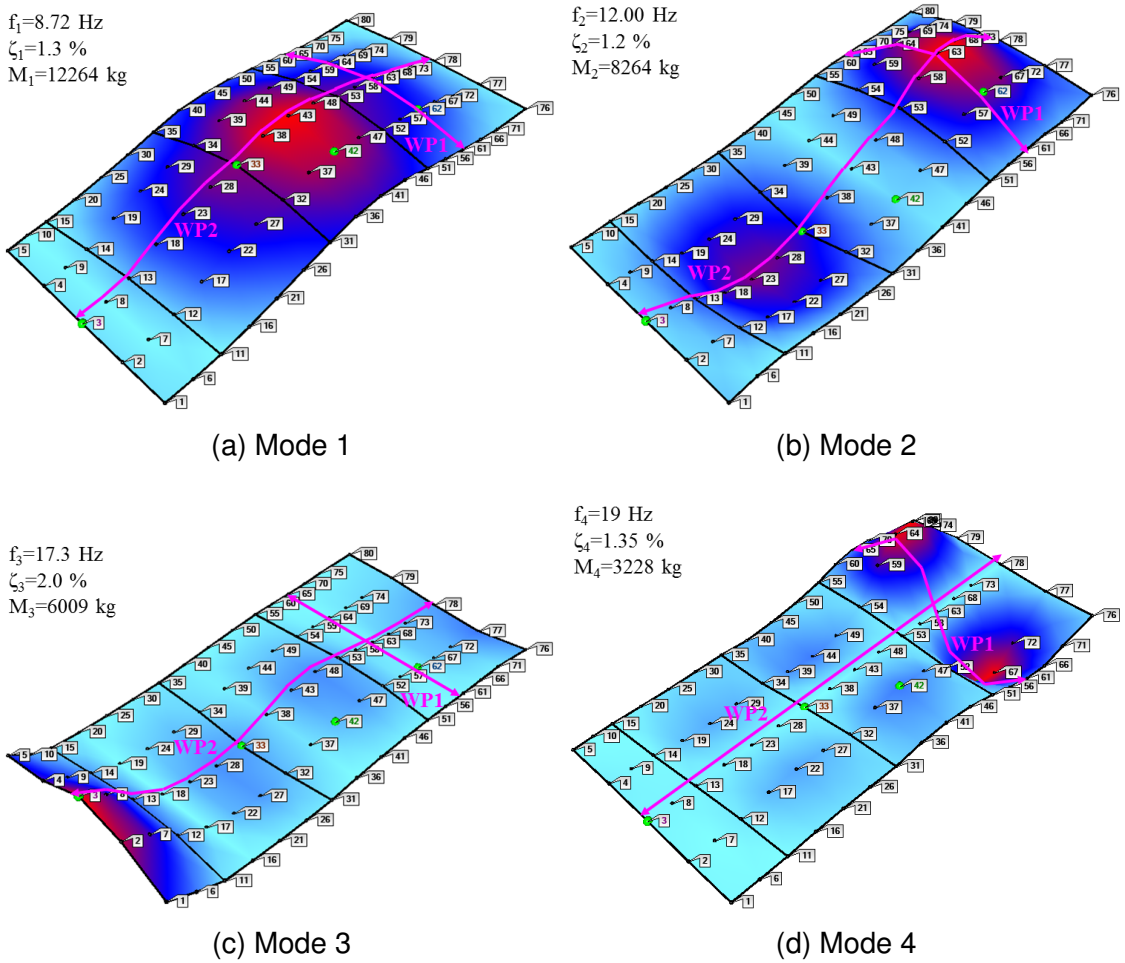

Figure 4.12: Mode shapes of the lowest four modes of vibration for Floor B when it was empty from occupants.

The 16 accelerometers were then placed at certain TPs, while the locations of the shakers were kept the same, to repeat the FRF measurements when the structure was empty and occupied by a single pedestrian walking along WP1 (Figure 4.13). As the tests conducted on this floor were for a different project, this walking path was chosen to investigate the effect of a walking individual on a mode of vibration with a frequency of 19.60 Hz, rather than for the lowest mode of vibration. However, the effects on the first mode was clear despite the non-critical walking path (Figure 4.14). Figure 4.14 shows the corresponding FRF magnitude measured at TP42 and TP62. A reduction in FRF magnitude of up to 20% can be observed at the fundamental frequency (Figure 4.14a) while no noticeable reduction can be observed at 19.60 Hz.

Figure 4.13: FRF measurement of Floor B when occupied by an individual walking along WP1 (Figure 4.11).

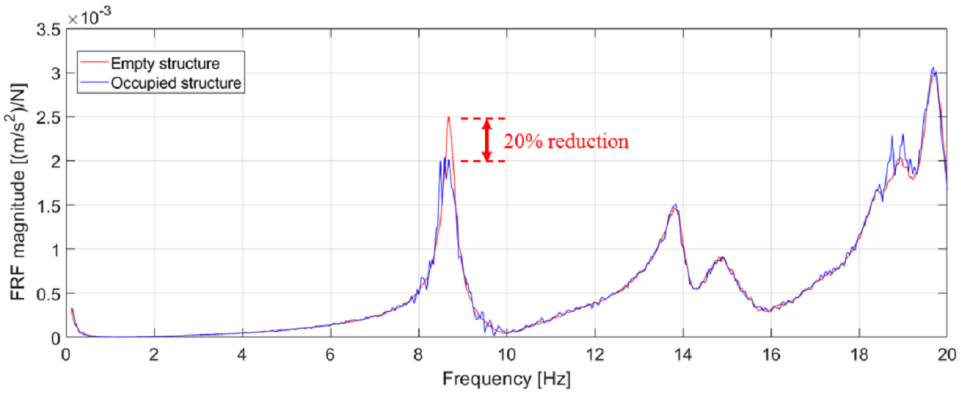

(a) TP42

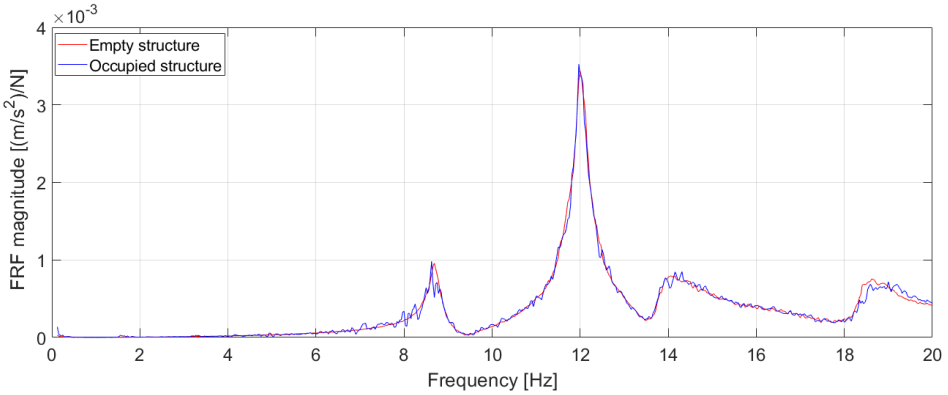

(b) TP62

Figure 4.14: FRF magnitude measured at (a) TP42 and (b) TP62 (Figure 4.11) on Floor B when it was empty and occupied by a pedestrian walking along WP1 (Figure 4.11).

Interestingly, there was no noticeable change in FRF magnitude at the frequency of the second mode of vibration, with f_n=12.0 Hz, despite the fact that the occupant was walking across the anti-node of that mode (Figure 4.14b).

4.2.4 Floor C

The floor, level 1 of the building shown in Figure 4.15, is a normal weight steel-concrete composite system, having 130 mm deck thickness, under construction. The floor was tested as a bare structure and before installing façade, raised floors, ceiling panels and other mechanical ducts. As the west and east wings of the first floor are almost identical, only the west wing was tested. Figure 4.16 shows the testing area and its corresponding key structural elements.

Figure 4.15: Panoramic view of the building containing Floor C. The testing area is in the far half of the first floor.

4.2.4.1 FRF measurements of the empty and occupied floor

The test grid used for modal testing of Floor C is shown in Figure 4.18. Three shakers - two APS400 (APS Dynamics Inc., 2013) and one APS113 (APS Dynamics Inc., 1996) shakers, were placed at TP24, TP42 and TP64, respectively, and 20 Honeywell QA750 accelerometers were used to measure the corresponding structural acceleration at the test grid in five ‘swipes‘ (Figure

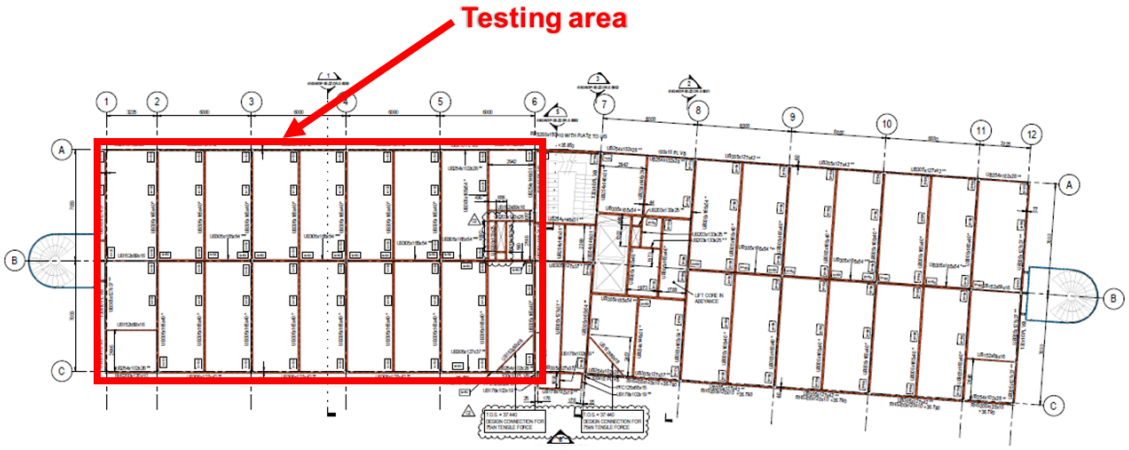

(a) Plan view of the first floor of the building and the testing area.

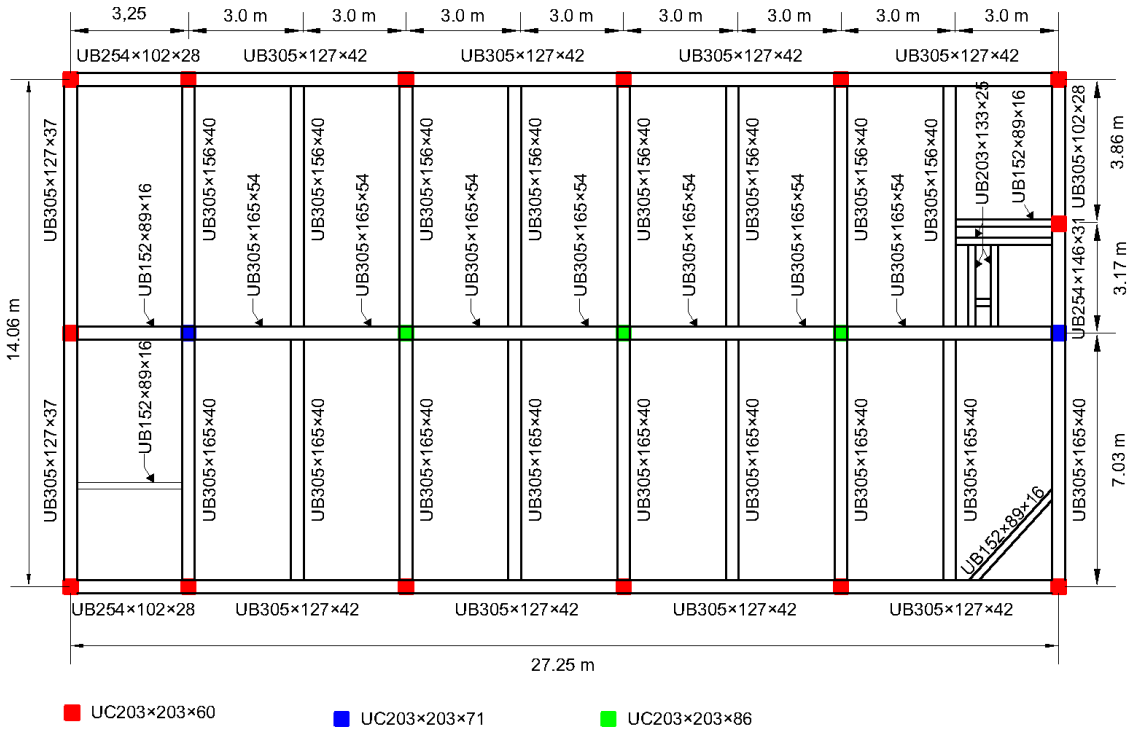

(b) Key structural elements in the testing area of Floor C.

Figure 4.16: (a) Testing area of Floor C and (b) the corresponding key structural elements. Red, blue and green squares refer to columns locations.

4.18). The measurements of the FRFs were conducted when the floor was empty. The test lasted about ten minutes, during which 20 data blocks, each lasting 40 s, were collected, and the corresponding frequency resolution was 0.025 Hz. Figure 4.17 shows one block of input force, related to the shaker at TP42, and the

corresponding vibration response measured at the same point.

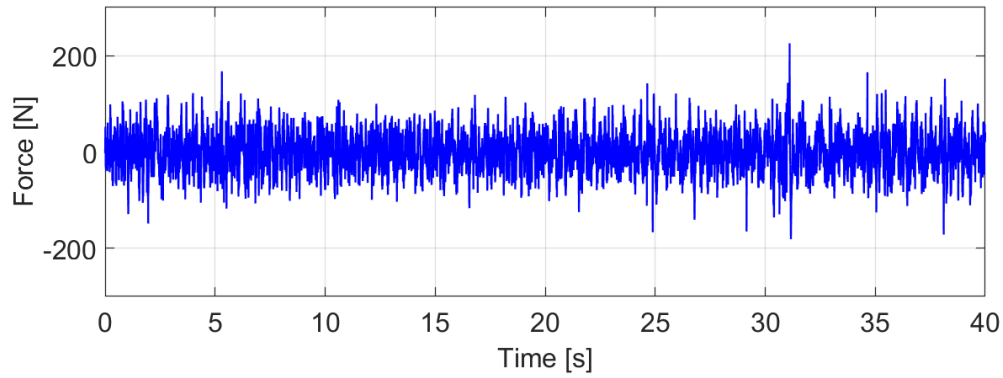

(a) Input force.

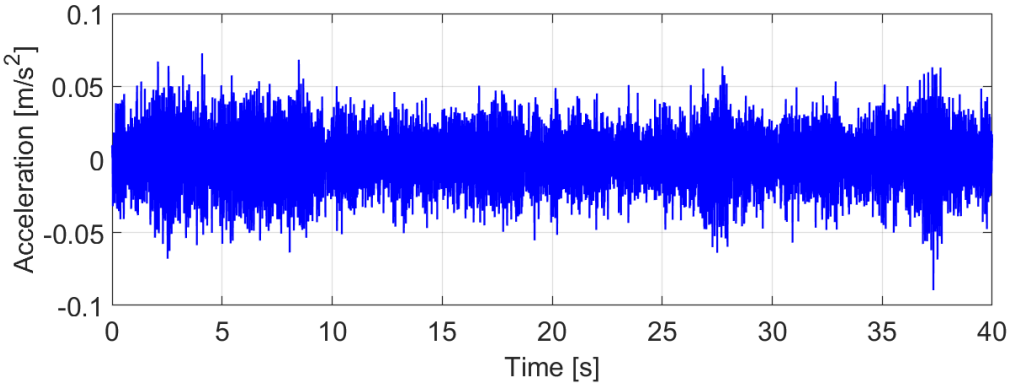

(b) Measured acceleration.

Figure 4.17: (a) Input force, related to the shaker at the TP42, and (b) the corresponding acceleration response measured at the same point.

The corresponding mode shapes of the lowest four modes of vibration corresponding to an empty floor are shown in Figure 4.19.

To measure the FRF corresponding to an empty and an occupied floor, one accelerometer and the three shakers were placed at TP44, i.e. the anti-node of the first, third and fourth modes of vibration. This test setup was made to maximise the excitation energy applied to these modes. A swept sine excitation with a frequency spanning between 8 Hz and 11 Hz, which covers the range of frequencies of the lowest four modes of vibration (Figure 4.19), was used to run the correlated shakers. Each test lasted about five minutes, during which 10 data blocks, each lasting 40 s, were collected with frequency resolution of 0.025 Hz.

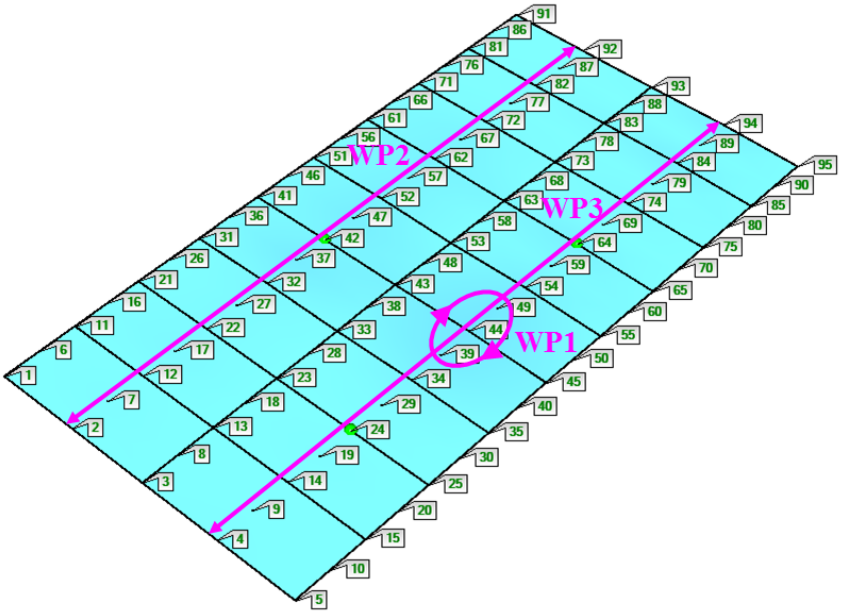

Figure 4.18: Test grid used for modal testing of Floor C.

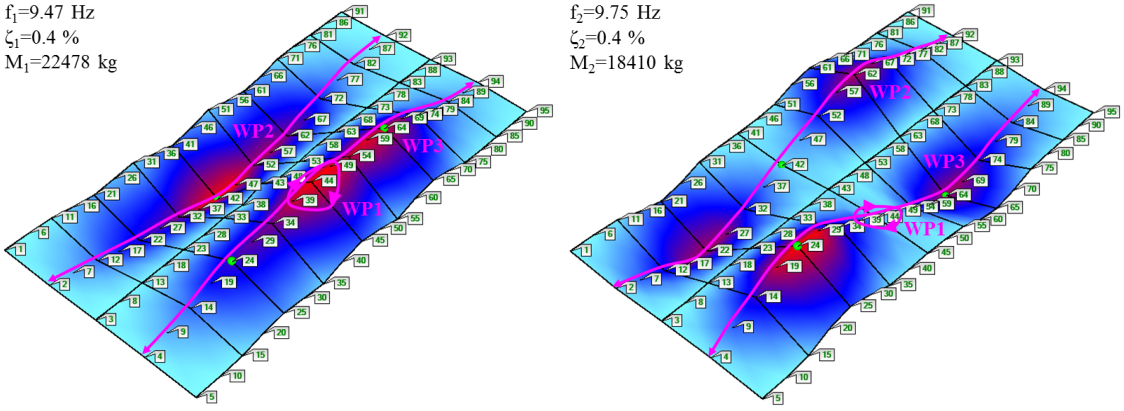

(a) Mode 1

(b) Mode 2

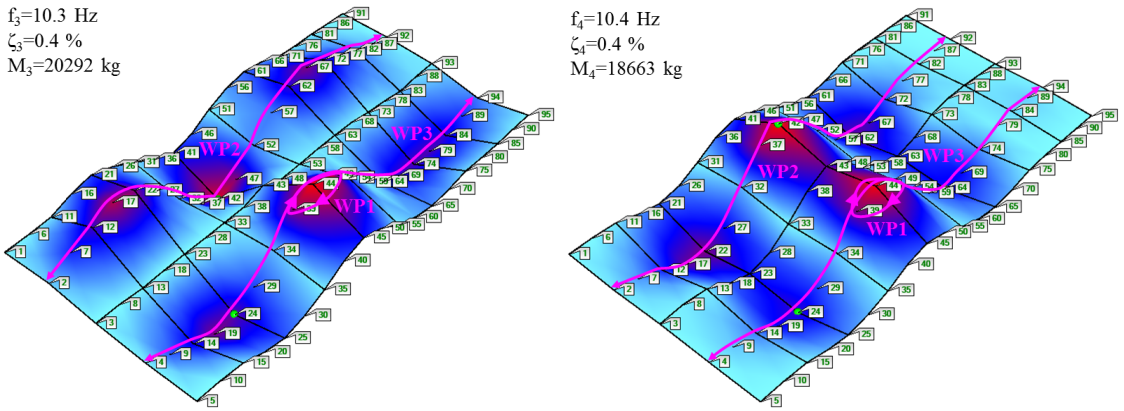

(c) Mode 3

(d) Mode 4

Figure 4.19: Mode shapes of the lowest four modes of vibration for Floor C when it was empty from occupants.

The FRFs were measured three times, during which the testing area was empty and occupied by six pedestrians walking along two WPs (Figure 4.20). In the first test (Figure 4.20a), the pedestrians were walking along a circular walking path around the shakers, i.e. WP1, while in the second test, shown in Figure 4.20b, they were walking along WP2 and WP3 in two groups. These walking paths were chosen to maximise the energy applied on the dominant modes of vibration as it is expected that the influence of walking individuals on the FRF magnitude is small due to the relatively high modal masses and natural frequencies of the floor. This is the reason that these walking paths were chosen differently to those utilised for Floor A.

(a) Six pedestrians walking in a circular path on WP1.

(b) Six pedestrians walking across WP2 and WP3 in two groups.

Figure 4.20: FRF measurement of Floor C (at TP44) when occupied by six pedestrians walking (a) on WP1 or (b) along WP2 and WP3 (Figure 4.18).

Figure 4.21 shows the FRF magnitude at TP44 when the testing area was empty and when it was occupied by the walking pedestrians. The reduction in FRF magnitude at the fundamental frequency, 9.47 Hz, was approximately 10% and 22% when the pedestrians were walking along WP1 and when they were walking along WP2 and WP3, respectively, compared to when the testing area was empty (Figure 4.21).

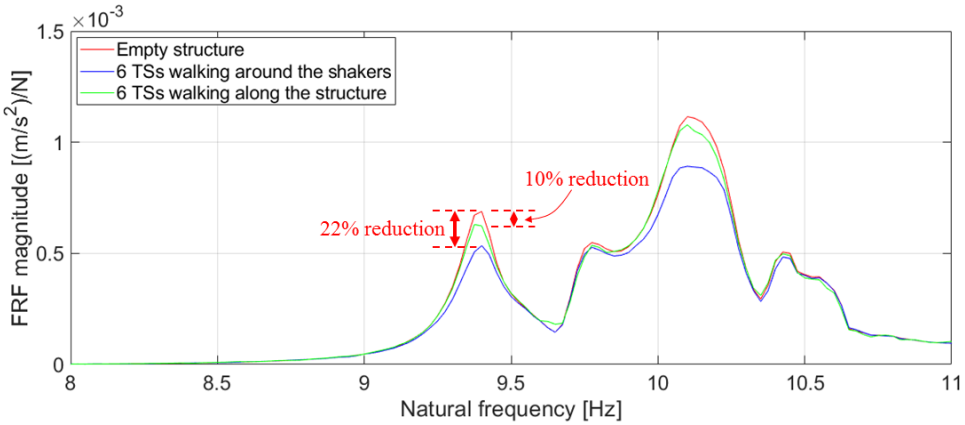

Figure 4.21: FRF magnitude at TP44 on Floor C when it was empty and occupied by six walking pedestrians (Figure 4.20).

4.2.5 Discussion

Table 4.1 summarises the approximate reductions in FRF magnitudes at the fundamental frequency of the three floors when occupied by walking pedestrians compared to those when the floors were empty. The results summarised in Table 4.1 show that the influence of HSI on the FRF magnitude of floors varies between different types of floor systems. The highest reduction in FRF magnitude at the fundamental frequency was noticed for Floor A, i.e. 62%, (Table 4.1).

Table 4.1: Reduction in FRF magnitude at the fundamental frequency of three floors when occupied by walking pedestrians.

Floor	Fundamental frequency [Hz]	No. of pedestrians	Mode of walking	Reduction in FRF magnitude at fundamental frequency [%]
Floor A	6.36	2	Random	44
		4	Random	46
		6	Random	62
Floor B	8.72	1	Along WP1 (Figure 4.12a)	20
Floor C	9.47	6	Along WP1 (Figure 4.19a)	22
			Along WP2 and WP3 (Figure 4.19a)	10

For floor B, the WP followed by the pedestrian was relatively far from the anti-node of the first mode of vibration (Figure 4.12a). It is expected that an even higher

reduction in the FRFs at fundamental frequency would occur if the occupant was walking closer to the anti-node of the lowest mode of vibration, i.e. across WP2 as shown in Figure 4.12a. However, it is clear that there is no such obvious reduction in the FRF magnitude at the second mode of vibration, despite the fact that the pedestrian was walking across its anti-node (Figure 4.12b). Such reduction was not observed for higher modes of vibration and this indicates that the HSI phenomenon during walking could be frequency limited.

Floor C had a limited influence of walking pedestrians on its FRF magnitude at the fundamental frequency despite the fact that the six pedestrians were walking close to its anti-node. This could be related to its relatively high fundamental frequency and modal mass compared to that for Floor A and Floor B.

Despite having different configurations and number of pedestrians to quantify the effect of HSI on the three floors, certain trends can be observed. It is apparent that the reduction in the FRF magnitude at fundamental frequency is higher for floors with lower natural frequency and modal mass. It is not obvious whether the same trend applies to modal damping ratios as the lowest modes for Floor A and Floor C have similar modal damping ratios. A higher reduction was also noticed when a higher number of pedestrians were walking on the floor (Table 4.1). The reduction in the FRF magnitude at fundamental frequency for Floor A was 62% when the floor was occupied by six pedestrians, compared to 44% when it was occupied by two pedestrians. Hence, it is apparent that the reduction in the magnitude of the FRFs depends on the modal properties of the floor and the number of walking occupants. This reduction in FRF magnitude can result in a significant reduction in the corresponding human-induced vibration of floors. Interestingly, the reduction in the FRF magnitude is comparable to that reported

by other studies conducted on footbridges (Shahabpoor, 2014; Živanović and Pavic, 2009). For example, Živanović and Pavic (2009) reported around around 25%, 50% and 55% reduction in the FRF magnitude of the fundamental frequency of a footbridge when two, four or six pedestrians, respectively, were walking along the footbridge (Živanović and Pavic, 2009). Therefore, the next section describes a methodology to consider HSI in the calculation of footfall-induced vibration specifically of floors.

4.3 Methodology

In this section, a revised methodology to consider HSI between walking pedestrians and building floors in the calculation of human-induced vibration is proposed. An overview of the methodology is presented, followed by a description of how it is derived before explaining its implementation.

4.3.1 Overview

When a pedestrian walks on a flexible structure, the corresponding acceleration of the structure can be transmitted to their body and results in an interaction force which is applied back to the structure (Figure 4.22) (Bocian et al., 2013; Dang, 2014). This 'exchange' of structural acceleration and interaction force between the structure and a walking occupant form the HSI, and its influence on vibration levels increases for high human-to-structure mass ratio (Ahmadi et al., 2018). Its effect is equivalent to the modification of the modal properties or FRF of the structure, as reported in the literature (Van Nimmen et al., 2016). In essence, the modal properties of the occupied structure can be considered the same as that for an empty structure if structural acceleration and the corresponding interaction

force exchanged between the structure and a walking occupant are addressed adequately. This is the basis of the currently available HSI models where MSDs, related to the whole-body dominant mode of vibration for an individual walker, are used to simulate the interaction between walking individuals and the supporting structures.

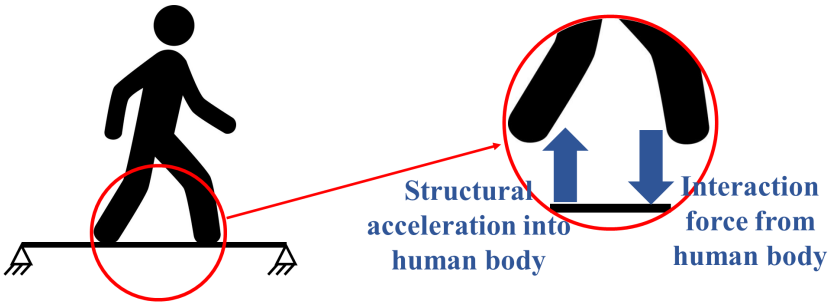

Figure 4.22: 'Exchange' of structural acceleration and interaction force between a walking pedestrian and a supporting structure.

It is worth mentioning that vibration of structures also affects the gait of individual walkers as they try to adapt to structural motion during walking (Bocian et al., 2013; Ahmadi et al., 2018). However, Dang and Živanović (2016) showed that the influence of the vibrating structure on the kinematics of the walker increases for high structural vibration levels. Hence, this study assumes that vibration levels of floor structures are generally not high enough, as for footbridges, for example, to significantly alter the gait of the walker. Furthermore, this study assumes that the influence of the structural acceleration transmitted to the walker and the corresponding interaction force, on the vibration response, is equivalent to that related to the H2S and S2H components of HSI (Ahmadi et al., 2019).

In this study, the dynamics of walking individuals were simulated using experimentally-based transfer functions which represent the dynamics of the walker over a range of frequencies, 1-10 Hz, instead of using a MSD as for the models reported in the literature. These transfer functions were used to calculate

the structural acceleration and the corresponding interaction force.

Previous studies showed that the vertical acceleration of the 7th cervical vertebrae (C7) is well correlated with the corresponding GRF (Bocian et al., 2016; Shahabpoor and Pavic, 2018). Hence, the proposed HSI methodology assumes that human body mass can be treated as a concentrated mass at the location of C7. The elements of the proposed HSI model are (Figure 4.23):

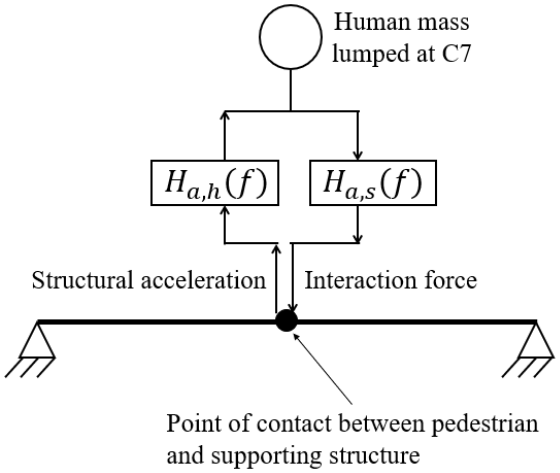

Figure 4.23: Components of the proposed HSI model.

- A single mass representing the mass of a human body,
- The supporting structure,
- A function, $H_{a,h}(f_i)$, to calculate the vertical acceleration of the human body mass from structural acceleration, where a refers to the relative acceleration between human body mass and the structure at the point of contact between them, h refers to the human body mass and f_i is the frequency of mode i related to an empty structure [Hz], and
- A function, $H_{a,s}(f_i)$, to calculate the interaction force, applied on the structure, from the relative vertical acceleration (a) between human body mass and the structure at the point of contact between them, where s

denotes the structure.

A detailed description of $H_{a,h}(f_i)$, $H_{a,s}(f_i)$ and the implementation of the proposed HSI methodology is presented below. Furthermore, the proposed methodology presented in this section assumes linear behaviour for both of human dynamics and structural dynamics.

4.3.2 Acceleration of human body mass

Following the principle of superposition, GRF related to an individual walking on a flexible structure can be treated as a summation of two components, as shown in Figure 4.24 (Van Nimmen et al., 2016; Shahabpoor et al., 2017a):

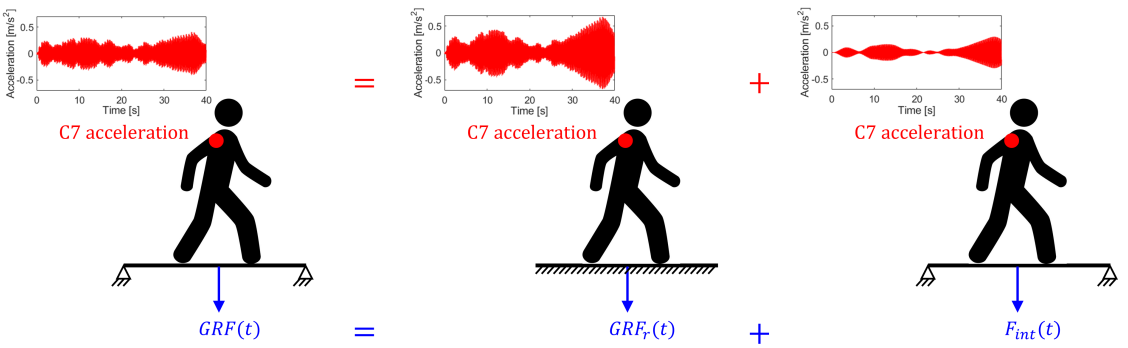

Figure 4.24: Schematic representation of C7 acceleration and the corresponding ground reaction force for an individual walking on a flexible structure.

- Ground reaction force component, related to walking on a *rigid* surface, $GRF_r(t)$, where r denotes a rigid surface and t is time, and
- Interaction force between the walking individual and the structure ($F_{int}(t)$), where int denotes the interaction term.

Similarly, this study assumes that the acceleration of human body mass has two components:

- Acceleration related to walking on a rigid surface, $GRF_r(t)$, (Figure 4.24)

caused by the desire of the pedestrian to walk, and

- Acceleration caused by vibration of the supporting surface which corresponds to the interaction force, $F_{int}(t)$) Figure 4.24).

The former component of acceleration is implicitly taken into account in $GRF_r(t)$ while the later is calculated as described in the rest of this subsection. It is worth mentioning that the proposed method assumes that $GRF_r(t)$ does not change for individuals walking on floor structures.

Matsumoto and Griffin (1998) measured the transmissibility of vertical acceleration between a vibrating platform and the 4th lumbar vertebrae (L4) for 12 individual test subjects *standing* on it. They described the transmissibility mathematically as in Equation 4.1.

$$H_{a,h}(f) = S_{sl}(f)/S_{ss}(f) \quad , \tag{4.1}$$

where, $H_{a,h}(f)$ is the transmissibility at frequency f, $S_{sl}(f)$, in [(m/s^2)^2/Hz], is the cross spectral density between vertical acceleration of the supporting surface, i.e. platform, and vertical acceleration of L4, where, s and l denote the supporting surface and L4, respectively. $S_{ss}(f)$, in [(m/s^2)^2/Hz], is the power spectral density of the vertical acceleration of the supporting surface.

Power spectral density, $S_{ss}(f)$, is the Fourier transform of the auto-correlation function, $R_{ss}(\tau)$ of the acceleration at the supporting surface, $s(t)$, as mathematically described in Equations 4.2 and 4.3. $S_{ss}(f)$ describes how the power of a signal is distributed in the frequency domain (McConnell and Varoto, 2008).

$$S_{ss}(f) = \frac{1}{2\pi} \int_{-\infty}^{\infty} R_{ss}(\tau)\ e^{-j\,2\pi f\,\tau}\ d\tau \quad , \tag{4.2}$$

$$R_{ss}(\tau) = \mathbf{E}[s(t)\ s(t+\tau)] \quad , \tag{4.3}$$

where, τ is time lag.

Cross spectral density, $S_{sl}(f)$, is the Fourier transform of the cross-correlation, $R_{sl}(\tau)$, between $s(t)$ and $l(t)$, where, $l(t)$ is the acceleration at L4. $S_{sl}(f)$ can be mathematically described in Equations 4.4 and 4.5 (McConnell and Varoto, 2008).

$$S_{sl}(f) = \frac{1}{2\pi} \int_{-\infty}^{\infty} R_{sl}(\tau)\ e^{-j\,2\pi f\,\tau}\ d\tau \quad , \tag{4.4}$$

$$R_{sl}(\tau) = \mathbf{E}[s(t)\ l(t+\tau)] \quad , \tag{4.5}$$

Figure 4.25 shows the transmissibility magnitude and its corresponding phase for the 12 test subjects, as presented by Matsumoto and Griffin (1998). In this study, the median transmissibility magnitude and phase were calculated at each frequency and elaborated in the same figure, i.e. Figure 4.25, in red. As the data in Figure 4.25 correspond to an even number of test subjects, i.e. 12, the median can be obtained by sorting the values related to each frequency in ascending order and calculating the average of the two values in the middle. The advantage of using the median, instead of the total average, is that it does not significantly change with extreme values of some of the data, i.e. outliers.

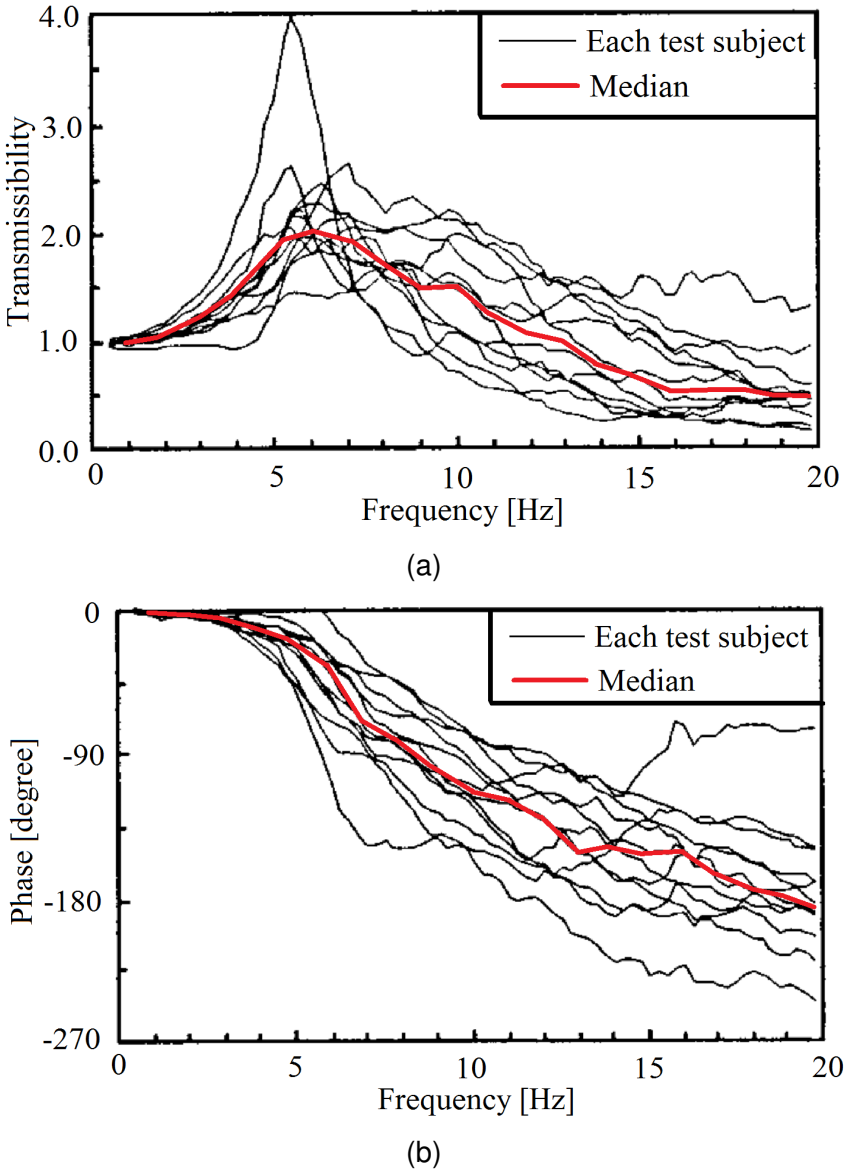

Figure 4.25: (a) Transmissibility magnitude of vertical acceleration between the vibrating platform and the L4 and (b) the corresponding phase lag for 12 standing test subjects (Matsumoto and Griffin, 1998).

Our study utilises the above mentioned transmissibility, $H_{a,h}(f)$, to calculate the acceleration at C7, instead of L4, of walking, instead of standing, individuals. These assumptions were made due to the lack of similar data related to C7 and walking individuals. If such measurements become available in the future, they can improve the proposed HSI model. However, Hagena et al. (1985) showed that vertical transmissiblity between the scrum and both C7 and L4 of standing people are relatively close. Furthermore, Shahabpoor and Pavic (2018) showed that there is a strong correlation between the acceleration measured at both C7

and the 5th lumbar vertebra (L5), which is located next to the L4. Hence, this study suggests that the acceleration of human body mass can be calculated as follows:

- Calculate *modal* acceleration of the structure, $a_{m,i}(t)$, for mode i and corresponding to $GRF_r(t)$ at time step t, where m denotes the modal acceleration and r for rigid surface.

- Calculate the contribution of mode i to the physical response, $a_{p,i}(t)$, using Equation 4.6, where p denotes the *physical* response.

$$a_{p,i}(t) = \Phi_i(v_p.t) \quad a_{m,i}(t) \quad , \tag{4.6}$$

  where, $\Phi_i(v.t)$ is the mode shape amplitude of mode i at a location of a moving pedestrian walking at a constant speed v_p [m/s] at time t.

- The acceleration of human body mass at C7, related to mode i, i.e. $a_{h,i}(t)$), can be obtained after calculating the impulse response function, $h_{a,h}(t)$, related to $H_{a,h}(f)$, as mathematically described in Equations 4.7 and 4.8 (McConnell and Varoto, 2008).

$$a_{h,i}(t) = \int_{-\infty}^{\infty} a_{p,i}(\tau) \;\; h_{a,h}(t-\tau) \;\; d\tau \quad , \tag{4.7}$$

$$h_{a,h}(t) = \frac{1}{2\pi} \quad \int_{-\infty}^{\infty} H_{a,h}(f) \;\; e^{j\,2\pi f\,t} \;\; df \quad , \tag{4.8}$$

  where, τ is the time step of the integration.

  The impulse response function, $h_{a,h}(t)$, describes the response of a system,

$H_{a,h}(f)$, in the time domain. Hence, there is no need to convert to the frequency domain.

4.3.3 Interaction force

In this section, the calculation of the interaction force applied by a walking pedestrian on the supporting structure is described. This interaction force was assumed to be a function of the relative vertical acceleration between human body mass and the supporting structure at the point of contact between them, as shown in Figure 4.23. This function, $H_{a,s}(f)$, was derived by utilising previously conducted measurements (Bocian et al., 2016) of vertical acceleration of:

- human body at C7, and three other locations on human body not utilised in this study (Bocian et al., 2016), using inertial measurement units (IMUs), and,
- the corresponding ground reaction force, for individuals walking on an instrumented treadmill.

This work was inspired by previous studies which linked between the acceleration of human body and the corresponding GRF (Toso et al., 2015; Shahabpoor and Pavic, 2018).

Figure 4.26 shows test configurations for one test subject (TS). Each TS performed at least eight minutes of walking on the treadmill as a 'warm up' before conducting the tests. Six walking tests, at the constant speed of the treadmill belt, between 0.6 m/s and 1.4 m/s, were carried out by each TS. The duration of each test was about three minutes. A detailed description of the experiments is available elsewhere (Bocian et al., 2016).

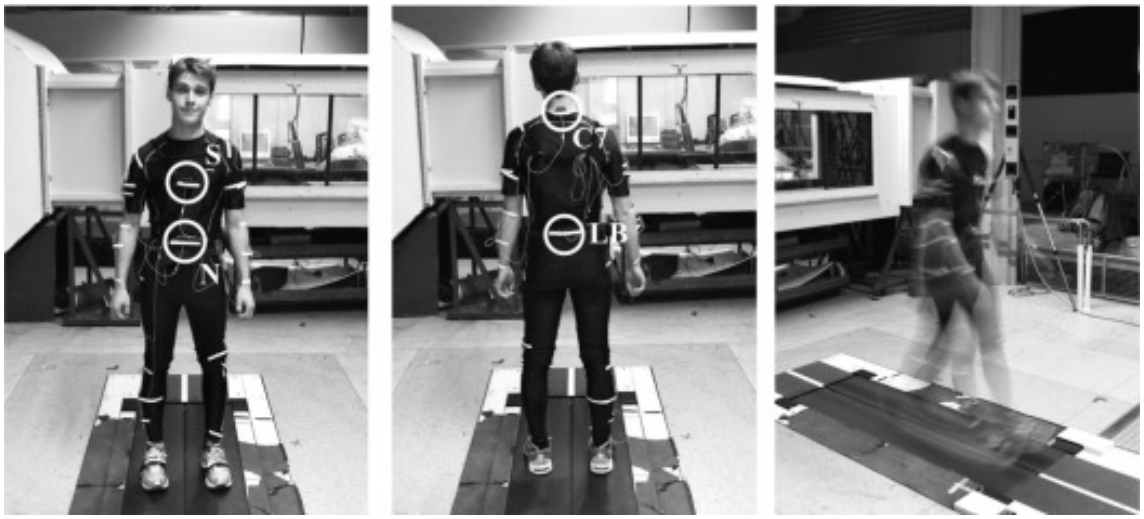

Figure 4.26: Test configurations showing the location of the IMUs (Bocian et al., 2016).

In the analysis described in this section, only two minutes of measurements, taken at the middle of each measurement, corresponding to five TSs, were considered. Figure 4.27 shows one measured time history of vertical acceleration at C7 and the corresponding ground reaction force for one TS.

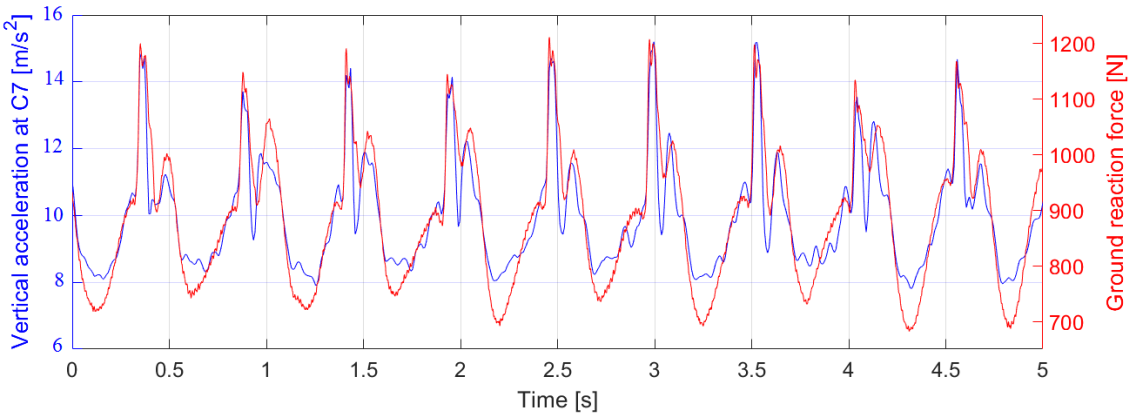

Figure 4.27: Sample of vertical acceleration measured at C7 and the corresponding GRF for one test subject while walking at a pacing frequency of 1.9 Hz.

A system identification process was carried out to derive a transfer function, $H_{a,s}(f)$, between vertical acceleration at C7 and the corresponding ground reaction force as an input and output for $H_{a,s}(f)$, respectively. Both signals were passband filtered between 1-10 Hz. This range of frequencies was chosen because of two reasons: firstly, it covers the range of fundamental frequency

for most floors, and therefore, the transfer functions and the proposed model can be used for such floors. Secondly, the signal-to-noise ratio at this range of frequencies is higher than that at higher frequencies due to the relatively strong harmonics at integer multiples of pacing frequencies (Živanović and Pavic, 2009). The ground reaction forces were also normalised by the corresponding human body weight. To simplify the identification process, $H_{a,s}(f)$ corresponding to each test subject was assumed to be independent from the walking speed. Hence, one $H_{a,s}(f)$ was derived for each TS, as explained below.

The form of the transfer function was obtained by increasing the number of parameters, in the numerator and denominator, gradually from 1 to 10. The fitting process was performed for each case as explained below. The transfer function form, related to the minimum error, i.e. objective function, is described in Equation 4.9.

$$H_{a,s}(f) = \frac{P_1(j\omega)^6 + P_2(j\omega)^5 + P_3(j\omega)^4 + P_4(j\omega)^3 + P_5(j\omega)^2 + P_6(j\omega)^1 + P_7}{P_8(j\omega)^6 + P_9(j\omega)^5 + P_{10}(j\omega)^4 + P_{11}(j\omega)^3 + P_{12}(j\omega)^2 + P_{13}(j\omega)^1 + P_{14}} \quad , \tag{4.9}$$

where, $\omega = 2\pi f$ is the angular frequency, in [rad/s] and $P_{1,2,...,14}$ are the constants to be obtained in the system identification by minimising the objective function described in Equation 4.10, based on the Non-linear Least Squares method.

$$E = \sum_{n=1}^{6} \sum_{t_i=0}^{T} (F_m(t_i, n) - F_s(t_i, n))^2 \quad , \tag{4.10}$$

where, E is a scalar value to be minimised, n refers to each walking test conducted by a TS, t_i is time step, T is the time duration of the signal, $F_m(t_i, n)$

is the measured ground reaction force at time step t_i for walking test n. $F_s(t_i, n))$ is the simulated ground reaction force at time step t_i for walking test n, which can be obtained by simulating the discrete-time response of the transfer function, $H_{a,s}(f)$, when subjected to an input signal, i.e. measured vertical acceleration at C7, (Gopalan, 2012). The transfer functions, $H_{a,s}(f)$, corresponding to the fitted parameters are shown in Figure 4.28.

Interestingly, the frequency of the first peak in the magnitude of $H_{a,s}(f)$ (Figure 4.28) is around 3-3.5 Hz which is within the range of frequency reported in the literature for walking individuals, i.e. 2-4 Hz, (Caprani et al., 2011; da Silva and Pimentel, 2011; Van Nimmen et al., 2015; Shahabpoor et al., 2016a). The second and third peaks, at around 7-7.5 Hz and 9.5-10 Hz, respectively, could refer to possible whole-body modes of vibration for walking individuals at these frequency ranges. It is worth mentioning that an attempt was made to fit individual peaks, in the transfer functions shown in Figure 4.28, as individual SDOF oscillators but it was challenging to obtain good fits, indicating that utilising a more complex multi-degree-of-freedom (MDOF) system might be more convenient to fit them. However, the HSI model presented in this study utilises these transfer functions directly to simulate HSI, eliminating the need to fit them into approximate SDOF or MDOF models.

To verify the applicability of the derived transfer function, one $H_{a,s}(f)$ was utilised to simulate the ground reaction force by using the acceleration measured at C7 as an input to $H_{a,s}(f)$. Figure 4.29 shows that the simulated ground reaction force is quite comparable to its measured counterpart on the treadmill. For comparison, Bocian et al. (2016) generated GRF of walking individuals using their body mass and the vertical acceleration at C7 on their body. They showed that the dynamic

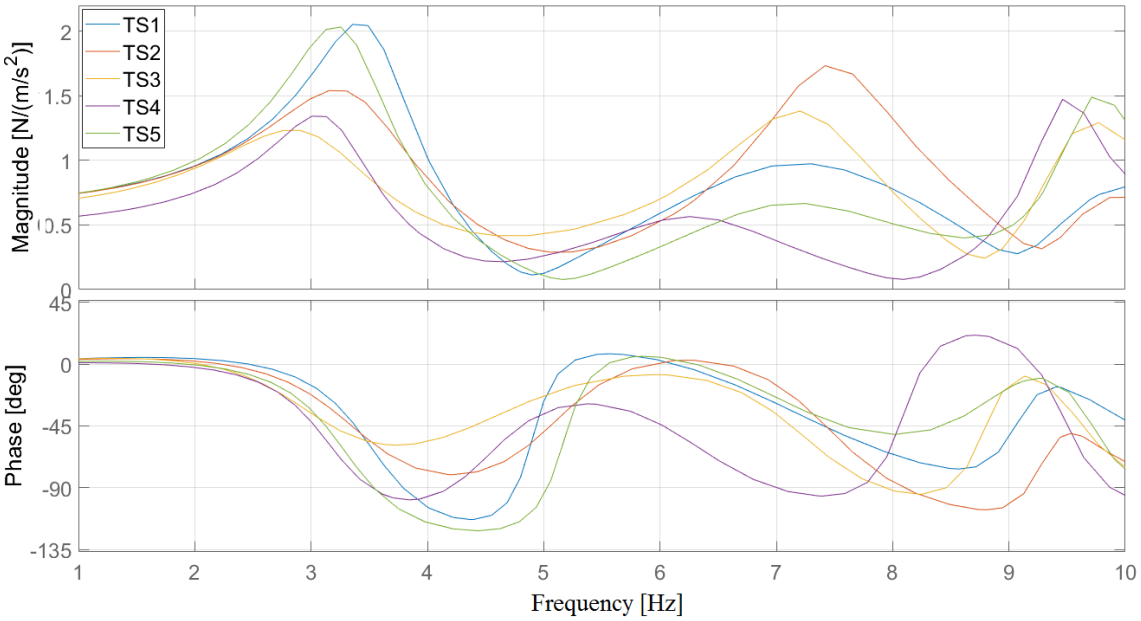

Figure 4.28: The derived transfer functions , $H_{a,s}(f)$, between vertical acceleration of C7 and the corresponding ground reaction force.

load factor of the generated GRF has an error of up to 18% when compared to that recorded on an instrumented treadmill. This can be compared to an error of around 7% for the example shown in Figure 4.29. This provides the confidence in the derived transfer function $H_{a,s}(f)$ to be used in the proposed HSI methodology. This is presented and explained in the next subsection.

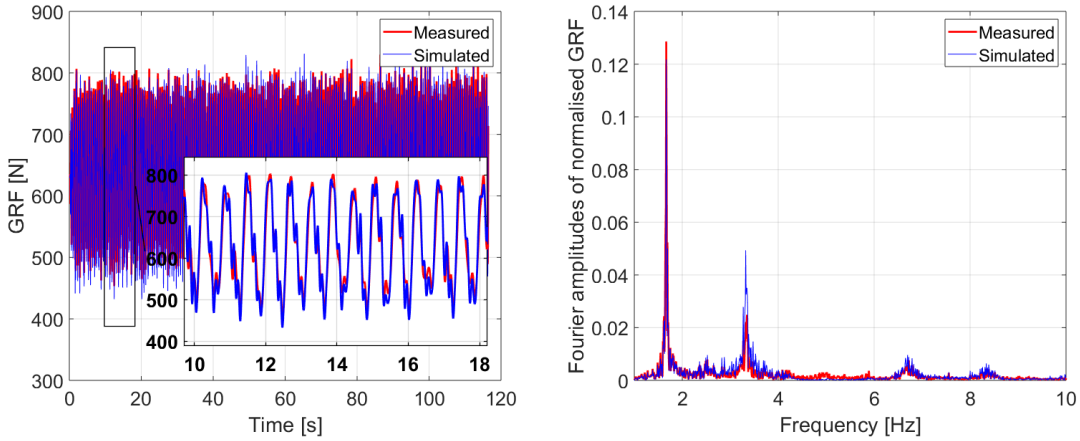

(a) Time domain. (b) Frequency domain.

Figure 4.29: Measured and simulated ground reaction force using measured acceleration at C7 and one derived transfer function, $H_{a,s}(f)$.

4.3.4 Implementation

The two above mentioned transfer functions, $H_{a,h}(f_i)$ and $H_{a,s}(f_i)$, are to be used in each time step to simulate the interaction between the walking individual and the supporting floor. The step-by-step procedure to implement the proposed HSI methodology in the response calculation of human-induced vibration is presented below and illustrated in Figure 4.30.

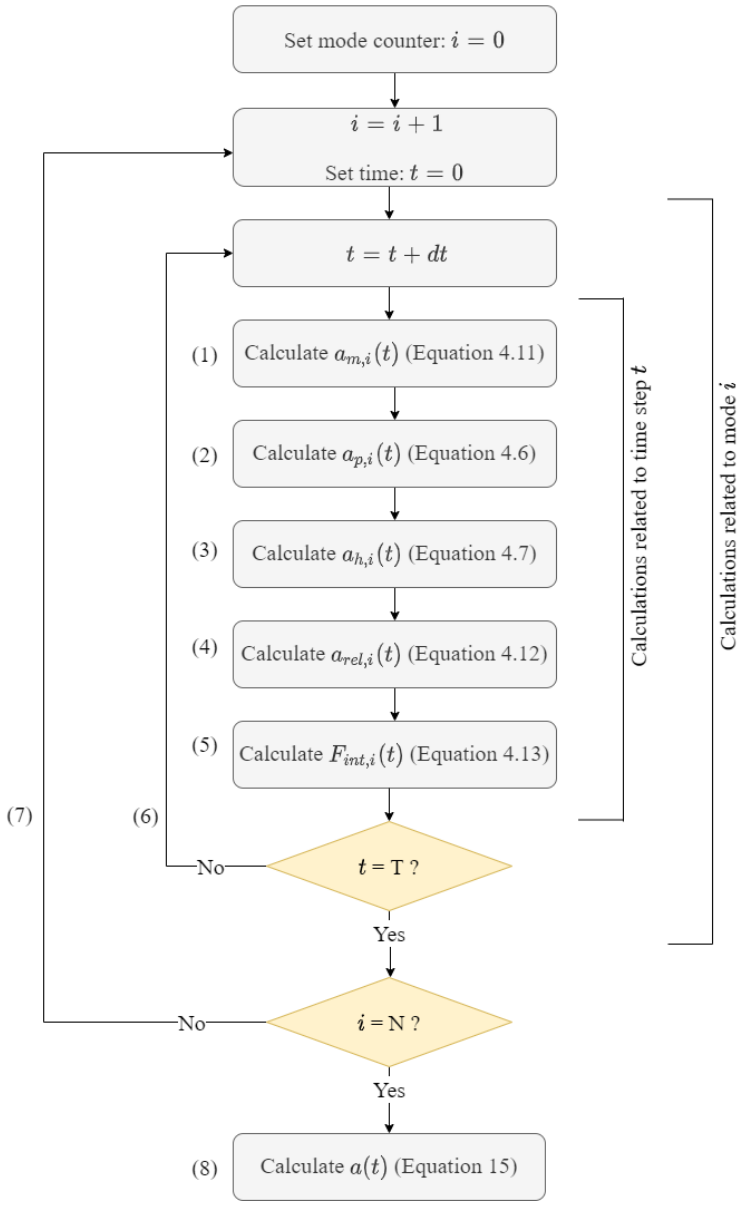

Figure 4.30: Flowchart showing the steps of implementing the proposed HSI methodology.

1. Calculate the modal acceleration response, $a_{m,i}(t)$, for mode i and time step

t, by solving the equation of motion, as described in Equation 4.11. Note that $F_{int}(t - dt)$ is equal to zero at $t = 0$.

$$M_i a_{m,i}(t) + C_i v_{m,i}(t) + K_i d_{m,i}(t) = GRF_r(t)\Phi_i + F_{int}(t)\Phi_i(v_p.t) \quad , \quad (4.11)$$

where, M_i, C_i and K_i are the modal mass [kg], damping coefficient [N.s/m] and stiffness [m/N] related to mode i of vibration, respectively, $v_i(t)$ and $d_i(t)$ are the modal velocity [m/s] and modal displacement [m] responses related to mode i and time step t, respectively and Φ_i is the mode shape amplitude related to mode i and the location of the walker.

2. Calculate the contribution of mode i in the physical response at time step t, $a_{p,i}(t)$, using Equation 4.6.

3. Calculate the vertical acceleration of human body mass related to mode i at time step t ($a_{h,i}(t)$), as mathematically described in Equation 4.7.

4. Calculate the relative vertical acceleration, $a_{rel,i}(t)$, between human body mass and the supporting structure, at the point of contact between them, related to mode i and time step t, using Equation 4.12.

$$a_{rel,i}(t) = a_{h,i}(t) - a_{p,i}(t)) \quad , \quad (4.12)$$

5. Calculate the interaction force related to mode i and time step t ($F_{int,i}(t)$), using Equations 4.13 and 4.14.

$$F_{int,i}(t) = \int_{-\infty}^{\infty} a_{rel,i}(\tau) \;\; h_{a,s} \tag{4.13}$$

$$h_{a,s}(t) = \frac{1}{2\pi} \;\; \int_{-\infty}^{\infty} H_{a,s}(f) \tag{4.14}$$

here, τ is the time step of the integration.

6. Repeat steps 1-5 for for all time steps until $t = T$, where T is the total duration of the simulation [s].

7. Repeat the above mentioned steps for all modes of vibration.

8. Calculate the total physical response of the floor at a location of interest, $a(t)$, using Equation 4.15.

$$a(t) = \sum_{i=1}^{N} a_i(t) \;\; \phi_i(k) \quad , \tag{4.15}$$

where, N is the number of modes considered in the analysis and $\phi_i(k)$ is the mode shape amplitude corresponding to mode i at the node of interest (k).

4.4 Experimental verification

This section verifies the performance of the proposed HSI methodology using experimental acceleration response obtained from floors A, B and C. Simulations were carried out to calculate the corresponding vibration responses when HSI was neglected or taken into account using the proposed methodology. The calculated responses were compared with the measurements using their

maximum transient vibration value ($MTVV$), in [m/s^2], which is equal to the maximum 1 s RMS. A brief discussion about the results is presented at the end of this section.

4.4.1 Floor A

A walking test was conducted by an individual walking along WP1 (Figure 4.4). The test subject conducted a controlled walking test at a pacing frequency (f_p) of 1.6 Hz to achieve resonant response. The corresponding vibration response was measured at the centre of the floor, i.e. TP11 in Figure 4.4. The measured response was low-pass filtered to eliminate the contribution of modes of vibration other than the first mode. This is because the proposed HSI method is designed for modes with natural frequencies up to 10 Hz which covers only the first mode of vibration for this floor.

The corresponding response calculation was conducted when HSI was taken into account or neglected. Previously measured ground reaction force for the same test subject while walking on an instrumented treadmill (Racic and Brownjohn, 2011; Brownjohn et al., 2015), at the same f_p as mentioned above - 1.6 Hz, was available to be utilised for this analysis. The modal force corresponding to the first mode of vibration (Figure 4.5a) was obtained by multiplying the ground reaction force of the walking pedestrian by mode shape amplitudes corresponding to WP1 (Figure 4.4). The modal vibration response related to the neglected effect of HSI was calculated directly using the Newmark integration method (Paz and Leigh, 2004). The corresponding physical response was calculated by multiplying the modal accelerations by the mode shape amplitude corresponding to TP11 (Figure 4.4). Vibration response was also calculated using the proposed HSI

methodology, as explained in Section 4.3.4.

To take into account the perception of humans to vibrations in the calculated responses, the W_b weighting curve was used to obtain the weighted acceleration response, $a_w(t)$, where t is time [s] (Institution, 1987). The running root-mean-square (RMS) acceleration, $a_{w,rms}(t)$, was calculated using Equation 4.16.

$$a_{w,rms}(t) = \sqrt{\frac{1}{T}\int_0^T a_w^2(t)dt} \quad , \tag{4.16}$$

where, T is the RMS duration (1 s) and dt is the duration of each time step [s].

Figure 4.31 shows the calculated and measured vibration responses. Figure 4.31 shows that there is a significant overestimation of the vibration response when the influence of HSI was neglected. Implementing the proposed methodology has reduced the MTVV by around 30% and resulted in much closer vibration responses to their measured counterparts (Figure 4.31).

4.4.2 Floor B

Walking tests were conducted by two TSs walking individually along WP2 (Figure 4.11) at f_p of 2.2 Hz. This f_p was chosen to achieve a resonant response corresponding to the first mode of vibration, where the fundamental frequency is 8.72 Hz. The responses were measured at TP43 (Figure 4.11), which is the anti-node of the first mode of vibration (Figure 4.12a). The responses were low-pass filtered to eliminate the contribution of modes of vibration other than the first mode.

There were no ground reaction force data available for the test subjects who

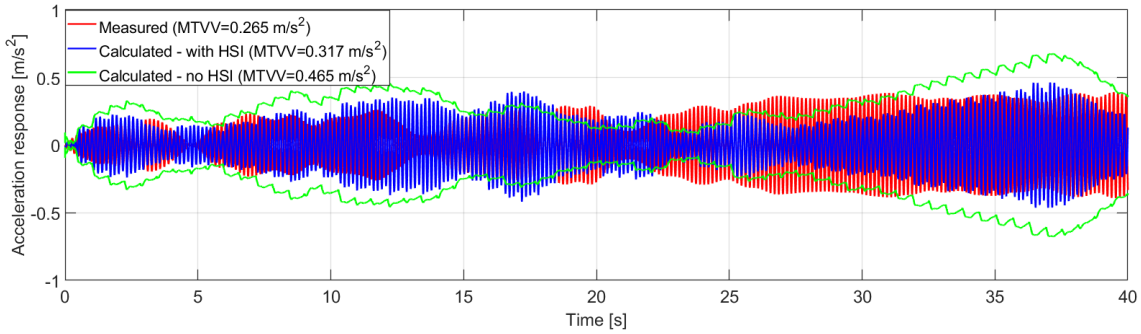

(a) Time history.

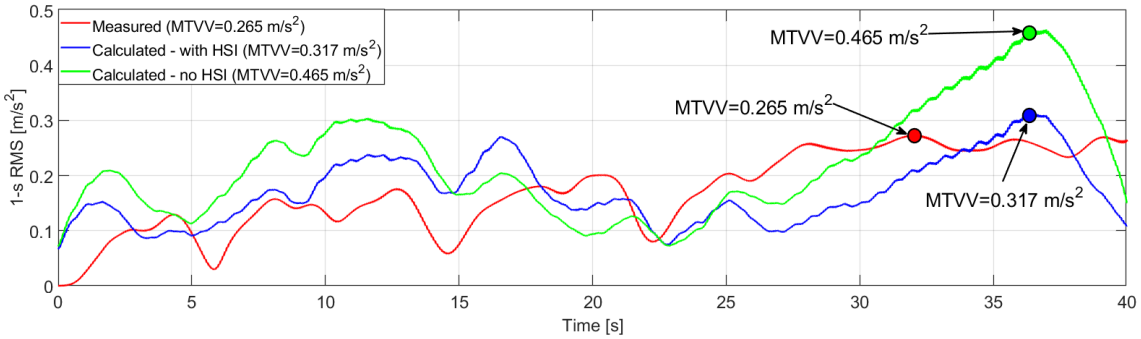

(b) RMS.

Figure 4.31: (a) Vibration response related to walking along WP1 on Floor A (TP11) at f_p of 1.6 Hz (resonance) and (b) the corresponding running RMS.

participated in these walking tests at f_p of 2.2 Hz. Therefore, 20 measured GRFs, using an instrumented treadmill (Racic and Brownjohn, 2011; Brownjohn et al., 2015), related to other people, who were chosen randomly, walking at the same f_p, i.e. 2.2 Hz, were used in the response calculations. These GRFs were normalised to match the body mass of each test subject. Similarly to the previous section, the responses were calculated twice: when HSI was neglected and when it was taken into account, as described in Section 4.3.4. This means there were 40 vibration responses calculated for each person, i.e. 20 for neglected HSI and 20 when the proposed HSI method was utilised. For comparing $MTVV$ for several vibration responses, a box plot can be used for for this purpose, as shown in Figure 4.32.

Figure 4.32 shows that despite using measured ground reaction forces in the response calculation, which are more realistic than the simplified footfall load

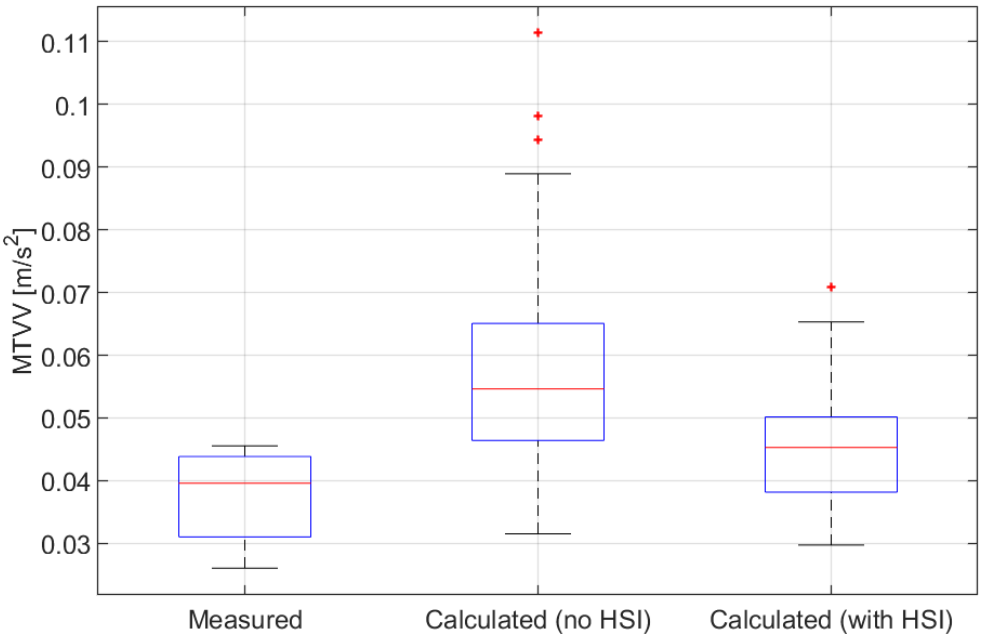

Figure 4.32: $MTVV$ corresponding to measured and simulated responses for two individuals walking on Floor B along WP2 (Figure 4.11).

models available in the literature, there was still around 50% overestimation of the vibration responses when HSI was neglected. Taking into account HSI in the response calculation, using the proposed HSI method, has resulted in less overestimation of the calculated vibration levels compared to that when neglecting the HSI effects in vibration response calculations.

4.4.3 Floor C

Walking tests were conducted by six individual test subjects, with known body mass, walking on Floor C along WP2 (Figure 4.18). f_p for each test was 1.9 Hz, where its fifth integer multiple, i.e. 9.5 Hz, is close to the measured fundamental frequency, which is 9.47 Hz. The responses were measured at TP42 (Figure 4.18), which is the anti-node of the first mode of vibration (Figure 4.19a) and low-pass filtered to eliminate the contribution of all modes of vibration other than the first mode.

Similarly to the analysis conducted in Section 4.4.2, 20 measured ground reaction forces related to other people, chosen randomly, walking at the same f_p, i.e. 1.9 Hz, were used in the response calculations. This was repeated when the effect of HSI was neglected and when taken into account in the response calculations. The $MTVV$ corresponding to the measured and simulated responses is presented as a box plot in Figure 4.33.

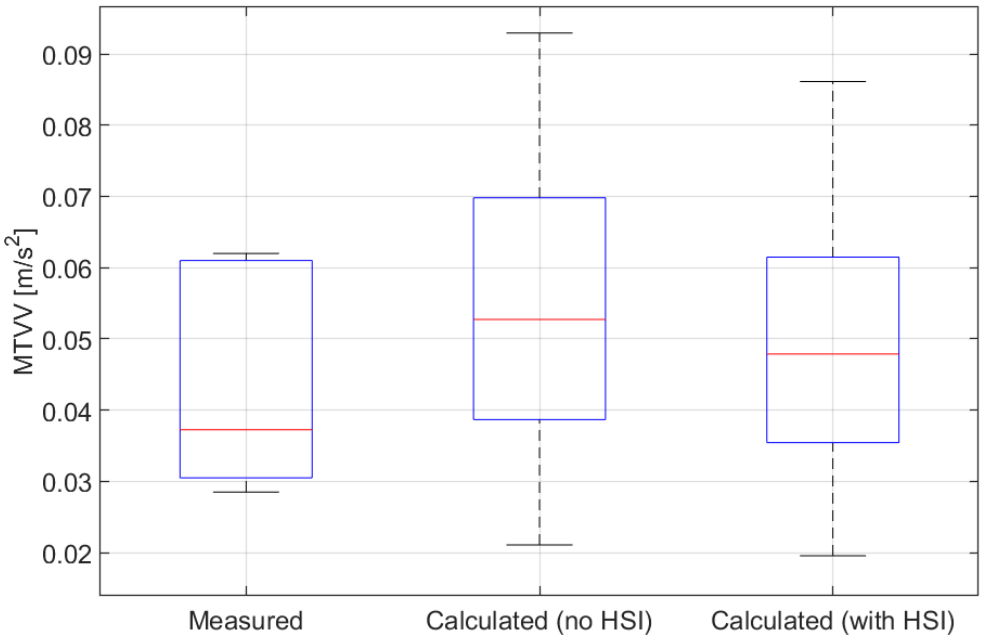

Figure 4.33: $MTVV$ corresponding to measured and simulated responses for six individuals walking on Floor C along WP2 (Figure 4.18).

Figure 4.33 shows that when HSI was taken into account using the proposed method, there was an average reduction in $MTVV$ of about 10% compared to that when HSI was neglected. This reduction is apparently similar for most of the responses with low and high vibration levels. This small reduction indicates that HSI did not have significant influence on the response calculations, and therefore, such interaction could be neglected for such cases. GRF is expected to have more influence on the predicted responses for such cases.

4.4.4 Discussion

The results presented in this section show that, in most cases, utilising the proposed HSI methodology has resulted in reduced vibration levels and more accurate prediction of vibration responses than that when HSI was neglected. For Floor C, there was no significant influence of HSI on the calculated responses, especially for the highest response levels, indicating that HSI can be neglected for such cases, and the footfall loading could have more significant influence on the response prediction.

The average reduction in $MTVV$ for Floor B and Floor C when HSI was taken into account, 20% and 10%, as shown in Figures 4.32 and 4.33, respectively, was less than that for Floor A, 30%, as shown in Figure 4.31. Interestingly, the maximum reduction in $MTVV$ for each floor is comparable to the reduction of its FRF magnitude at the fundamental frequency when occupied by single or multiple pedestrians (Table 4.1) despite the differences between the two concepts. Furthermore, the reduction in the $MTVV$ for Floor A is comparable to those reported in the literature for footbridges (Shahabpoor, 2014; Dang, 2014) while Floor B and Floor C showed lower reduction than that. This is believed to be related to the higher natural frequency and modal mass for Floor B and Floor C compared to that for Floor A.

The results presented in this section show that utilising the proposed HSI methodology has resulted in an improved estimation of human-induced vibration levels for floors. This is confirmed by the tests conducted on the three floors discussed in this chapter. However, even when the proposed model was ustilised, there was an overestimation in the vibration levels. This could be caused by

neglecting the influence of structural vibration on the gait of the walker and the corresponding footfall loading, which was reported in the literature (Ahmadi et al., 2018).

4.5 Parametric study

In this section, a parametric study was conducted to examine how the dynamic properties of a floor modelled as SDOF oscillator, i.e. natural frequency, modal mass and modal damping ratio, affect the influence of HSI on the vibration responses. This was achieved by calculating vibration response, corresponding to the lowest mode of vibration, related to an imaginary scenario of a pedestrian walking on Floor B and across WP2 (Figure 4.11). For each case explained below, the $MTVV$ was calculated when HSI was neglected and when it was taken into account using the proposed HSI method, and the reduction in $MTVV$ was utilised for comparison, as explained below.

4.5.1 Natural frequency effects

The influence of the natural frequency on HSI can be examined by using the same modal mass, i.e. 12,264 kg, and modal damping ratio, i.e. 1.3%, as measured for Floor B (Figure 4.12a) but with different natural frequencies. The choice of natural frequencies is explained below.

Six ground reaction forces, measured previously using an instrumented treadmill (Racic and Brownjohn, 2011; Brownjohn et al., 2015), were chosen for random individuals walking at different f_p , i.e. 1.6, 1.75, 1.85, 1.9, 2.1 and 2.3 Hz. As the influence of HSI on vibration responses is relatively high in the case of a resonant response, it was decided to make the natural frequency equal to an

integer multiple of f_p but below 10 Hz. Table 4.2 shows the natural frequencies used with each f_p. The reduction in $MTVV$ was calculated for each pair of f_p and a corresponding natural frequency (Table 4.2), and the results are shown in Figure 4.34a.

Table 4.2: f_p and the corresponding natural frequencies used in the parametric study.

f_p [Hz]	Corresponding natural frequencies [Hz]
1.60	1.60, 3.20, 4.80, 6.40, 8.00 and 9.60
1.75	1.75, 3.5, 5.25, 7.0 and 8.75
1.85	1.85, 3.7, 5.85, 7.4 and 9.25
1.90	1.90, 3.80, 5.70, 7.60 and 9.50
2.10	2.10, 4.20, 6.30 and 8.40
2.30	2.30, 4.60, 6.90 and 9.20

4.5.2 Modal mass and modal damping ratio effects

The influence of the modal mass on HSI was examined by using the measured fundamental frequency, i.e. 8.72 Hz, and modal damping ratio of the first mode of vibration, i.e. 1.3% as indicated in Figure 4.12a, but with varying value of modal mass between 3,000 kg and 30,000 kg. The range of the chosen modal mass corresponds to a mass ratio, the ratio between human body mass and the modal mass for the lowest mode of vibration, between 2.5% and 0.25%. The corresponding reduction of $MTVV$ is shown in Figure 4.34b.

Similarly, the influence of the modal damping ratio on HSI was examined by using the measured fundamental frequency, i.e. 8.72 Hz, and modal mass, i.e. 12,264 kg, of the first mode (Figure 4.12a) but with varying value of modal damping ratio between 0.5% and 5%. The corresponding reduction of $MTVV$ is shown in Figure 4.34c.

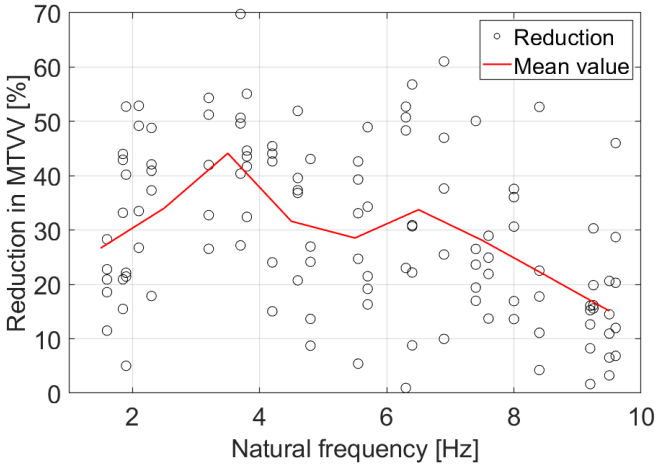

(a) Reduction in $MTVV$ for different natural frequencies of the empty floor.

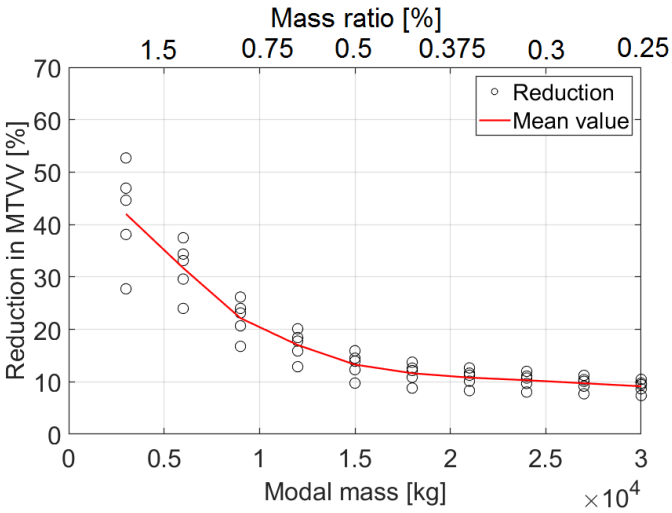

(b) Reduction in $MTVV$ for different modal masses and mass ratios of the empty floor.

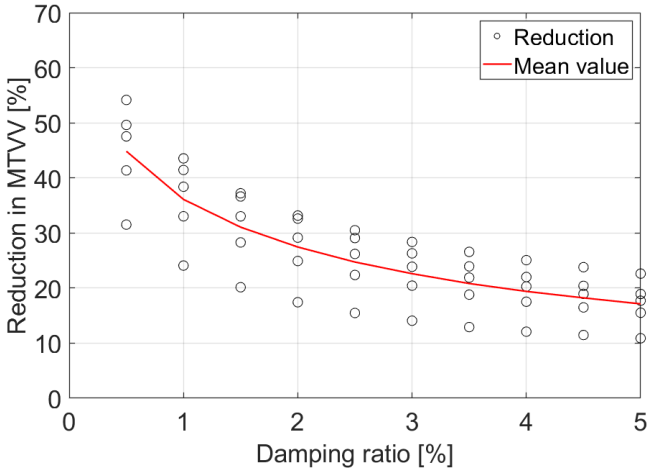

(c) Reduction in $MTVV$ for different modal damping ratios of the empty floor.

Figure 4.34: The influence of (a) natural frequency, (b) modal mass and (c) modal damping ratio on the reduction in $MTVV$ when HSI was taken into account.

4.5.3 Discussion

Figure 4.34a shows that maximum reduction in $MTVV$, related to utilising the proposed HSI model, appears at 3-4 Hz and 7-8 Hz. This is comparable with the peaks of $H_{a,s}(f)$ magnitude as shown in Figure 4.28. Furthermore, higher modal mas, i.e. lower mass ratio, and/or damping ratio has resulted in less reduction in $MTVV$, as shown in Figure 4.34b and Figure 4.34c.

The results presented in Figure 4.34 can assist designers in estimating the range of reduction in $MTVV$ for a floor. For example, Figure 4.34 can be used to estimate the reduction in $MTVV$ for Floor C when only the first mode of vibration is considered (Figure 4.19a) as follows:

- An initial reduction in $MTVV$ can be picked from Figure 4.34a as around 10%, which is the average reduction in $MTVV$ corresponding to a fundamental frequency of 9.47 Hz.
- As the data presented in Figure 4.34a corresponds to a modal mass and damping ratio of 12,264 kg and 1.3%, respectively (Figure 4.19a), interpolation should be made, using Figure 4.34b and Figure 4.34c, to adjust the initial reduction in $MTVV$ accordingly. This will result in an around 13% reduction in $MTVV$, which is comparable to the 10% reduction observed in the analysis in Section 4.4.3.

4.6 Conclusions

This work quantifies the effect of walking pedestrians on the FRF magnitude for three floors and presents an improved methodology that takes into account the dynamics of walking individuals over a frequency range between 1 Hz and

10 Hz to simulate HSI in the response calculation of human-induced vibration of floors. Experimental measurements of three floors show the potential for a significant reduction in their FRF magnitude when they are occupied by walking pedestrians. The amount of this reduction is apparently affected mostly by the natural frequency and modal mass.

In contrast to other HSI models available in the literature, the proposed model takes into account human dynamics using two experimentally-based transfer functions that describe the dynamics of walking individuals over a range of frequencies of 1-10 Hz rather than using MSD models which correspond to only the whole-body dominant mode of vibration. The advantage of this modelling approach is that it utilises the transfer functions directly in the response calculations rather than using approximate SDOF or MDOF systems. These transfer functions can be used to calculate:

- Acceleration of the human body due to structural acceleration of the supporting structure, and
- The corresponding interaction force acting on the structure.

The performance of the proposed model was verified using experimental measurements of individuals walking on three floors. The responses calculated using the proposed model were lower than those calculated when HSI was neglected but still higher than their measured counterparts. This implies that the proposed model can be utilised for improved vibration response prediction of floors. However, the vibration levels of the simulated responses were relatively dispersed compared with the measured responses. It is believed that by performing further measurements dedicated to derive transfer functions related

to walking individuals, similar to those presented in this study, the proposed model can be statistically further improved. Furthermore, the proposed HSI methodology should be used only for floor modes of vibrations with a natural frequency of less than 10 Hz, i.e. low-frequency floors. This is so because the transfer functions, related to the proposed method, was derived for this range of frequencies.

Preface to Chapter 5

Chapter 5 describes how an Ultra-WideBand location tracking system was utilised to collect unique data on people's locations on floors, model their occupancy and movement patterns and utilise it in a comprehensive framework for vibration serviceability assessment of floors. Furthermore, this chapter proposes an improved method to predict VDV anywhere on the floor based on the simulated people's movements.

The experimental works and analyses related to this chapter were conducted by the author of this thesis. Members in the Vibration Engineering Section at the University of Exeter assisted in the experimental works.

The contents of this chapter were adopted from the following journal paper to be submitted to the Sound and Vibration. Slight amendments were made to make the style of this chapter compatible with the rest of the thesis.

Mohammed, A. and Pavic, A. Utilising indoor people tracking system for the application of vibration serviceability of floors. *Sound and Vibration*.

Chapter 5

Utilising indoor people tracking system for the application of vibration serviceability of floors

Abstract

The design of modern buildings is increasingly governed by the vibration serviceability criterion related to occupants' walking activities. However, the current design guidelines for floor vibration serviceability lack reliable representation of walking scenarios on floors. Instead, the guidelines adopt the extreme scenario for a single person walking on the most responsive walking path causing resonance. In principle, utilising an extreme scenario for a serviceability check can result in overestimated vibration levels. There is only limited, and not conclusive, research in the literature regarding utilising walking scenarios in the design for vibration serviceability of floors. This work utilises an Ultra-WideBand positioning tracking system to collect unique data on people's locations on floors,

model their occupancy and movement patterns and utilise it in a comprehensive framework for vibration serviceability assessment of floors. For normal daily floor operation, the measurements show that a multiple pedestrian walking scenarios may result in higher floor vibration levels than that for a single person. The simulations conducted using the framework shows that vibration levels experienced by floor occupants could be significantly less than the peak response on the floor, indicating the benefits of utilising vibration levels experienced by the occupants in the design. Moreover, a simplified, and improved, method to predict the vibration dose value which takes into account realistic walking paths and the number of movements across the floor is proposed in this study. The outcome of this study can assist the designers in more reliably predicting footfall-induced vibration of open-plan office floors.

5.1 Introduction

Vibration serviceability criterion is increasingly governing the design of modern civil structures, such as building floors. This is due to the advancements in design tools and construction materials, resulting in slender floors with long spans. For such structures, footfall-induced vibration could be problematic, and is becoming a crucial factor in the design (Brownjohn et al., 2015).

Several UK and international design guidelines related to footfall-induced vibration of floors are currently available (Pavic and Willford, 2005; Willford and Young, 2006; Feldmann and Heinemeyer, 2007; Smith et al., 2009; AS 3623—1993, 1993; Fanella and Mota; Murray et al., 2016). The latest versions of most of them were published more than 10 years ago (Pavic and Willford, 2005; Willford and Young, 2006; Feldmann and Heinemeyer, 2007; Smith et al., 2009),

so they are based on knowledge about footfall-induced vibration available which is 10-20 years old. Since then, there has been advancements in measurement and design tools that have the potential to be utilised to update and improve the performance of these guidelines. However, there is still lack of guidance regarding realistic walking scenarios in buildings and utilising them in the design. This aspect was rarely researched in the context of vibration serviceability of floors, and therefore, current design guidelines recommend utilising critical walking scenarios, related to extreme vibration levels in the design. This walking scenario is still a useful design approach when information regarding floor layout is not available. However, if such information is available, realistic walking scenarios can be utilised to calculate vibration levels likely to occur when the floor is in operation. This can be done, for example, to check vibration serviceability performance of a floor with a new layout before doing commissioning, or refurbishment, works. It can be used also as a vibration remedy technique to optimise floor layout and minimise vibration levels. Hence, realistic walking scenarios can be utilised to improve the following aspects in the vibration serviceability design guidelines:

1. The current guidelines adopt the scenario of *single person walking at a pacing frequency related to a resonant response* as a worst-case scenario for design. This assumption has two aspects. Firstly, it is not the only walking scenario that occurs in many building floors, such as open-plan office floors and retail premises where multiple pedestrians are likely to walk simultaneously. Secondly, it was reported that utilising single person walking scenario may result in lower (Chen et al., 2015) or higher (Živanović et al., 2012) vibration levels than that for multiple pedestrian walking scenarios. Hence, single person walking may not be the worst case

scenario for the design for vibration serviceability.

2. The current guidelines adopt *the worst walking path and pacing frequency* corresponding to resonant response as a conservative assumption for design no matter how unlikely these two assumptions occur. As this scenario could still occur, it is useful in the design of floors requiring stringent criterion on vibration levels, such as operating theatres and laboratories. For other types of floors, such as offices, where there is some tolerance about the permitted vibration levels and the number of times it can be exceeded, the assumption of utilising the most responsive walking path and pacing frequency in the design may not be relevant for a serviceability criterion and may result in overestimation of vibration levels.

3. Vibration serviceability criterion is widely assessed using a *single number*, usually referred to as the response (R) factor which typically corresponds to 1 s root-mean-square (RMS) averaging of floor acceleration response (Pavic and Willford, 2005). Its simple form and dependence on short duration high peaks, related to most responsive walking scenario, makes it relatively easy to use in practice. However, it is argued that it is too sensitive to, and depends on, very short duration peaks, i.e. 1 s, in the response and may not describe vibration levels for the vast majority of the time (Reynolds and Pavic, 2015; Muhammad et al., 2018). Reynolds and Pavic (2015) carried out vibration monitoring of an in-service office floor for 10 days. They found that the peak R factor was reached for a very short duration and the R factor related to 90% probability of non-exceedance was significantly lower than the peak R factor. One way to improve this vibration descriptor is by utilising R factor related to certain probability of non-exceednace in

the design, which requires understanding of people's movements and their statistical patterns. Another vibration descriptor is the vibration dose value (VDV). The advantage of VDV is that it takes into account the duration of exposure to vibration throughout the day in its calculations. The main challenge of using VDV in the design is the estimation of the number of floor occupants' walking events and their walking paths (Pavic and Willford, 2005; Smith et al., 2009).

It can be concluded that these aspects of design guidelines are all related to lack of understanding of occupants' movements across floors. Predicting the exact movements of floor occupants could be practically impossible due to their complexity, but understanding their patterns and statistical features is essential to model these movements and utilise them for innovative data-driven vibration serviceability assessment. In general, measurement and modelling of people occupancy and movements on floors can be used to improve design tools for vibration serviceability of floors by:

1. Deriving occupancy and movement models on floors from experimental data. Such models can be used to model realistic footfall loading scenarios for vibration serviceability applications.

2. Utilising vibration levels experienced by floors' occupants in the design instead of relying on vibration levels occurring at positions that may not be occupied by the occupants during most of the day.

3. Studying the subjective rating of vibration levels by floors' occupants, experimentally, by comparing the actual vibration levels they perceived, based on their positions, and their assessment to these vibration levels.

This chapter demonstrates the application of an indoor location tracking system in the context of vibration serviceability by:

1. Conducting simultaneous measurements of people's locations and their corresponding footfall-induced vibrations in real-life situations to understand the relationship between the number of people walking simultaneously and their corresponding vibration levels,

2. Utilising the collected data of people's locations to develop a full time history occupancy model that can be used for vibration serviceability applications,

3. Proposing a framework for vibration serviceability assessment of floors subjected to footfall loading of multiple occupants based on the occupancy model proposed in this study, and

4. Proposing an improved method to calculate VDV based on the location and frequency of people's movements.

Section 5.2, of this chapter, provides brief description about indoor location tracking systems and describes the tracking system utilised in the experimental measurements (Section 5.3). The proposed movements and occupancy model is presented in Section 5.4. Section 5.5 describes an improved method for predicting VDV based on people's locations, while Section 5.6 describes a proposed framework for vibration serviceability assessment of floors. Finally, Section 5.7 presents conclusions of this study.

5.2 Indoor position tracking

There are many studies in the literature (Balvedi et al., 2018; Dong et al., 2018) that focus on either measurement and modelling of general people occupancy, i.e. number of occupants in an office at time intervals, or the detailed walking behaviour of individuals within crowds of people (Helbing and Farkas, 2002). Only a small proportion of them was carried out to model the full time history of floors occupants' locations. However, even these studies are based on inaccurate measurements of people's locations due to the limitations of available indoor people tracking equipment (Balvedi et al., 2018; Dong et al., 2018).

For vibration serviceability applications, developing an occupancy model, based on experimental measurements, can be useful in the design, as discussed above. Such model can be developed using experimentally acquired locations of people on floors. The accuracy of such measurement can affect the reliability of the derived model. For example, if a tracking system is not precise enough, it might, wrongly, show that an occupant is sitting in, say, a meeting room while he/she is, in reality, sitting in an adjacent office or kitchen. This may affect the derived occupancy models and the corresponding walking paths and vibration levels of other floors with different layout where the meeting room, as for the example above, is located away from the office or the kitchen.

There are various devices and techniques related to indoor people location tracking, such as cameras, motion sensors, ranging devices and inertial sensors. Most of them are difficult to deploy to track people's locations outside laboratory conditions or has limited accuracy. Vision-based tracking techniques, based on cameras, are gaining a growing interest in the past few years. While the

data collected using such systems are useful to trace the movements on floors, it is difficult to use them for modelling the occupancy of individual occupants, especially where multiple cameras are needed to monitor the movements (Teixeira et al., 2010). The occlusion is an another challenge for such systems. Other techniques, such as those based on Bluetooth signals can be easily used to track the location of mobile phones of the occupants but their accuracy is considerably low, i.e. the error is typically higher than 2-3 m (Teixeira et al., 2010), which may affect the reliability of the derived occupancy model. Tracking systems based on Ultra-WideBand (UWB) technology have relatively high accuracy, around 0.5-1.0 m, and capability to track individual floor occupants. However,they require floor occupants to wear tags so that their position can be monitored.

It can be concluded that different tracking systems have their advantages and disadvantages. However, to minimise the influence of the accuracy of measured locations on the derived occupancy model, it is decided to utilise the UWB tracking system in this study.

5.2.1 UWB tracking system

The UWB system comprises wearable signal emitters, i.e. tags, which send pulse signals to nearby receivers, i.e. anchors, as shown in Figure 5.1.

UWB tags' locations are calculated based on a two-way ranging algorithm, where signals are exchanged between tags and anchors to determine the distance between them (Dardari et al., 2015). Each anchor reports the data to a central server, through a WiFi signal, where at least three anchors are needed to calculate the location of a tag using the triangulation technique (Figure 5.1).

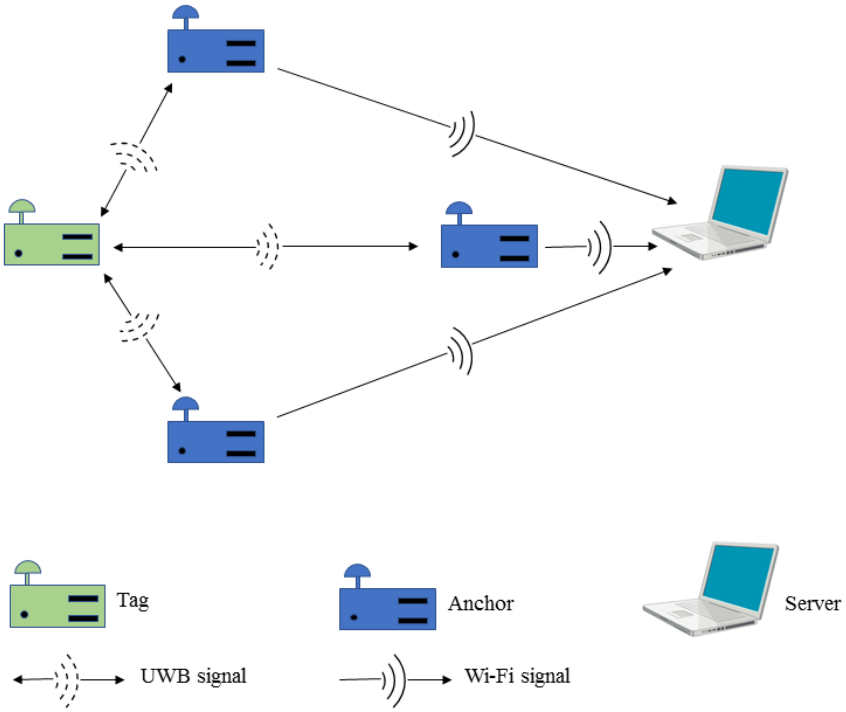

Figure 5.1: Overview of the UWB tracking system described in this study.

5.2.2 Testing of the UWB tracking system

A simple experiment was conducted on a laboratory floor in the Structures Lab at the University of Exeter to test the accuracy of the deployed UWB system, as shown in Figure 5.2a. The floor is 7.5m long and 5.0m wide. A detailed description of the floor is available elsewhere (Hudson and Reynolds, 2016).

Four anchors were deployed just outside the floor, as shown in Figure 5.2a. A video recording from a point around 5m above the floor was made and synchronised with the UWB system for comparison purposes. Two test subjects (TSs) participated in the test and each wore a UWB tag on the left wrist, as shown in Figure 5.2a. The frequency of the UWB tracking system was set to 1 Hz, i.e. UWB tags' locations were determined every 1 s. The two TSs walked across two different diagonals of the floor simultaneously, as shown in Figure 5.2b.

The identified locations of the UWB tags are illustrated in Figure 5.2b. The green and blue circles, shown in Figure 5.2b, represent the identified locations of the

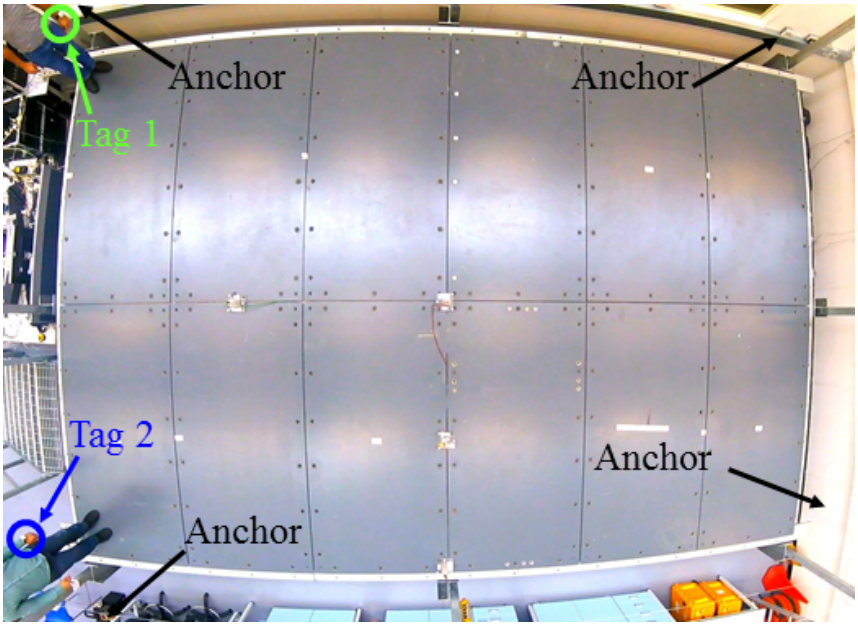

(a) Locations of anchors.

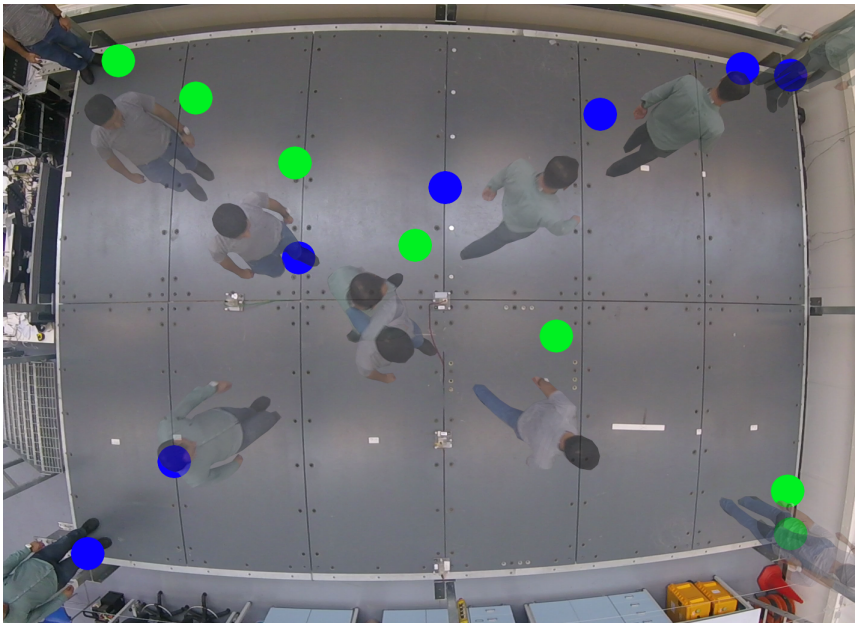

(b) Actual location of the test subjects and the corresponding tracked locations of their UWB tags.

Figure 5.2: (a) Locations of the UWB tags and anchors related to the UWB tracking system and (b) the corresponding identified locations of the UWB tags (Mohammed and Pavic, 2018).

UWB tags worn by TS1 and TS2, respectively, during one diagonal crossing. These locations are visually quite comparable to their actual counterparts, from the video recordings, as shown in Figure 5.2b. The performance of the utilised tracking system is in-line with previous reports regarding the accuracy of the

UWB tracking systems which was found to be around 0.5-1.0 m (Maalek and Sadeghpour, 2016). With this level of accuracy, it is believed that the errors related to the identified locations of floor occupants can be minimised, i.e. it is less likely that a person located in, say, a meeting room is recorded as located in an adjacent kitchen. This may have an influence on the derived occupancy models and the corresponding walking paths for other floors with different layouts.

5.3 Experimental measurements

This section describes the tested structure and the experiments conducted on it. Modal testing of the empty floor is firstly described, followed by a description of the logistics and preparations made for the people's location tracking and vibration monitoring tests. The main results are presented after that followed by a brief discussion.

5.3.1 Test floor

The test was conducted in the west wing of the first floor of a newly constructed in-service building, as shown in Figure 5.3. It is the same part of the building where the measurements described in Section 4.2.4 were conducted during the construction stage. The key structural elements of the testing area comprise a normal weight composite floor supported by steel beams and columns as illustrated in Figure 5.4. The testing area is 27.25m long and 14.0m wide and comprises an open-plan office with two meetings rooms, a discussion room, printing areas, kitchen, free area and toilets, as shown in Figure 5.5a.

(a) Overview of the building.

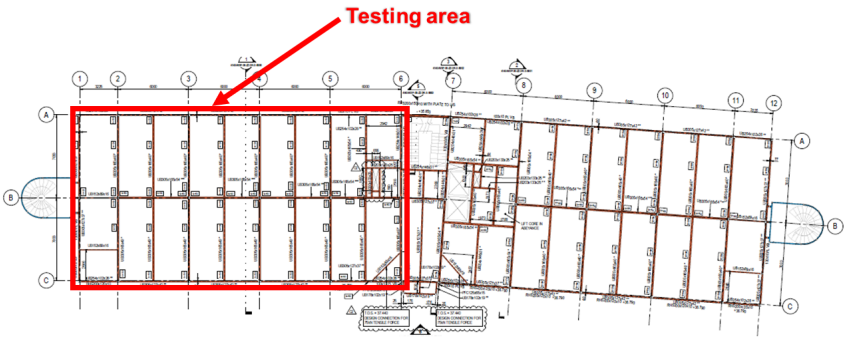

(b) Testing area.

Figure 5.3: Overview of the building and testing area.

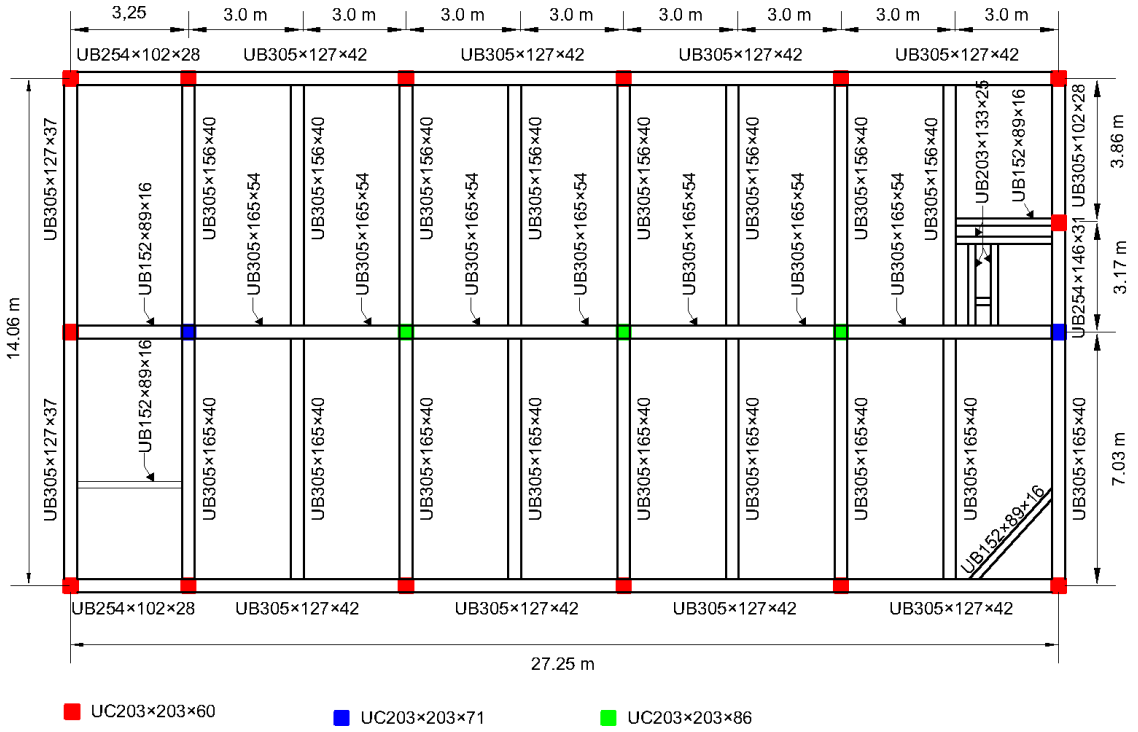

Figure 5.4: Key structural elements of the testing area.

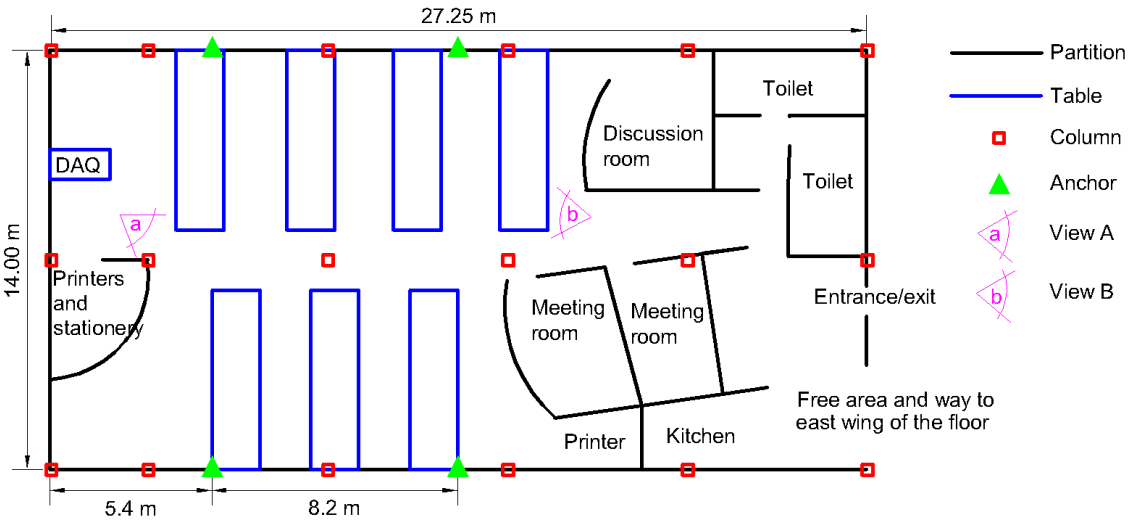

(a) Layout of the testing area.

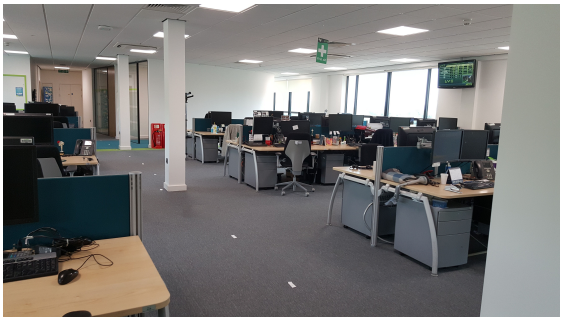

(b) View A (Figure 5.5a).

(c) View B (Figure 5.5a).

Figure 5.5: Overview of the test floor.

5.3.2 Modal testing

Modal testing was conducted on the testing area of the empty floor to measure the frequency response functions (FRFs) which were used to calculate natural frequency, mode shape, damping ratio and modal mass of its dominant modes of vibration. Multi-input multi-output (MIMO) modal testing was conducted where two APS400 (APS Dynamics Inc., 2013) and one APS113 (APS Dynamics Inc., 1996) shakers were placed at TPs 24, 42 and 64, shown in Figure 5.6, respectively, and used to apply uncorrelated random forces on the floor structure. The shakers were placed on the concrete structure after false floor panels were lifted at their locations, as shown in Figure 5.7. Their input force was calculated by multiplying the acceleration of the armature, measured using an Endevco

7754A-1000 piezoelectric accelerometer, by its mass. The corresponding structural response was measured by Honeywell QA750 accelerometers placed on specific TPs on the false floor, as indicated in Figure 5.6.

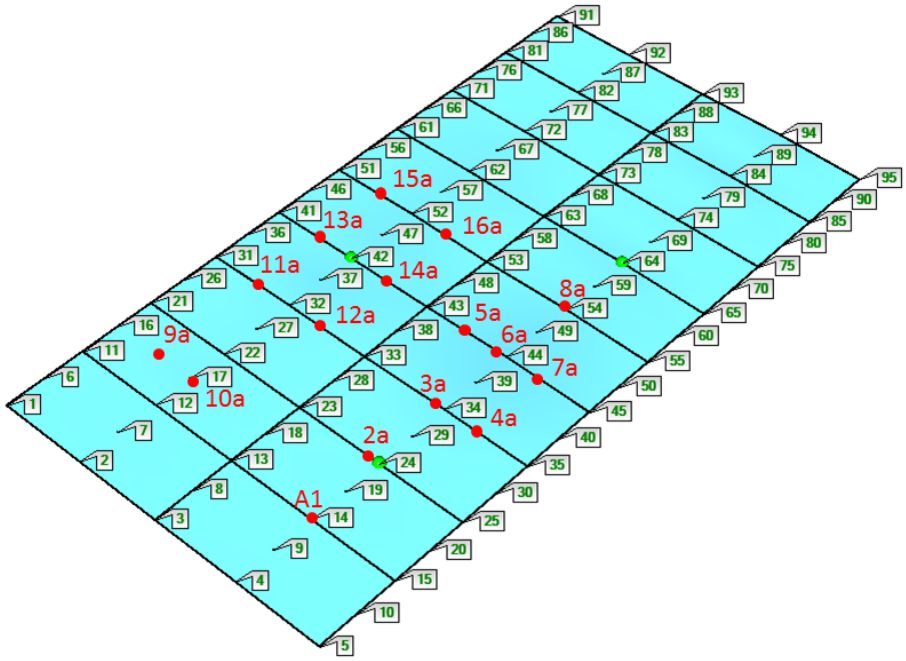

Figure 5.6: Test grid used for the modal testing (TPs' numbers are written in green) and vibration monitoring (TPs' numbers are written in red) of the floor. Green dots represent shakers' locations.

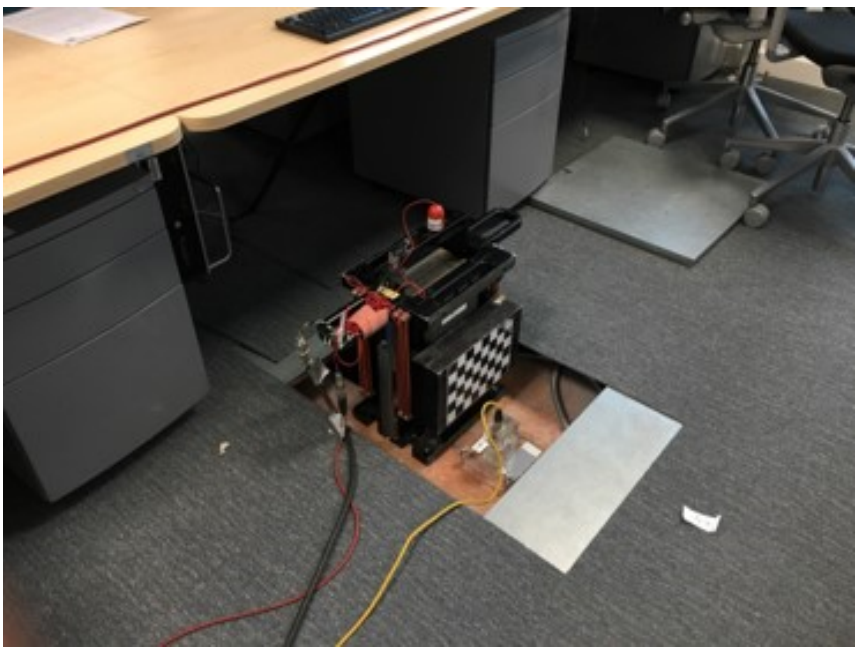

Figure 5.7: Placement of a shaker on the concrete surface.

The floor input force and output acceleration signals were processed using Data

Physics Spectrum Analyser DP730 to calculate the FRFs (Ewins, 2000). A Hanning window with 75% overlap was used for this purpose. Curve fitting of the calculated FRFs was carried out using ME'scope software (Vibrant Technology Inc., 2018) to extract natural frequency, mode shape, damping ratio and modal mass corresponding to modes of vibration of interest. The test lasted about ten minutes, during which 20 data blocks, each lasting 40 s, were collected, and the corresponding frequency resolution was 0.025 Hz. Figure 5.8 shows one block of input force, related to the shaker at TP42, and the corresponding vibration response measured at the same point.

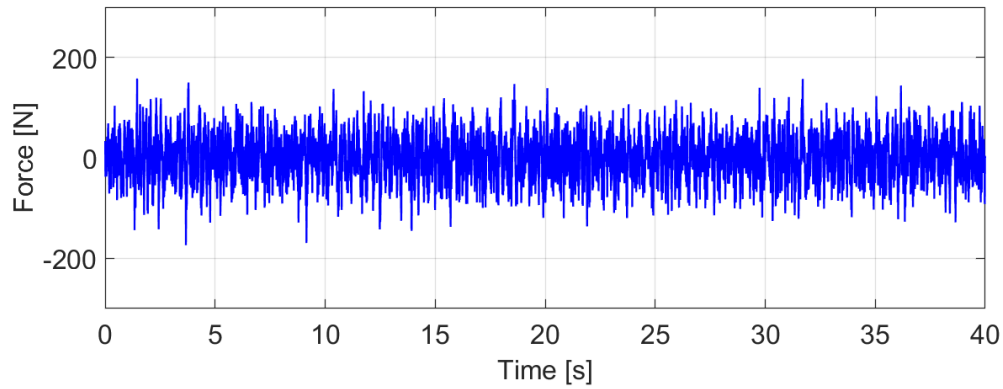

(a) Input force.

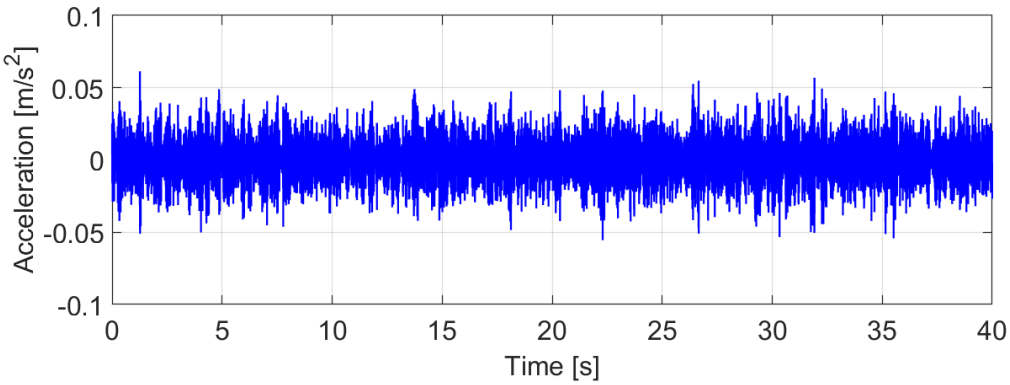

(b) Measured acceleration.

Figure 5.8: (a) Input force, related to the shaker at TP42, and (b) the corresponding acceleration response measured at the same point.

The fitting of the FRFs is illustrated in Figure 5.9 while the corresponding identified mode shapes of the lowest six modes of vibration are shown in Figure 5.10. It

is worth mentioning that this modal test is nominally identical to that described in Section 4.2.4, and the differences in their modal properties are believed to be related to the different construction stages when these two tests were conducted, i.e. when the building was a bare structure during construction and then when it was in operation. Further investigation regarding the influence of non-structural elements on the modal properties is outside the scope of this study.

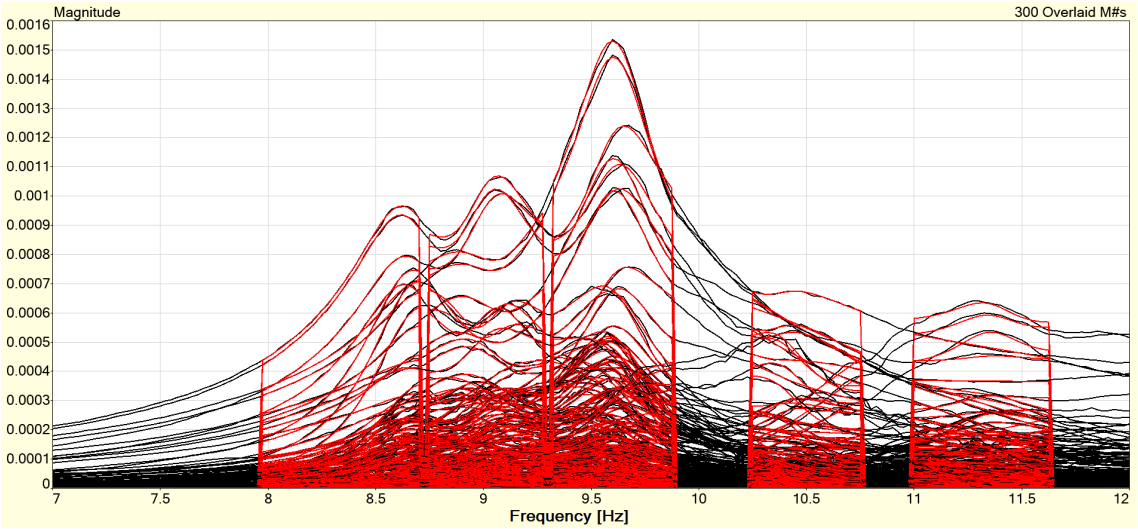

Figure 5.9: The estimated FRFs (black curves) and the corresponding curve fitting (red curves) for the lowest six modes of vibration.

5.3.3 People location tracking and vibration monitoring systems

There were around 40 people working in the testing area, and this number fluctuated slightly over the six testing days. They were mainly based in this area of the floor, so they had little interaction with the rest of the building. Only 30 UWB tags related to the location tracking system were available, and they were all charged overnight before distributing them randomly to floor occupants on each day of testing. The tags have an internal accelerometer to detect their movements, and they were configured for measurement at a frequency of 1 Hz while in stationary mode and 5 Hz during movements. The floor occupants

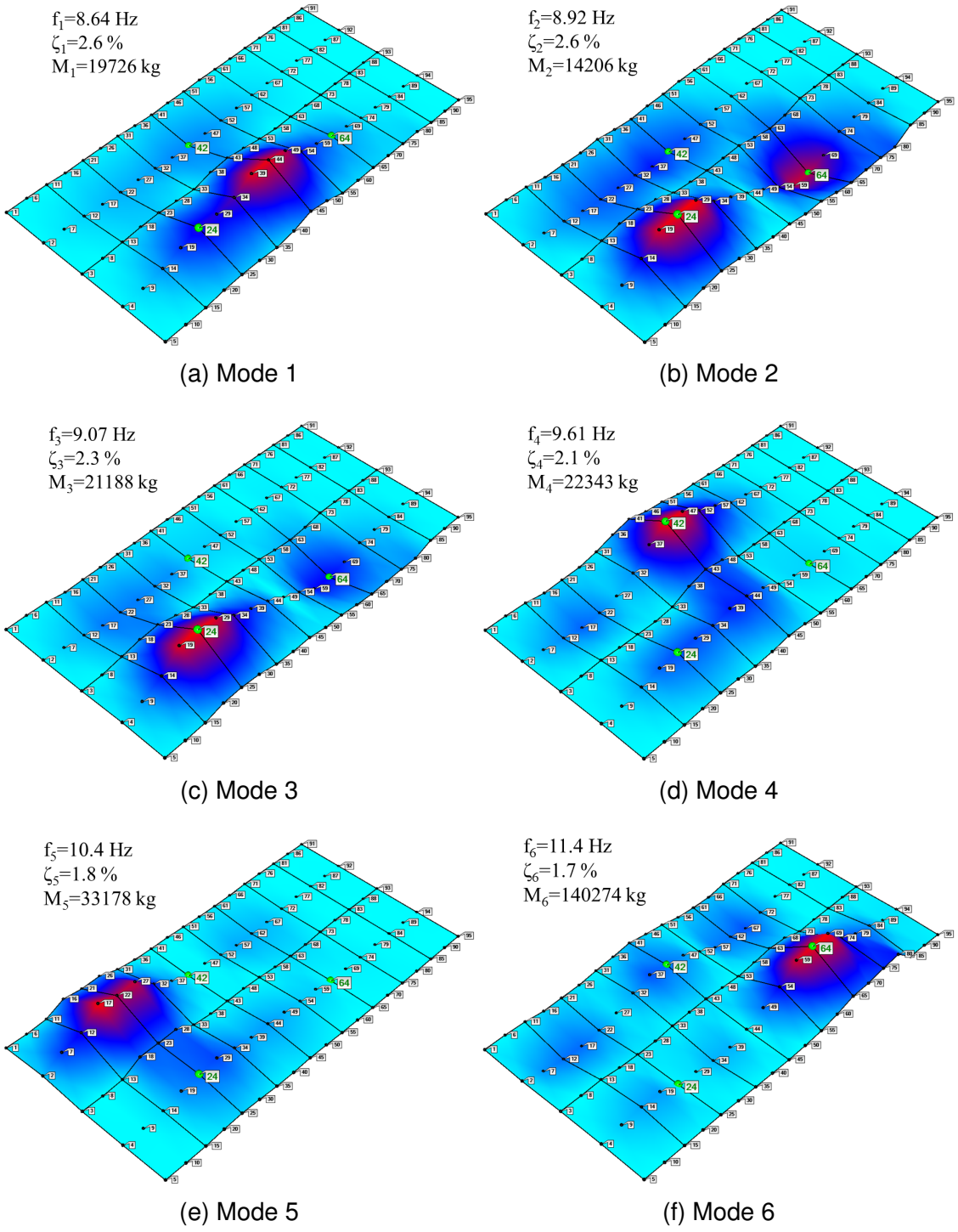

(a) Mode 1 (b) Mode 2

(c) Mode 3 (d) Mode 4

(e) Mode 5 (f) Mode 6

Figure 5.10: Mode shapes of the lowest six modes of vibration of the test floor when it was empty from occupants.

wore the tags using a lanyard during their presence on the floor, as indicated in Figure 5.11. Four anchors were attached to the windows frames, i.e. green triangles in Figure 5.5a, in the open-plan area where anchors have line-of-sight between them. While they can work in battery mode, they were connected to the power mains to ensure continuous operation. Participation in the location tracking

measurements was voluntary, and the floor occupants were approached by the management of the building to ask for volunteers before an approval was made to conduct the measurements.

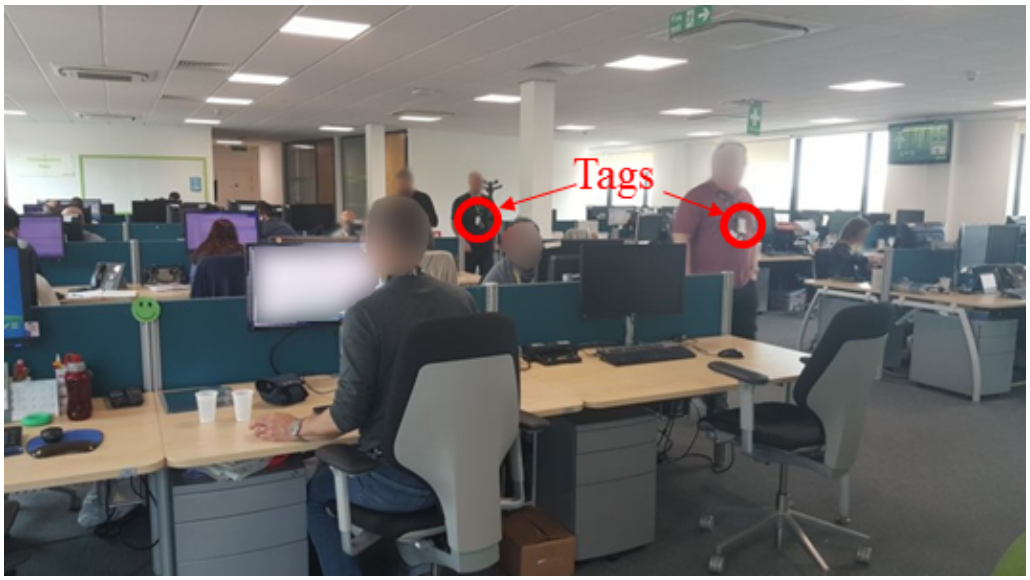

Figure 5.11: UWB tags worn by the floor occupants.

In total, 16 Honeywell QA750 accelerometers were deployed at the test grid shown in Figure 5.6 (red dots) to monitor the in-service vibration of the floor. The data acquisition (DAQ) centre for both systems was placed at the left edge of the floor (Figure 5.5a).

The test was conducted from Monday 30/04/2018 to Saturday 06/05/2018. During each day, the measurements were started at 08:00 and finished around 21:00. Most of the floor occupants arrived between 08:00 and 09:00 and left between 17:00 and 18:00. A second shift of floor occupants were there between 17:00 and 21:00.

Due to logistical difficulties, it was not possible to deploy the UWB tags immediately at the arrival of the floor occupants. However, most of the tags were deployed before 10:00. This is considered in the post-processing where the data collected before 10:00 were filtered out. It is worth mentioning that some of the

test subjects did not carry or wear their tags during their presence on the floor, i.e. between 10:00 and their departure. Notes about these tags were made during the test and their corresponding data were later filtered out in the post-processing.

5.3.4 Results and discussion

This section describes the results of the people's location tracking and vibration monitoring tests conducted on the floor described in the previous section. Firstly, the results related to the measured vibration responses, and their correlation with the corresponding number of walking floor occupants are presented. Key statistics about single and multiple pedestrian movements are illustrated, before presenting a brief discussion about the results.

The results presented in this section are related to three days of measurements when clear data were obtained for both the people's location tracking and vibration monitoring systems. These days are Wednesday, Thursday and Friday, 03/05/2018 to 05/05/2018, and they are referred to in this chapter as Day1, Day2 and Day3, respectively. The number of floor occupants whose location data were fully obtained, i.e. between 10:00 and their departure, is 17, 18 and 19 during Day1, Day2 and Day3, respectively.

5.3.4.1 Measured vibration responses

To take into account the perception of humans to vibrations, frequency weighting was applied to the vibration responses. Typical W_b frequency weighted (Institution, 1987) acceleration response time history related to Day2, i.e. $a_w(t)$, is presented in Figure 5.12 with the corresponding 1 s running RMS. As most floor occupants arrived on the floor between 08:00 and 09:00 and left by 18:00, the vibration results and analysis presented below correspond to the measurement

conducted between 08:00 and 18:00.

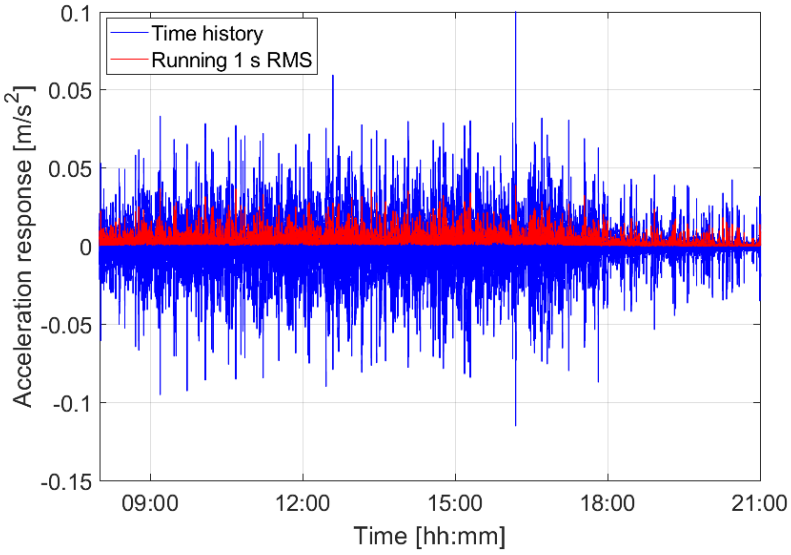

Figure 5.12: Typical weighted acceleration response related to Day2, at TP5a (Figure 5.6), and the corresponding 1 s running RMS.

To calculate the R factor, the RMS acceleration, $a_{w,rms}(t)$, was calculated using Equation 5.1.

$$a_{w,rms}(t) = \sqrt{\frac{1}{T}\int_0^T a_w^2(t)dt} \quad , \tag{5.1}$$

where, T is the total duration and dt is the duration of each time step (1 s).

The maximum transient vibration value ($MTVV$), which is equal to the peak $a_{w,rms}(t)$, can be utilised to calculate the R factor, as described in Equation 5.2 (Pavic and Willford, 2005).

$$R = MTVV/0.005 \quad , \tag{5.2}$$

The maximum R factor obtained from the measurements is 7.8, which is related to Day2 of measurements and TP5a (Figure 5.6). Moreover, statistics of R factors can be calculated for blocks of 1 s, in a similar way as described in Equations 5.1

and 5.2, and for the whole duration of the measurements. The corresponding cumulative distribution function (CDF) of the R factor values indicates how often a certain value of R factor was exceeded, as shown in Figure 5.13.

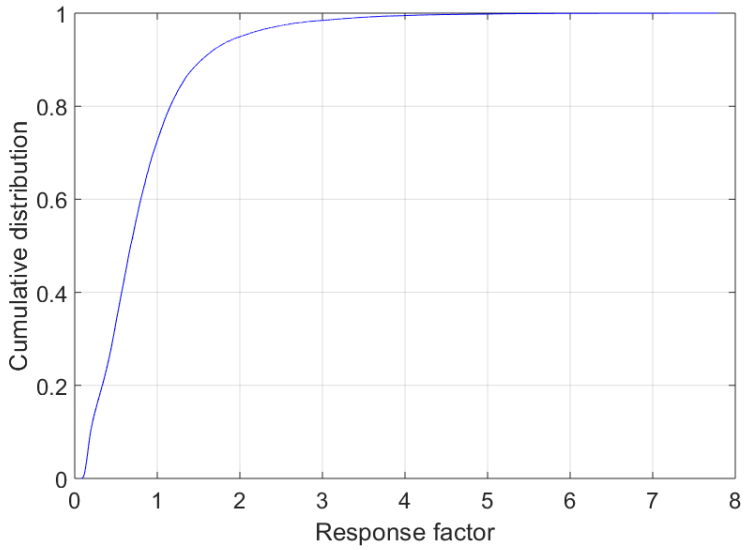

Figure 5.13: CDF of R factor related to blocks of 1 s of the vibration response.

Similar trends of vibration levels were obtained for the three days of measurements. For cumulative distribution of 75%, R factor did not exceed 1, which is the threshold for human perception to vertical vibration (BS6472:1992). The R factor of 4 was not exceeded for around 99.5% of the 1 s blocks. However, the remaining 0.5% of the R values, when R factor exceeded 4, represented around 250 seconds uniformly distributed over the day, as shown in Figure 5.14. The R factor of 8 was never reached in the three days of measurements.

to calculate the VDV, in [m/s$^{1.75}$], for the measured responses, Equation 5.3 can be utilised.

$$VDV = \left(\int_0^T a_w^4(t)\, dt \right)^{0.25} , \tag{5.3}$$

To facilitate the comparison between the measured VDV for 10 hours, between

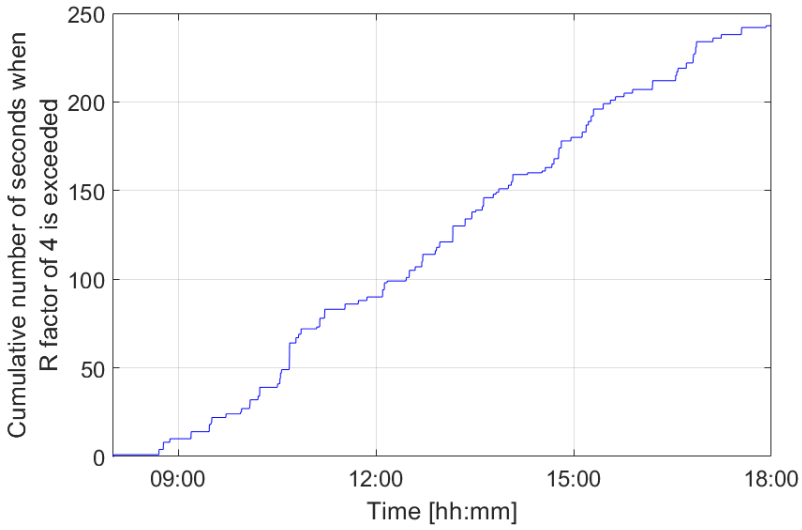

Figure 5.14: Number of times when R factor of 4 was exceeded at TP5a during Day 2.

08:00 and 18:00, and the tolerance limits given by BS 6472-1:2008 (2008), which correspond to 16 hours of exposure to vibrations, Equation 5.4 describes a normalised vibration dose value (VDV_{norm}) related to 16 hours of exposure to vibration.

$$VDV_{norm} = \left(\int_0^T a_w^4(t)\, dt \right)^{0.25} \left(\frac{16}{10} \right)^{0.25} , \tag{5.4}$$

The maximum VDV_{norm} obtained from the measurements was 0.157 m/s$^{1.75}$, occurred at TP5a on Day2. The cumulative VDV related to the measurements conducted on Day2 is presented in Figure 5.15.

5.3.4.2 Correlation between the number of pedestrians and their corresponding vibration levels

As the location tracking and the vibration monitoring systems were synchronised, it was possible to track the walking events related to maximum R factor, which was 7.8. It was found that the maximum R factor occurred when two floor occupants were walking along the dotted red lines, top to bottom, shown in Figure 5.16.

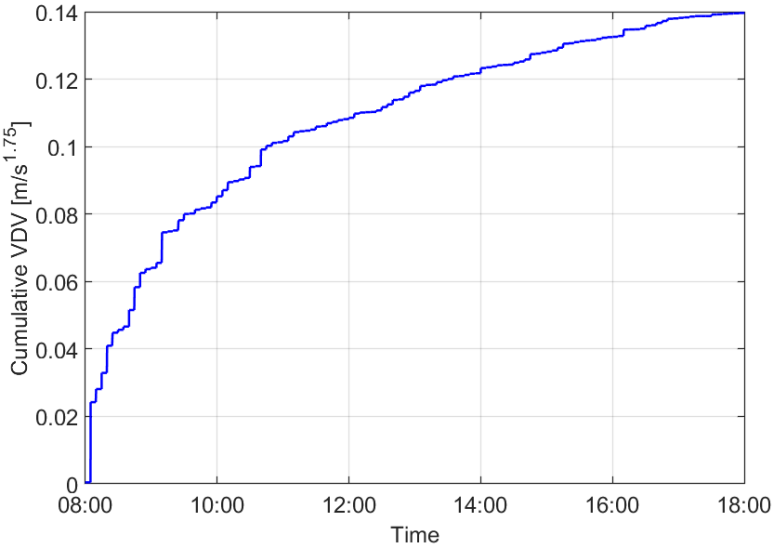

Figure 5.15: Cumulative VDV corresponding to the period between 08:00 and 18:00 at TP5a.

However, as not all floor occupants were wearing the tracking system tags, it is not known if more floor occupants were walking when the maximum R factor occurred.

Apart from the tracking system, certain walking events were noted manually when single or multiple pedestrians were walking on random walking paths across the testing area and their corresponding times were recorded. The aim was to compare the vibration response related to single and multiple pedestrians walking events. The time was recorded for 30 single pedestrian walking events and ten walking events for 2, 3, and 4 walking pedestrians, i.e. the total is 50 walking events. Figure 5.17 compares the R factor corresponding to these walking events.

Figure 5.17 shows a clear correlation between the number of pedestrians walking simultaneously and their corresponding R factor, i.e. the higher number of pedestrians walking simultaneously the higher the R factor, which is potentially a significant finding.

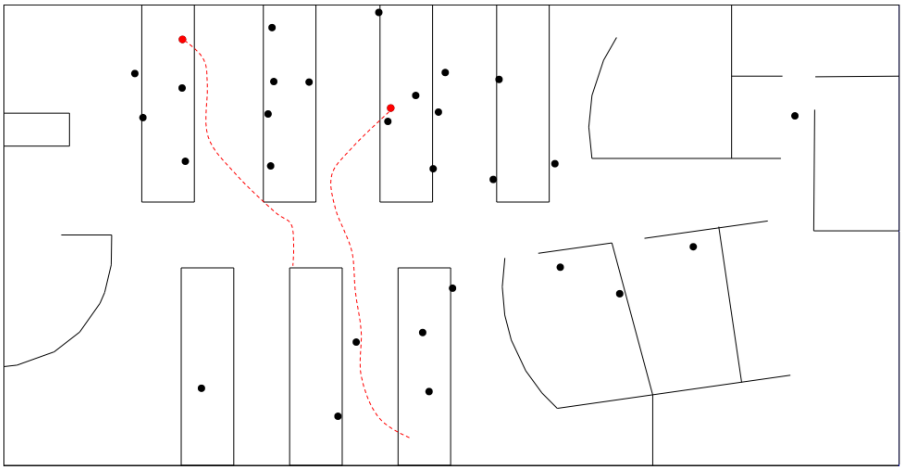

(a) Walking paths, top to bottom, related to maximum R factor (7.8).

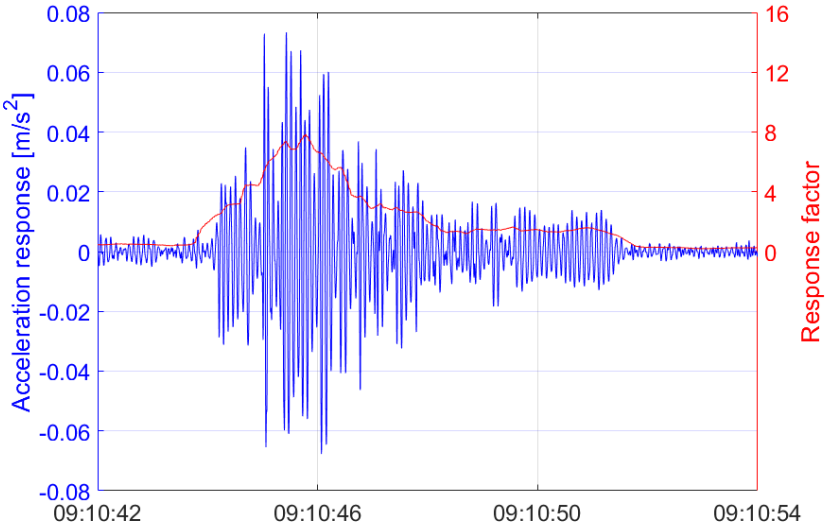

(b) Maximum vibration response (R factor) recorded at TP5a.

Figure 5.16: (a) Walking paths (top to bottom) related to maximum R factor (7.8) and (b) the corresponding vibration response.

5.3.4.3 Single and multiple pedestrian walking events

The Steel Construction Institute's design guideline (Smith et al., 2009) utilises a relationship, proposed by Ellis (2001), between the VDV and the corresponding number of walking events on a floor and their corresponding peak RMS acceleration, $a_{w,rms}(t)$, as mathematically described in Equation 5.5.

$$VDV = 0.68\ a_{w,rms,peak}(t)\ \sqrt{N_a T_a} \quad , \tag{5.5}$$

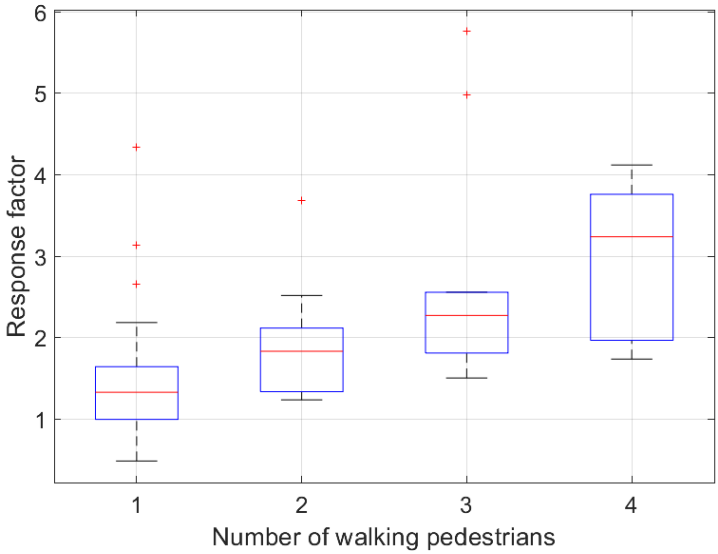

Figure 5.17: R factor corresponding to single and multiple pedestrian walking events.

where, N_a and T_a are the number and duration of individual walking activities, respectively.

Hence, it was interesting to count the average number of walking events conducted by floor occupants during the measurements. This can be useful to predict the number of walking events for other similar open-plan offices. In this study, a *walking event* is defined as the event when a *single* floor occupant walks for at least three meters and at least three seconds. These temporal and spatial limits were made to exclude short movements from the analysis. Figure 5.18 shows the cumulative probability distribution of the number of *individual walking events* conducted by floor occupants from 10:00 until 18:00.

The measurements show that the median number of walking events conducted by each floor occupant, between 10:00 and 18:00, is 16, and the average value is around 20. For simplicity, the average number can be interpolated for other duration of a working day, i.e. the average is 25 for 10 hours between 08:00 and 18:00.

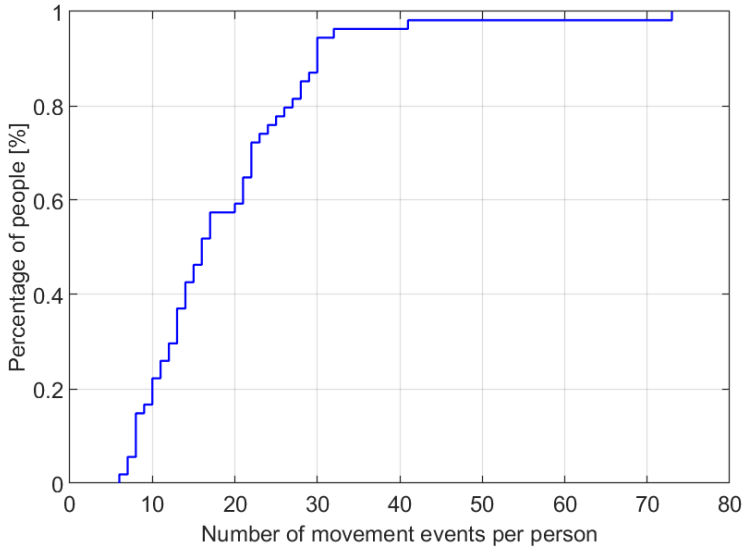

Figure 5.18: Number of individual walking events observed for the floor occupants.

Furthermore, it is expected that the higher the number of people on a floor, the more chance that a higher number of simultaneous walking events occur. A *simultaneous walking event* is defined in this study as an event when *two or more* single walking events, correspond to two or more floor occupants, occur simultaneously and overlap for at least 3 seconds. To verify this, it was possible to count the number of simultaneous walking events for different numbers of pedestrians, i.e. from those who were wearing tracking system tags. Figure 5.19 shows the average number of simultaneous walking events for a varying number of floor occupants. For example, for 15 occupants, there were 33 simultaneous walking events occurred by two or more of those occupants, as shown in Figure 5.19.

5.3.4.4 Discussion

The results, presented in Section 5.3.4.2, show that multiple pedestrian walking events are likely to produce a higher R factor than that for single pedestrian walking events. A controlled walking test, using a metronome, and conducted

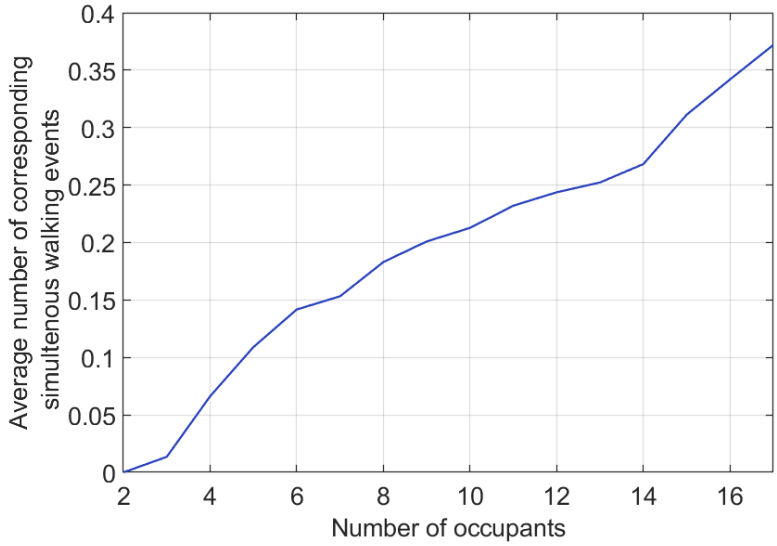

Figure 5.19: Number of simultaneous walking events for various number of floor occupants.

by a TS walking at a pacing frequency of 2.16 Hz, i.e. fourth integer multiple coincidences with the fundamental frequency of the floor as shown in Figure 5.10a, at various walking paths on the floor has produced a maximum R factor of 5.3. This is still less than the recorded maximum R factor related to multiple pedestrian walking events (Figure 5.16). The higher vibration levels related to multiple floor occupants, than that related to individual occupants, was also reported by Chen et al. (2015). However, Živanović et al. (2012) reported lower vibration levels for an in-service office floor, occupied by multiple occupants, than that related to single person walking tests. Hence, it is evident that utilising only single person walking scenario in the design could lead to an underestimation or overestimation of vibration levels.

The maximum VDV_{norm} obtained from the measurements, 0.157 m/s$^{1.75}$, was way below the threshold for low probability of adverse comment for offices given by BS 6472-1:2008 (2008), i.e. 0.4-0.8 m/s$^{1.75}$. This threshold is based on the assumption of continuous exposure to vibration, which is not the case for typical footfall-induced vibration of floors (BS 6472-1:2008, 2008; Pavic and Willford,

2005) where people tend to walk intermittently. The Concrete Society's design guideline (Pavic and Willford, 2005) adopts a relationship between the proportion of time when floor occupants are exposed to vibration and a corresponding scaling factor for the VDV tolerance, as shown in Figure 5.20. For example, for continuous exposure to vibration, a scaling factor of 1.0 is to be utilised.

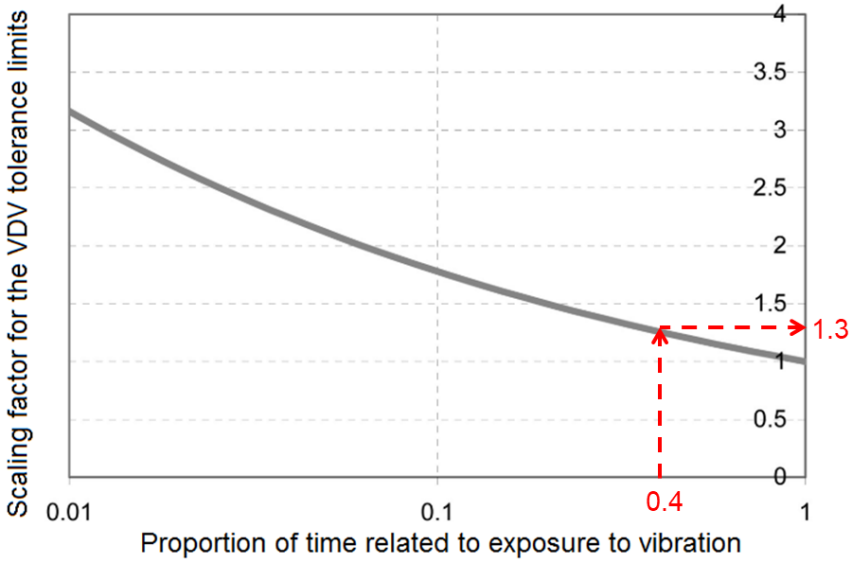

Figure 5.20: Relationship between a constant VDV and proportion of time of actual vibration required to cause such constant VDV (Pavic and Willford, 2005).

The proportion of time related to occupants' exposure to footfall-induced vibrations can be estimated using the collected data of people's movements. It is assumed that the occupants were only exposed to vibration when single of multiple occupants were walking. Figure 5.21 shows the ratio between the total recorded duration of movements from 10:00 to 18:00, by single or multiple floor occupants, and the total duration which is 8 hours.

Figure 5.21 shows an approximately linear relationship between the number of floor occupants and their corresponding proportion of time when single or multiple floor occupants were walking on the floor. For example, if the floor only included 17 occupants, the proportion of time when a single or multiple occupants were walking on the floor was around 17%. Similarly, and by extrapolation, it is

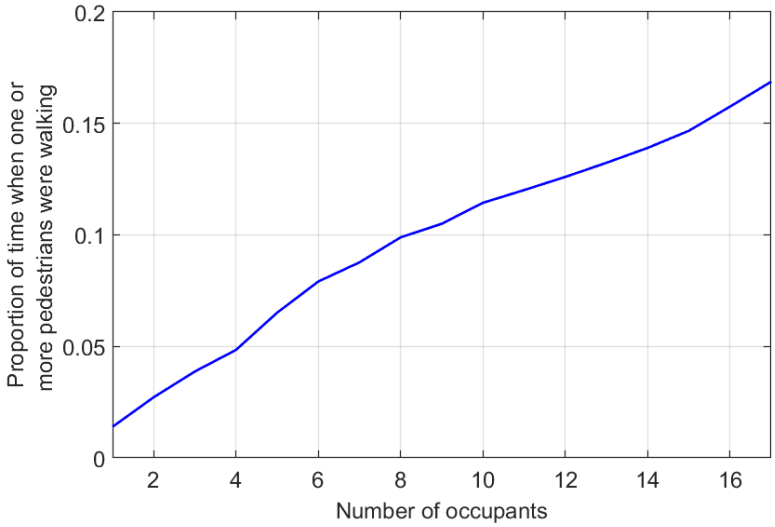

Figure 5.21: Proportion of time when single or multiple floor occupants were walking on the floor.

expected that for 40 occupants, the proportion of time when a single or multiple occupants were walking on the floor was 40%, as shown in Figure 5.21. As this number is a proportion of time, it applies for 8 hours or any other duration. This proportion was also assumed to be equal to the proportion of time related to exposure to footfall-induced vibration. This corresponds to an increased VDV limit, according to Figure 5.20 (BS 6472-1:2008, 2008), by a factor of 1.3. Therefore, the relevant tolerance VDV limit for low probability of adverse comments is $1.3 \times (0.4 - 0.8) = (0.52 - 1.04)$ m/s$^{1.75}$, which is significantly higher than the measured VDV_{norm}, 0.157 m/s$^{1.75}$. Since the threshold for low probability of adverse comment is a range between two numbers, 0.52-1.04 m/s$^{1.75}$, its higher limit, i.e. 1.04 m/s$^{1.75}$, is likely to be used in practice which is more than six times higher than that calculated from the measurements, 0.157 m/s$^{1.75}$).

A questionnaire created for 30 random floor occupants (Figure 5.22) shows that no one of them complained about any excessive or clear vibration levels.

Bearing in mind the questionnaire results and the difference between the VDV obtained from the measurements, VDV_{norm} = 0.157 m/s$^{1.75}$, and its tolerance

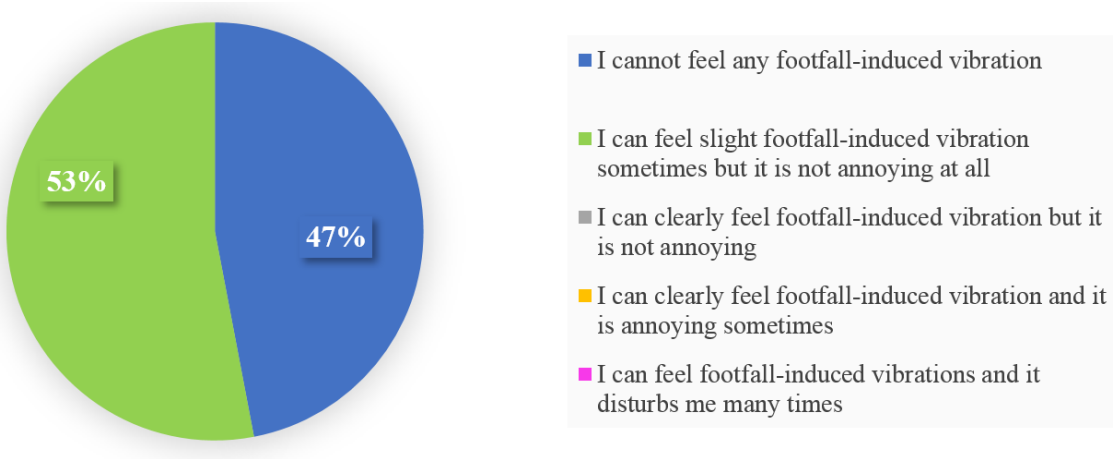

Figure 5.22: Questionnaire results about perceived vibration levels.

limit, 1.04 m/s$^{1.75}$, it is unlikely that vibration responses related to VDV_{norm} six times higher than that obtained from the measurements will still have low probability of adverse comments.

Hence, it appears that both of the R factor and VDV failed to describe reliably vibration serviceability performance of the floor. The main problem of utilising R factor in the design is its dependence on a single value related to the peak RMS response. Utilising R factor related to specific probability of exceedance can describe more reliably vibration levels than using only the peak R factor. The VDV takes into account the duration of exposure to vibration in its calculations as described above, but it is apparent that its tolerance limits need calibration for footfall-induced vibration of office floors. A similar conclusion regarding utilising VDV in the design was reached by Reynolds and Pavic (2015). The other issue related to utilising VDV in the design is the need to estimate the number and location of walking events needed to calculate VDV in the design stage.

5.4 Modelling of people occupancy

This section provides a description of modelling of people's occupancy and movements on open-plan office floors and simulation of the full time history

related to their locations. These time history data are useful to conduct either full simulation of footfall-induced vibrations or to assess vibration levels of floors using VDV, as explained in the next two sections. The proposed model is based on data regarding people's locations collected in the experiment described in Section 5.3.

In this section, statistical data (Section 5.4.1) regarding the measurements were presented before describing the structure of the model (Section 5.4.2). The performance of the model is demonstrated in Section 5.4.3.

5.4.1 Statistical data

To model movement patterns, the floor was divided into zones based on their function. The zones are presented in Figure 5.23 and as follows:

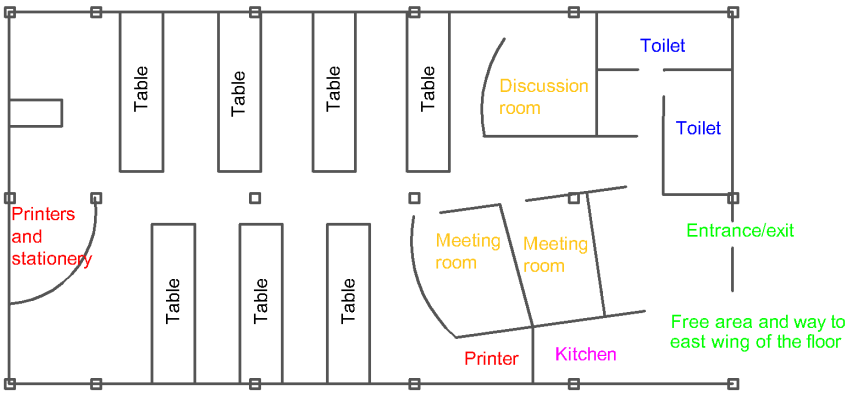

Figure 5.23: Zones on the test floor. Zones 1 and 2 in black, Zone 3 in red, Zone 4 in yellow, Zone 5 in blue, Zone 6 in pink and Zone 7 in green.

1. Zone 1 is the own desk of each individual. This desk could be related to any of the annotated tables in Figure 5.23.

2. Zone 2 is a desk related to any colleague on the test floor. This is to take into account the scenario when a person walks to a colleague, e.g. for a quick discussion.

3. Zone 3 covers two floor areas housing printing and stationery.

4. Zone 4 represents two meeting areas and a discussion room where floor occupants meet from time to time.

5. Zone 5 represents the toilets area.

6. Zone 6 is a kitchen where floor occupants can get a coffee or store their food.

7. Zone 7 represents a free area where floor occupants occasionally sit for lunch or to make phone calls. Due to its distant location, compared with the anchors (Figure 5.5a), the signals received by the UWB tags in this area were weak and disappearing. Hence, sometimes it was not possible to distinguish if a person was located at the far end of that area or if he/she left the floor. Therefore, it was decided that Zone 7 included the free area and any other area that floor occupants may go beyond.

Figure 5.24 presents the CDF of the time durations spent by each floor occupant at these zones between each two subsequent walking events. The data presented in Figure 5.24 correspond to the aggregate data for 17, 18 and 19 floor occupants in Day1, Day2 and Day3, respectively.

As it was not possible to deploy the UWB tags for the occupants immediately after their arrival, no reliable measurement was made before 10:00. However, there are studies available in the literature regarding the first arrival rate (Reinhart, 2004), which can be measured using simple techniques.

Departure times were the times when floor occupants returned their UWB tags at the end of each day before their final departure. The time duration between the

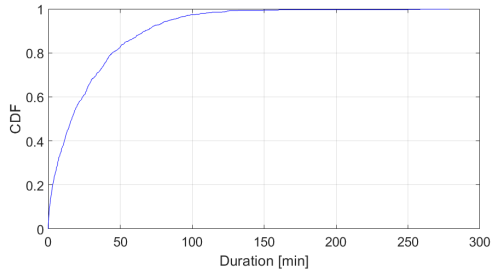

(a) Duration at Zone 1 between two walking events.

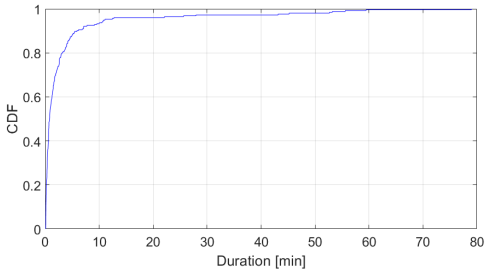

(b) Duration at Zone 2 between two walking events.

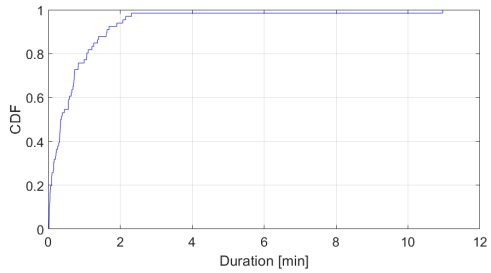

(c) Duration at Zone 3 between two walking events.

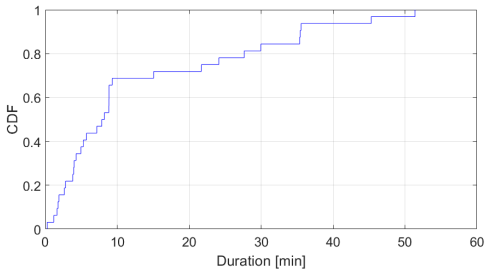

(d) Duration at Zone 4 between two walking events.

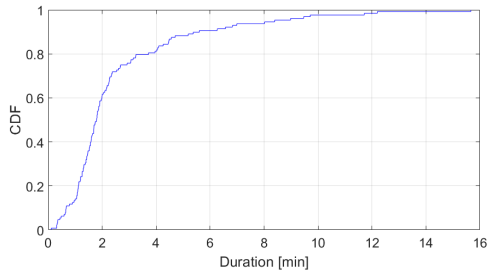

(e) Duration at Zone 5 between two walking events.

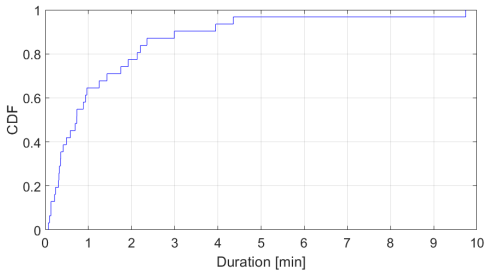

(f) Duration at Zone 6 between two walking events.

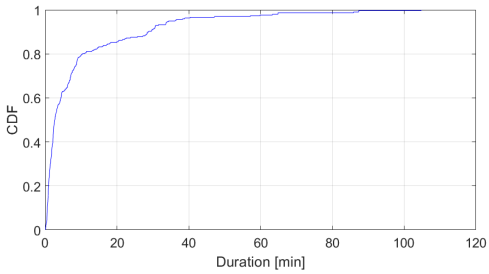

(g) Duration at Zone 7 between two walking events.

Figure 5.24: CDF of the time spent by individual floor occupants at zones 1-7 between two subsequent walking events.

departure of each two subsequent floor occupants was extracted. Figure 5.25 shows the CDF of the duration between each two subsequent departures by two floor occupants.

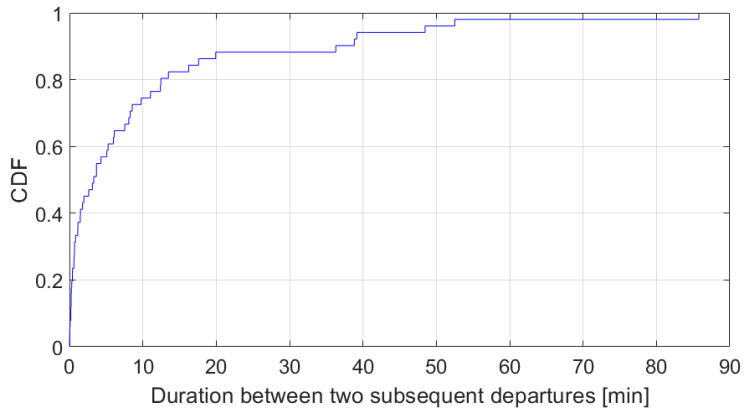

Figure 5.25: The CDF of the duration between two subsequent final departures of two floor occupants.

These data could be utilised to model walking paths on office floors by describing origin-destination pairs related to walking events.

Furthermore, natural walking speed was calculated for 100 walking events chosen randomly. The walking path and the corresponding duration related to 100 walking events, from the measurements, were used for this purpose. The CDF of the calculated walking speeds is presented in Figure 5.26.

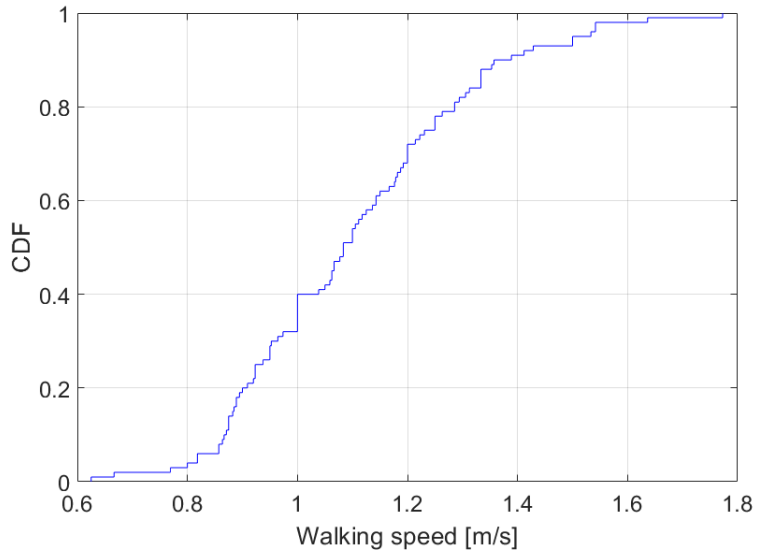

Figure 5.26: Walking speed obtained from the people's location tracking measurements.

5.4.2 Model structure

The model mainly comprises building a 'schedule' for each floor occupant during a day. The corresponding movements are conducted using the social force model which takes into account the features of natural walking and interaction with other floor occupants and the surrounding boundaries in an agent-based framework, as explained below (Helbing and Farkas, 2002). While the social force model is sensitive to the parameters related to physical contact between the occupants and the surroundings (Helbing and Farkas, 2002), this is not expected to be an issue when the model is used to simulate movements in normal conditions, i.e. not evacuation scenarios where pedestrians are less likely to touch the walls and other boundaries during walking. Further details regarding the social force model and its implementation can be found elsewhere (Helbing and Farkas, 2002; Mohammed and Pavic, 2019).

The key elements of occupants' 'schedules' are explained below and are shown in Figure 5.27:

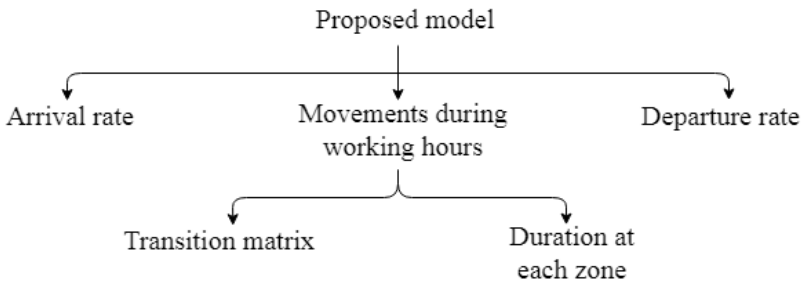

Figure 5.27: The key elements of occupants' 'schedules'.

1. While no reliable measurements for the arrival rate were obtained in this study, uniform distribution could be assumed for the arrival of the floor occupants. Alternatively, other data available in the literature can be used for this purpose (Page et al., 2008).

2. The intermediate movements between the first arrival and last departure. This is the focus of the proposed model, where accurate and high time-resolution data of the people's locations were used. This is discussed below in more detail.

3. The departure rate. This can be based on the measurements described in this chapter or from the literature (Page et al., 2008).

Modelling the intermediate movements is a more complex task than that for the arrival and departure rates. Table 5.1 shows the total number of walking events conducted by 17, 18 and 19 floor occupants during Day1, Day2 and Day3, respectively. For example, there were 37 recorded movements from the own desks to the printing areas and 19 movements from the meeting areas to the own desks.

Table 5.1: Number of walking events conducted by 17, 18 and 19 floor occupants during Day1, Day2 and Day3, respectively, from one zone to another.

		To						
	Zone	Own desk	Other desks	Printing areas	Meeting areas	Toilets area	Kitchen area	Free areas
From	Own desk	0	140	37	18	58	6	152
	Other desks	121	40	5	3	10	0	128
	Printing areas	40	3	0	4	0	0	9
	Meeting areas	19	4	4	0	0	3	4
	Toilet area	54	5	3	3	0	4	28
	Kitchen area	9	3	4	4	0	0	14
	Free areas	168	12	3	2	29	21	0

These intermediate movements between different zones of the floor can be visualised as a chord diagram, as shown in Figure 5.28. The thickness of the curves in this figure corresponds to the number of walking events between each two zones.

Figure 5.28 shows that most of the movements were occurred between Zone

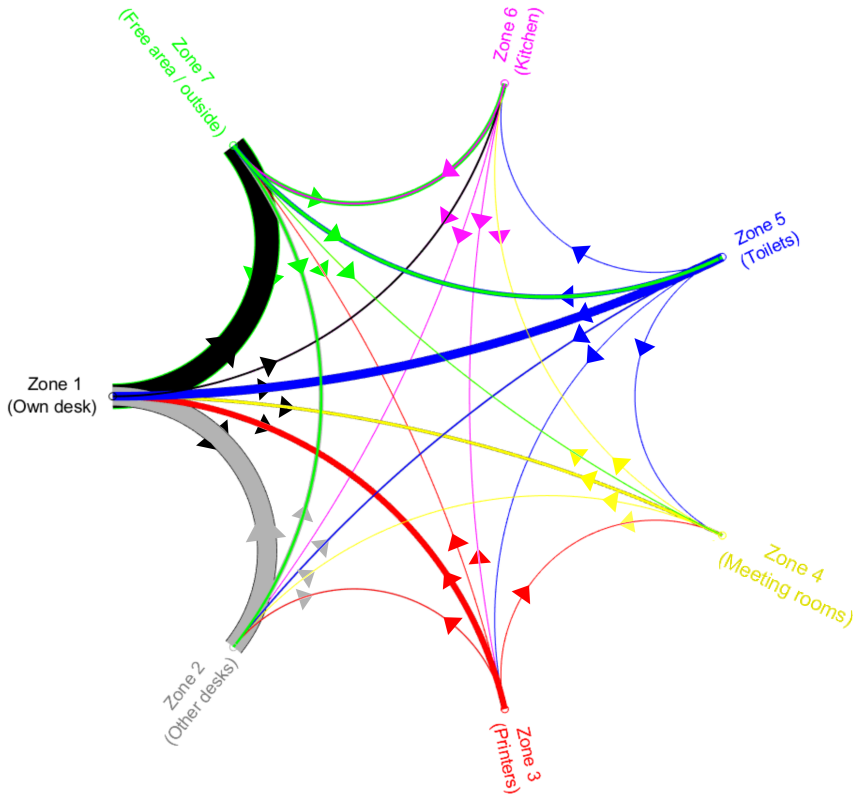

Figure 5.28: Chord diagram showing the intermediate movements between different zones on the floor. The thickness of the curves corresponds to the number of walking events between each two zones.

1, i.e. own desk of floor occupants, and other zones, while some of them were in-between the desks, i.e. Zone 1 and Zone 2. A convenient strategy to model this pattern of movements is to use the transition matrix, also known as Markov matrix or stochastic matrix (Page et al., 2008). It is a square matrix which can describe the probability of transition from one state to another based on the current state. All entries in the transition matrix should be real values between 0 and 1.0. The Markov chain, the basis of the Markov matrix, has proven its efficiency to describe the occupancy patterns as reported in the literature (Page et al., 2008). The transition matrix was formed by identifying the number of transitions made from each zone to all other zones, i.e one row in Table 5.1. These numbers were then divided by the total number of transitions occurred from that zone, i.e. summation of each row in Table 5.1. The resulting transition matrix is shown in Table 5.2.

Table 5.2: Transition matrix corresponding to occupants' movements from one zone to another.

		To						
	Zone	Own desk	Other desks	Printing areas	Meeting areas	Toilets area	Kitchen area	Free areas
From	Own desk	0	0.341	0.09	0.044	0.141	0.015	0.37
	Other desks	0.585	0.193	0.024	0.014	0.048	0	0.135
	Printing areas	0.714	0.054	0	0.071	0	0	0.161
	Meeting areas	0.559	0.118	0.118	0	0	0.088	0.118
	Toilet area	0.557	0.052	0.031	0.031	0	0.041	0.289
	Kitchen area	0.265	0.088	0.118	0.118	0	0	0.412
	Free areas	0.715	0.051	0.013	0.009	0.123	0.089	0

The probabilities of a floor occupant moving from Zone 1, as an example, to other zones are presented in the first row of the matrix shown in Table 5.2. The same applies to movements from other zones. Hence, the summation of all probabilities related to moving from one zone should equal 1.0. This approach ensures probabilistic, instead of deterministic, treatment of the movements.

5.4.3 Demonstration

This section demonstrates the capability of the proposed model by simulating the movements of 18 floor occupants in the same floor layout described in Section 5.3. The results is presented in the form of heatmaps, where it is possible to visualise the simulated locations.

5.4.3.1 Heatmaps related to walking paths

Figure 5.29a presents all recorded locations related to walking events of a individual floor occupant during Day2. The corresponding heatmap, shown in Figure 5.29b, can be calculated as follows.

1. At each point (j) on the heatmap, identify the duration of time when an individual g was walking within 0.5m, measured horizontally or vertically,

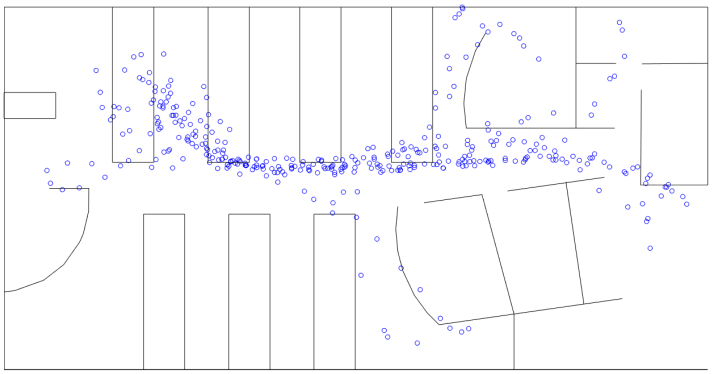

(a) Recorded locations of a walking occupant on Day2.

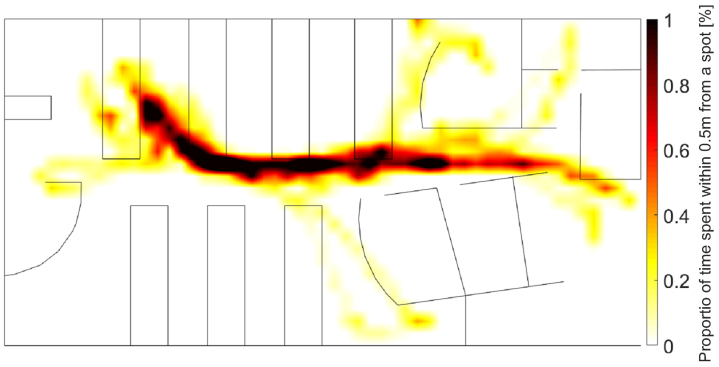

(b) The corresponding heatmap.

Figure 5.29: (a) Recorded walking locations related to a typical occupant on Day2 and (b) the corresponding heatmap.

from its coordinates $t_{j,g}(x, y)$, where, x and y represent the horizontal and vertical coordinates of point j, respectively.

2. Identify the total duration spent by the individual g walking on that day (T_g).

3. Calculate the proportion of time spent by individual g walking within 0.5m, measured horizontally or vertically, from point j ($k_{j,g}(x, y)$), as mathematically described in Equation 5.6.

$$k_{j,g}(x, y) = \frac{t_{j,g}(x, y)}{T_g} \quad , \tag{5.6}$$

4. Repeat the same for all other points on the floor, and plot $k_{j,g}(x, y)$, as shown

in Figure 5.29b.

In Figure 5.29b, the color on each point on the map refers to the proportion of time spent by the occupant walking within 0.5 m, measured horizontally or vertically, from that point. The same principle can be followed to generate a heatmap corresponding to multiple floor occupants for each day of the measurement. These heatmaps are generated as follows:

1. Calculate $k_{j,g}(x, y)$ for every pedestrian, i.e. for N_p number of pedestrians separately.

2. Calculate $K_j(x, y)$, the average proportion of time spent by floor occupants walking within 0.5m from point j, as described in Equation 5.7.

$$K_j(x, y) = \frac{\sum_{g=1}^{N_p} k_{j,g}(x, y)}{N_p} \quad , \tag{5.7}$$

3. Repeat the same for all other coordinates and plot $K_j(x, y)$ corresponding to each day of measurement.

5.4.3.2 Heatmaps generated from simulations and measurements

The heatmaps were generated from measured and simulated locations of floor occupants during walking, as shown in Figure 5.30. The heatmap related to the proposed model (Figure 5.30b) is comparable with those related to the measurements (Figure 5.30a). There are also clear differences between them, but the locations of hotspots are similar between them. However, the simulations are not expected to reproduce the exact locations as those obtained from the measurements due to the probabilistic nature of the proposed model.

The proposed movement model can be applied to model people's movements for

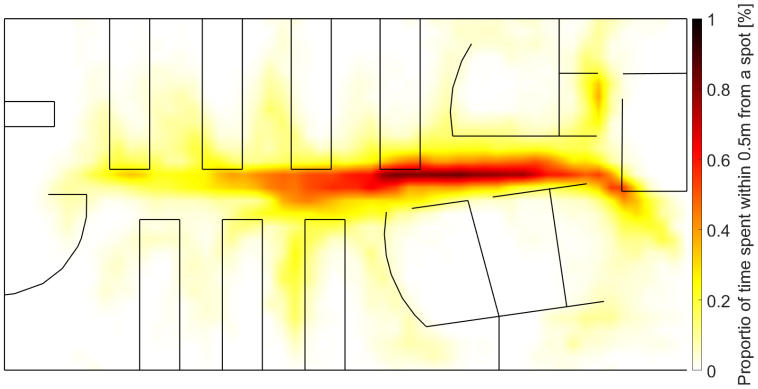

(a) Heatmap generated from the measurements.

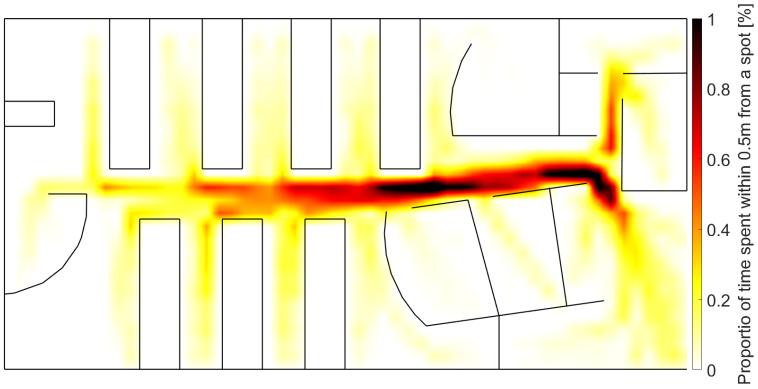

(b) Heatmap generated from the simulations.

Figure 5.30: Heatmaps generated from (a) measurements and (b) simulations, showing the proportion of time spent by all occupants walking within 0.5m, measured horizontally or vertically, from any point on the floor.

other office floors. For other types of floors, more experimental measurements are needed to derive the time that floor occupants spend at each zone (Figure 5.24) and their corresponding transition matrix (Table 5.2).

5.5 Improved method for predicting VDV

Equation 5.5, which can be used to calculate VDV from the peak weighted RMS acceleration and number and duration of walking events, does not take into account the variable locations of floor occupants during walking and their number of occurrences. Hence, this section describes an improved method for predicting

VDV based on realistic movements of occupants which takes into account the variable locations of the occupants.

The proposed method is based on representing people's movements for one day as a heatmap, as explained below. Hence, the steps needed to generate heatmaps related to floor occupants' movements are explained before presenting a description related to utilising these heatmaps in the proposed method for predicting VDV.

5.5.1 Methodology

The term under the square root in Equation 5.5, i.e. N_a and T_a, represents the total duration of walking events related to all floor occupants. This term can be replaced by a duration obtained from the heatmap, which takes into account the spatial and temporal locations of floor occupants during walking. Hence, Equation 5.8 is the revised equation to calculate the VDV, as explained below.

$$VDV_{j,i} = 0.68\ a_{w,rms,j,i}\ \sqrt{T_{eff,i}} \quad , \tag{5.8}$$

where, $VDV_{j,i}$, in [m/s$^{1.75}$], is the VDV at the response point i corresponding to a footfall force applied at excitation point j , $a_{w,rms,j,i}$ is the maximum 1 s RMS weighted acceleration obtained at the response point i and corresponding to footfall force applied at excitation point j [m/s^2] and $T_{eff,j}$ is the effective time spent walking at the excitation point j [s], as described below.

The steps needed to implement the proposed method, which is inspired by the method presented by the Concrete Society (Pavic and Willford, 2005) for low-frequency floors, are illustrated in a flow-chart in Figure 5.31 and summarised

below:

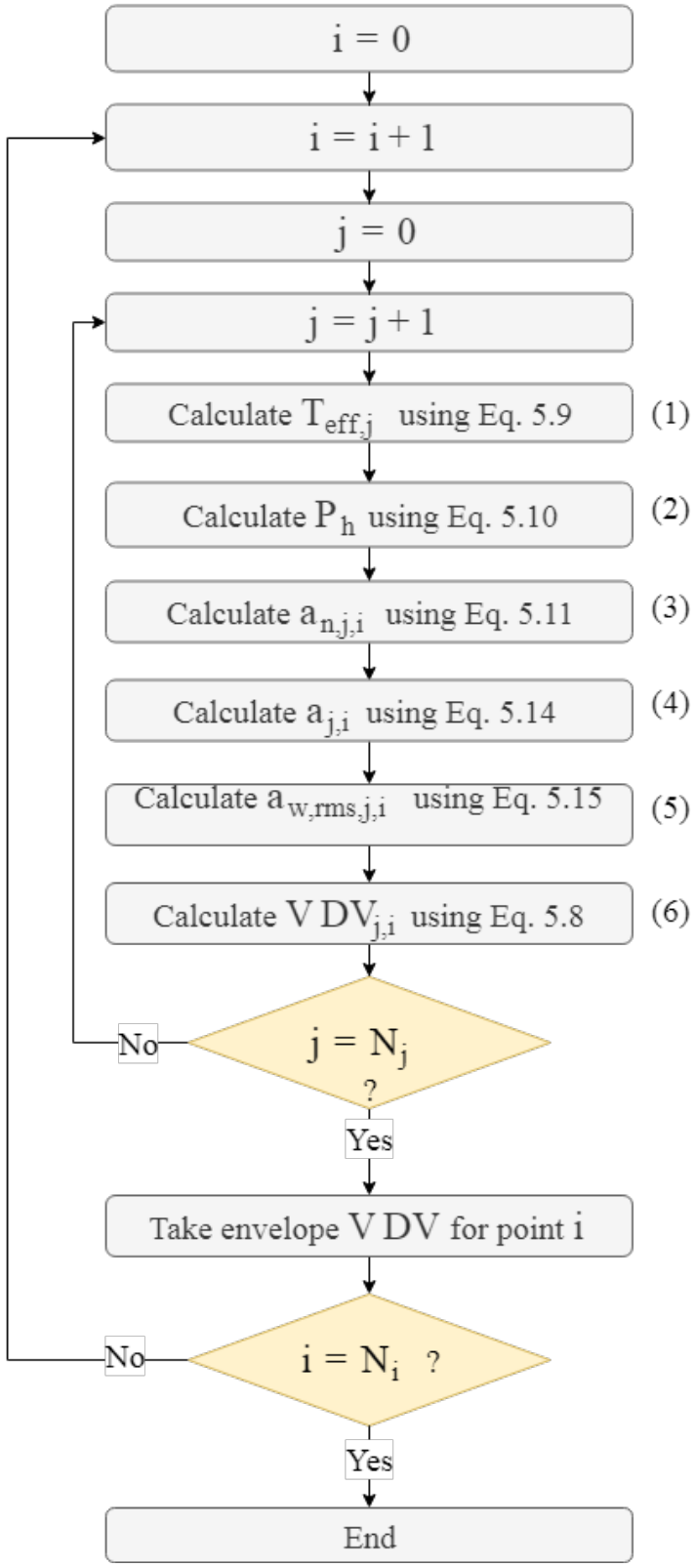

Figure 5.31: Flow-chart showing the proposed methodology to calculate VDV.

1. Calculate $T_{eff,j}$, as described in Equation 5.9.

$$T_{eff,j} = K_j(x,y)\ N_e\ T_e\ N_p \quad , \tag{5.9}$$

where, N_e is the average number of single walking events carried out by each individual (Figure 5.18) and T_e is the average duration of single walking events, which can be obtained from the measured or simulated walking events, as explained below.

2. Calculate harmonic force amplitude, P_h, for each harmonic, as described in Equation 5.10.

$$P_h = \alpha_h W \quad , \tag{5.10}$$

where, α_h is the Fourier coefficient of the hth harmonic and W is the weight of human body [N].

3. Calculate modal response, $a_{n,j,i}$, related to mode n, using Equation 5.11.

$$a_{n,j,i} = \sqrt{\sum_{h=1}^{4} a_{n,h,j,i}^2 (h f_p)} \quad , \tag{5.11}$$

$$a_{n,h,j,i} = u_{i,n} u_{j,n} \left(\frac{h f_p}{f_n}\right)^2 \frac{P_h}{M_n}\ DMF_{h,n} \quad , \tag{5.12}$$

$$DMF_{h,n} = \frac{1}{\left(1 - \left(\frac{h f_p}{f_n}\right)^2\right) + \sqrt{-1}\left(2\zeta_n\left(\frac{h f_p}{f_n}\right)\right)} \quad , \tag{5.13}$$

where, $a_{n,h,j,i}$ is harmonic modal acceleration related to mode n and harmonic h at point i related to excitation at point j. f_p is the pacing

frequency and $u_{j,n}$ and $u_{i,n}$ are mode shape amplitudes at the excitation and response points related to mode n, respectively. f_n, M_n and ζ_n are the natural frequency [Hz], modal mass, i.e. unity-scaled, [kg] and damping ratio related to mode n of vibration, respectively, and $DMF_{h,n}$ is the dynamic magnification factor for mode n and harmonic h.

4. Calculate the physical response at point i due to excitation at point j ($a_{j,i}$) following the principle of superposition, as described in Equation 5.14.

$$a_{j,i} = \sum_{n=1}^{N_m} a_{n,j,i}(t) \quad , \tag{5.14}$$

where, N_m is the total number of modes with a natural frequency less than 12 Hz (Pavic and Willford, 2005).

5. Apply W_b weighting, using Figure 5.32, to obtain the weighted acceleration, $a_{w,j,i}$, and calculate the RMS acceleration, $a_{w,rms,j,i}$, using Equation 5.15.

$$a_{w,rms,j,i} = 0.707\ a_{w,j,i} \quad , \tag{5.15}$$

6. Calculate $VDV_{j,i}$ using Equation 5.8.

7. Repeat the above mentioned steps for all N_j excitation points and all N_i response points and extract the maximum vibration response at to each response point across range of pacing frequencies, related to excitation, to be included in the analysis.

It is worth mentioning that the same resonance scaling approach, as in the Concrete Society design guideline (Pavic and Willford, 2005), can be applied to

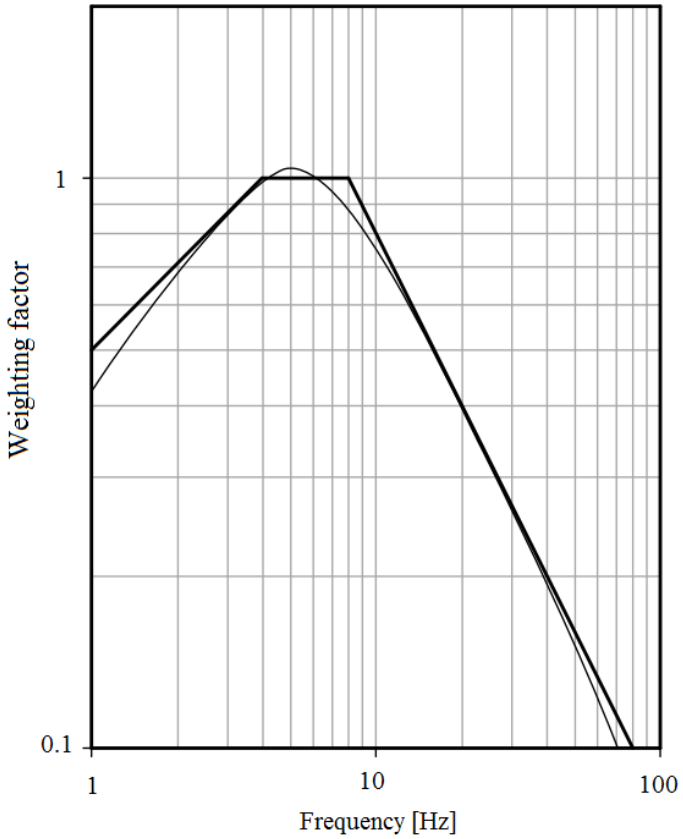

Figure 5.32: W_b frequency weighting curve for z-axis (light curve) and its approximation (thick curve) (BS6472:1992).

take into account the varying location of walking pedestrians and the build-up time needed to achieve resonant response.

5.5.2 Verification

This method was utilised to calculate the VDV of the tested floor, and comparison was made with the VDV obtained from the measurements (Section 5.3.4.1).

The average pacing frequency, 1.7 Hz, was calculated from an average walking speed of 1.1 m/s, taken from Figure 5.26, as mathematically described in Equation 5.16 (Smith et al., 2009).

$$v = 1.67 f_p^2 - 4.83 f_p + 4.5 \quad , \tag{5.16}$$

In Section 5.3.4.3, it was found that the average number of single movement events is 20 (Figure 5.18), which corresponds to 8 hours, i.e. between 10:00 and 18:00. Hence, N_e for 10 hours, from 08:00 to 18:00, can be extrapolated to N_e =40 for 16 hours. T_e was assumed to be around 10 s, from observation of the collected data, and N_p was taken as 40.

The modal properties obtained from the measurements (Figure 5.10) were utilised in the analysis to calculate the vibration responses.

The VDV from measurements (Section 5.3.4.1) and the proposed method, equivalent to 16 hours, are illustrated in Figure 5.33. The figure shows that the VDV from measurements, i.e. circles in Figure 5.33, and the proposed method, i.e. the contour in Figure 5.33, are comparable at the lower part of the floor. While the maximum VDV from measurements is 0.157 m/s$^{1.75}$, the maximum VDV from the proposed method is 0.22 m/s$^{1.75}$. These peak values are located closely in the middle of the lower floor panels (Figure 5.33).

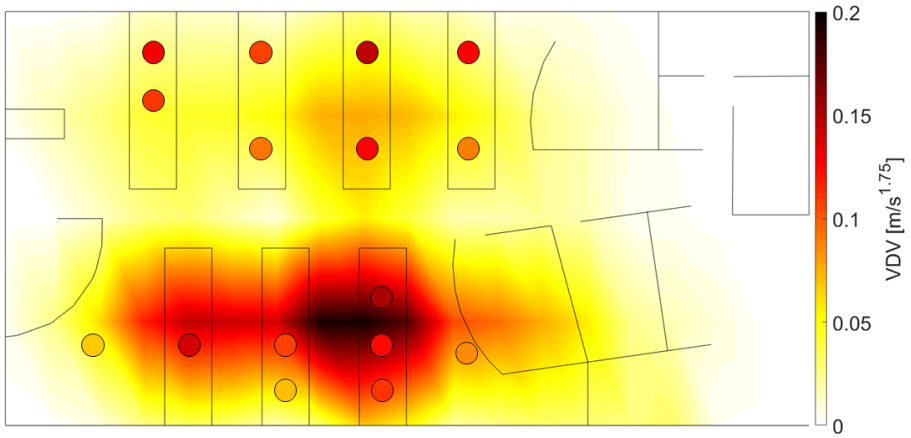

Figure 5.33: VDV from measurements (circles) and proposed method (contour).

There are clear differences between the VDV obtained from measurements and those calculated using the proposed method at the upper part of the floor. This could be caused by missing local modes of vibration at the upper part of the floor during modal testing, as only one shaker was deployed there (Figure

5.6). Moreover, the analysis presented above utilised only the average pacing frequency, i.e. 1.7 Hz, and utilising other pacing frequencies in the proposed method could affect the results. Furthermore, the missing information regarding the locations of other floor occupants, who were not tracked, can also affect the simulated responses.

This method can be used for any floor, provided that the described heatmap of people locations is available. The model presented in the previous section can be utilised to generate this heatmap.

5.6 Framework for vibration serviceability assessment of floors

A framework for vibration serviceability assessment of floors is proposed in this section. Firstly, the procedure for vibration response calculation was presented (Section 5.6.1) before describing the assessment procedure in Section 5.6.2. The influence of floor layout on vibration serviceability performance is demonstrated afterwards in Section 5.6.3.

5.6.1 Simulation of footfall-induced vibration

This study proposes calculating vibration responses through two stages:

1. Modelling of people's occupancy and movements, and
2. Calculation of the corresponding vibration responses.

The former can be performed using the model presented in Section 5.4. For response calculation, measured or modelled ground reaction force (GRF) time-history can be assigned to each floor occupant based on the corresponding

walking speed. Modal properties of the floor structure, i.e. natural frequencies, modal damping ratios, modal masses and mode shapes, can be obtained from either a finite element model or experimental measurements. The following steps show how to utilise the principle of superposition to calculate the vibration responses:

- Calculate modal force, $F_n(t)$, related to mode n, as described in Equation 5.17 (Craig Jr. and Kurdila, 2011).

$$F_n(t) = \sum_{p=1}^{N_p} \Phi_{p,n}(v_p.t)\ F_p(t) \quad , \tag{5.17}$$

  where, $\Phi_i(v_p.t)$ is the mode shape amplitude of mode n at a location of a moving pedestrian p walking at a constant speed v_p [m/s] at time t and $F_p(t)$ is the physical force time history related to each floor occupant [N].

- Solve the equation of motion, i.e. Equation 5.18, and calculate the modal accelerations, $a_n(t)$, using any method available in the literature (Craig Jr. and Kurdila, 2011).

$$M_n a_n(t) + C_n v_n(t) + K_n d_n(t) = F_n(t) \quad , \tag{5.18}$$

  where, M_n, C_n and K_n are the modal mass [kg], damping coefficient [N.s/m] and stiffness [m/N] related to mode n of vibration, respectively, and $v_n(t)$ and $d_n(t)$ are the modal velocity [m/s] and modal displacement [m] responses related to mode n, respectively.

- Calculate the physical response at point i, $a_i(t)$, on the floor following the principle of superposition, using Equation 5.19 (Craig Jr. and Kurdila, 2011).

$$a_i(t) = \sum_{n=1}^{N_m} a_n(t) \;\; \phi_{n,i} \quad , \tag{5.19}$$

where, N_m is the number of modes considered in the analysis and $\phi(n,i)$ is the mode shape amplitude corresponding to mode n at the response point i.

- The above mentioned steps can be utilised to obtain the full-day time history responses related to each point on the floor. An appropriate frequency weighting is to be applied to the calculated response to obtain the frequency-weighted acceleration, $a_{i,w}(t)$.

- The RMS acceleration, $a_{i,w,rms}(t)$, can be calculated using Equation 5.20 and its peak value is equal to the maximum transient vibration value ($MTVV$). $MTVV$ can be utilised in Equation 5.21 to obtain the R factor (Pavic and Willford, 2005).

$$a_{i,w,rms}(t) = \sqrt{\frac{1}{T}\int_0^T a_{i,w}^2(t)dt} \quad , \tag{5.20}$$

where, T is the total duration and dt is the duration of each time step (1 s).

$$R = MTVV/0.005 \quad , \tag{5.21}$$

- Furthermore, the VDV, in [m/s$^{1.75}$], related to any point on the floor, can be calculated using Equation 5.22 (Pavic and Willford, 2005).

$$VDV = \left(\int_0^T a_{i,w}^4(t)\; dt \right)^{0.25} \quad , \tag{5.22}$$

5.6.1.1 Verification

The verificaiton was performed based on an experiment conducted on the floor described in Section 5.3.

The analysis assumes 40 floor occupants exist on the floor with the same layout (Figure 5.5a) and modal properties (Figure 5.10) as those obtained in the experiment. The transition matrix (Table 5.2), durations that floor occupants stay stationary at each zone of the floor (Figure 5.24) and departure rates (Figure 5.25) were also taken from the results of the experiment described in Section 5.3. The arrival rate was assumed to be uniform in that all floor occupants arrived at the floor within one hour.

The simulations were conducted for a working day of 10 hours, i.e. occupants started arriving at 08:00 and they departed by 18:00. Walking speeds of floor occupants were assigned randomly based on the cumulative distribution provided in Figure 5.26. Body mass is reported to be different between various countries. In this study, the body mass was selected probabilistically based on a mean and standard deviation of 78.15 kg and 15.8 kg, respectively, from a study related to people in England (Sperrin et al., 2016). GRFs were assigned to floor occupants from a pool of data measured using an instrumented treadmill (Racic and Brownjohn, 2011; Brownjohn et al., 2015). The GRFs were scaled to take into account the body mass assigned to floor occupants.

The measured responses were low-pass filtered at 12 Hz to filter out the contribution of higher modes of vibration than those considered in the analysis (Figure 5.10).

The contour plots related to the calculated R factor and VDV are shown in Figure

5.34. The figure also shows the R factor and VDV calculated from the measured vibration responses at 16 test points.

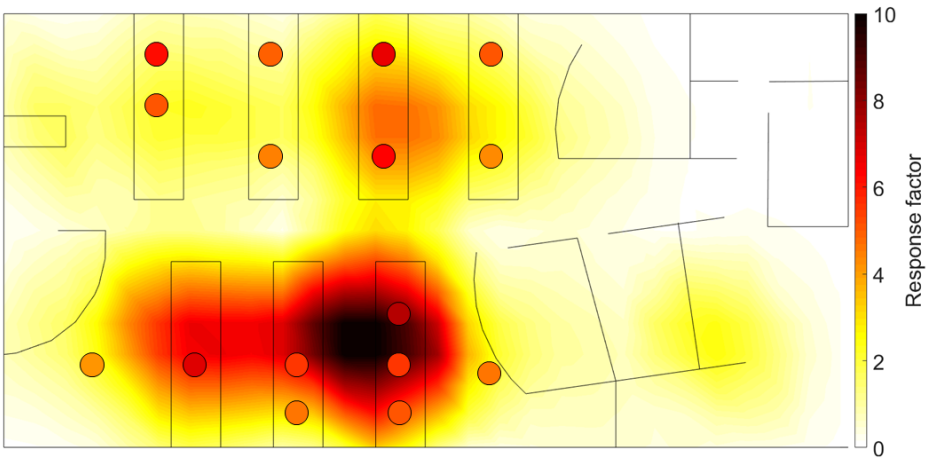

(a) R factor

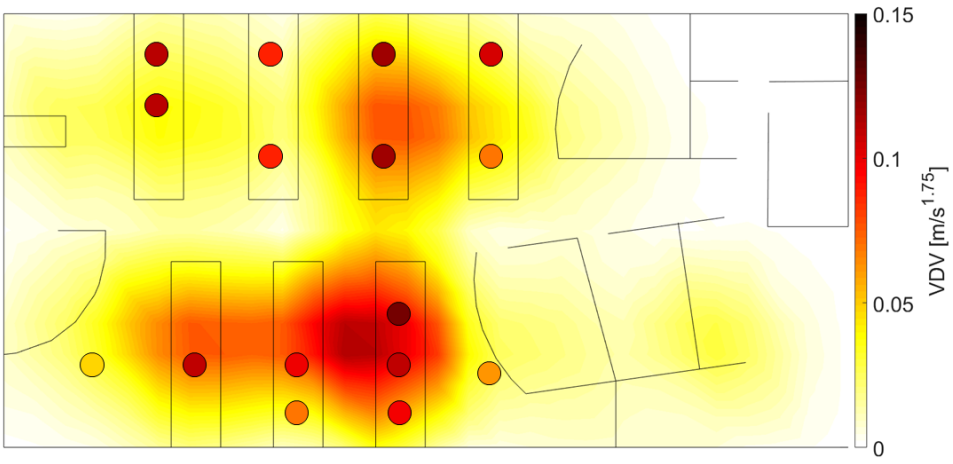

(b) VDV

Figure 5.34: R factor and VDV calculated using the proposed method (contours) and measurements (circles).

The maximum R factor obtained from the simulations, i.e. R=10, is higher than that obtained from the measurements, i.e. R=7.4, while the maximum VDV related to the simulations, VDV=0.115 m/s$^{1.75}$, slightly underestimates the

maximum measured VDV, 0.133 m/s$^{1.75}$.

Both of these $VDVs$ correspond to 10 hours of simulation/measurement, between 08:00 and 18:00. The measured responses, i.e. R factor and VDV, at the upper part of the floor are clearly higher than those obtained from the simulations. This could be related to a local mode of vibration that was missed from the modal testing, as only one shaker was located at the upper half of the floor during modal testing (Figure 5.10). However, the vibration levels, i.e. max R factor and VDV, calculated using the proposed method are comparable to those calculated from the measured vibration responses.

5.6.2 Vibration serviceability assessment

Figure 5.34 shows that the traditional ways of presenting the measured or simulated vibration responses do not provide clear information about people's experience of vibration levels. This is because floor occupants, by their nature, do not stay stationary at their desks all the time. This section shows how floor occupants' experience of vibration levels can be used for vibration serviceability assessment.

The analysis presented in this section utilises the simulated vibration responses, presented in Section 5.6.1.1, the recorded locations of 18 floor occupants on one day of the measurements and the simulated locations of 40 floor occupants (Section 5.6.1.1). The occupants' experience of the simulated vibration levels were obtained using either their measured or simulated locations. The calculated R factor and VDV experienced by floor occupants were only considered when the floor occupants were stationary. This is to take into account the fact that walking people have a higher threshold of perception of vibration than that of

seated people (BS 6472-1:2008, 2008).

5.6.2.1 Simulated vibration response at the recorded locations of floor occupants

The R factor and VDV related to the vibration responses (Section 5.6.1.1) experienced by 18 floor occupants whose locations were recorded are shown in Figure 5.35.

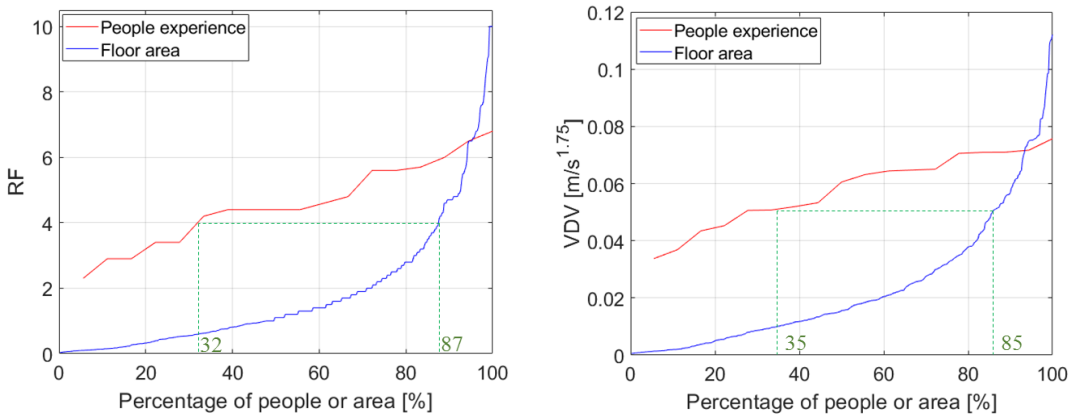

(a) R factor (b) VDV

Figure 5.35: (a) R factor and (b) VDV related to recorded locations of 18 floor occupants and simulated vibration responses.

Figure 5.35 shows that vibration levels, i.e. R factor or VDV, related to various percentages of floor area significantly differ from those related to people's experience. Around 87% of the floor area has R factor less than 4, compared with only 32% for people's experience. Similarly, around 85% of the floor area has VDV less than 0.05 m/s$^{1.75}$ compared with 35% for people's experience. However, the peak R factor and VDV for the floor area are higher than those experienced by the occupants.

5.6.2.2 Simulated vibration response at the simulated locations of floor occupants

The comparison made in Section 5.6.2.1 can be extended to study the vibration levels experienced by 40 floor occupants whose locations were simulated. Figure 5.36 shows the R factor and VDV related to various percentages of floor area and occupants' experience.

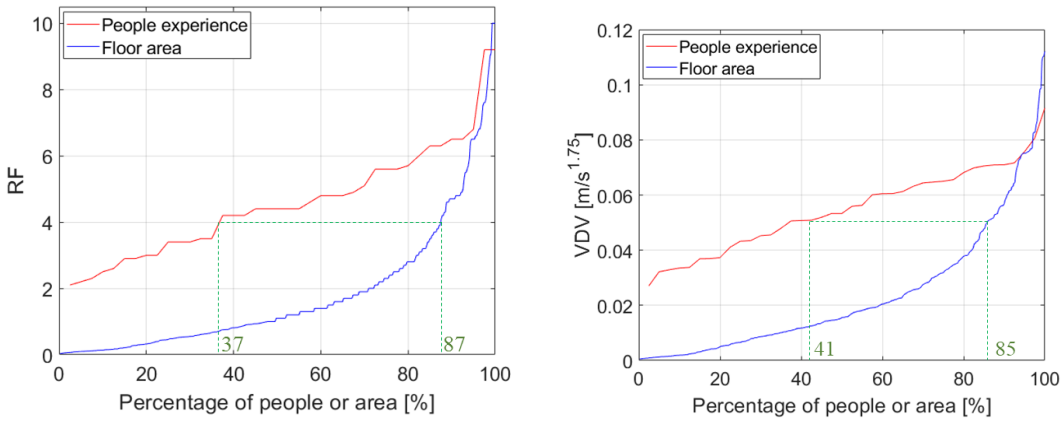

(a) R factor (b) VDV

Figure 5.36: (a) R factor and (b) VDV related to simulated locations of 40 floor occupants and simulated vibration responses.

Around 87% of the floor area has R factor less than 4, compared with only 37% for people's experience. Similarly, around 85% of the floor area has VDV less than 0.05 m/s$^{1.75}$ compared with 41% for people's experience. However, the peak R factor and VDV for the floor area are only slightly higher than those experienced by the occupants.

Furthermore, R factor corresponding to various percentages of time and either floor area or floor occupants' experience can be represented as contour plots, as shown in Figure 5.37.

Figure 5.37b shows that during 95% of the time, all floor occupants experienced R factor less than 1, which is the threshold for human perception of vibrations in

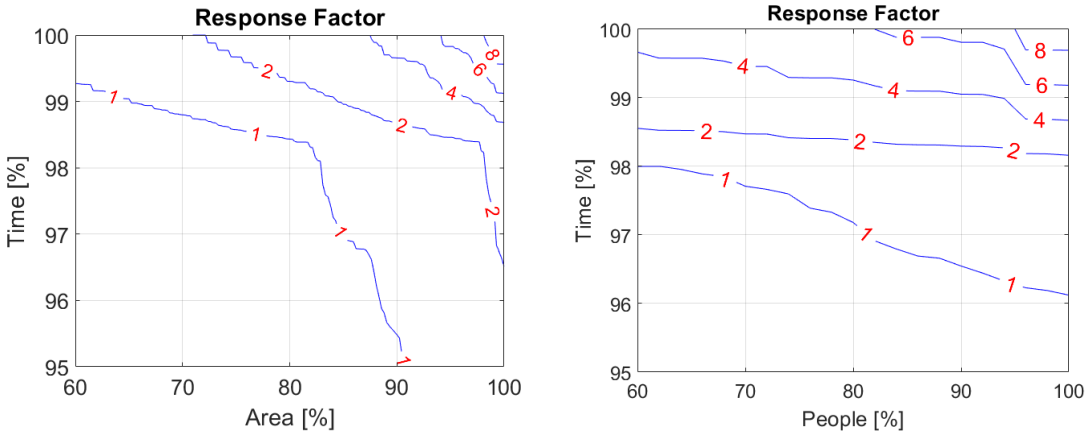

(a) (b)

Figure 5.37: R factor related to various percentages of time and (a) floor area or (b) floor occupants' experience based on simulated vibration responses and simulated locations of 40 floor occupants.

the vertical direction (BS 6472-1:2008, 2008). All floor occupants experienced R factor higher than 4 for less than 2% of the time, while only 5% of floor occupants experienced R factor higher than 8 for less than 0.5% of the time, i.e. around 3 minutes. Similar statistics can be observed for similar percentages of floor area (Figure 5.37b).

5.6.2.3 Discussion

The results presented above show that vibration levels related to certain percentages of floor area could differ significantly from those related to what floor occupants experience. This is because certain areas on floors where vibration levels are relatively low, e.g. edges and corners, are unlikely to be occupied by people. These areas count as a percentage of the floor area but do not count as a percentage of occupants' experience. Furthermore, footfall-induced vibrations of floors are intermittent by their nature, and do not occur continuously throughout the day. This means that while floor occupants walk and change their locations during the day, they can miss periods of high vibration levels at certain locations.

The way how Figure 5.36 and Figure 5.37 are presented can allow designers

to gain information about the temporal and spatial description of vibration levels and allow for vibration serviceability assessment to be conducted based on people's experience rather than peak values. If certain levels of R factor are to be allowed in the design for a certain time duration, higher vibration limits, i.e. peak R factor or VDV, than those stated in current design guidelines, could be allowed. This has the potential to influence the design of floors for vibration serviceability and reduce the corresponding construction costs, as less stringent vibration serviceability criterion could be utilised. The next section shows how these measures can be used to assess vibration serviceability for different layouts of a floor as part of the design.

5.6.3 Influence of floor layout on vibration serviceability performance

As one of the main improvements of the proposed vibration serviceability method in this chapter is utilising people's occupancy and movements model, it is likely that the design for vibration serviceability can be directly influenced by the floor layout and walking paths followed by the occupants of the floor. This feature can be used by designers to optimise the design of floors for vibration serviceability by optimising the layout of the floor. While changing floor layout will have an influence on the modal properties of the floor, especially natural frequency and modal damping, this influence is not taken into account in this study as it is outside its scope. Optimising the layout of structures to minimise their footfall-induced vibration responses was reported in the literature for footbridge structures (Venuti and Bruno, 2013).

This section compares the vibration levels corresponding to the actual layout of

the floor, i.e. Layout 1, shown in Figure 5.5a, which was utilised in the above mentioned analysis, i.e. Section 5.6.2.2, and two other imaginary layouts (Layout 2 and Layout 3, as shown in Figure 5.38b and Figure 5.38c, respectively). The actual layout, shown in Figure 5.5a, is illustrated in Figure 5.38a for comparison purposes.

Layout 2, shown in Figure 5.38b, and Layout 3, shown in Figure 5.38c, were generated with random configurations, but the same dimensions and zones, i.e. desks, printing area, meeting area, toilets, kitchen and free area, as in Layout 1. The people occupancy and movement model proposed in this study was utilised to obtain people's trajectories on the floor and all other model inputs were the same as those utilised in the analysis described in Section 5.6.2.2.

5.6.3.1 Results and discussion

Figures 5.39 and 5.40 show the contour plot related to the R factor and VDV corresponding to the three layouts, respectively. They show a considerable difference in terms of maximum responses, i.e. R factor and VDV, related to the three layouts.

The responses related to Layout 3, i.e. Figure 5.39c and Figure 5.40c, have a slightly different spatial distribution from those for Layout 1, i.e. Figure 5.39a and Figure 5.40a, and Layout 2, i.e. Figure 5.39b and Figure 5.40b. This could be related to the locations of tables where people often walk in-between. When the tables in the lower part of the floor, shown in Figure 5.39a, were shifted from the area of maximum response towards areas with lower responses, shown in Figure 5.39b, the vibration levels in the lower part were reduced, as shown in Figure 5.39b, compared to those for Layout 1. When the tables were shifted to the upper

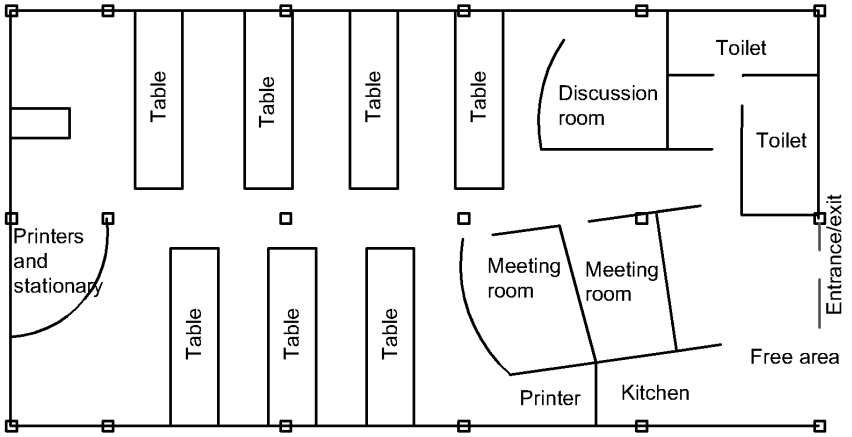

(a) Layout 1

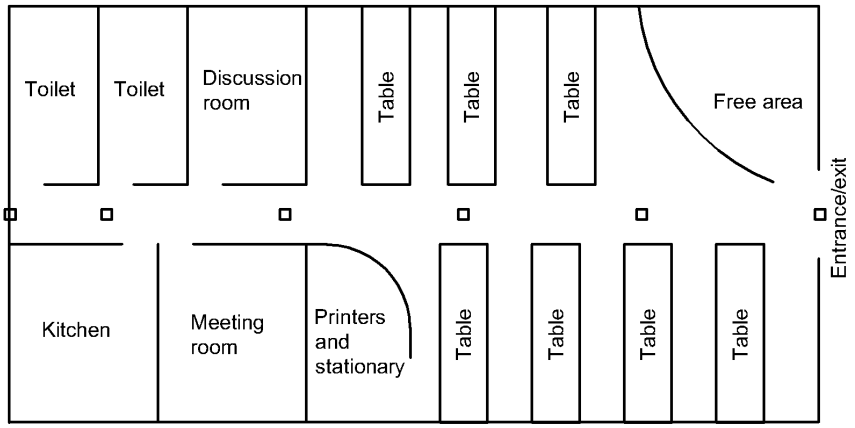

(b) Layout 2

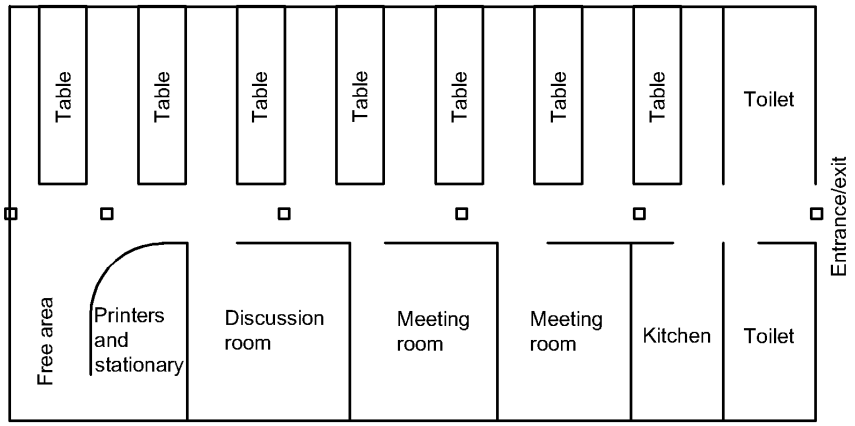

(c) Layout3

Figure 5.38: (a) Layout 1 (actual) (b) Layout 2 (imaginary) and (c) Layout 3 (imaginary) of the floor.

part of the building, in Layout 3, as shown in Figure 5.39c, the response in the lower part of the floor reduced even more, but a higher response occurred at the upper part, as shown in Figure 5.39c. The same pattern was observed for VDV

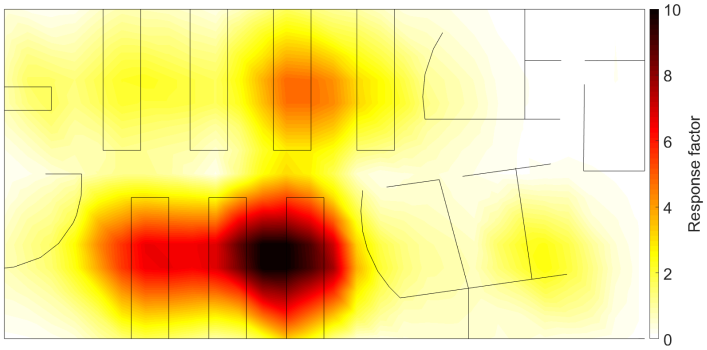

(a) R factor related to Layout 1

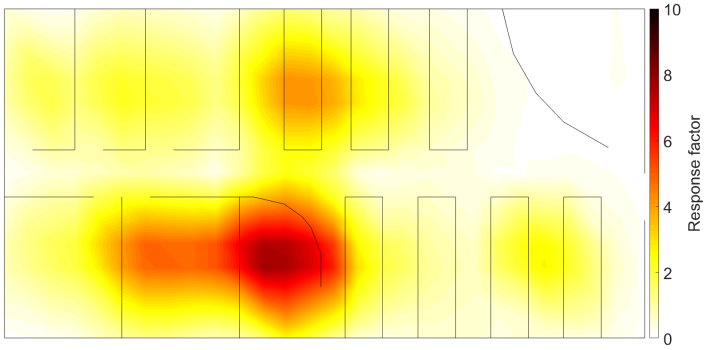

(b) R factor related to Layout 2

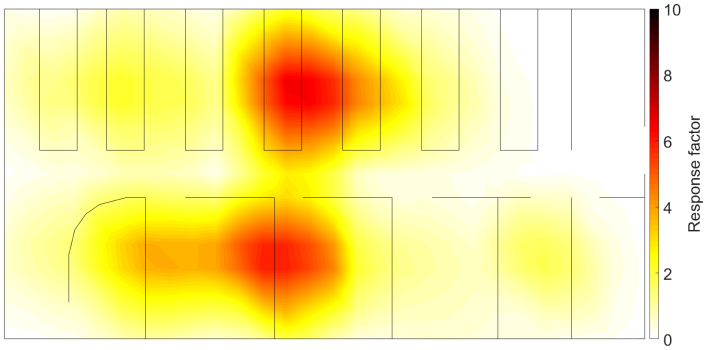

(c) R factor related to Layout 3

Figure 5.39: R factor calculated using the proposed method for (a) Layout 1, (b) Layout 2 and (c) Layout 3 of the floor.

in Figure 5.40.

Similar observations, to those mentioned above, were made for Figure 5.41 and

Figure 5.42. The maximum R factor and VDV for Layout 1, shown in Figure 5.41a

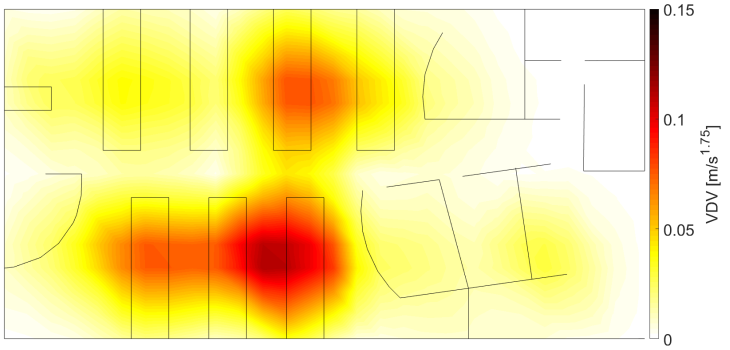

(a) VDV related to Layout 1

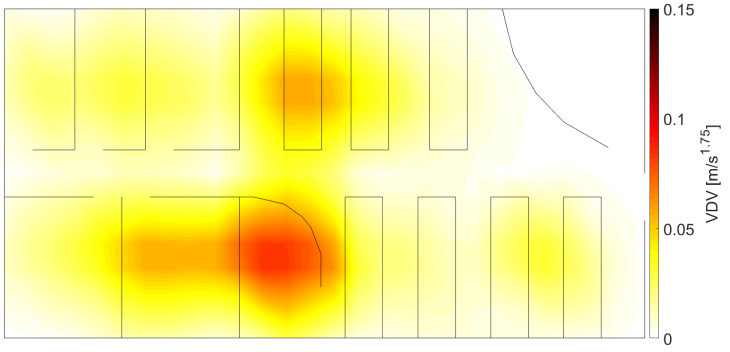

(b) VDV related to Layout 2

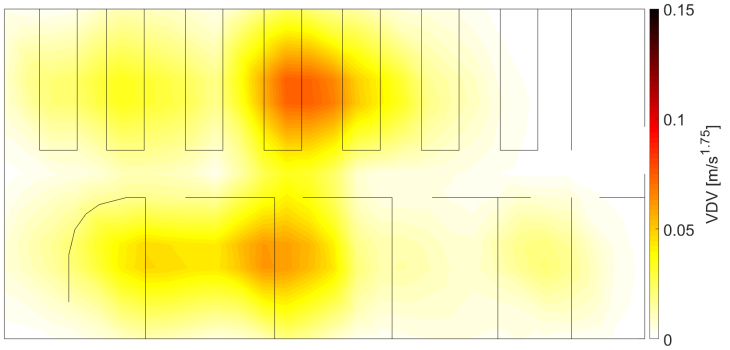

(c) VDV related to Layout 3

Figure 5.40: VDV calculated using the proposed method for (a) Layout 1, (b) Layout 2 and (c) Layout 3 of the floor.

and Figure 5.42a, were higher than those for Layout 2, as shown in Figure 5.41b and Figure 5.42b, and Layout 3, as shown in Figure 5.41c and Figure 5.42c. It is worth mentioning that for Layout 3, vibration levels, i.e. R factor and VDV, related to various percentages of the floor area, i.e. Figure 5.41c and Figure 5.42c, were

relatively close to that of occupants' experience. This was in contrast to that for Layout 1, as shown in Figure 5.41a and Figure 5.42a, where vibration levels related to various percentages of the floor area were significantly less than those related to occupants' experience. These differences are expected to be caused by the distribution of tables with respect to locations of high vibration levels.

The results presented in this section show the potential of utilising optimised floor layouts to improve vibration serviceability performance of floors.

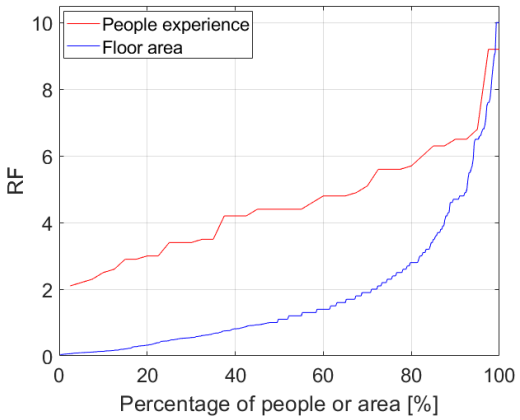

(a) R factor related to Layout 1

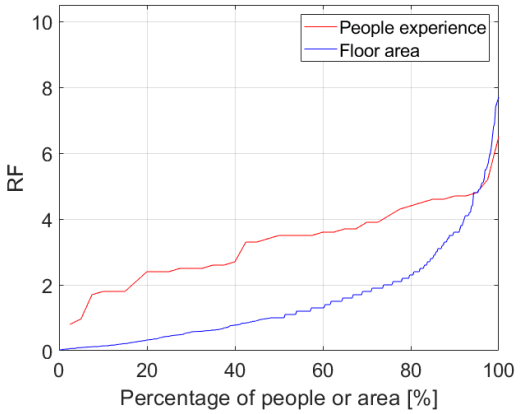

(b) R factor related to Layout 2

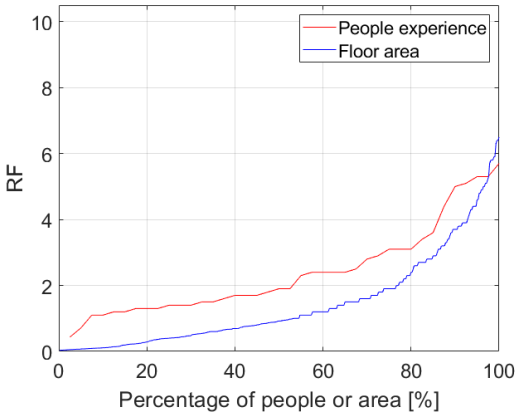

(c) R factor related to Layout 3

Figure 5.41: R factor related to (a) Layout 1, (b) Layout 2 and (c) Layout 3 and corresponding to various percentages of floor area and occupants' experience.

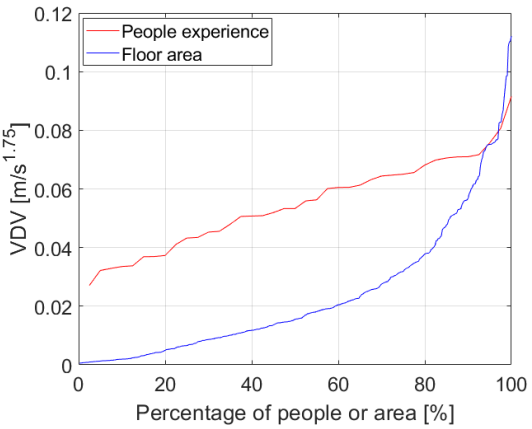

(a) VDV related to Layout 1

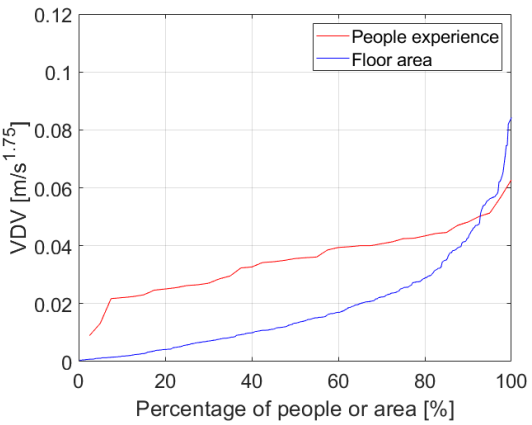

(b) VDV related to Layout 2

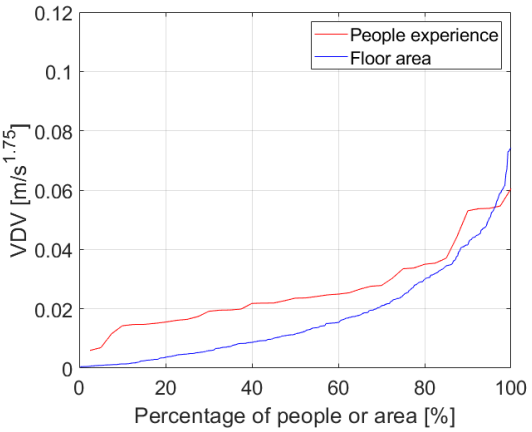

(c) VDV related to Layout 3

Figure 5.42: VDV related to (a) Layout 1, (b) Layout 2 and (c) Layout 3 and corresponding to various percentages of floor area and occupants' experience.

5.7 Conclusions

People movements on an office floor and their correlation with footfall-induced vibration levels were studied experimentally in this chapter. A comprehensive framework for vibration serviceability assessment of floors is proposed based on that.

It is shown that neglecting multiple pedestrian walking scenario in the design for vibration serviceability may result in an underestimation of vibration levels. Predicting people's movements, to calculate their vibration levels, is obviously more complicated than that for single pedestrians. Hence, this study utilises a location tracking system to collect data regarding people's locations on an office floor and model their occupancy and movements. This model was utilised to predict the floor occupants' movements and the corresponding vibration levels they are likely to experience. It is shown that vibration levels, i.e. R factor and VDV, experienced by floor occupants could be significantly less than the peak response on the floor area. This means there is a potential of utilising relaxed vibration tolerance limits in the design, compared to the limits stated in current design guidelines. Furthermore, it was found that floor layout can be optimised to reduce vibration levels experienced by the occupants. This is particularly useful for floors with problematic vibration levels where other vibration remedies are more expensive.

The proposed occupancy and movements model was also utilised for an improved, and simplified, method of predicting VDV. The method utilises heatmaps, related to people movements, to take into account walking patterns on floors in the calculation of VDV. Higher, but comparable, VDV was obtained

using this model when compared to that calculated from the measurements. This method is computationally less demanding than the above mentioned framework and can be utilised for preliminary vibration serviceability checks.

Chapter 6

Conclusions and Recommendations for Future Work

The work presented in this thesis aimed to improve the vibration serviceability design methods of floors related to single and multiple pedestrian footfall excitation. This was achieved by identifying the main drawbacks of the current design guidelines which were not addressed sufficiently in the literature. The main conclusions are listed below followed by recommendations for future work.

6.1 Conclusions

1. An improved probabilistic method for predicting vibration levels of floors in sensitive facilities was proposed. The model is based on single pedestrian walking scenario as it is the most likely walking scenario for such floors. The improved model was based on Arup's model for high-frequency floors but it was improved to predict vibration levels related to any probability of non-exceedance. This is far more flexible than Arup's original model which was designed to provide vibration levels related to 75% of non-exceedance.

The performance of the proposed model was compared with simulations of a finite element model of a floor subjected to GRFs measured using an instrumented treadmill. It was shown that the proposed model can predict vibration levels for more than 90% of cases. Furthermore, a cut-off frequency of 14 Hz was derived so that floors in sensitive facilities with requirements of low-level vibration limit can be designed to have a fundamental frequency of 14 Hz.

2. It was found that the presence of single or multiple pedestrians on lightweight floors can significantly reduce the floor's FRFs magnitude, which is a similar finding to that from other studies conducted in the past for footbridge structures. The amount of this reduction was mostly affected by natural frequency and modal masses, i.e. mass-ratio between individual walkers and the floor, related to the floor's dominant modes of vibration as well as the number of walking occupants. A new model was proposed to take into account the HSI in the prediction of vibration responses related to footfall excitation. In contrast to other HSI models available in the literature, the proposed model takes into account whole-body dynamics *over a range of frequencies*, 1-10 Hz, using two transfer functions. The performance of the proposed model was verified using experimental measurements of individuals walking on three different floors.

3. Vibration levels related to multiple pedestrian footfall excitation could be higher than those related to single pedestrian. This is in contrast to the general understanding and current design guidelines which utilise single person walking scenario in the design as the worst-case scenario. For open-plan offices it was shown that multiple pedestrians frequently walk

simultaneously. For other types of floors, such as those in sensitive facilities, the multiple pedestrian walking scenario is less likely to occur. Therefore, walking scenarios utilised for the vibration serviceability checks could be decided based on the usage of the building.

4. An experimentally-based model capable of producing full location time-history of floor occupants was proposed. The model takes into account realistic patterns related to people's movements on floors. The model was built based on experimental data collected utilising an advanced UWB indoor location tracking system. The model can be used for various applications related to vibration serviceability of office floors. For other types of floors, experimental measurements need to be conducted to collect data related to people's movements on such floors before updating the parameters of the model.

5. A revised methodology to predict the VDV based on people's movements was presented. This model utilises the above mentioned people's occupancy and movements model to predict people's movements before calculating the VDV. A comparison between the VDV predicted using the proposed model and those obtained from the measurements shows that the model can produce comparable VDV to those obtained from the measurements.

6. A fully probabilistic framework to simulate footfall-induced vibration of floors and quantify the occupants' exposure to vibration was presented. It utilises the above mentioned model related to people's occupancy and movements to simulate the locations of walking people, i.e. footfall loading, and the

stationary people, i.e. receivers of vibration. The framework was utilised to predict vibration levels of a tested in-service office floor. The results showed close predictions of vibration levels compared to those obtained from the measurements. As the framework requires that a layout of the floor is known, it can be utilised for vibration serviceability checks for floors before conducting commissioning or refurbishment works in a building. Furthermore, it was shown that the layout of the floor can be used efficiently to optimise the vibration serviceability performance by checking the vibration levels experienced by the occupants for different floor layouts. Hence, the model can be utilised also as an alternative vibration remedy solution for floors with problematic vibration levels related to footfall loading.

6.2 Recommendation for future work

1. The proposed model related to footfall-induced vibration of floors in sensitive facilities has shown a good performance when the predicted vibration levels obtained using this model was compared with simulations of a finite element model. However, comparison with experimental measurements for such floors need to be conducted to verify the performance of the proposed model.

2. The derived transfer functions related to the proposed HSI model were made for five test subjects. The parameters of these transfer functions were shown to be different for different people. Hence, there is a need to conduct further experiments with higher number of test subjects to derive their corresponding transfer function parameters. This can allow for probabilistic treatment of human dynamics in the prediction of vibration

levels. Furthermore, one of the transfer functions utilised in the model was derived using measurements of individuals standing on a platform due to the absence of facilities where such data can be collected for individuals walking on a structure vibrating at various frequencies. Hence, when such a facility becomes available for conducting such tests, the transfer functions can be updated accordingly.

3. The proposed people's occupancy and movements model was derived based on experimental data conducted on one open-plan office floor. More experimental data are needed for other similar floors to verify its performance and input parameters for this type of floors. Furthermore, if the model is to be utilised to simulate people's occupancy and movements on other types of floors, further experimental work is needed to collect data from other similar floors regarding people's occupancy and movements to update the model parameters.

References

Ahmadi, E., Caprani, C., Živanović, S., and Heidarpour, A. (2018). Vertical ground reaction forces on rigid and vibrating surfaces for vibration serviceability assessment of structures. *Engineering Structures*, 172(June):723–738.

Ahmadi, E., Caprani, C., Živanović, S., and Heidarpour, A. (2019). Assessment of human-structure interaction on a lively lightweight GFRP footbridge. *Engineering Structures*, 199(March).

Allen, D. E. and Murray, T. M. (1993). Design criterion for vibrations due to walking.

Amick, H., Hardash, S., Gillett, P., and Reaveley, R. J. (1991). Design of Stiff, Low-Vibration Floor Structures. In *Proceedings of International Society for Optical Engineering*, volume 1619, pages 180–191. SPIE.

ANSYS Inc. (2016). ANSYS® Academic Research, Release 17.1.

APS Dynamics Inc. (1996). *Instruction manual, ELECTRO-SEIS, Model 113 Shaker*. APS Dynamics, Inc.

APS Dynamics Inc. (2013). *Instruction manual, ELECTRO-SEIS, Model 400 Shaker*. APS Dynamics, Inc.

AS 3623—1993 (1993). Domestic metal framing.

Azizi, S., Nair, G., and Olofsson, T. (2019). Demand-controlled energy systems in commercial and institutional buildings : a review of methods and potentials. *eceee 2019 Summer Study proceedings*, (June):1443–1450.

Balvedi, B. F., Ghisi, E., and Lamberts, R. (2018). A review of occupant behaviour in residential buildings. *Energy and Buildings*, 174:495–505.

Baumann, K. and Bachmann, H. (1988). Dynamic loads caused by humans and their effect on beam structures. Technical report.

Beirlant, J., Goegebeur, Y., Teugels, J., and Segers, J. (2005). *Statistics of extremes: Theory and applications*.

Bocian, M., Brownjohn, J. M. W., Racic, V., Hester, D., Quattrone, A., and Monnickendam, R. (2016). A framework for experimental determination of localised vertical pedestrian forces on full-scale structures using wireless attitude and heading reference systems. *Journal of Sound and Vibration*, 376:217–243.

Bocian, M., Macdonald, J. H. G., and Burn, J. F. (2013). Biomechanically inspired modeling of pedestrian-induced vertical self-excited forces. *Journal of Bridge Engineering*, 18(12):1336–1346.

Brownjohn, J. M. W. and Middleton, C. J. (2008). Procedures for vibration serviceability assessment of high-frequency floors. *Engineering Structures*, 30(6):1548–1559.

Brownjohn, J. M. W., Pavic, A., and Omenzetter, P. (2004). A spectral density approach for modelling continuous vertical forces on pedestrian structures due to walking. *Canadian Journal of Civil Engineering*, 31(1):65–77.

Brownjohn, J. M. W., Racic, V., and Chen, J. (2015). Universal response spectrum procedure for predicting walking-induced floor vibration. *Mechanical Systems and Signal Processing*, pages 1–15.

BS 6472-1:2008 (2008). Guide to evaluation of human exposure to vibration in buildings Part 1 : Vibration sources other than blasting.

BS6472:1992. Evaluation Of Human Exposure To Vibration In Buildings (1 Hz to 80 Hz) - Guide For The Evaluation Of Human Exposure To Whole-Body Vibration.

Caprani, C. (2014). Application of the pseudo-excitation method to assessment of walking variability on footbridge vibration. *Computers & Structures*, 132:43–54.

Caprani, C. C., Keogh, J., Archbold, P., and Fanning, P. (2011). Characteristic Vertical Response of a Footbridge Due to Crowd Loading. (July):4–6.

Chen, J., Zhang, M., and Liu, W. (2015). Vibration Serviceability Performance of an Externally Prestressed Concrete Floor during Daily Use and under Controlled Human Activities. *Journal of Performance of Constructed Facilities*, page 04015007.

Craig Jr., R. R. and Kurdila, A. J. (2011). *Fundamentals of Structural Dynamics*.

da Silva, F. T. and Pimentel, R. L. (2011). Biodynamic walking model for vibration serviceability of footbridges in vertical direction. In *Eurodyn 2011*, number July, pages 1090–1096.

Dang, H. (2014). *Experimental and Numerical Modelling of Walking Locomotion on Vertically Vibrating Low-Frequency Structures*. PhD thesis, University of Warwick, UK.

Dang, H. and Živanović, S. (2016). Influence of Low-Frequency Vertical Vibration on Walking Locomotion. *Journal of Structural Engineering (United States)*, 142(12):1–12.

Dardari, D., Closas, P., and Djuric, P. M. (2015). Indoor tracking: Theory, methods, and technologies. *IEEE Transactions on Vehicular Technology*, 64(4):1263–1278.

Deloitte (2018). London Office Crane Survey Building momentum. Technical report.

Dong, B., Yan, D., Li, Z., Jin, Y., Feng, X., and Fontenot, H. (2018). Modeling occupancy and behavior for better building design and operation—A critical review. *Building Simulation*, 11(5):899–921.

Duives, D., Daamen, W., and Hoogendoorn, S. (2013). State-of-the-art crowd motion simulation models. *Transportation Research Part C: Emerging Technologies*, 37:193–209.

Ebrahimpour, A., Sack, R., and Van Kleek, P. (1989). Computing crowd loads using a nonlinear equation of motion. volume 2;, pages 47–52, London. Civil-Comp Press.

Ebrahimpour, A. and Sack, R. L. (2005). A review of vibration serviceability criteria for floor structures. *Computers & Structures*, 83(28-30):2488–2494.

Ellis, B. R. (2001). Serviceability evaluation of floor vibration induced by walking loads. *The Structural Engineer*, 79(21):30–36.

Ellis, B. R., Ji, T., and Littler, J. D. (2000). The response of grandstands to dynamic crowd loads. *Proceedings of ICE: Structures and Buildings*, 140(4):355–365.

Eriksson, P. E. (1994). Vibration of low-frequency floors - dynamic forces and response prediction.

Ewins, D. J. (2000). *Modal Testing: Theory, Practice and Application*. Research Studies Press Ltd., Baldock, Hertfordshire, England.

Fanella, D. A. and Mota, M. *Design Guide for Vibrations of Reinforced Concrete Floor Systems*. CRSI, 1st edition.

Feldmann, M. and Heinemeyer, C. (2007). *Human Induced Vibration of Steel Structures - Vibration Design of Floors: Guideline*. Research for coal and steel.

Feldmann, M., Heinemeyer, C., Butz, C., Caetano, E., Cunha, A., Galanti, F., and Goldack, A. (2009). Design of floor structures for human induced vibrations, JRC Report - EC3. Technical report.

Ferdous, W., Bai, Y., Ngo, T. D., Manalo, A., and Mendis, P. (2019). New advancements, challenges and opportunities of multi-storey modular buildings – A state-of-the-art review. *Engineering Structures*, 183(October 2018):883–893.

Gaetani, I., Hoes, P. J., and Hensen, J. L. (2016). Occupant behavior in building energy simulation: Towards a fit-for-purpose modeling strategy. *Energy and Buildings*, 121:188–204.

Galbraith, F. W. (1970). Ground Loading from Footsteps. *The Journal of the Acoustical Society of America*, 48(5B):1288.

Gopalan, K. (2012). *Introduction to Signals and Systems Analysis*. Cengage Learning, Inc, Belmont, CA, United States.

Gorodon, C. (1988). The Control of Vibration in Buildings. Technical report, BBN Laboratories, Cambridge, MA.

Griffin, M. J. (1990). Handbook of human vibration - appendices and glossary.

Hagena, F., Wirth, C., Piehler, J., Plitz, W., Hofmann, G., and Zwingers, T. (1985). In-vivo experiments on the response of the human spine to sinusoidal GZ-vibration. In *AGARD Conference Proceedings*, pages 1–12.

Hanagan, L. M. and Murray, T. M. (1997). Active Control Approach for Reducing Floor Vibrations. *Journal of Structural Engineering*, 123(11):1497–1505.

Helbing, D. and Farkas, I. (2002). Simulation of pedestrian crowds in normal and evacuation situations. *Pedestrian and evacuation dynamics*, 21(January):21–58.

Helbing, D., Farkas, I., and Vicsek, T. (2000). Simulating Dynamical Features of Escape Panic. 794(July):487–490.

Hicks, S. J. and Smith, A. L. (2011). Design of floor structures against human-induced vibrations. *Steel Construction*, 4(2):114–120.

Hudson, E. J. and Reynolds, P. (2013). Implications of structural design on the effectiveness of active vibration control of fl oor structures. *Structural Control and Health Monitoring*, 21(5):685–704.

Hudson, E. J. and Reynolds, P. (2016). Design and Construction of a Reconfigurable Pedestrian Structure. *Experimental Techniques*.

Inman, D. J. (2007). *Engineering Vibration*. Pearson Education, Inc., 3rd edition.

Institution, B. S. (1987). BS6841: 1987 Measurement and evaluation of human exposure to whole-body mechanical vibration and repeated shock.

ISO (1989). Part 2: Continuous and shock-induced vibration in buildings (1 to 80Hz).

ISO 10137:2007 (2007). *ISO 10137:2007 Bases for design of structures - Serviceability of buildings and walkways against vibrations*. International Standards Organisation, 2nd edition.

ISO 2631-2-2003 (2003). *ISO 2631-2-2003 Mechanical vibration and shock — Evaluation of human exposure to whole-body vibration - Part 2, vibrations in buildings (1-80Hz)*, volume 2003. International Organization for Standardization, Geneva, Switzerland.

Kerr, S. C. (1998). *Human induced loading on staircases*. PhD thesis, University College London, London, UK.

Kotz, S. and Nadarajah, S. (2000). *Extreme value distributions*. Number x.

Liu, D. and Davis, B. (2014). Walking Vibration Response of High-Frequency Floors Supporting Sensitive Equipment. *Journal of Structural Engineering*, 141(8):04014199.

Maalek, R. and Sadeghpour, F. (2016). Accuracy assessment of ultra-wide band technology in locating dynamic resources in indoor scenarios. *Automation in Construction*, 63:12–26.

Matsumoto, Y. and Griffin, M. J. (1998). Dynamic response of the standing human body exposed to vertical vibration: Influence on posture and vibration. *Journal of Sound and Vibration*, 212(1):85–107.

McConnell, K. G. and Varoto, P. S. (2008). *Vibration testing: theory and practice*. John Wiley & Sons, Inc., 2nd edition.

Middleton, C. (2009). *Dynamic Performance of High Frequency Floors*. Phd thesis, University of Sheffield.

Middleton, C. J. and Brownjohn, J. M. W. (2010). Response of high frequency floors: A literature review. *Engineering Structures*, 32:337–352.

Mohammed, A. and Pavic, A. (2017). Effect of Walking people on Dynamic Properties of Floors. *Procedia Engineering*, 199:2856–2863.

Mohammed, A. and Pavic, A. (2019). Simulation of people's movements on floors using social force model. *Conference Proceedings of the Society for Experimental Mechanics Series*, pages 39–46.

Mohammed, A. S. and Pavic, A. (2018). Utilising an advanced technology of people tracking in vibration serviceability application. In *Lecture Notes in Civil Engineering*, volume 5, pages 388–396.

Muhammad, Z. and Reynolds, P. (2020). Probabilistic Multiple Pedestrian Walking Force Model including Pedestrian Inter- and Intrasubject Variabilities. *Advances in Civil Engineering*, 2020.

Muhammad, Z., Reynolds, P., Avci, O., and Hussein, M. (2018). Review of Pedestrian Load Models for Vibration Serviceability Assessment of Floor Structures. *Vibration*, 2(1):1–24.

Muhammad, Z. O. and Reynolds, P. (2019). Vibration Serviceability of Building Floors: Performance Evaluation of Contemporary Design Guidelines. *Journal of Performance of Constructed Facilities*, 33(2):04019012.

Murray, T. M., Allen, D. E., and Ungar, E. E. (1997). *Floor Vibrations Due to Human Activity - AISC DG11*. American Institute of Steel Construction, 1st edition.

Murray, T. M., Allen, D. E., Ungar, E. E., and Davis, D. B. (2016). Vibrations of Steel-Framed Structural Systems Due to Human Activity: AISC DG11 Second Edition. Technical report, American Institute of Steel Construction (AISC).

Nag, P. K. (2018). *Office Buildings: Health, Safety and Environment*. Springer.

National Building Code of Canada (2005). User's Guide - NBC 2005: Structural Commentaries (Part 4 of Division B) Commentary D.

Nguyen, H. A. U. (2013). Walking Induced Floor Vibration Design and Control. page 340.

Ohlsson, S. (1982). *Floor Vibrations and Human Discomfort*. Phd thesis, Chalmers University of Technology.

Ohlsson, S. V. (1988). Ten Years of Floor Vibration Research - A Review of Aspects and Some Results. In *In: Proceedings of the Symposium/Workshop on Serviceability of Buildings (Movements, Deformations, Vibrations)*, volume 1, pages 419–434, Ottawa, Canada.

Page, J., Robinson, D., Morel, N., and Scartezzini, J. L. (2008). A generalised stochastic model for the simulation of occupant presence. *Energy and Buildings*, 40(2):83–98.

Pavic, A. and Reynolds, P. (2002). Vibration serviceability of long-span concrete building floors. Part 1: Review of background information. *Shock and Vibration Digest*, 34(3):191–211.

Pavic, A., Reynolds, P., Prichard, S., and Lovell, M. (2003). Evaluation of mathematical models for predicting walking-induced vibrations of high-frequency floors. *International Journal of Structural Stability and Dynamics*, 3(1):107–130.

Pavic, A. and Willford, M. R. (2005). Appendix G: Vibration serviceability of post-tensioned concrete floors.

Paz, M. and Leigh, W. (2004). *Structural Dynamics*. Springer US, Boston, MA.

Petrovic-Kotur, S. P. (2016). *Vibrations of Lightweight Steel Floors in Prefabricated Buildings and Effects of Non-Structural Walls on Their Modal Properties*. Doctoral dissertation (in serbian), “Union – Nikola Tesla” Faculty of Construction Management.

Pimentel, R. (1997). *Vibrational performance of pedestrian bridges due to human-induced loads*. PhD thesis, Sheffield.

Qin, J. W., Law, S. S., Yang, Q. S., and Yang, N. (2013). Pedestrian-bridge dynamic interaction, including human participation. *Journal of Sound and Vibration*, 332(4):1107–1124.

Racic, V. and Brownjohn, J. M. W. (2011). Stochastic model of near-periodic vertical loads due to humans walking. *Advanced Engineering Informatics*, 25(2):259–275.

Racic, V. and Brownjohn, J. M. W. (2012). Mathematical modelling of random narrow band lateral excitation of footbridges due to pedestrians walking. *Computers & Structures*, 90-91:116–130.

Racic, V. and Pavic, A. (2009). Mathematical model to generate asymmetric pulses due to human jumping. *ASCE Journal of Engineering Mechanics*, 135(10):1–6.

Racic, V., Pavic, A., and Brownjohn, J. M. W. (2009). Experimental identification and analytical modelling of human walking forces: Literature review. *Journal of Sound and Vibration*, 326(1-2):1–49.

Reinhart, C. F. (2004). Lightswitch-2002: A model for manual and automated control of electric lighting and blinds. *Solar Energy*, 77(1):15–28.

Reynolds, P. and Pavic, A. (2015). Reliability of assessment criteria for office floor vibrations. In *50th United Kingdom Conference on Human Responses to Vibration*, Southampton, UK.

Rubinstein, R. and Kroese, D. (2017). *Simulation and the Monte Carlo Method*. John Wiley & Sons, Inc.

Scheaffer, R., McClave, J., and Franklin, C. (2010). *Probability and statistics for engineers*. Cengage Learning, Boston, MA, USA, 5th edition.

Schwarz, G. (1978). Estimating the Dimension of a Model. *The Annals of Statistics*, 6:461–464.

Shahabpoor, E. (2014). *Dynamic Interaction of Walking Humans with Pedestrian Structures in Vertical Direction*. Phd thesis, University of Sheffield.

Shahabpoor, E. and Pavic, A. (2018). Estimation of vertical walking ground reaction force in real-life environments using single IMU sensor. *Journal of Biomechanics*, 79:181–190.

Shahabpoor, E., Pavic, A., and Racic, V. (2016a). Identification of mass–spring–damper model of walking humans. *Structures*, 5:233–246.

Shahabpoor, E., Pavic, A., and Racic, V. (2016b). Interaction between Walking Humans and Structures in Vertical Direction: A Literature Review. *Shock and Vibration*, 2016:12–17.

Shahabpoor, E., Pavic, A., and Racic, V. (2017a). Structural vibration serviceability : New design framework featuring human-structure interaction. *Engineering Structures*, 136:295–311.

Shahabpoor, E., Pavic, A., Racic, V., and Živanović, S. (2017b). Effect of group walking traffic on dynamic properties of pedestrian structures. *Journal of Sound and Vibration*, 387:207–225.

Smith, A. L., Hicks, S. J., and Devine, P. J. (2009). *Design of floors for vibration - A new approach SCI P354, Revised Ed*, volume SCI P354. The Steel Construction Institute.

Sperrin, M., Marshall, A. D., Higgins, V., Renehan, A. G., and Buchan, I. E. (2016). Body mass index relates weight to height differently in women and older adults: Serial cross-sectional surveys in England (1992-2011). *Journal of Public Health (United Kingdom)*, 38(3):607–613.

Teixeira, T., Dublon, G., and Savvides, A. (2010). A Survey of Human-Sensing: Methods for Detecting Presence, Count, Location, Track, and Identity. *ACM Computing Surveys*, 5(1):1–35.

Teunissen, P. J. G. (1990). Nonlinear least squares. *Manuscripta Geodaetica*, 15(3):137–150.

Toso, M., Gomes, H., da Silva, F., and Pimentel, R. (2015). Experimentally fitted biodynamic models for pedestrian–structure interaction in walking situations. *Mechanical Systems and Signal Processing*, pages 1–17.

Ungar, E. E. and White, R. W. (1979). Footfall-induced vibrations of floors supporting sensitive equipment.

Van Nimmen, K., Lombaert, G., De Roeck, G., and Den Broeck, P. V. (2016). Reduced-order models for vertical human-structure interaction. *Journal of Physics: Conference Series*, 744(1).

Van Nimmen, K., Maes, K., Živanović, S., Lombaert, G., De Roeck, G., and Van den Broeck, P. (2015). Identification and modelling of vertical human-structure interaction. In *Conference Proceedings of the Society for Experimental Mechanics Series*, volume 2, pages 319–330. Springer International Publishing.

Venuti, F. and Bruno, L. (2013). Mitigation of human-induced lateral vibrations on footbridges through walkway shaping. *Engineering Structures*, 56:95–104.

Vibrant Technology Inc. (2018). ME'Scope VES - VT560 Visual SDM Pro.

Willford, M. R. and Young, P. (2006). *A Design Guide for Footfall Induced Vibration of Structures - CCIP-016*. The Concrete Centre, Slough.

Willford, M. R., Young, P., and Field, C. (2005). Improved methodologies for the prediction of footfall-induced vibration. In *Proceedings of the Sixth European Conference on Structural Dynamics EURODYN*.

Willford, M. R., Young, P., and Field, C. (2007). Predicting footfall-induced vibration: Part 2.

Wyatt, T. A. (1989). *Design Guide on the Vibration of Floors SCI P076*. The Steel Construction Institute, Construction Industry Research and Information Association, London.

Wyatt, T. A. and Dier, A. F. (1989). Building in steel, the way ahead.

Yi, K. (2011). The Effects of Shoe Type on Ground Reaction Force. *Korean Journal of Sport Biomechanics*, 21(1):9–16.

Zhang, M., Georgakis, C., Qu, W., and Chen, J. (2015). SMD Model Parameters of Pedestrians for Vertical Human-Structure Interaction. pages 311–317. Springer International Publishing.

Zhang, S. (2017). *Vibration Serviceability of Cold-Formed Steel Floor Systems*. Phd thesis, University of Waterloo.

Živanović, S. (2012). Benchmark Footbridge for Vibration Serviceability Assessment under the Vertical Component of Pedestrian Load. *Journal of Structural Engineerig*, 138(10):1193–1202.

Živanović, S. and Pavic, A. (2009). Probabilistic modeling of walking excitation for building floors. *Journal of Performance of Constructed Facilities*, 23(3):132–143.

Živanović, S., Pavic, A., and Racic, V. (2012). Towards modelling in-service pedestrian loading of floor structures. *Conference Proceedings of the Society for Experimental Mechanics Series*, 1:85–94.

Publications produced during working on thesis

- Mohammed, A. and Pavic, A and Racic, V. (2018). Improved model for human induced vibrations of high-frequency floors. *Engineering Structures*, 168:950–966. ISSN 01410296. doi: $10.1016/j.engstruct.2018.04.093$.

- Mohammed, A. and Pavic, A. (2019). Simulation of people's movements on floors using social force model. *Conference Proceedings of the Society for Experimental Mechanics Series*, pages 39–46. ISSN 21915652. doi: $10.1007/978-3-319-74421-66$.

- Mohammed, A. and Pavic, A. (2017). Evaluation of Mass-Spring-Damper Models for Dynamic Interaction Between Walking Humans and Civil Structures. *Conference Proceedings of the Society for Experimental Mechanics Series Dynamics of Civil Structures*, Volume 2, 169-177. doi: $10.1007/978-3-319-54777-0_21$.

- Mohammed, A. and Pavic, A. (2018). Utilising an advanced technology of people tracking in vibration serviceability application. In *Lecture Notes in Civil Engineering*, volume 5, pages 388–396. doi: 10.1007/978-3-319-67443-8 33. doi: $10.1007/978-3-319-54777-0_21$.

- Mohammed, A. and Pavic, A. (2017). Effect of Walking people on Dynamic Properties of Floors. *Procedia Engineering*, 199:2856–2863. ISSN 18777058. doi: $10.1016/j.proeng.2017.09.561$.

- Mohammed, A. and Pavic, A. and Racic, V. (2016). Improved footfall model for vibration of high-frequency floors. *Insights and Innovations in Structural Engineering, Mechanics and Computation*, 202-205. doi: $10.1016/j.engstruct.2018.04.093$.